# Investigating negative selection of pathogenic mtDNA variants in the blood

Imogen Grace Franklin

Doctor of Philosophy

Biosciences Institute

November 2024

## Author declaration

This thesis is submitted for the degree of Doctor of Philosophy at Newcastle University. I declare that all work described has not been submitted for any other qualification and was carried out by myself, unless otherwise stated.

## Abstract

The most common cause of adult mitochondrial disease is the pathogenic mitochondrial DNA (mtDNA) variant m.3243A>G. This variant is heteroplasmic, meaning that it does not affect all mtDNA molecules. The level of m.3243A>G in post-mitotic tissues remains stable throughout life. In mitotic tissues such as the blood, the level of pathogenic mtDNA is consistently decreased in comparison to post-mitotic levels and further declines with age. This work aims to characterise this decline in different cell types and understand the mechanism underlying this process.

By investigating m.3243A>G level within 15 cell populations from 26 individuals, I observed enhanced mutation loss in six cell subtypes; this included all cells investigated within the T-cell compartment. Single cell analysis in six individuals supported these findings; all T-cell subsets exhibited an increased proportion of cells with low mutation levels compared to progenitor, myeloid and B-cell groups. This shift was more marked in memory compared to naïve T-cells and followed consistent trends between patients throughout maturation. Notably, this pattern was also observed in samples carrying the m.8344A>G variant, which remains stable in whole blood with age, but not for any investigated protein-coding variants.

Flow cytometry data revealed a lower proportion of T-cells in m.3243A>G patients compared to controls and higher T-cell expression of exhaustion marker PD-1, suggesting that m.3243A>G impacts blood homeostasis. Parallel sequencing of mtDNA and the transcriptome revealed high levels of cellular stress and abnormal interleukin signalling in T-cells with high m.3243A>G heteroplasmy, indicating decreased fitness of these cells. This was supported by *in vitro* studies which demonstrated increased cell death in patient T-cells following stimulation.

Understanding selection can give an invaluable insight into disease prognosis and help to identify therapeutic targets. These findings lay the foundations for further exploration into cellular fitness as a driver of negative selection in the blood.

**Acknowledgements.**

Firstly, I want to express my gratitude to my supervisors, Sarah, Ollie, and Matt, for their invaluable guidance and support throughout my PhD journey. Sarah and Ollie, you have gone above and beyond for me over the past four years, and I cannot thank you enough for your unwavering patience and encouragement. The two of you make such a great team and I hope you continue to mentor students together (but also don't because I'll get jealous). Your faith in me, especially during times when I struggled to believe in myself, has meant more than I can express. I'd also like to give a special mention to Paul for always being a source of wisdom and advice. Big shout out for enduring all those long days on the cell sorter – especially the ones where I did not stop talking!!

I would next like to acknowledge the Flow Cytometry core facility and thank the individuals who donated their blood for this work as well as the incredible clinical staff who coordinated recruitment, especially with a pandemic to contend with! Susie, Barbara, Ana, and all of the team in oxford, thank you for allowing me to visit and welcoming me with open arms.

It has been a pleasure to work on the 4$^{th}$ floor with so many incredible people. I've been so lucky to make lifelong friends among the past and present members of the big office; thank you for the laughter and for creating such a friendly and supportive community. Roisin, I am so grateful for you, your support has been a constant boost when I needed it most. A big thank you to my dearest friends Chloe, Carol-Ann, Charlotte, Callum, Niamh, Catherine, and Aleah despite none of them really knowing what it is I do. Carol-Ann, I'm so glad we have gone on this journey together and pulled each other out the other side. Not sure I would have managed it without a housemate like you!!

To my big sister pip, writing this thesis would not have been possible without you. Without you, I would have probably been homeless and without a fully functioning right ankle! You put up with me at my lowest, driving me up and down the country to hospital appointments and didn't ask for anything in return (well maybe a dogsitter). So, this is as much your achievement as it is mine. Thank you and love you so much!!! Jess I can always rely on you to bring a smile to my face, you mean more to me than you know and I'm so grateful to call you all family. Finally, Mum and dad, thank you for being my biggest supporters both emotionally and financially (sorry! IOU). You make even the smallest achievements feel special and I am so lucky to have a crazy pair like you.

## Publications

**Franklin, I.G.**, Milne, P., Childs, J., Boggan, R.M., Barrow, I., Lawless, C., Gorman, G.S., Ng, Y.S., Collin, M., Russell, O.M. and Pickett, S.J., 2023. T cell differentiation drives the negative selection of pathogenic mitochondrial DNA variants. Life Science Alliance, 6(11).

# Contents

**List of Figures**

**List of tables**

## List of equations

**List of abbreviations**

| Abbreviation | Meaning |
|---|---|
| **APC** | Antigen presenting cell |
| **APS** | Adenosine 5' phosphosulfate |
| **ATAC-seq** | Assay for transposase-accessible chromatin with sequencing |
| **ATP** | Adenosine triphosphate |
| **BCR** | B cell receptor |
| **BMDM** | Bone marrow derived macrophages |
| **cDNA** | Complementary DNA |
| **CI** | NADH:ubiquinone oxidoreductase |
| **CII** | Succinate dehydrogenase |
| **CIII** | Ubiquinol:cytochrome *c* oxidoreductase |
| **CIV** | Cytochrome *c* oxidase |
| **CMP** | Common myeloid progenitors |
| **CMV** | Cytomegalovirus |
| **CN** | Copy number |
| **ConA** | Concanavalin A |
| **CPEO** | Chronic progressive external ophthalmoplegia |
| **CTV** | Cell trace violet |
| **CV** | ATP synthase |
| **D** | Diversity |
| **D loop** | Displacement loop |
| **DAMP** | Damage associated molecular patterns |
| **DEG** | Differentially expressed gene |
| **DN** | Double negative |
| **dNTP** | Deoxyribonucleotide triphosphate |
| **DP** | Double positive |
| **EBV** | Epstein–Barr virus |
| **ELISpot** | Enzyme linked immunospot assay |
| **ER** | Endoplasmic reticulum |
| **ERAD** | ER-associated degradation |
| **ERSE** | ER stress response elements |

| | |
|---|---|
| **ETC** | Electron transport chain |
| **FACS** | Fluorescence activated cell sorting |
| **FAD** | Flavin adenine dinucleotide |
| **FAO** | Fatty acid oxidation |
| **FBS** | Foetal bovine serum |
| **FDR** | False discovery rate |
| **FMN** | Flavin mononucleotide |
| **GC** | Germinal centres |
| **GEM** | Gel Beads in-emulsion |
| **GMP** | Granulocyte–macrophage progenitors |
| **GO** | Gene ontology |
| **GSEA** | Gene set enrichment analysis |
| **HPO** | Human Phenotype Ontology |
| **HSC** | Haematopoietic stem cell |
| **IL** | Interleukin |
| **IMM** | Inner mitochondrial membrane |
| **IMS** | Intermembrane space |
| **iNeurons** | iPSC derived neurons |
| **ISFET** | Ion-sensitive field-effect transistor |
| **ISP** | Ion sphere particle |
| **ISR** | Integrated stress response |
| **J** | Join |
| **KO** | knockout |
| **LHON** | Leber's hereditary optic neuropathy |
| **LMP** | Common lymphoid progenitors |
| **LMPP** | Lymphoid primed multipotent progenitors |
| **LPS** | Lipopolysaccharides |
| **MAIT** | Mucosal associated invariant T cells |
| **mDC** | Myeloid dendritic cell |
| **MELAS** | Mitochondrial encephalomyopathy, lactic acidosis and stoke like episodes |
| **MEP** | Megakaryocyte erythroid progenitors |
| **MERRF** | Myoclonic epilepsy with ragged red fibres |

| | |
|---|---|
| **MHC** | Major histocompatibility complex |
| **MitoCohort** | Mitochondrial Research Patient Cohort |
| **MLASA** | Mitochondrial Myopathy, Lactic Acidosis, and Sideroblastic Anaemia |
| **MPP** | Multipotent progenitor cell |
| **Mt-aaRSs** | Mitochondrial aminoacyl-tRNA synthetases |
| **mtDNA** | Mitochondrial DNA |
| **mt-tRNA** | Mitochondrial tRNA |
| **MW** | Molecular Weight |
| **NAD** | Nicotinamine adenine dinucleotide |
| **NARP** | Neuropathy, ataxia, retinitis pigmentosa syndrome |
| **NK** | Natural killer |
| **NMDAS** | Newcastle Mitochondrial Disease adult scale |
| **NUMT** | Nuclear mitochondrial DNA segments |
| **$O_H$** | Heavy strand origin of replication |
| **$O_L$** | Light strand origin of replication |
| **OMM** | Outer mitochondrial membrane |
| **OXPHOS** | Oxidative phosphorylation |
| **PAMP** | Pathogen associated molecular pattern |
| **PBMC** | Peripheral blood mononuclear cells |
| **PBS** | Phosphate buffered saline |
| **PCR** | Polymerase chain reaction |
| **pDC** | Plasmacytoid dendritic cell |
| **PGC** | Primordial germ cell |
| **PPi** | Pyrophosphate |
| **PRR** | pattern recognition receptors |
| **QC** | Quality control |
| **$QH_2$** | Ubiquinol |
| **RBC** | Red blood cell |
| **ROS** | Reactive oxygen species |
| **scRNA seq** | Single cell RNA sequencing |
| **SD** | Standard deviation |
| **TAE buffer** | Tris-acetate-EDTA buffer |

| | |
|---|---|
| **TCA** | Tricarboxylic acid cycle |
| **$T_{CM}$** | Central memory T cell |
| **TCR** | T cell receptor |
| **$T_{eff}$** | Effector T cell |
| **$T_{EM}$** | Effector memory T cell |
| **$T_{EMRA}$** | T effector memory cells re-expressing naïve marker CD45RA |
| **$T_{Naive}$** | Naïve T cell |
| **Treg** | Regulatory T cell |
| **UPR** | Unfolded protein response |
| **UV** | Ultraviolet |
| **V** | Variable |
| **WB** | Whole blood |
| **WT** | Wild type |

# Chapter 1 Introduction

## 1.1 Origin of mitochondria

Mitochondria are double-membraned organelles found within all nucleated cells. They are thought to have originated from a symbiotic relationship between an alpha-proteobacterium and an archaeon (Wang and Wu, 2015, Roger,Muñoz-Gómez and Kamikawa, 2017). Phylogenetic analysis was able to trace the host cell lineage to that of the Asgard Archaea (Spang *et al.*, 2015, Liu *et al.*, 2021). The rationale for integration of the α-proteobacteria into the Asgard archaea is that it is thought to present a survival benefit (Sagan, 1967, Margulis, 1971); the exact benefit is widely debated (Mills *et al.*, 2022, Searcy, 2003). The α-proteobacterium retained a portion of its genome which is now known as mitochondrial DNA (mtDNA) and is the only source of extra-nuclear DNA in human cells (Gray,Burger and Lang, 1999, Martijn *et al.*, 2018). The contents of this thesis will refer to human mitochondria unless stated otherwise.

## 1.2 Mitochondrial structure and dynamics.

Mitochondria are encapsulated by two phospholipid membranes; the outer mitochondrial membrane (OMM) and inner mitochondrial membrane (IMM), separated by the intermembrane space (**Figure 1.1A**). The IMM is protein dense (Horvath and Daum, 2013) and consists of invaginations known as cristae which hold protein complexes involved in the generation of ATP via oxidative phosphorylation (OXPHOS) (section 1.4.2). The formation of OXPHOS complexes is important in the maintenance of cristae structure (Blum *et al.*, 2019). The IMM surrounds the matrix, which houses mtDNA and is the site of fatty acid oxidation and the tricarboxylic acid (TCA) cycle (section 1.4.1). Metabolites, proteins and most ions can only access the matrix via specific transporters including the adenine nucleotide translocator (ANT) due to the IMM being essentially impermeable.

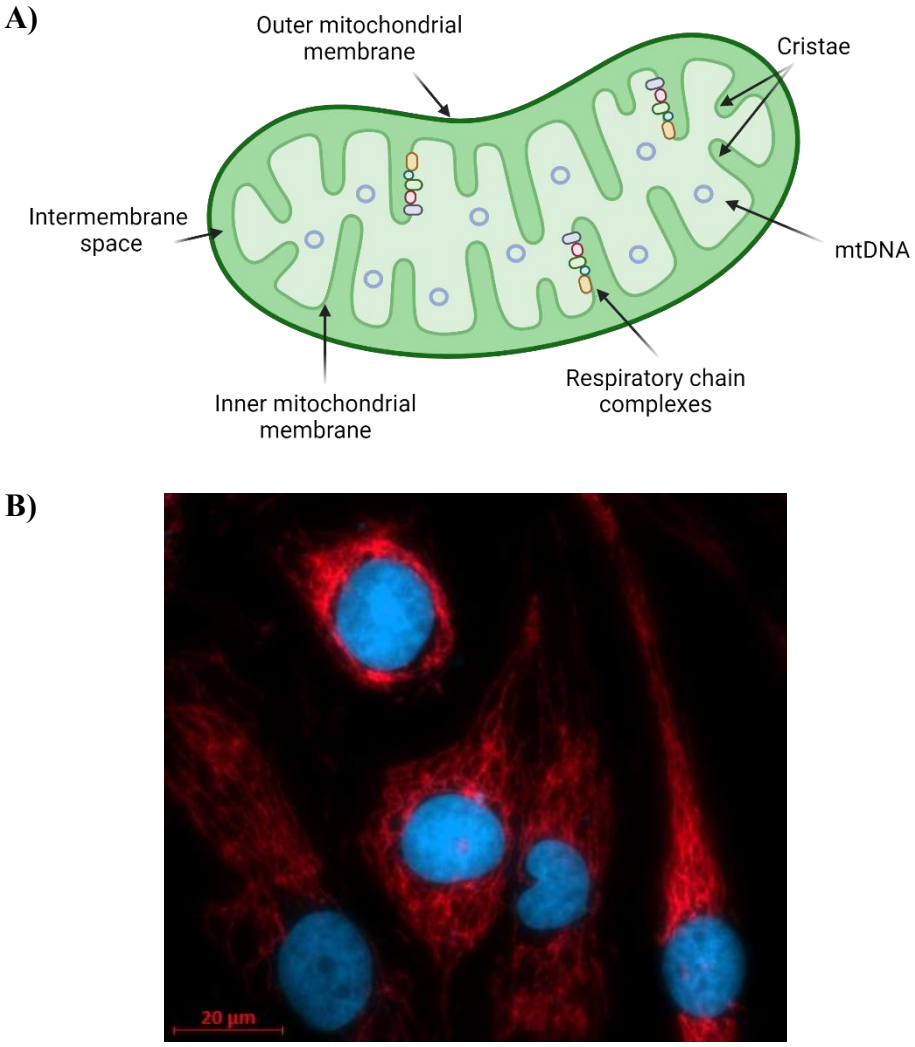


***Figure 1.1 Mitochondrial structure.*** *A) A cartoon demonstrating basic mitochondrial structure (made using biorender.com) B) A microscopy image demonstrating the mitochondrial network (red) in fibroblasts via TOMM20 staining and Hoechst staining for nuclei (blue).*

Mitochondria are dynamic organelles and are continuously undergoing fission and fusion, forming a network which maintains efficient distribution of mitochondrial contents throughout a cell (**Figure 1.1B)**. Two mitochondria fuse using three GTPases found on the OMM and IMM: Mitofusin 1 (MFN1), Mitofusin 2 (MFN2) and OPA1 Mitochondrial Dynamin Like GTPase (OPA1). MFN1 and MFN2 facilitate outer membrane fusion (Cao *et al.*, 2017) followed by OPA1 fusing two IMM (Ishihara *et al.*, 2006). Regulation of mitochondrial fusion is carried out by an opposing process, fission, which divides a mitochondrion in two. Fission is controlled by Dynamin related protein 1 (DRP1) (Smirnova *et al.*, 2001); DRP1 is recruited to the OMM by human mitochondrial

dynamics protein 49 (MID49), 51 (MID51), mitochondrial fission 1 protein (FIS1) or mitochondrial fission factor (MFF) following ER constriction of the mitochondrion (Gandre-Babbe and van der Bliek, 2008, Otera *et al.*, 2010, Palmer *et al.*, 2013, Losón *et al.*, 2013). ER constriction via ER tubules is required to reduce mitochondrial diameter from up to 500nm to 150nm, a size which allows DRP1 to form a ring-like structure around the mitochondrion (Friedman *et al.*, 2011) inducing further restriction. GTP hydrolysis of DRP1 recruits Dynamin 2 (DNM2) which severs at the restriction site (Lee *et al.*, 2016). There is debate as to the importance of DNM2 in the scission of the mitochondrion; Kamerkar *et al.* (2018) report that DRP1 is capable of fission without the recruitment of DNM2 (Kamerkar *et al.*, 2018).

## 1.3 Mitochondrial genetics

### 1.3.1 The mitochondrial genome

The mitochondrial genome is a small circular double stranded DNA molecule, approximately 16.57kb in length that encodes 37 genes: 13 protein coding genes, 2 rRNAs & 22 tRNAs (**Figure 1.2**). The majority of these (28) are encoded by the guanine-rich heavy strand and the remaining nine are found on the cytosine-rich light strand (Anderson *et al.*, 1981). Each strand can be segregated according to their buoyancy using a caesium chloride density gradient (Vinograd *et al.*, 1963). mtDNA does not contain introns, and has only one major non-coding region, known as the displacement loop (D loop) (Arnberg,van Bruggen and Borst, 1971, Walberg and Clayton, 1981). The D loop is a 1.1kb region which contains the origin of replication, TFAM (transcription factor A, mitochondrial) binding sites and two promotor regions (the H-strand promoter and the L-strand promoter) (Kasamatsu,Robberson and Vinograd, 1971). All protein coding genes encoded by the mtDNA are involved in facilitating generation of ATP via OXPHOS (section 1.4.2).

mtDNA is found in multiple copies per mitochondrion. Most somatic cells contain between 10s-1000s of copies mtDNA per cell, this varies between tissues; for example, those which have a high metabolic demand such as neurological and muscle tissue possess the highest proportion of mtDNA (Rath *et al.*, 2024). mtDNA reside in the

mitochondrial matrix as part of a nucleoid, associated with TFAM and other transcription, translation and replication machinery (Garrido *et al.*, 2003, Bogenhagen,Rousseau and Burke, 2008).

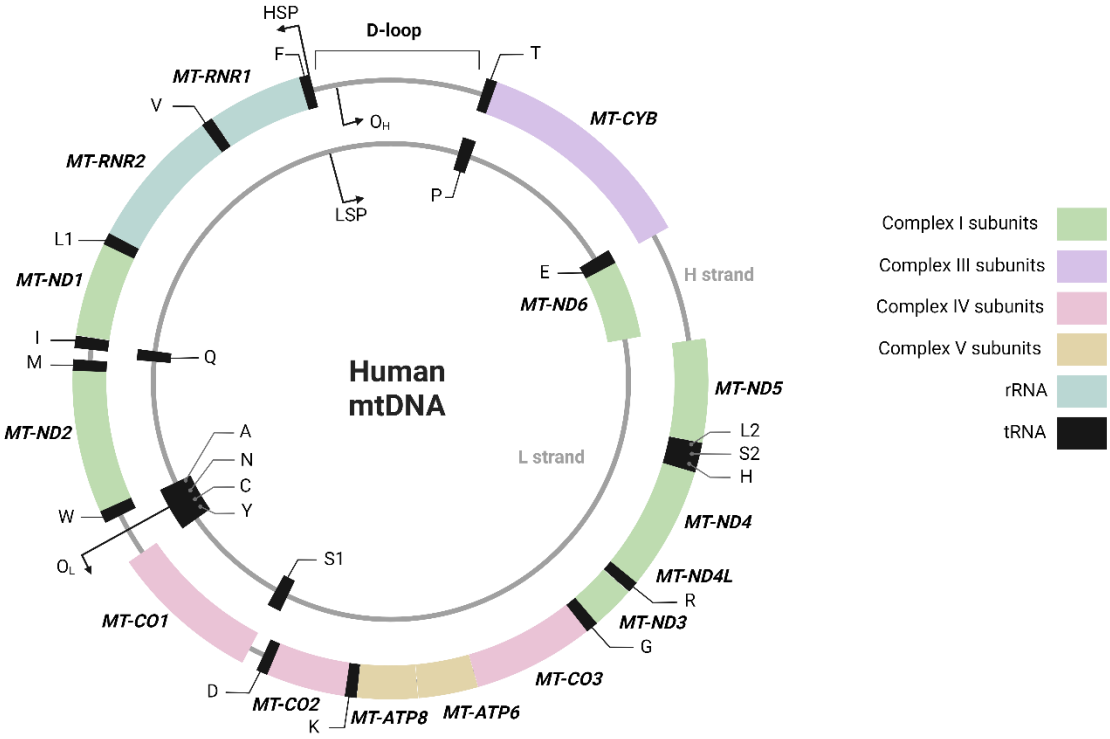


***Figure 1.2 Map of human mitochondrial DNA.*** *Human mtDNA is a double stranded circular DNA molecule which encodes 37 genes. These are 22 tRNAs (black), two rRNAs (blue) and 13 polypeptides (coloured according to the respiratory chain complex they are associated with). The majority of these genes are encoded by the heavy strand (H-strand) and the remaining 9 genes (8 tRNAs and 1 protein encoding gene) are encoded by the light strand (L strand). Each strand has its own origin of replication as demonstrated by the OL and HL labels. tRNAs are represented as an abbreviation of the cognate amino acid. Figure adapted from biorender template.*

### 1.3.2 mtDNA Replication

As well as occurring linked with the cell cycle, mtDNA replication occurs independently of the cell cycle in a process known as relaxed replication (Bogenhagen and Clayton, 1977). Two origins of replication can be found on mtDNA, one on the light strand ($O_L$) and one on the heavy strand ($O_H$). $O_H$ is located within the D-loop and $O_L$ within a tRNA

cluster ~11000 bp downstream. The exact mechanism of mtDNA replication is not established; there are three prevailing models of mtDNA replication which debate as to whether the synthesis of each strand occurs asynchronously or synchronously (extensively reviewed in (Falkenberg, 2018)). All theories agree that replication is reliant on nuclear encoded DNA polymerase γ and mtDNA helicase Twinkle. Twinkle binds the H strand at the replication fork and unwinds the mtDNA strand 5' -3 (Korhonen *et al.*, 2004), the mitochondrial single-stranded DNA-binding protein (mtSSB) binds the now single stranded, H strand to prevent formation of secondary structures allowing polγ mediated nascent strand synthesis (Miralles Fuste *et al.*, 2014).

### 1.3.3 Mitochondrial transcription

mtDNA transcription occurs bidirectionally and originates from two heavy strand promoters (HSP1 & HSP2) and one light strand promoter (LSP) within the D-loop. HSP1 initiates transcription from the 5' end of $tRNA^{Phe}$ to 16S RNA, therefore producing a single transcript containing $tRNA^{Phe}$, $tRNA^{Val}$ and two rRNAs. HSP2 is proposed to begin transcription at 12S RNA and transcribes the remaining length of the heavy strand, generating one long polycistronic transcript consisting of the majority of the mitochondrial heavy strand (Montoya *et al.*, 1982, Montoya,Gaines and Attardi, 1983). Similarly, initiation originating at the LSP also generates one long polycistronic transcript of the light strand (Chang and Clayton, 1984). Recently, a second light strand promotor has been identified: LSP2 which has lower transcriptional activity compared to LSP1 (Tan *et al.*, 2022).

TFAM binds upstream of these promotors inducing a bend in the mtDNA which enables recruitment of mitochondrial RNA polymerase (POLRMT) to form the preinitiation complex (Ngo,Kaiser and Chan, 2011, Hallberg and Larsson, 2011) . POLRMT undergoes a conformational change allowing mitochondrial transcription factor B2 (TFB2M) binding, thus forming the mitochondrial transcription initiation complex (Falkenberg *et al.*, 2002). Binding of TFB2M induces further conformational changes in POLRMT which enables entry of the mtDNA strand into the catalytic site (**Figure 1.3**) (Gustafsson,Falkenberg and Larsson, 2016). Upon initiation of transcription, TFB2M

dissociates allowing for binding of mitochondrial transcription elongation factor (TEFM). TEFM facilitates elongation of long transcripts greatly by stabilising the affinity of POLMRT to template and preventing termination upon POLMRT stalling (Minczuk *et al.*, 2011, Posse *et al.*, 2015).

Transcription termination is incompletely understood; currently only one termination factor has been characterised: mitochondrial transcription termination factor 1 (MTERF1), which is believed to play a role in termination of all 3 transcripts (Asin-Cayuela *et al.*, 2005, Yakubovskaya *et al.*, 2010). Initial hypotheses suggested that MTERF1 bends the mtDNA, joining HSP1 to *MT-TL1,* inducing termination from HSP1 through base flipping and DNA unwinding (Yakubovskaya *et al.*, 2010, Jiménez-Menéndez *et al.*, 2010). There is debate as to the existence of two heavy strand promotors as HSP2 transcription initiation has been difficult to recapitulate *in vitro* and knockout of Mterf1 in mice did not affect rRNA levels and appears to terminate transcription from LSP rather than HSP (Terzioglu *et al.*, 2013). However, there is the possibility that human and murine systems differ in the number of promoters present.

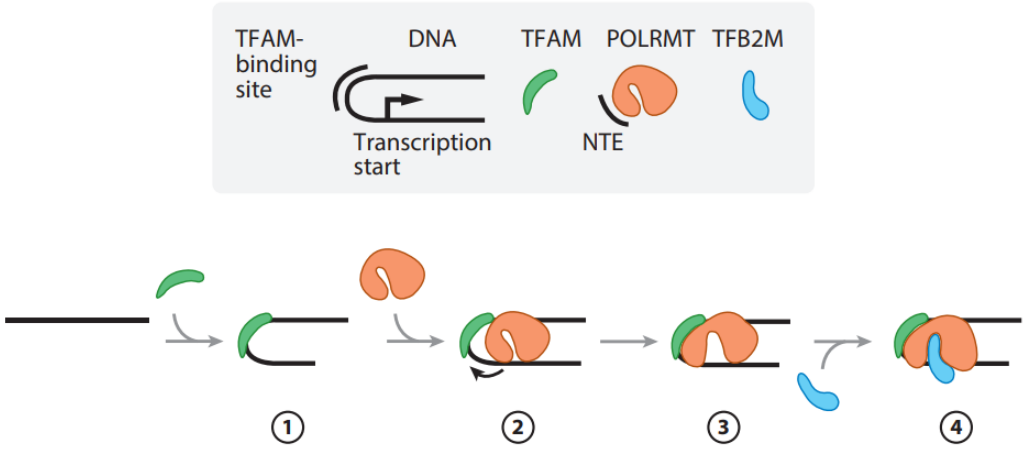


***Figure 1.3 Initiation of mitochondrial transcription.*** *TFAM binds upstream of transcription promotors (1) inducing a bend in the mtDNA and enabling binding of POLRMT (2). POLRMT undergoes a conformational change (3) allowing mitochondrial transcription factor B2 (TFB2M) binding (4). TBF2M induces further conformational changes in POLRMT which enables entry of the mtDNA strand into the catalytic site. Taken from Gustafsson,Falkenberg and Larsson (2016)*

### 1.3.3.1 Transcript Processing

The tRNA punctation model dictates that 22 tRNA genes encoded by the mitochondrial genome act as a guide for processing of the large polycistronic transcript (Ojala,Montoya and Attardi, 1981). Each tRNA is excised via ribonuclease P (RNase P) from the 5' end and ribonuclease Z (RNase Z) from the 3' end (Brzezniak *et al.*, 2011). This model can explain the release of tRNA flanked rRNA and protein coding genes from the transcript. A small number of the mtDNA encoded genes are not flanked by tRNA on both sides (*MT-ND6, MT-CO3, MT-ND5, MT-CYB, MT-ATP6/8*) and therefore require further processing via G-Rich RNA Sequence Binding Factor 1 (GRSF1) or Pentatricopeptide Repeat Domain 2 (PTCD2) (Xu *et al.*, 2008, Antonicka *et al.*, 2013).

Once all transcripts are released, all mRNAs except *MT-ND6* are polyadenylated by mitochondrial poly(A) polymerase (mtPAP) (Tomecki *et al.*, 2004). The addition of a poly(A) tail generates a complete stop codon (UAA) in seven transcripts (Temperley *et al.*, 2010). tRNA molecules undergo a vast number of post-transcriptional modifications which induce folding of secondary and tertiary structures; those at the anti-codon stem wobble base are essential for tRNA function. The addition of a -CAA sequence to the 3' end of each tRNA enables aminoacylation via a complementary mitochondrial aminoacyl tRNA synthetase (mt-aaRS) (Nagaike *et al.*, 2001).

### 1.3.4 Mitochondrial translation

Mitochondria possess their own translation machinery, termed the mitoribosome. The mitoribosome is made up of two subunits, one consisting of the mitochondrially encoded 16S rRNA and ~50 nuclear encoded subunits known as the large or 39S subunit (LSU) and another with the 12S rRNA and 30 nuclear subunits known as the small subunit (SSU) (Amunts *et al.*, 2015). Mitochondrial translation takes place tethered to the IMM (Itoh *et al.*, 2021).

Initiation of transcription is facilitated by mitochondrial initiation factor mtIF3. mtIF3 associates with the SSU and acts to position the mRNA start codon at the P site of the SSU (**Figure 1.4**) (Bhargava and Spremulli, 2005). Like cytosolic protein synthesis, mitochondrial translation is initiated at a methionine residue; however, unlike cytosolic

protein synthesis the mitoribosome recognises non-AUG initiation codons such as AUU and AUA. A single $tRNA^{met}$ is used to trigger initiation and during elongation (Spremulli *et al.*, 2004). A formylated molecule of methionine associated with $tRNA^{Met}$ ($fMet\text{-}tRNA^{Met}$) functions to initiate as this post transcriptional modification increases its affinity to mtIF2 which aids in assembly of the mitoribosome (Spencer and Spremulli, 2004).

Mitochondrial tRNA molecules (mt-tRNA) are loaded with their corresponding amino acid via the nuclear-encoded family of mitochondrial aminoacyl-tRNA synthetases (mt-aaRSs). Elongation is facilitated by mitochondrial elongation factor Tu (mtEF-Tu). mtEF-Tu is associated with GTP and directs the tRNA to the acceptor (A) site to allow base pairing with the mRNA (**Figure 1.4**), hydrolysis of the associated GTP catalyses the formation of a peptide bond (Cai *et al.*, 2000).

Termination of transcription most commonly occurs in the instance of a canonical UAA or UAG stop codon. In human mitochondria, the standard stop codon UGA is reassigned to tryptophan. Termination at stop codons relies on the actions of mitochondrial translation release factor A (mtRF1a) which catalyses a GTP dependent cleavage of a nascent polypeptide as it exits the large subunit (Soleimanpour-Lichaei *et al.*, 2007). In the event of a non-canonical stop codon, as is suggested at the end of *MT-ND6* and *MT-CO1* transcripts, mitochondrial release factor 1 (mtRF1) has recently been implicated as the primary catalyst using mtRF1 knock out HEK293 cells (Krüger *et al.*, 2023, Temperley *et al.*, 2010).

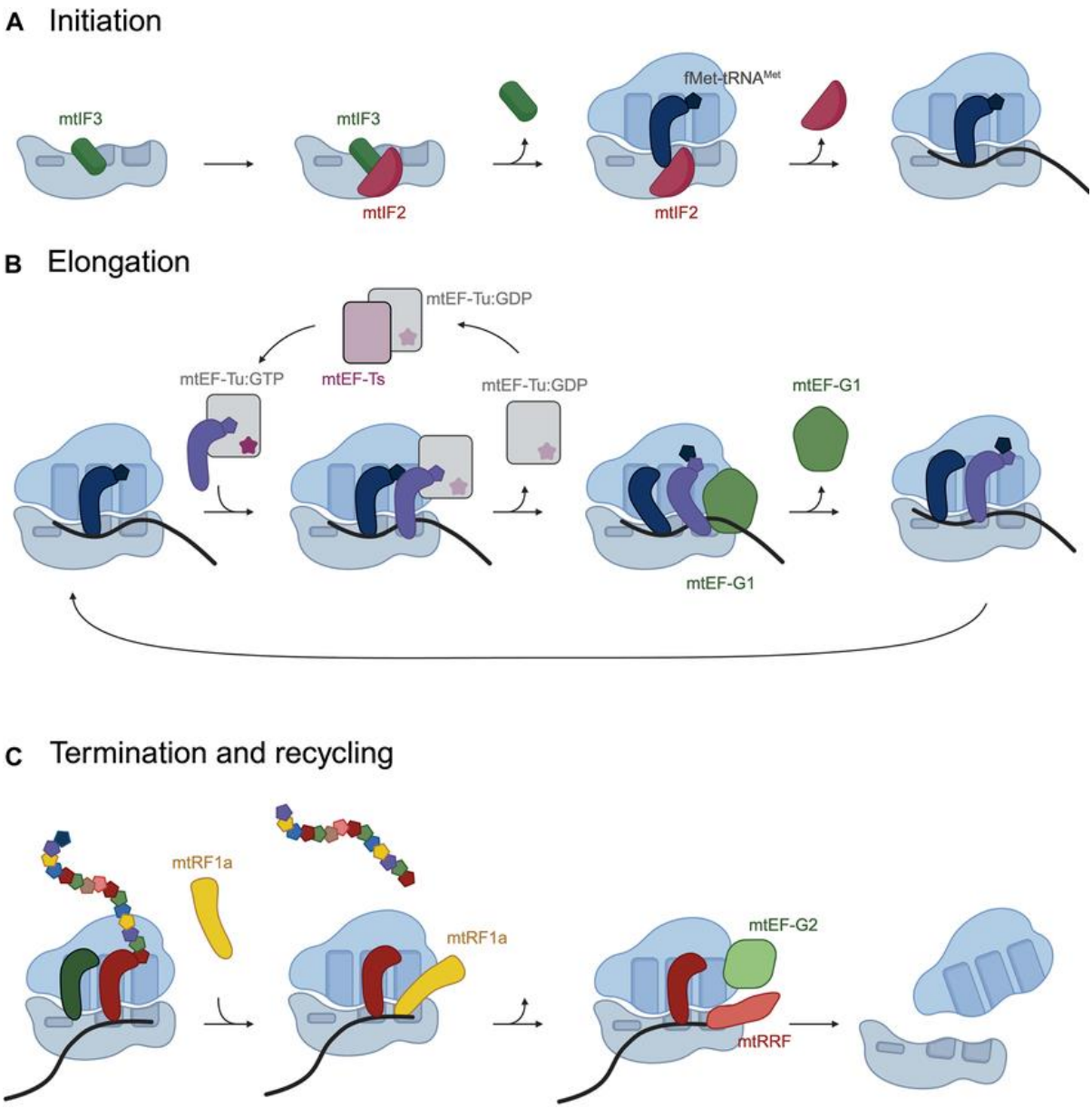


***Figure 1.4 Mitochondrial translation.*** *Mitochondrial translation is initiated via the binding of mitochondrial initiation factor 3 (mtIF3) to the small subunit of the mitoribosome. fMet-tRNAMet is recruited to the formed mitoribosome via mtIF2 where it initiates translation. mtEF-Tu is associated with GTP and directs a loaded tRNA to the acceptor site to allow base pairing with the mRNA, hydrolysis of the associated GTP catalyses the formation of a peptide bond. Translation termination occurs when mtRF1a recognises a stop codon and terminates translation. mtEF-G2 and mtRRF disband the mitoribosome after the polypeptide is released. Figure taken from (Antolínez-Fernández et al., 2024)*

## 1.4 Functions of the mitochondrion

As mentioned above, the IMM is the site of ATP generation via OXPHOS using products from matrix reactions. However, the importance of mitochondrial function to the cell is not limited to ATP production. In excess of 1000 nuclear genes contribute to mitochondrial function beyond OXPHOS (Boengler,Heusch and Schulz, 2011, Rath *et al.*, 2021) including processes such as cell development, apoptosis, calcium buffering and iron sulphur (Fe-S) cluster biosynthesis (Buck *et al.*, 2016, Westermann, 2010, Stehling and Lill, 2013). Fe-S clusters play a key role in electron transfer in the respiratory chain (section 1.4.2), haem biosynthesis and are critical for all polymerase functions and are therefore indispensable for DNA repair (Netz *et al.*, 2012); the biosynthesis mechanism is highly conserved across species making it one of the mitochondrion's most important functions.

### 1.4.1 Bioenergetics

As mentioned above, OXPHOS relies on upstream reactions which generate reduced forms of nicotinamine adenine dinucleotide (NAD) and Flavin adenine dinucleotide (FAD). These include glycolysis, a reaction which generates pyruvate from glucose in the cytosol, forming four molecules of ATP. Pyruvate is then oxidised and input into the TCA cycle as acetyl CoA or converted into lactic acid. The TCA cycle involves a series of redox reactions, originating from acetyl CoA, generating the reduced electron carriers NADH and $FADH_2$ (**Figure 1.5**). Like glycolysis, fatty acid oxidation (FAO) also supplies the TCA cycle with acetyl CoA via the breakdown of long chain fatty acids into acetyl CoA generating 4ATP, $FADH_2$ and NADH (de Carvalho and Caramujo, 2018). Another reaction, glutaminolysis, involves the breakdown of glutamine into α-ketoglutaric acid, which is then input into the TCA cycle (**Figure 1.5**), this process also generates non-essential amino acids which can be used in nucleotide synthesis, therefore, glutaminolysis is utilised often in proliferating cells.

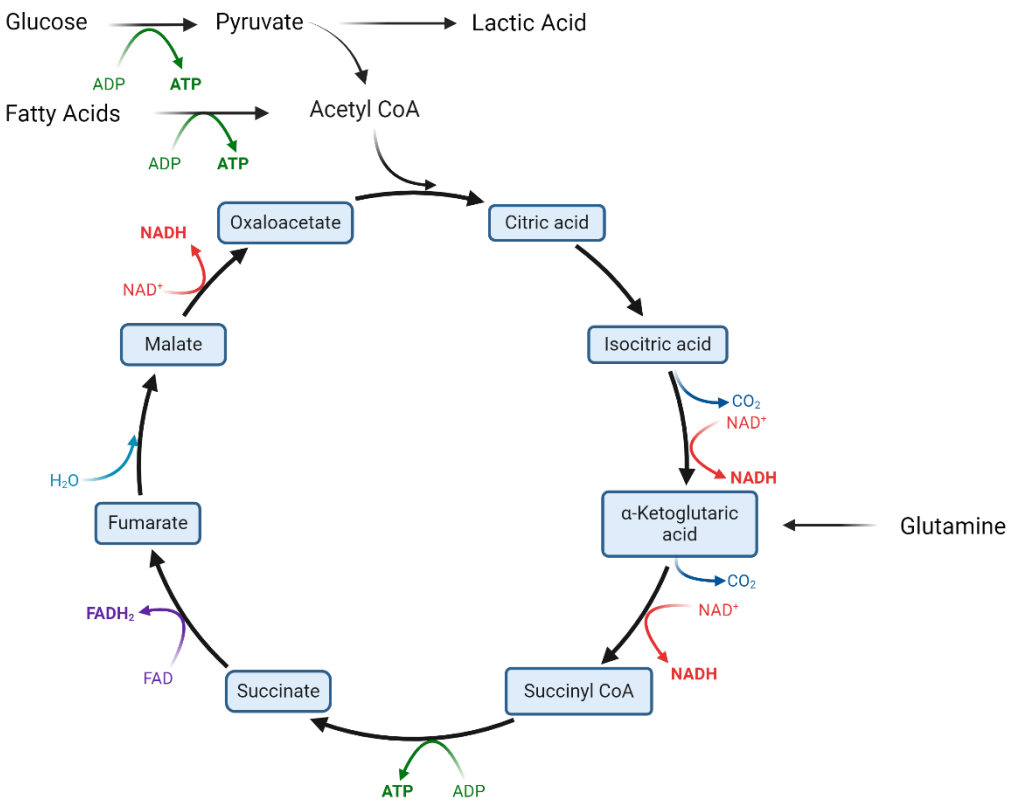


***Figure 1.5 The tricarboxylic acid cycle.*** *The TCA cycle denotes the conversion of acetyl CoA to CoA via eight intermediate redox reactions taking place in the mitochondrial matrix. Four of these reactions are catalysed by the reduction of NAD+ or FAD, generating NADH or FADH2 which act as electron donors and are the entry point of electrons into the electron transport chain. Figure adapted from biorender template*

### 1.4.2 OXPHOS.

OXPHOS involves the transfer of electrons between four protein complexes situated on the IMM. This induces a proton gradient which drives ATP synthase (Complex V; CV), thus, generating ATP. Electrons enter the electron transport chain via NADH, which donates an electron to NADH:ubiquinone oxidoreductase (Complex I; CI) or via $FADH_2$ to succinate dehydrogenase (Complex II; CII). From both complexes, an electron is transferred to ubiquinol:cytochrome *c* oxidoreductase (complex III; CIII) via ubiquinone, and from CIII to cytochrome *c* oxidase (complex IV; CIV) via Cytochrome *c* (CytC). As this process occurs, each reaction releases energy which drives translocation of protons

from the matrix to the intermembrane space via CI, CIII and CIV. The proton gradient established induces the synthesis of ATP by CV (Mitchell, 1961).

Both the nuclear and mitochondrial genome encode components of these multi-protein complexes, meaning that the process is under duel genetic control. All OXPHOS complexes contain both mitochondrial and nuclear encoded subunits, with the exception of complex II, which is entirely nuclear encoded (**Figure 1.6**).

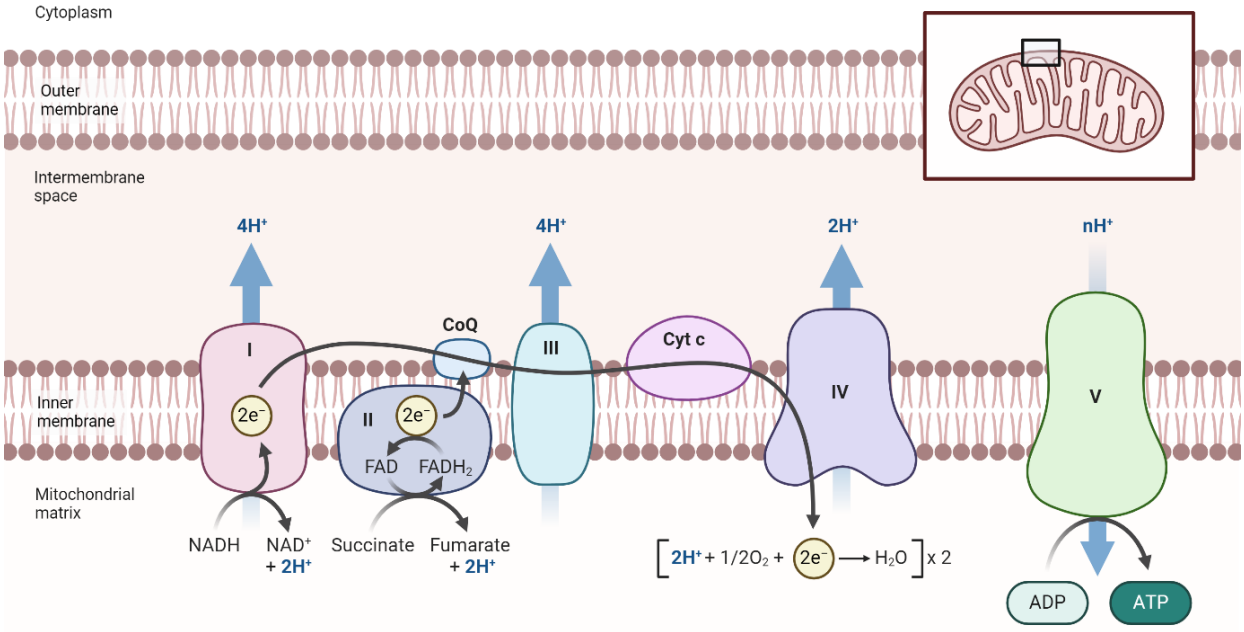


***Figure 1.6 Oxidative phosphorylation.*** *The electron transport chain (ETC) is made up of four multi subunit complexes within the inner mitochondrial membrane. Electrons enter the ETC via oxidation of NADH at CI and FADH2 at CII, these electrons reduce ubiquinone to ubiquinol. Ubiqinol donates electrons to CIII which reduces cytochrome c. Reduced cytochrome c donates electrons to reduce oxygen, catalysing the formation of H2O. The reaction at complexes I, III and IV catalyse the transfer of protons across the IMM into the intermembrane space. The proton gradient generated fuels ATP formation by ATP synthase. Figure adapted from Biorender.com template.*

### 1.4.2.1 NADH:ubiquinone oxidoreductase

NADH:ubiquinone oxidoreductase or CI is the largest OXPHOS complex and the point of entry for electrons donated by NADH. Mammalian CI is an L shaped structure residing in the IMM and made up of 44 subunits which are encoded by a combination of nuclear and mtDNA genes (37 nuclear and 7 mtDNA) (Carroll *et al.*, 2006, Zickermann *et al.*, 2015). Fourteen of these are considered to be 'core' CI subunits which are evolutionary conserved across bacteria and humans and essential for CI function; all 7 mtDNA encoded are considered core subunits. The remaining 31 accessory subunits are involved in complex assembly rather than having a direct role in CI function (Stroud *et al.*, 2016).

CI structure can be segmented into 3 functionally independent modules: N, Q and P (Zickermann *et al.*, 2015). The N-module is located at the tip of the hydrophilic arm extending into the matrix and is the site of NADH oxidation to $NAD^{+;}$ the released electrons are transferred to flavin mononucleotide (FMN) to form $FMNH_2$. The Q-module, also located within the matrix arm, contains a chain of eight iron-sulphur (Fe-S ) clusters, between which an electron is transferred which ultimately reduces ubiquinone to ubiquinol ($QH_2$) inducing a conformational change which allows the transfer of four protons from the matrix into the intermembrane (IMS) in the P-module (**Equation 1**) (Galkin and Moncada, 2017).

$$NADH + Q + 5H^{+}_{matrix} \rightarrow NAD^{+} + QH_2 + 4H^{+}_{IMS}$$

***Equation 1****. Complex I reaction.*

### 1.4.2.2 Succinate:ubiquinone oxidoreductase

Complex II is the smallest OXPHOS complex, made up of just 4 nuclear encoded subunits and is the only complex to be made up entirely of nuclear encoded proteins. Two hydrophobic subunits anchoring the complex to the IMM (SDHC & SDHD) and two catalytic subunits extending into the matrix (SDHA & SDHB) (Sun *et al.*, 2005). It is an alternative entry point for electrons into the ETC and, unlike CI, CIII and CIV, does not have proton pump capabilities. However, CII does play an essential role in the TCA cycle

via the oxidation of succinate to fumarate (**Equation 2**). Following this reaction FAD is reduced to $FADH_2$. As in CI, electrons are transferred along a chain of Fe-S clusters before transferal to ubiquinone to form $QH_2$ (Bezawork-Geleta *et al.*, 2017).

$$Succinate + Q \rightarrow Fumarate + QH_2$$

***Equation 2**. Complex II reaction*

### 1.4.2.3 Ubiquinol:cytochrome c oxidoreductase

Ubiquinol:cytochrome *c* oxidoreductase (CIII) is made up of 11 subunits, one of which is encoded by the mtDNA (cytochrome *b*). CIII exists as a homodimer with a catalytic core consisting of cytochrome *b* which contains two b-type hemes ($b_L$ and $b_H$), cytochrome $c_1$ which contains one c-type heme and a Rieske Fe-S cluster protein (Xia *et al.*, 1997, Fernandez-Vizarra and Zeviani, 2018).

Electron transfer by CIII takes place in a process known as the 'Q cycle' which originates with $QH_2$ derived from CI binding to the $Q_0$ site. Two electrons are then donated to the Rieske Fe-S cluster and cytochrome $c_1$ and cytochrome *b,* respectively. The electron donated to the Rieske Fe-S cluster then reduces cytochrome *c* resulting in its release from CIII and two protons being pumped into the IMS. The second electron is transferred between the two haem groups within cytochrome *b* which in two cycles reduces Q to $QH_2$. Two cycles of this process are represented by **Equation 3**.

$$2QH_2 + Q + 2Cytc_{ox} + 2H^+_{matrix} \rightarrow 2Q + QH_2 + 2Cytc_{red} + 4H^+_{IMS}$$

***Equation 3.** Complex III reaction*

### 1.4.2.4 Cytochrome c oxidase

Cytochrome *c* oxidase or CIV is the final enzyme of the ETC which reduces oxygen to generate $H_2O$. This process utilises four electrons and four protons from four reduced cytochrome c molecules while also driving the transfer of four protons into the IMS (Faxén *et al.*, 2005). It is made up of 14 subunits: 3 core mtDNA subunits and 11 nuclear encoded (Yoshikawa,Shinzawa-Itoh and Tsukihara, 1998). Two mtDNA encoded subunits: *MT-COI* and *MT-COII* form the catalytic core, making them essential to enzyme function. MT-COI contains two haem groups and a copper binding site while MT-COII contains a second copper binding site ($Cu_B$). Electrons are donated from reduced cytochrome *c* to $Cu_A$ and transferred to $haem_a$ which forms a catalytic site with $Cu_B$. Here, one electron reduces $Cu_B$ and the other $haem_{a3}$ establishing a peroxide bridge between the two. A second set of electrons transferred to the catalytic site break this peroxide bridge by reducing the oxygen molecules, thus forming $H_2O$ (Faxén *et al.*, 2005). This process pumps four protons into the IMS and can be summarised in **Equation 4**.

$$4CytC_{red} + 8H^+ + O_2 \rightarrow 4CytC_{ox} + 2H_2O + 4H^+_{IMS}$$

***Equation 4**. Complex IV equation*

### 1.4.2.5 ATP synthase

CV, also known as ATP synthase, catalyses the synthesis of ATP from ADP + inorganic phosphate (Pi). This enzyme is made up of two functional domains, termed $F_O$ and $F_1$. $F_O$ is a pore residing in the IMM and $F_1$ is a rotary module which extends into the matrix (Abrahams *et al.*, 1994). Two of the nineteen subunits making up ATP synthase are mtDNA derived (encoded by *MT-ATP6* and *MT-ATP8*) and both are found within the $F_O$ domain.

As a result of the proton gradient established via the actions of CI, CIII & CIV, protons pass through the $F_O$ module back into the matrix which drives the rotation of the F1 subunit (Watt *et al.*, 2010). During this rotation, the subunits which bind ADP and Pi (β

subunit) undergo conformational changes which bring ADP and Pi together to synthesise ATP (Devenish,Prescott and Rodgers, 2008).

#### 1.4.2.6 Super complexes

It is important to note that, these complexes often exist in multi-complex units known as supercomplexes. The most well-established of these is known as the respirasome and consists of CI, dimerised CIII and ~four units of CIV in close association (Moreno-Lastres *et al.*, 2012). Two other, smaller supercomplexes exist made up of either CI and CIII or CIII and CIV (Heinemeyer *et al.*, 2007). So far, CII and ATP synthase have not been identified as being part of a supercomplex structure. The role of supercomplexes is a widely debated field. It has been proposed that they are important for complex stability, for example, CI may be unstable in the absence of CIII or CIV (Acín-Pérez *et al.*, 2004, Diaz *et al.*, 2006). This suggests that the dysfunction of one complex may have negative consequences to those complexes making up the same supercomplex. Recent work, which depleted the levels of the respirasome in mice indicated that these structures were dispensable for OXPHOS function. They knocked out three amino acids within UQCRC1 (CIII) which controls respirasome stability and found no change in respiratory chain activity (Milenkovic *et al.*, 2023). However, these mice possess a novel supercomplex species migrating above free CI which, although dismissed by the authors, may present a compensation mechanism for respirasome deficiency. Another suggestion is that they function to minimise production of ROS; disruption of the CI + CIII supercomplex increases ROS output, suggesting a protective role (Maranzana *et al.*, 2013).

### 1.4.3 Generation of ROS

The generation of ROS has long been considered a negative byproduct of respiration. Electron 'leakage' from CI and CIII can cause interaction with surrounding oxygen to form superoxide ($O_2^{\cdot -}$) which promotes DNA damage via hydroxyl-radical formation (Keyer and Imlay, 1996). More recently, ROS have been identified as key signalling molecules involved in a wide variety of cellular processes (Hart *et al.*, 2015, Sies and Jones, 2020). Generation of a superoxide is favoured when the NADH/NAD+ ratio of the matrix is high and when mitochondria are not generating ATP causing a high

protonmotive force and a large pool of reduced CoQ (Kudin *et al.*, 2004, Lambert and Brand, 2004). Direct oxidation of partially reduced CoQ is a prominent route of $O2^{\cdot -}$ formation. Mitochondrial dysfunction such as supercomplex disruption can hinder the production of ATP and increase ROS generation through this mechanism.

Excess mitochondrial ROS can be detrimental; there is evidence to suggest that ROS can induce loss of function in proteins, promote apoptosis and initiate abhorrent cellular signalling. At moderate levels, ROS signalling is important in the differentiation and function of many cell types, with particular importance in cells of the immune system. For example, low concentrations of ROS signalling are importance in the maintenance of the activated T cell state during infection (Sena *et al.*, 2013)(discussed further in 1.9.1.2).

### 1.4.4 Calcium homeostasis

The maintenance of intracellular calcium levels is key for cell migration, proliferation and in the case of muscle cells, contraction as these processes are all reliant on calcium dependent signalling. The endoplasmic reticulum (ER) and the mitochondria are the main cellular stores of calcium ions ($Ca^{2+}$) (Romero-Garcia and Prado-Garcia, 2019). Mitochondrial $Ca^{2+}$ is required for the regulation of mitochondrial processes such as the TCA cycle and ATP synthesis (McCormack and Denton, 1979, Jouaville *et al.*, 1999). A complex interplay between the ER and mitochondria, aided by numerous close contact sites such as at MFN2, regulate entry of calcium ions into the mitochondria and protect against severe cytosolic calcium overload. $Ca^{2+}$ signalling is key in the activation of the leukocyte T cell. The prolonged elevation of cytosolic required for activation is maintained via interaction of the mitochondria with membrane residing calcium channels. Mitochondria localise $Ca^{2+}$ away from sites which would induce opening of $Ca^{2+}$ release channels (Hoth,Button and Lewis, 2000).

### 1.4.5 Apoptosis

Apoptosis or programmed cell death can be induced as a result of extrinsic or intrinsic pathways. The intrinsic pathway typically originates in the mitochondria in response to

cellular stress such as ultraviolet (UV) damage, high cytosolic $Ca^{2+}$ or growth factor restriction. Mitochondrial outer membrane permeability is regulated via the Bcl-2 protein family including BAX, which is localised to the cytosol, and BAK which is localised to mitochondria (Todt *et al.*, 2015). These molecules are activated under stress via the binding of BH3 proteins such as PUMA, BID and BIM resulting in conformational changes of BAX/BAK (Dewson *et al.*, 2008, Czabotar *et al.*, 2013, Moldoveanu *et al.*, 2013). BH3 binding leads to homodimerization of BAX and BAK on the OMM which then form larger oligomer pores and thus inducing mitochondrial outer membrane permeabilization (Dewson *et al.*, 2009, Subburaj *et al.*, 2015). Following this, extensive cristae remodelling occurs due to OPA1 cleavage by OMA1 and the opening of cristae junctions (Estaquier and Arnoult, 2007, Jiang *et al.*, 2014). Cytochrome *c* is released from the matrix, which interacts with the apoptotic protease activating factor-1 (APAF1) in the cytosol, triggering a caspase cascade including caspase-9 and caspase-3 (Riedl *et al.*, 2005) (**Figure 1.7**). This leads to DNA fragmentation and ultimately, cell death (Li *et al.*, 1997).

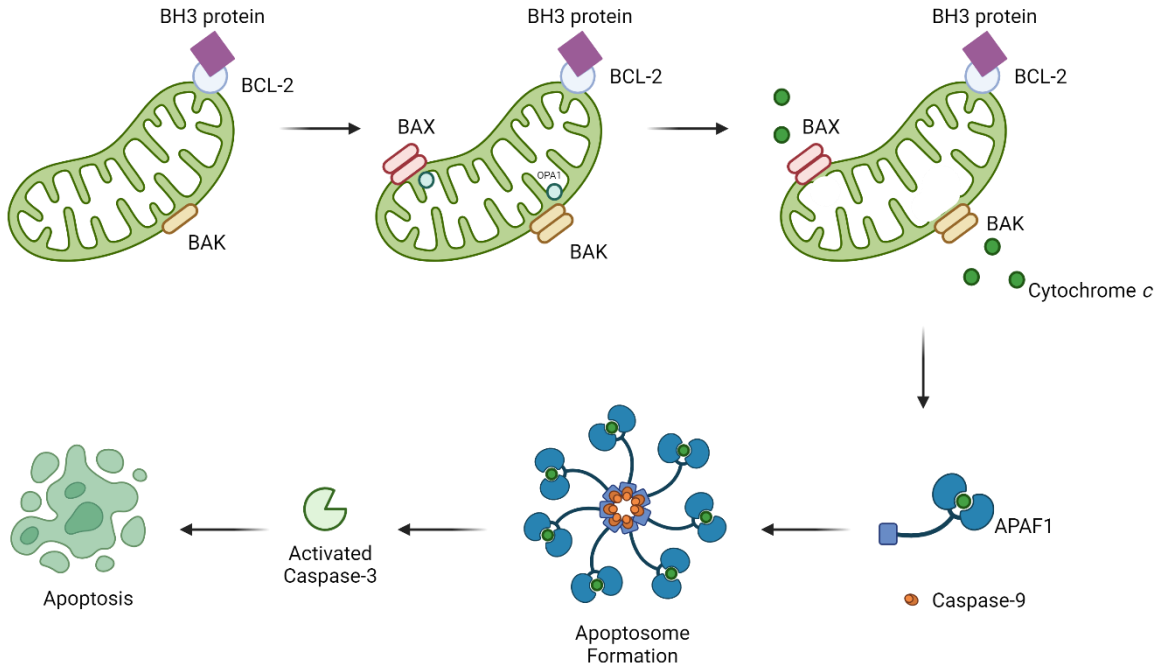


***Figure 1.7 Mitochondrial Apoptosis***. *Internal stress such as UV induced DNA damage triggers the binding of BH3 proteins to the Bcl-2 family proteins found on the outer mitochondrial membrane. Following this BAX and BAK form homodimers on the outer membrane, initiating pore formation. OPA1 is cleaved by OMA1, opening cristae junctions, allowing the release of cytochrome c into the cytosol. Cytochrome c binds APAF1 and caspase-9 forming the apoptosome which activates caspase-3 inducing apoptosis. Figure made using biorender.com*.

## 1.5 Mitochondrial disease

Mitochondrial disease encompasses a group of heterogenous, multisystemic conditions which are induced as a result of mitochondrial dysfunction. As over 99% of the genes required for healthy mitochondrial function are nuclear encoded, alterations of both the mtDNA and nDNA can result in mitochondrial disease (Rath *et al.*, 2021). Examples of nuclear encoded mitochondrial disease include those which affect replication machinery such as *POLG (Van Goethem et al., 2003, Naviaux and Nguyen, 2004)*, translation

machinery such as mitoribosomal proteins (Gardeitchik *et al.*, 2018) or structural genes such as *OPA1 (Delettre et al., 2001)*.

### 1.5.1 mtDNA disease & heteroplasmy

mtDNA-related disease arises due to alterations to the mtDNA genome; this is often in the form of a single nucleotide variant or deletion. As multiple copies of mtDNA are present per cell, it is possible for only a proportion of mtDNA molecules to carry the pathogenic variant. Heteroplasmy is the term used to describe a state in which two or more species of mtDNA co-exist within the same cell, for example, wild type mtDNA and pathogenic mtDNA occupying the same cell (**Figure 1.8**). Homoplasmy is a state in which all mtDNA is identical in nature. Heteroplasmy of a pathogenic variant is represented as a percentage; high proportions of pathogenic mtDNA (~60-80%) typically exceed a biochemical threshold in which the wild-type (WT) mtDNA can no longer compensate for a respiratory deficit and respiratory dysfunction is induced (**Figure 1.8**) (Rossignol *et al.*, 2003). The biochemical threshold can differ between tissues and cell types as well as the variant in question (Shoffner *et al.*, 1990).Typically large scale mtDNA deletions have a lower threshold than point mutations.

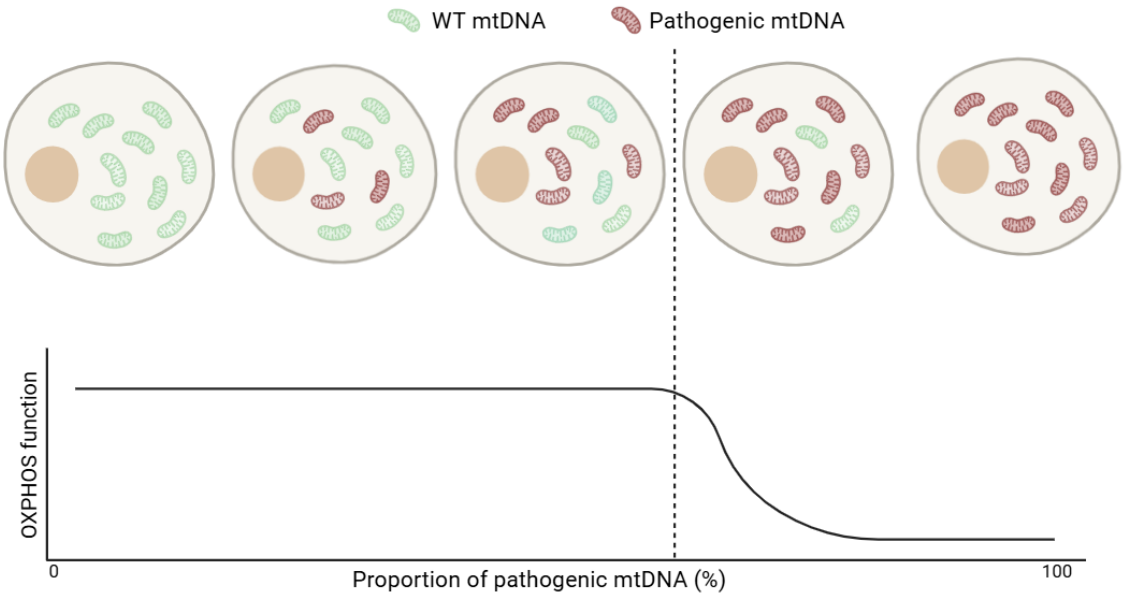


***Figure 1.8 The mitochondrial threshold effect.*** *Heteroplasmic mtDNA variants induce biochemical dysfunction once a threshold is surpassed (60-80% pathogenic mtDNA). Until this point, the wild type mtDNA is able to compensate for the dysfunctional mtDNA. Figure generated using biorender.com.*

### 1.5.2 Maternal Inheritance

The oocyte is the most mtDNA concentrated cell within the human body, containing over 100,000 mitochondria (Chen *et al.*, 1995). All of the mitochondria within a developing embryo are inherited from the oocyte in a process termed maternal inheritance (Hutchison *et al.*, 1974, Giles *et al.*, 1980). There has been research to suggest that, rarely, bi-parental inheritance of mtDNA can occur (Luo *et al.*, 2018), however this research is limited. Using WGS trio data the authors found paternal mtDNA sequences in offspring data, however it is likely that paternal mitochondrial genes are transferred into the paternal nuclear genome forming nuclear mitochondrial DNA segments (NUMTs) which are then autosomally transmitted to offspring. These NUMTs could be mistaken for paternal transmission, therefore more research is needed to determine if bi-parental inheritance is real phenomena or an artefact (Wei *et al.*, 2020). In 2023, the use of digital droplet PCR revealed spermatozoa contain ~0.58 mtDNA copies per cell; this low value was confirmed using whole genome sequencing which estimated an average of 0.14 copies

per spermatozoa. The group then used RNAscope to show that spermatozoa contain no mtDNA and the minor amounts being measured were likely a result of leukocyte contamination (Lee *et al.*, 2023). This provides strong evidence against paternal transmission.

### 1.5.3 Alterations in heteroplasmy and the genetic bottleneck

The mitochondrial genetic bottleneck describes a phenomenon in which a small pool of mtDNA in the parent results in highly variable transmission of mtDNA heteroplasmy to offspring upon an increase in mtDNA (Cree *et al.*, 2008). This phenomenon was first described in Holstein cows (Olivo *et al.*, 1983, Ashley,Laipis and Hauswirth, 1989). This can be observed in the inheritance of mtDNA disease; two siblings can be born with a very different mutation heteroplasmy, which can also differ from the mother (Jenuth *et al.*, 1996, Wai,Teoli and Shoubridge, 2008, Hellebrekers *et al.*, 2012).

A bottleneck is thought to occur during the formation of primordial germ cells (PGCs) in early embryonic development as the mtDNA content of PGCs is ~1000 fold lower than oocytes (Floros *et al.*, 2018). Daughter cells with a randomly allocated pool of mtDNA then increase mtDNA content upon maturation to oocyte, giving rise to siblings with differing levels of heteroplasmy (**Figure 1.9**). A low mtDNA level in tissues during development can result in tissue-specific bottlenecks and differences in heteroplasmy in different tissues (Floros *et al.*, 2018). As mtDNA are capable of relaxed replication, some theories suggest that preferential replication of variant mtDNA could increase the heteroplasmy in offspring. Preferential replication of pathogenic mtDNA molecules has been observed in human cell lines and animal models (Diaz *et al.*, 2002a, Clark *et al.*, 2012) and this could offer an explanation as to why, in some individuals with mtDNA disease, the onset of symptoms does not occur until later in life.

During cell division, mtDNA is thought to be distributed to daughter cells randomly in a process known as vegetative segregation. In the event of heteroplasmy, this means that an unequal proportion of mutant mtDNA may be transmitted to each daughter cell (Birky, 2001). This can result in a mutation level drift in populations of dividing cells. A bottleneck occurring during cell division, for example due to a pathogenic variant having

negative effects on cellular function inducing cell death or inhibiting proliferation, could have a purifying selection effect.

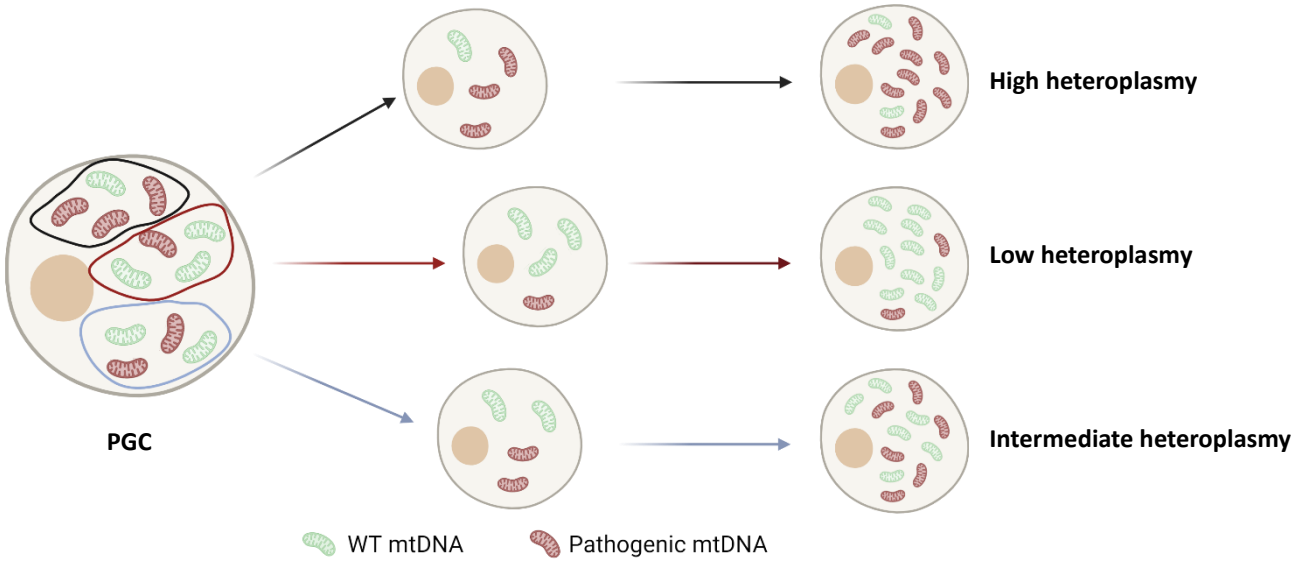


***Figure 1.9 The mitochondrial genetic bottleneck.*** *A primordial germ cell undergoes a period of mitosis followed by meiosis in order to differentiate into mature gametes as represented by the middle cells. During division, daughter cells are generated with a random distribution of wild type and pathogenic mtDNA; these cells have a low mtDNA content and must induce replication of mtDNA to increase mtDNA to healthy levels. This expansion generates daughter cells with a level of pathogenic mtDNA which has shifted from the parent cell. Figure generated using biorender.com.*

### 1.5.4 Selection of mtDNA

Whilst random distribution of mtDNA during division can result in discrepancies between generations, active selection for or against variants can also occur. This can be observed in the case of both human and murine mtDNA variant transmission to offspring. For example, the $tRNA^{Ala}$ mouse, a mouse model with a m.5024C>T variant, exhibited biased transmission of WT mtDNA in that the number of pups with a high level of pathogenic mtDNA was reduced compared to the number expected under neutral drift (Kauppila *et*

*al.*, 2016). This could reflect an incompatibility of cell viability at high mutation levels, consistent with the observation that pups with >80% ear tag heteroplasmy were not observed. Interestingly, analysis of mother-offspring pairs carrying the m.3243A>G variant in human mtDNA, identified positive selection of the pathogenic mtDNA at low heteroplasmy levels (<30%) which then switched to negative selection at high levels, suggesting that germline selection follows a bell curve (Franco *et al.*, 2022). Strong purifying germline selection has been observed in the germline of mice with ~30 mtDNA variants generated via POLG mutator mice cross breeding (Stewart *et al.*, 2008). Authors found low incidences of non-synonymous mutations and mutations occurring within the first and second codon positions of protein coding genes in offspring, a trend which is highly suggestive of purifying selection. This germline selection is consistent with that observed in human mtDNA data. There is strong negative selection of large, single deletions in the human germline; these are rarely transmitted to offspring (Chinnery *et al.*, 2004)

Selection is not isolated to the germline and has been observed in somatic tissues, perhaps the most well established being the loss of the pathogenic mtDNA variant m.3243A>G from mitotic tissues such as the blood and gut as individuals age (Rahman *et al.*, 2001, Pyle *et al.*, 2007, de Laat *et al.*, 2016, Grady *et al.*, 2018, Langdahl *et al.*, 2018). The literature surrounding m.3243A>G selection patterns will be discussed in more depth in section 3.1.1. Selection of mtDNA variants has also been observed for non-pathogenic variants. Using an engineered heteroplasmic mouse model which possessed mtDNA pertaining to that of NZB and C57BL/6N mice on a C57BL/6N nuclear background (Lechuga-Vieco *et al.*, 2020), Lechuga-Vieco and colleagues demonstrated tissue specific discrepancies in selection. This is a phenomenon which has been observed in other heteroplasmic murine models such as BALB/c x CAST/Ei (Battersby,Loredo-Osti and Shoubridge, 2003). Proliferative tissues such as the blood, spleen and thymus accumulated C57BL/6N mtDNA and quiescent tissues such as hepatic, renal and brain accumulated NZB mtDNA (Lechuga-Vieco *et al.*, 2020). Further investigation via environmental and pharmacological interventions, identified that segregation of haplotypes was likely a result of cell type specific OXPHOS reliance. NZB mtDNA promotes lipid metabolism, whereas C57 mtDNA promotes glucose utilization (Latorre-Pellicer *et al.*, 2019). A shift towards NZB was observed in hepatocytes and CD8+ T cells

upon proliferation. The authors demonstrated the negative impact of heteroplasmy and speculated that this selection was occurring intracellularly (Lechuga-Vieco *et al.*, 2020).

When discussing selection in somatic tissues, it is important to consider random drift and the potential of fixation at extremes of heteroplasmy. For example, a mouse model carrying a heteroplasmic mt-tRNA variant (m.5019A>G) appears to positively select for the variant in the brain and spleen with age. However, single cell data reveals a drift to either extreme (0 and 100%). Once cells reach a homoplasmic state of either mtDNA molecule, the proportion of the alternate mtDNA molecule cannot be increased as it is not present to amplify resulting in fixation, giving the illusion of selection (Glynos *et al.*, 2023).

There is much debate in the literature as to whether selection occurs at the genome (relaxed replication), cell (cell death) or organelle level. Selection at the organelle level may involve degradation of pathogenic mitochondria via mitophagy or in a more recently described process, the exchange of mitochondria between cells via tunnelling nanotubules (Needs *et al.*, 2024). Mitophagy is a form of autophagy which can result from both Ubiquitin-dependent or independent pathways. The most well established is the ubiquitin dependent PTEN induced putative kinase 1 (PINK1)-Parkin pathway. This process is induced by alterations to mitochondrial membrane potential which prevents passage of PINK1 through the IMM resulting in the accumulation of PINK1 on the OMM (Matsuda *et al.*, 2010). This accumulation activates Parkin, an E3-ubiquitin ligase which tags the mitochondria with ubiquitin and signals it for degradation via an autophagosome (Geisler *et al.*, 2010).

### 1.6 m.3243A>G

The m.3243A>G pathogenic mtDNA variant was first identified in 1990 in association with the mitochondrial encephalopathy, lactic acidosis and stoke like episodes (MELAS) phenotype and is the most common cause of adult mitochondrial disease (Goto,Nonaka and Horai, 1990, Gorman *et al.*, 2015). It is estimated that the carrier frequency is 140-150 per 100,000, but due to many individuals being asymptomatic, the disease prevalence is between 40-70x lower (Elliott *et al.*, 2008, Pickett *et al.*, 2018).

This pathogenic variant is located within the *MT-TL1* gene, which encodes mitochondrial tRNA$^{Leu(UUR)}$. Under healthy conditions, mt-tRNA$^{Leu(UUR)}$ facilitates leucine incorporation into mtDNA-encoded polypeptides during protein synthesis. A number of key post-transcriptional modifications are required to ensure the stabilisation of the clover leaf structure (**Figure 1.10**). Modifications at position 34 on the anticodon stem, also known as the wobble position, are important to mitochondrial tRNA molecules; in the case of tRNA$^{Leu(UUR)}$ a taurinomethylation (τm5U) at this site is crucial for facilitating its role in translation (Kirino *et al.*, 2005, Suzuki *et al.*, 2002).

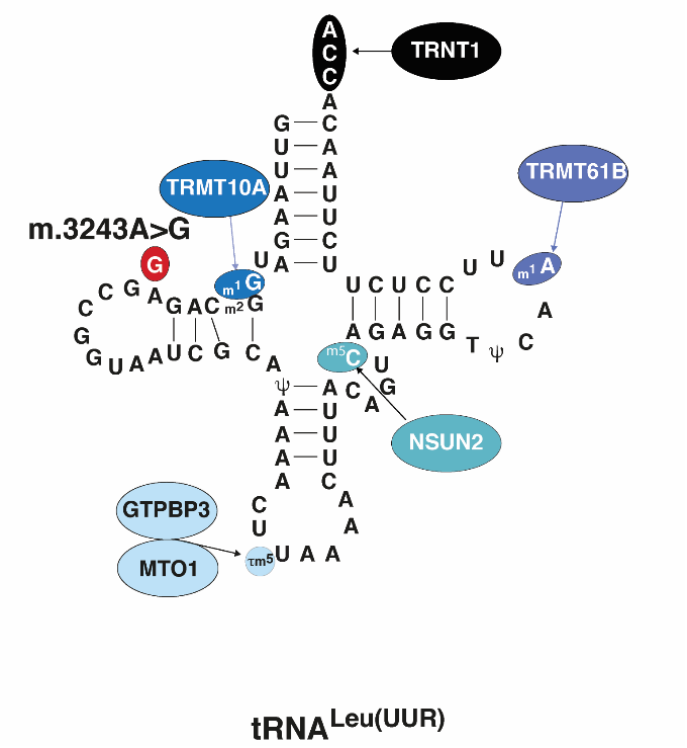


***Figure 1.10 The secondary structure of mt-tRNA$^{Leu(UUR)}$.*** *The m.3243A>G variant is highlighted in red at position 14 (dihydrouridine loop). Post transcriptional modifications and the enzymes responsible for these are highlighted. m1G = 1-methylguanosine, τm5U = 5-taurinomethyluridine, m5C = 5-methylcytidine, m1A = 1-methyladenosine. Figure taken from Richter et al. (2021)*

### 1.6.1 Molecular mechanism

The exact pathogenesis of m.3243A>G has not been confirmed, however the consensus is that the m.3243A>G point mutation has been found to impair mt-tRNA$^{Leu(UUR)}$ function inducing a mitochondrial translational defect (Hess *et al.*, 1991a). This defect negatively impacts the number of functional OXPHOS complexes inducing a respiratory deficiency and therefore m.3243A>G related disease. The severity of the respiratory defect varies across studies (Hess *et al.*, 1991a, King *et al.*, 1992, Janssen,Maassen and van den Ouweland, 1999, Chomyn *et al.*, 2000, Wittenhagen and Kelley, 2002). However, a consistent finding is the reduction in CI and CIV activities, which is perhaps unsurprising as these are the complexes with the highest number of mitochondrially encoded subunits (Chung *et al.*, 2021, Garrido-Maraver *et al.*, 2015, Yokota *et al.*, 2015). The oxygen consumption of patient fibroblasts worsens with increasing m.3243A>G level, but interestingly this is not always reflected in reduced ATP production (Yokota *et al.*, 2015, Chung *et al.*, 2021).

Some of the first investigations detail impairment of 16S transcription termination (Hess *et al.*, 1991b). As mentioned in section 1.3.3, transcription of mtDNA forms two transcripts, one of which terminates within the *MT-TL1* gene. Hess et al (1991) suggests that the smaller transcript encoding for just the rRNAs and 2 tRNAs is not formed due to m.3243A>G inhibiting termination factor binding. Only the full length polycistronic transcript was found, indicating a reduced rate of ribosome biogenesis in these cells. This claim was supported by reduced termination factor binding compared to WT. These conclusions were directly contradicted a year later in a study that utilised transmitochondrial cybrid cell lines with differing m.3243A>G levels. This revealed a similar reduced affinity for mTERF to m.3243A>G mtDNA compared to WT but this was not accompanied by a significant change in the steady-state level of the mt-rRNAs, indicating that a transcription defect was not being driven by a reduction in mitoribosome biogenesis (Chomyn *et al.*, 1992).

Other investigations imply the main driver of pathogenesis is the disruption to the taurine modification at the wobble position in mt-tRNA$^{Leu(UUR)}$. The first piece of evidence driving this theory was the discovery that mitochondrially encoded proteins in Epstein–Barr virus (EBV)- transformed B cells carrying 70% m.3243A>G showed decreased

leucine incorporation. When compared to controls, there were identical proportions of other amino acids such as phenylalanine, lysine and proline (Flierl,Reichmann and Seibel, 1997). Amino acid misincorporation was confirmed in further investigations using cybrids; Janssen and colleagues suggested that misincorporation reduced the stability of mitochondrial proteins and subjected them to increased degradation (Janssen,Maassen and van den Ouweland, 1999), thus explaining a translation defect with no real change in rate of protein synthesis. This altered function was speculated to be due to reduced stability driven by alterations to the secondary modification of the uridine at the first position of the anticodon of mt-tRNA$^{Leu(UUR)}$ (Yasukawa *et al.*, 2000, Kirino *et al.*, 2005) and possible alterations to the tertiary structure (Helm *et al.*, 1999, Chomyn *et al.*, 2000).

However, when attempting to corroborate this data by interrogating CIV mitochondrially encoded proteins for mis-incorporated amino acids, Janssen and colleagues found all proteins showed the correct sequence (Janssen *et al.*, 2007). This study focuses on CIV only and shows a clear difference in the impact of the variant on different CIV subunits, likely due to the number of UUR codons per polypeptide. Much of the research in this area, uses transmitochondrial cybrid cell lines. The process of transmitochondrial cybrid generation requires treating cell lines, usually cancer cell lines, with ethidium bromide to deplete mtDNA (Rho0) before fusion with an enucleated cell containing pathogenic mtDNA (King and Attardi, 1989). Not only are the cell lines used aneuploid and genetically unstable but treatment of cells with ethidium bromide can vastly alter the transcriptome, particularly the mitochondrial transcripts (Danielson *et al.*, 2005). Therefore, these cells are not always a reliable experimental model of m.3243A>G related dysfunction.

Investigations using immortalised patient myoblasts homoplasmic for m.3243A>G demonstrated a failure of complex I, VI and V assembly that could be partially rescued by the overexpression of elongation factors EFTu and EFG2. These investigations revealed a reduced rate of global protein synthesis (~70% of control) with specific polypeptides, ND5 and ND6, being disproportionately affected and residual enzyme activity ~6% of control levels. These data support amino acid mis-incorporation resulting in premature translation termination while also demonstrating an increased rate in translation of ATP6 and ATP8, leading authors to conclude that the m.3243A>G mutation induces both gain and loss of function consequences (Sasarman,Antonicka and Shoubridge, 2008).

Considering these investigations, it is likely that m.3243A>G induced disruption to the post transcriptional modifications causes the mt-tRNA to decode all UUX codons resulting in the misincorporation of amino acids into the polypeptide. Stable respiratory complexes fail to form leading to swift degradation of complexes and a biochemical defect. A summary of investigations into m.3243A>G pathogenesis can be found in **Table 1. 1**.

| *Author (Year)* | *Key Findings* | *Cell Model* |
|---|---|---|
| *Hess et al. 1991* | ▪ Impairment of 16S transcription termination, resulting in only full-length transcript.<br>▪ Reduced termination factor binding | Human KB cell |
| *Chomyn et al. 1992* | ▪ Reduced affinity for mTERF but no significant change in the steady-state level of the mt-rRNAs | Transmitochondrial cybrid cell line (143B & $p^0206$) |
| *Flierl et al. 1997* | ▪ Decreased leucine incorporation into mitochondrially encoded proteins than controls | EBV-transformed B-lymphoblastoid cell lines |
| *Janssen et al. 1999* | ▪ Translation defect with no decrease in rate of translation<br>▪ Amino acid misincorporation reduced the stability of mitochondrial proteins and subjected them to increased degradation. | Transmitochondrial cybrid cell line (143B & Bρ°-3 cells) |
| *Helm et al.1999* | ▪ Reduction in $m^2G10$ post-transcriptional modifications with m.3243A>G.<br>▪ Absence of methyl group can affect tRNA binding. | As in Chomyn *et al.* (1992) |
| *Chomyn et al. 2000* | ▪ Reduced methylation at A14 results in reduction in modifications at wobble base. | As in Chomyn *et al.* (1992) |
| *Park et al. 2003* | ▪ Reduced rate of protein translations due to 25-fold reduction in efficiency of aminoacylation of $tRNA^{Leu(UUR)}$<br>▪ Decreased steady state levels of $tRNA^{Leu(UUR)}$ | Transmitochondrial cybrid cell line (WS227) |
| *Kirino et al. 2004 & Kirino et al. 2005* | ▪ Deficiency in $\tau m^5U$ modification at wobble base results in UUG codon-specific translational defect<br>▪ A lack of this modification correlates with MELAS phenotype. | Purified tRNA from primary patient cells (fibroblast, placenta, liver, cardiac) |
| *Janssen et al. 2007* | ▪ Correct amino acid sequence in all CIV proteins. | Transmitochondrial cybrid cell line (143B) |
| *Sasarman et al. 2008* | ▪ Failure of complex I, IV and V assembly that could be partially rescued by the overexpression of elongation factors EFTu and EFG2.<br>▪ Evidence of amino acid misincorporation | Immortalised patient myoblasts |

***Table 1. 1 A summary of research into the molecular mechanisms behind m.3243A>G pathogenesis.***

### 1.6.2 Phenotypic presentation

As with many mitochondrial diseases, carriers of m.3243A>G present with a wide phenotypic spectrum affecting all tissues (**Figure 1.11**) (Nesbitt *et al.*, 2013). The most common phenotype combinations are segregated into syndromes; however, many patients do not present with symptoms complying to a syndrome, therefore these are being replaced with genetic diagnoses.

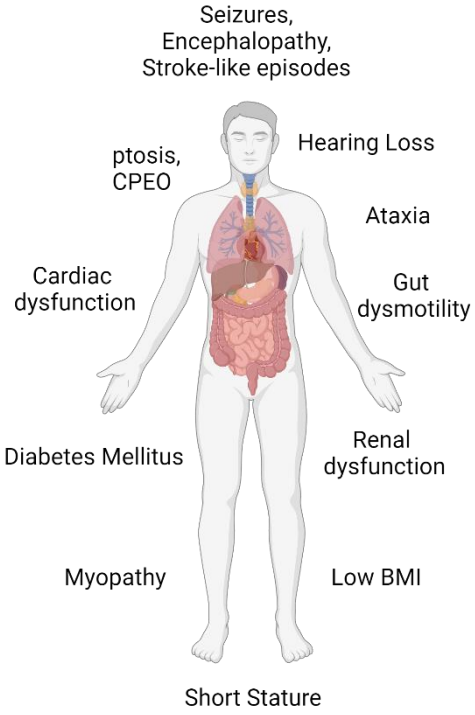


***Figure 1.11 Phenotypes associated with m.3243A>G.*** m.3243A>G related disease can affect a multitude of tissues simultaneously, with prevalence in the muscle and tissues of the nervous system. Figure generated using biorender.com.

For a long time, it was thought that phenotypes were induced when a threshold of OXPHOS deficiency (60-80% heteroplasmy) was surpassed (Karppa *et al.*, 2005, Petruzzella *et al.*, 1994), however, larger cohort studies have shown that the level of m.3243A>G in tissue does not explain the extent of variability in disease phenotype (Nesbitt *et al.*, 2013, Mancuso *et al.*, 2014, Grady *et al.*, 2018). The associated extensive range of clinical presentations makes disease prognosis difficult - currently the best predictor of disease progression is age-adjusted blood heteroplasmy (Grady *et al.*, 2018),

which is an estimation of whole blood m.3243A>G level at birth. This measurement is an estimation as in mitotic tissues, such as the blood, the proportion of mtDNA carrying m.3243A>G decreases with age (Sue *et al.*, 1998, Rahman *et al.*, 2001, Pyle *et al.*, 2007, Rajasimha,Chinnery and Samuels, 2008b, Grady *et al.*, 2018). However, even when taking age into account, m.3243A>G level only explains ~25% of the variation in disease burden. Therefore, a better indicator of disease progression is needed. There is evidence to suggest that the remainder of this variation can be partly-explained by the existence of nuclear modifiers; some phenotypes (psychiatric involvement, cognition, ataxia, migraine and hearing impairment) showed moderate to high heritability estimates in a pedigree-based study (Pickett *et al.*, 2018) and overexpression of mt-leucyl-tRNA synthetase alone can recover growth rates of m.3243A>G carrier cells cultured in galactose (Hornig-Do *et al.*, 2014).

m.3243A>G has not been found to reach homoplasmy in any tissue suggesting that, in vivo, the mitochondrial dysfunction induced is incompatible with tissue functionality; this is in contrast with other other pathogenic mtDNA variants, such as m.11778G>A, which can be found in a homoplasmic state (Yen *et al.*, 1999). Further to this, patients with low levels of m.3243A>G in postmitotic tissues as well as the blood can present with moderate disease symptoms, supporting the notion that the impact of this pathogenic variant on cell vitality is severe (de Laat *et al.*, 2016). Research using cultured cells with a near homoplasmic state of m.3243A>G offer mixed results; some suggest a replicative advantage at high levels, however, this may be confounded by high levels of glucose within culture media, allowing cells to bypass OXPHOS altogether (Yoneda *et al.*, 1992). Culturing of induced pluripotent stem cells (iPSCs) carrying high m.3243A>G levels demonstrates dysfunction in the form of a reduced oxidative reserve; prolonged passaging of the cells decreased the m.3243A>G level within these cells (Folmes *et al.*, 2013), providing evidence to link the decline in level of this variant to mitochondrial/cell division and selection against it.

There is currently no effective treatment for m.3243A>G-related disease; current treatment strategies focus on improving quality of life by controlling individual disease phenotypes, for example: insulin administration in the case of diabetes mellitus; organ transplants in the case of kidney disease; pain management and appropriate physiotherapy routes in the case of myopathy. The unique decline in m.3243A>G level in the blood

tissue with age is an underexplored area and understanding this process could enable the development of therapeutic strategies targeted at decreasing pathogenic mtDNA levels.

## 1.7 The blood

This thesis will explore the impact of m.3243A>G on haematopoietic cells; to do this, it is first important to understand the functions of these cells, their origins and their metabolism.

The blood is a vastly complex tissue with multiple functions, one of which is the identification and eradication of pathogens. It can be segmented into three distinct lineages: lymphoid cells, myeloid cells and erythroid cells, all derived from haematopoietic stem cells (HSC) in the bone marrow. The HSC is a well-characterised multipotent stem cell, first investigated in 1945 upon the discovery that radiation exposure led to immunological disorders. Its status as a stem cell was revealed in 1956, when lethally irradiated mice recovered following injection with donor bone marrow, supplementing the immune tissues with donor cells (Ford *et al.*, 1956, Nowell *et al.*, 1956). These findings were confirmed in later investigations which observed colonies containing cell types of myeloid origin arise in response to injection of donor marrow into lethally irradiated mice; the presence of a unique translocation allowed them to determine that these were all derived from the same progenitor cell (Siminovitch,McCulloch and Till, 1963). Although the bone marrow is the primary HSC location, they can also be found in the umbilical cord and more sparsely in peripheral blood (Broxmeyer *et al.*, 1989). It is rare that high levels of immature blood cells can be found in the peripheral blood and is often an indication of disease.

### 1.7.1 Adult haematopoiesis

HSCs preserve DNA integrity by infrequent, asymmetric replication into another stem cell and a daughter multipotent progenitor cell (MPP). MPP replicate more readily and are able to give rise to further progenitor cells: the lymphoid primed multipotent progenitors (LMPP), common myeloid progenitors (CMPs), common lymphoid progenitors (CLPs),

granulocyte–macrophage progenitors (GMPs) and megakaryocyte erythroid progenitors (MEP). LMPP and CMP are able to give rise to common lymphoid progenitors, granulocyte–macrophage progenitors and megakaryocyte erythroid progenitors which form 3 distinct lineages: the lymphoid lineage, the myeloid lineage and the erythroid lineage (**Figure 1.12**). This is a traditional view of blood tissue development and recent advances have suggested a more plastic differentiation process than a strict hierarchy.

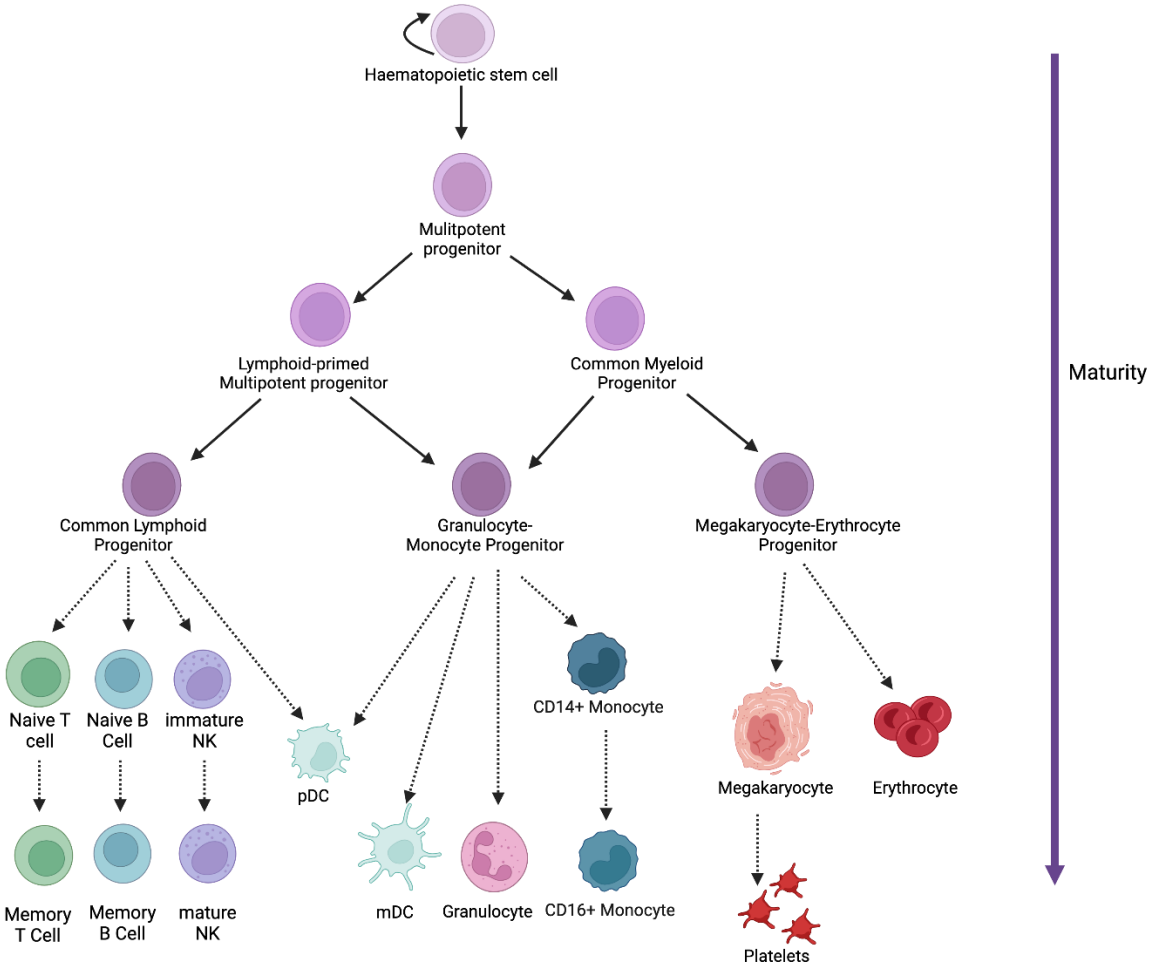


***Figure 1.12 Blood cell differentiation hierarchy.*** *All cells of the blood are derived from the haematopoietic stem cells (HSCs), which gives rise to multipotent progenitors (MPP) able to differentiate into lymphoid primed multipotent progenitors (LMPP) common myeloid progenitors (CMPs), common lymphoid progenitors (CLPs), granulocyte–macrophage progenitors (GMPs) and megakaryocyte erythroid progenitors (MEP). CLP are committed to the lymphoid lineage and are able to give rise to T, B, natural killer (NK) and plasmacytoid dendritic cells (pDC). GMPs give rise to cells of the myeloid lineage including myeloid dendritic cells (mDC), monocytes and granulocytes (basophil, eosinophil, and neutrophils). MEP differentiate into cells of the erythroid lineage such as megakaryocytes which are platelet precursors and erythrocytes.*

Long term HSC are largely quiescent and reside in a hypoxic environment, therefore, they are heavily dependent on anaerobic glycolysis for ATP production (Takubo *et al.*, 2010). This is thought to be protective as a reduction of OXPHOS activity limits the production of ROS and therefore limits the likelihood of cellular damage (Ito *et al.*, 2006, Mantel *et al.*, 2015). The primary metabolic source switches immediately upon differentiation to MPP when the vast majority of ATP is generated in the mitochondria via OXPHOS (Takubo *et al.*, 2013). Although glycolysis is the metabolic driver in HSC, OXPHOS function still plays a role in HSC maintenance, for example, high mitochondrial membrane potential inhibits reconstitution in mice (Sukumar *et al.*, 2016) and loss of CIII activity impairs differentiation (Ansó *et al.*, 2017).

The aforementioned progenitor cells and HSCs express a common extracellular marker: CD34, which allows for identification and isolation of immature cells from the marrow and peripheral blood. CD34 is a transmembrane phosphoglycoprotein with a poorly characterised function but it has been suggested that it enables binding to vascular beds via E and P-selection (AbuSamra *et al.*, 2017). Expression of this marker is lost as cells reach terminal differentiation.

## 1.8 Myeloid Lineage

Myeloid cells are the most abundant immune cells and are components of the innate immune system. Cells of the innate immune system are able to recognise pathogens via pattern recognition receptors (PRR) on the cell surface which bind pathogen/microbe associated molecular patterns (PAMPs/MAMPs) or damage associated molecular patterns (DAMPs). PAMPs are highly conserved molecular motifs shared across many pathogens but absent from the host, therefore PRRs have a broad spectrum. Examples of PAMPs include bacterial membrane components such as lipopolysaccharides (LPS) or cell wall components (Medzhitov and Janeway, 1997). PRRs were first described by Janeway and can be divided into three categories: cytoplasmic, secreted or transmembrane (Janeway, 1989). Although activation via structural components is the most well-characterised innate immune response, innate immune cells can also respond to the absence of self-signals from cells and pathogen virulence factors such as toxins (Remick,Gaidt and Vance, 2023). DAMPs include heat shock proteins, mtDNA and cell death signals.

Sensing of these often triggers an inflammasome response, inflammasomes are made up of a cytosolic PRR such as NLRP3, an adaptor molecule (e.g. apoptosis-associated speck-like protein containing a caspase recruitment domain/ASD) and caspase 1. The formation of an inflammasome induces the formation of the mature cytokine IL-1β (Cassel and Sutterwala, 2010). The IL-1 family of cytokines are master regulators of inflammation, they have the ability to act on lymphocytes by inducing inflammatory cytokine production by CD8+ T cells and Natural killer (NK) cells and macrophages (Garlanda,Dinarello and Mantovani, 2013). In recent years the release of mtRNA has been implicated as immunostimulatory (Dhir *et al.*, 2018). Accumulation of double stranded mtRNA occurred following pharmacological inhibition of fumarate hydratase (FH) in bone marrow derived macrophages (Hooftman *et al.*, 2023). This release induced a strong IFN type I response. A summary of myeloid cell properties and functions can be found in **Table 1. 2**.

| Cell type | Family | Function | Metabolism | Turnover | Reference |
|---|---|---|---|---|---|
| **CD14+ Monocyte** | Monocyte (Classical) | Anti-bacterial responses. Produce IL-6, IL-8, CCL2, CCL3 in response to LPS. Phagocytosis. Immature state. | Glycolytic + Pentose phosphate pathway metabolism. | 24hr in circulation | (Cros *et al.*, 2010, Schmidl *et al.*, 2014, Patel *et al.*, 2017, Williams *et al.*, 2023) |
| **CD16+ Monocyte** | Monocyte (Non-classical) | Anti-viral response. Produce TNFα IL-1β, CCL3 in response to LPS. Antigen presentation. Mature state. | OXPHOS metabolism. | 7.4 days in circulation | |
| **CD11c+ DC** | DC | Antigen presenting cell. Express MHC molecules, important in coordination of T cell response. | Quiescent state maintained by TCA cycle + OXPHOS. Glycolytic upon activation | ~3 days (mouse spleen) | (Kamath *et al.*, 2002, Wu *et al.*, 2023) |
| **pDC (CD123+)** | DC | Type I IFN response to virus mediated via TLR7 and TLR9 activation. APC | TLR7 stimulation = glycolytic TLR9 stimulation = FAO + OXPHOS | | (Ye *et al.*, 2020, Wu *et al.*, 2016, Bajwa *et al.*, 2016) |
| **Neutrophil** | Granulocyte | Pathogen killing via: Phagocytosis, respiratory burst, formation of neutrophil extracellular traps (NETs) & cytotoxic granule release. | Glycolysis – NETosis, phagocytosis OXPHOS – differentiation and ROS production | Reports of a half-life of 7 hours - 3.95 days | (Athens *et al.*, 1961, Pillay *et al.*, 2010, Kumar and Dikshit, 2019) |
| **Eosinophil** | Granulocyte | Anti-parasitic response. Release MBP, ECP, EDN and EPO cytotoxic proteins | OXPHOS | 24 hours in circulation | (Farahi *et al.*, 2012, Porter *et al.*, 2018) |
| **Basophil** | Granulocyte | Anti-parasitic response/Allergic response. Release histamine upon activation. | Glycolysis & possibly OXPHOS | 1-2 days | (Ohnmacht and Voehringer, 2009, Sumbayev *et al.*, 2009) |

***Table 1. 2 Functions of Myeloid cells.*** *DC = dendritic cell, pDC = plasmacytoid dendritic cell*

## 1.9 Lymphoid Lineage

The lymphoid lineage consists of the B and T cells, known as lymphocytes, and a number of innate lymphoid cells including NK cells and some plasmacytoid dendritic cells (**Table 1. 2**). NK cells are active in the innate immune response but originated from the CLP and, as a consequence, have a slower turnover compared to their myeloid counterparts (~13.5days) (Lutz *et al.*, 2011). NK cells can exist in the peripheral blood in an immature (CD56++CD16-) or a mature state (CD56+CD16++). Mature NK cells make up ~90% of the peripheral NK population. In their activated form, these cells release lysosomes containing perforin and cytotoxic granzymes which induce the death of infected cells. Immature NKs release IFNγ, TNF-β, IL-10, IL-13 and GM-CSF in response to cytokine stimulation and receptor ligation; these cells can be cytotoxic but need increased priming compared to mature NKs (O'Brien and Finlay, 2019). Resting NK cells are quiescent and have low rates of both OXPHOS and glycolysis, upon activation these rates increase significantly utilising aerobic glycolysis for ATP generation (Keating *et al.*, 2016).

### 1.9.1 T cells

T cells are involved in the adaptive immune response. These cells are CD3+ and make up 15-30% of all leukocytes. Conventional T cells can be functionally segregated depending on their ability to recognise major histocompatibility complex (MHC) molecules on antigen presenting cells (APCs). CD8+ T cells can recognise MHC type I and CD4+ T cells are capable of recognising MHC type II. CD4+ T cells, also known as T helper cells, coordinate the T cell response via interactions with other immune cell types. CD8+ cytotoxic T cells directly kill pathogens and infected cells. CD4+ T cells can be further divided into functionally distinct groups (**Table 1. 3**).

| CD4+ Cell type | Function | Cytokine production |
|---|---|---|
| **Th1** | Intracellular pathogen response via CD8+ T cell macrophage activity | IFNγ |
| **Th17** | Extracellular bacteria/fungi response via neutrophil activity | IL-17 |
| **Th2** | Extracellular parasite response via Basophil and eosinophil activity | IL-4, IL-5, IL-13 |
| **$T_{FH}$** | B cell response | IL-21 |
| **Treg** | Immunomodulatory response requiring TCR and IL-2 signalling via CD25. | IL-10, TGFβ |

***Table 1. 3 CD4+ T cell types.****(Plitas and Rudensky, 2016, Künzli and Masopust, 2023)*

#### 1.9.1.1 T cell development

Early T cell progenitors migrate from the bone marrow to the thymus, where they differentiate into double negative 2(DN2; CD4-CD8-) thymocytes (CD25+CD44+) (**Figure 1.13**). Proliferation and downregulation of CD44 represents differentiation into DN3 thymocytes (CD25+CD44-) which undergo T cell receptor (TCR) rearrangement before expressing αβ or γδ TCRs. At the DN3 stage, thymocytes commit to the T cell lineage and lose B cell potential (Heinzel *et al.*, 2007). Within the genes encoding the TCR are a series of variable (V), diversity (D) and join (J) regions which form VDJ segments. TCR rearrangement involves recombination of these genes within the V, D and J regions to generate a diverse pool of TCRs. Failure to produce a functional β chain prevents cells from progressing to α chain rearrangement; this is known as β selection. Upon completion of this process, thymocytes progress to DN4 (CD25-CD44-) and undergo high levels of proliferation before differentiation into a double positive (CD4+CD8+) state. DN1 and DN2 thymocytes are maintained in a quiescent state via a primarily OXPHOS driven metabolism regulated via AMPK signalling before a switch to highly glycolytic at DN4 facilitating high levels of proliferation (**Figure 1.13**) (Cao *et al.*, 2010, Chapman,Boothby and Chi, 2020).

Double positive (DP) thymocytes undergo α chain rearrangement and are then subject to a rigorous central tolerance process in the thymic cortex (Kisielow *et al.*, 1988). Central

tolerance consists of both positive and negative selection which just ~3% of all DP thymocytes survive (Goldrath and Bevan, 1999). During this process DP thymocytes interact with self-antigens presented by thymic stromal cell and dendritic cell MHC (Bousso *et al.*, 2002). The strength of this interaction dictates the thymocyte survival: low avidity binding induces survival signals and progression to a single positive (SP) state, high avidity reactions induce apoptosis, eliminating the risk of self-reactive T cells. SP cells mature in the thymic medulla before being released from the thymus as naïve T cells.

Following β selection, thymocytes undergo robust proliferation enabled by transitioning to an aerobic glycolytic metabolism facilitated by mTORC1, a crucial regulator of anabolism, before returning to quiescence at the DP and SP stage. Appropriate switches in metabolism are important in cell development, for example, alterations in mTOR signalling via the deletion of RAPTOR prevented αβ progression to DP stage and encouraged differentiation to γδ T cells (Yang *et al.*, 2018).

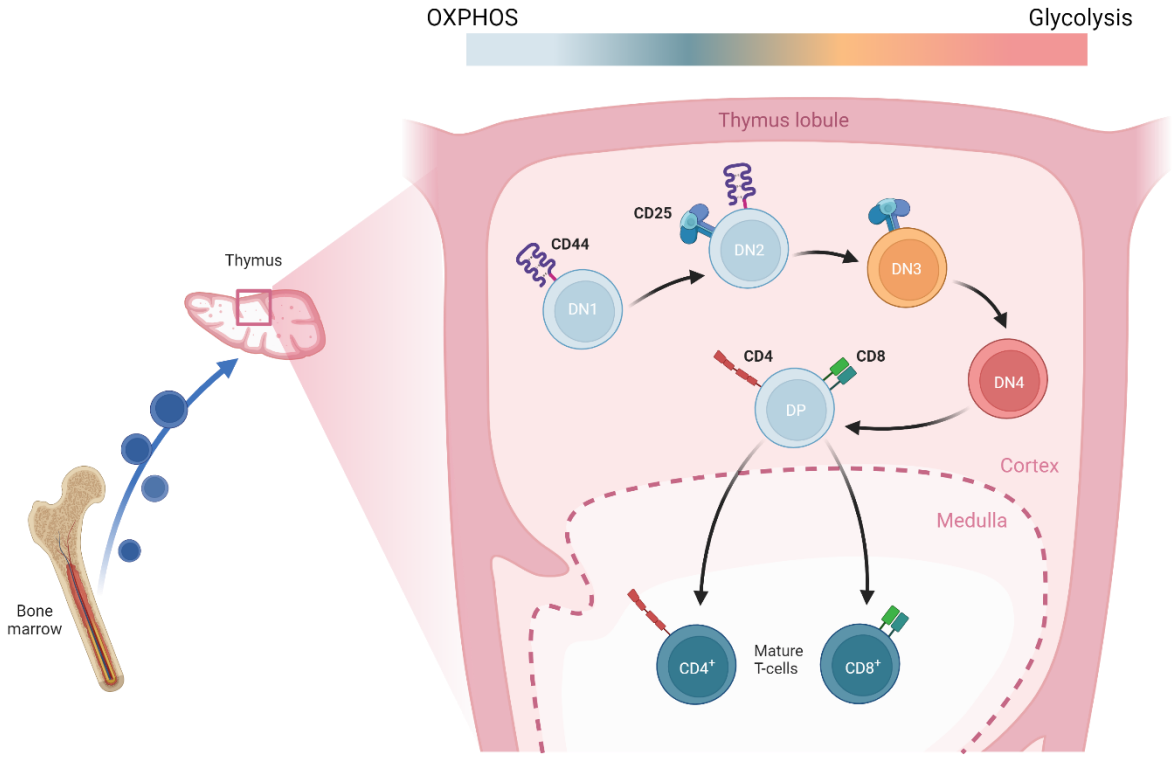


***Figure 1.13 $T_{Naive}$ cell development in the thymus.*** *Early thymic progenitors (DN1) migrate from the bone marrow into the thymus, these then commit to the T cell lineage upon differentiation to DN2. β selection occurs at DN3 stage, this is characterised by the rearrangement of T cell receptor (TCR) genes, those without a functional β cell receptor do not progress to the next cell stage. DN3 and DN4 thymocytes undergo mass proliferation enabled by a switch from a quiescent OXPHOS maintained state to a glycolytic metabolism. After development of a mature TCR a double positive cell undergoes central tolerance in which highly self-reactive and unreactive cells undergo programmed cell death and those with competent reactivity mature to single positive $T_{naive}$ cells. Cells are coloured according to cells preferred metabolism. Adapted from biorender template.*

Interestingly, the thymus does not continue to produce new naïve T cells throughout an individual's lifetime and undergoes involution, marked by the loss of functional thymic tissue and replacement with adipose tissue. This process begins at just 1 year of age and occurs extensively after 15 years of age (Steinmann,Klaus and Mullerhermelink, 1985). This coincides with an observed decrease in TCR repertoire diversity as the naïve T cell

pool replenishment decreases drastically resulting in supplementation of the T cell pool with memory T cells (Fagnoni *et al.*, 2000, Naylor *et al.*, 2005). Entry of progenitor cells into the thymus is not continuous and is theorised to be periodic, with a large number of cells arising from very few progenitors. Such a restricted window for naïve cell production is isolated to the T cell lineage. The closest relative of T cells, the B cell is continuously replenished throughout life, however, a decline in B cell number has also been observed with age, although, less substantial (Ademokun,Wu and Dunn-Walters, 2010).

#### 1.9.1.2 T cell activation and memory

Naïve T cells ($T_{naive}$) exist in a quiescent state, metabolically reliant on ATP generation via OXPHOS. This quiescent state is maintained via tonic TCR and IL-7 signalling facilitating OXPHOS (Fox,Hammerman and Thompson, 2005, Jacobs,Michalek and Rathmell, 2010). These cells persist for up to 10 years in humans, enabled by slow homeostatic proliferation every ~154 days (Vrisekoop *et al.*, 2008, Macallan *et al.*, 2003). Extracellular expression of CCR7, a lymphocyte-specific G-protein-coupled receptor, allows $T_{naive}$ cells to patrol the secondary lymphoid organs as well as the peripheral blood (Randolph *et al.*, 1999). In both naïve and memory states, T cells are capable of self-renewal meaning that they typically have a longer lifespan than mature myeloid cells which have a high turnover (**Table 1. 2**). Self-renewal capabilities of a T cell are correlated to CCR7 expression. CD4+ $T_{naive}$ mitochondria are enriched for one-carbon metabolism (Ron-Harel *et al.*, 2016), whereas CD8+ rely heavily on OXPHOS, although their mitochondrial activity is low (Cao,Rathmell and Macintyre, 2014).

Binding of a cognate antigen to the TCR, coupled with CD28 co-stimulation, triggers a switch to a glycolytic metabolism, known as the Warburg shift (Xu *et al.*, 2021). This switch is crucial for the clonal proliferation of an activated T cell as an anabolic metabolism facilitates the production of metabolic intermediates required for rapid proliferation. TCR signalling involves engagement of the PI3K/Akt/mTORCI axis which activates hypoxia-inducible factor α (HIF-α), a well-known driver of glycolytic metabolism. Increased glucose uptake, amino acid uptake and pentose phosphate pathway activity, which is required for de novo nucleotide synthesis and therefore DNA synthesis, are hallmarks of transition into an effector T cell ($T_{eff}$) state. mTOR activity is controlled

by leucine availability and therefore so is T cell activation (Schriever *et al.*, 2013). Deletion of *S*lc7a5, a transporter for large amino acids such as leucine, in murine T cells showed impaired T subset formation (Sinclair *et al.*, 2013). In this model, Th17 and Th1 subsets failed to form but Tregs formed effectively; CD8+ $T_{eff}$ cell formation was also impaired. This was found to be due to an inability to sustain c-myc signalling, which induces glucose and glutamine uptake into the T cell upon activation for mTORC1-driven metabolic reprogramming. Glycolytic, proliferating $T_{eff}$ have a vastly fragmented network in contrast to their naïve quiescent OXPHOS fuelled state, which shows a fused, elongated network (Buck *et al.*, 2016). Upon exit from its naïve, quiescent state, a T cell undergoes asymmetric cell division to generate an effector cell and a cell primed for memory T cell formation (Verbist *et al.*, 2016, Pollizzi *et al.*, 2016).

A second tolerance mechanism, peripheral tolerance acts at the point of activation to further limit the incidence of self-reactive $T_{eff}$. There are six mechanisms of peripheral tolerance: quiescence, ignorance, anergy, exhaustion, senescence and death (ElTanbouly and Noelle, 2021), all of which work to inhibit the activity of or induce death in autoreactive T cells. Ignorance and anergy are the primary peripheral tolerance mechanisms in naïve T cells; these mechanisms ensure that a high TCR affinity or high antigen concentration is required to illicit a response. Anergy describes a response to TCR stimulation in the absence of co-stimulation which results in a defect in RAS-mitogen activated protein kinase (MAPK) signalling and establishment of an anergic state in which IL-2 is suppressed (Fields,Gajewski and Fitch, 1996, Li *et al.*, 1996). In both quiescent and anergic states mTORC1 activity is suppressed preventing proliferation (Zheng *et al.*, 2007). The lack of co-stimulation can also induce cell death, the exact conditions which induce cell death over anergy have yet to be characterised. Cell death and exhaustion are the primary peripheral tolerance mechanisms in memory cells. Exhaustion is encountered during persistent antigen stimulation and describes a T cell which has decreased cytokine production, high levels of inhibitory receptors such as PD-1 and the inability to transition into a quiescent state (Gallimore *et al.*, 1998, Blackburn *et al.*, 2009, Wherry, 2011).

Although $T_{eff}$ cells are highly reliant on glycolysis for protein synthesis, OXPHOS is still required for activation, as demonstrated by activation defects induced by inhibition of CI and CIV (Yi *et al.*, 2006a, Tarasenko *et al.*, 2017a, Bailis *et al.*, 2019, Vardhana *et al.*, 2020a). This may be related to the reliance of T cell differentiation on ROS signalling.

CIII deficient T cells show reduced activation of the transcription factor nuclear factor of activated T cells (NFAT) (Sena *et al.*, 2013). As CIII is one of the largest producers of mitochondrial ROS, authors speculated ROS may be responsible and provided cells with exogenous $H_2O_2$ leading to NFAT activation and proliferative recovery. There is evidence to suggest that mTOR signalling, and therefore a glycolytic state, is dependent on ROS. ROS scavenging inhibited CD4+ T cell proliferation by inhibiting mTOR signalling (Previte *et al.*, 2017). NF-κB activation, a downstream target of mTOR signalling can be blocked via antioxidant treatment (Schreck,Rieber and Baeuerle, 1991). It is important to note that only a small level of ROS optimal for these reactions and high levels or chronic exposure can have opposing effects (Flescher *et al.*, 1994).

Memory cell subsets persist after the clearance of a pathogen and contraction of the clonally expanded effector cells (DeWitt *et al.*, 2015, Wieten *et al.*, 2016). Upon reinfection, these cells generate a fast and effective adaptive defence. Two memory cell subsets key in defence against reinfection are the central memory T cells ($T_{CM}$) and the effector memory T cells ($T_{EM}$). $T_{CM}$ are long-lived memory cells which possess lymphoid homing markers such as CCR7 which allows them, like naïve T cells, to populate the secondary lymphoid organs. $T_{EM}$ cells lack these markers and remain in the peripheral blood and more rarely in tissue (Sallusto *et al.*, 1999). Upon reinfection, $T_{EM}$ have a powerful effector function, but low proliferative potential and shorter lifespan, therefore, would act to contain the response immediately allowing for $T_{CM}$ cells to undergo rapid proliferation and generate a sufficient response.

Epigenetic analysis of T cell subsets of varying maturity (naïve, $T_{CM}$ and $T_{EM}$) revealed a progressive loss of gene methylation from naïve T to $T_{CM}$ to $T_{EM}$, suggesting that $T_{EM}$ are the most mature of the two (**Figure 1.14**). This was found to be the case in both CD8+ and CD4+ T-cells (Durek *et al.*, 2016, Abdelsamed *et al.*, 2017). However, it is unclear where T effector memory cells re-expressing naïve marker CD45RA ($T_{EMRA}$) cells sit in this differentiation pathway. These cells have the lowest level of methylation and low proliferative capacity which has led to the assumption that they are a terminally differentiated effector memory cells (Sallusto *et al.*, 1999). $T_{EM}$ and $T_{EMRA}$ have the highest propensity for cytokine production. The majority of $T_{EMRA}$ cells are CD8+; they are scarce in the CD4+ population. CD4+ $T_{EMRA}$ cells persist in individuals who have contracted viral infections such as dengue virus and human cytomegalovirus (Libri *et al.*, 2011, Weiskopf *et al.*, 2015), suggesting that these cells play vital roles in chronic viral

infection. Due to the ability of each memory cell to differentiate into an effector cell, it is likely that the differentiation of T cells is more fluid that the traditional linear model of T cell differentiation.

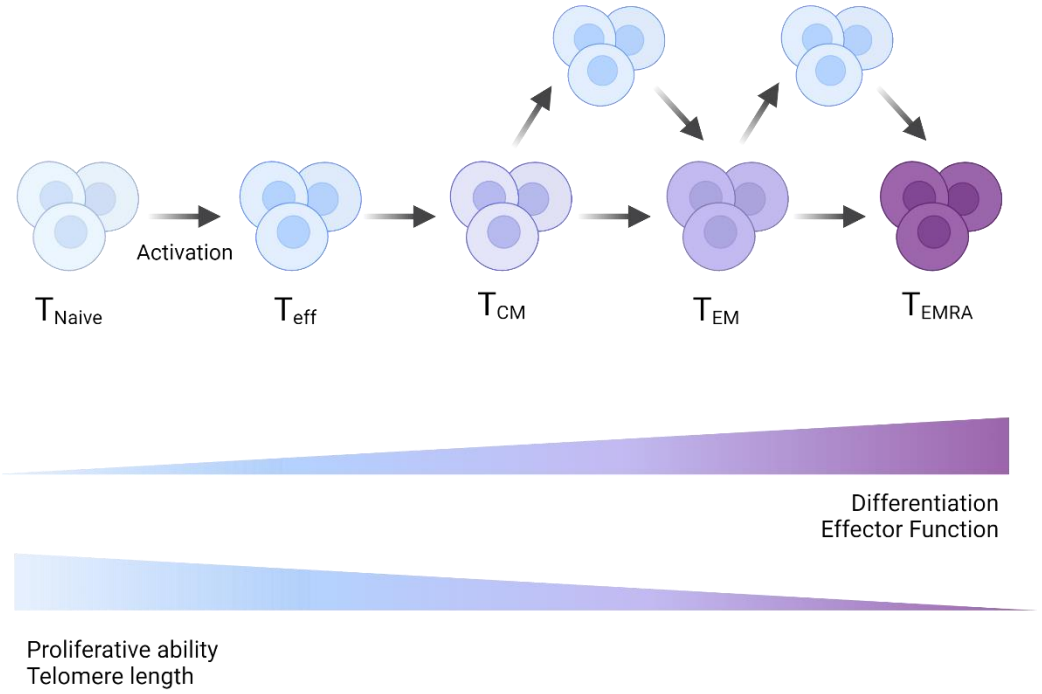


***Figure 1.14 Linear model of T memory cell differentiation.*** *$T_{Naive}$ cells differentiate into effector T cells ($T_{eff}$) upon antigen stimulation. $T_{eff}$ undergo mass clonal expansion to combat pathogen before retraction upon eradication of foreign antigens, after retraction, T memory cells remain, patrolling the peripheral blood and lymph tissues. T memory cells can be subdivided according to extracellular protein expression $T_{CM}$ (CD45RA-CD45RO+CD27+CCR7+), $T_{EM}$ (CD45RA-CD45RO+CD27-CCR7-), $T_{EMRA}$ (CD45RA+CD45RO-CD27-CCR7-). According to effector function and proliferative ability, $T_{CM}$ are considered the least differentiated and $T_{EMRA}$ cells the most terminally differentiated with $T_{EM}$ being intermediate according to the proposed linear hierarchy of memory T cell differentiation.*

Each memory T cell state is maintained by slight adjustments in the OXPHOS/glycolysis flux (**Figure 1.15**). While both are largely dependent on OXPHOS, $T_{EM}$ cells utilise glycolysis more than $T_{CM}$ (Ecker *et al.*, 2018). Both mechanisms are fuelled via fatty acid oxidation. $T_{EM}$ are dependent on the uptake of external fatty acids, whereas $T_{CM}$ take up glucose to form fatty acids which are subsequently broken down (Corrado and Pearce, 2022). CD28 costimulation during activation is vital for the formation of memory T cells

(Geltink *et al.*, 2017). CD28 signalling promotes expression of carnitine palmitoyltransferase 1a (Cpt1a), an enzyme which facilitates FAO. Reactivation of cells activated while cpt1a expression was inhibited resulted in failure to response to secondary antigen exposure. The authors also found CD28 signals were important in cristae integrity, which in turn enhanced spare respiratory capacity after stimulation resulting in competent memory cell formation.

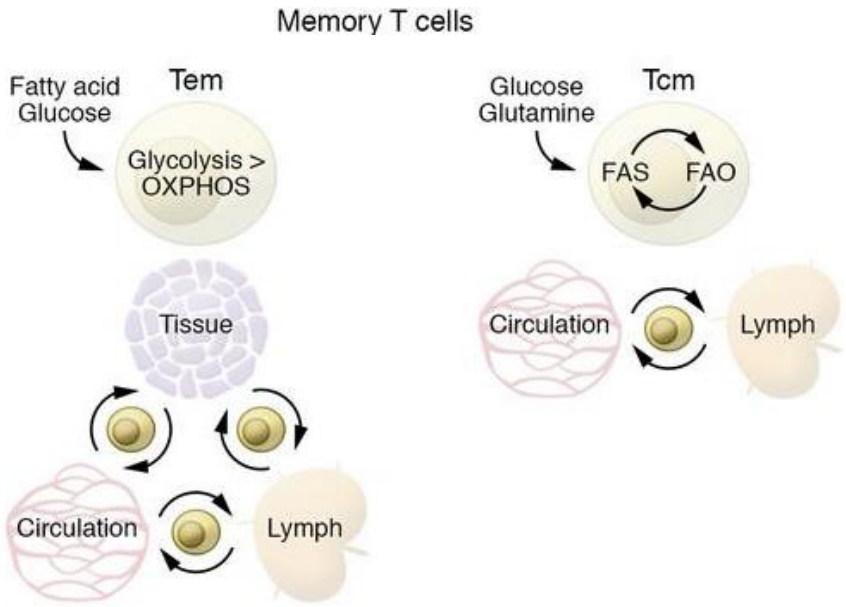


***Figure 1.15 Differing metabolism in T memory cell subsets.*** *T effector memory ($T_{EM}$) cells are slightly more glycolytic than central memory T cells ($T_{CM}$), likely related to their increased capacity to return to an effector state. Figure adapted from (Corrado and Pearce, 2022).*

Two replicative bottlenecks occur during T cell development (**Figure 1.16**). Depending on infection history, a memory T cell will have undergone at least two episodes of clonal proliferation to reach the memory state. The first occurs in the thymus at the DN3/DN4 stage and the second takes place in the secondary lymphoid tissues in response to antigen. Both events coincide with a metabolic shift from highly glycolytic metabolism to one governed by OXPHOS.

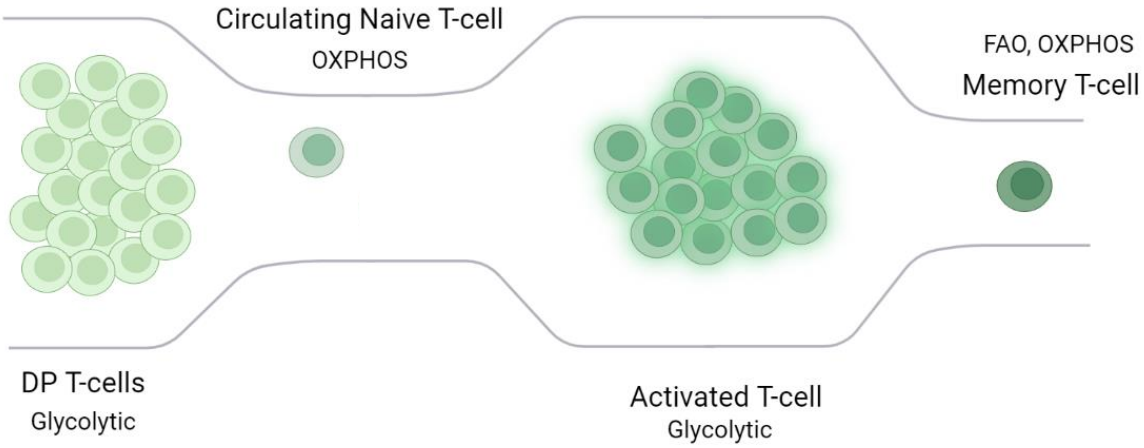


***Figure 1.16 Bottlenecks during T cell development.*** *Thymocytes undergo mass proliferation before central tolerance in the thymus; few cells (~3%) survive this selection process and exit the thymus as naïve T cells, thus generating the first bottleneck in T cell development. Stimulation with a cognate antigen results in clonal proliferation of an antigen specific T cell, exponentially increasing T cell number. Clearance of the pathogen is followed by retraction leaving only a small subset of memory T cells: the second bottle neck. Grey lines signify the changes in population size at each stage.*

### 1.9.2 B cells

B cells are responsible for the humoral immune response; this is characterised by the production of antibodies by terminally differentiated plasma cells. Like the myeloid cells, B cell development takes place in the bone marrow before release to the periphery as an immature B cell. During this development immunoglobulin gene rearrangement occurs to form a functional B cell receptor (BCR), in a process similar to TCR gene rearrangement, generating a diverse immunoglobulin repertoire. Again, similar to the T cell development process, B cells undergo a tolerance process to eliminate self-reactive clones and cells with a dysfunctional BCR. However, rather than an immediate apoptotic response, B cells can be rescued via receptor editing (Retter and Nemazee, 1998). This process allows rearrangement of the immunoglobulin light chain, typically the V-J regions until a functional BCR is generated. This suggests that B cell death during the central tolerance process is on a smaller scale than T cells.

Naïve B cells exist in an OXPHOS-maintained quiescent state and can become activated through either T cell dependent or independent mechanisms. All signals begin with antigen binding to the BCR, resulting in localised IgM clustering on the cell surface; a second signal is required to activate the B cell. Most antigen responses supply this second signal through a T cell dependent response. Upon binding the BCR, an antigen is endocytosed and presented extracellularly via an MHC class II molecule; antigen primed helper T cells bind this and CD40 to generate the additional signalling required for B cell activation (Chesnut and Grey, 1981), without a second signal the partially activated B cell will undergo apoptosis (Akkaya *et al.*, 2018).

Activation of B cells in this way triggers the formation of short-lived plasma cells with low binding affinity and recruitment of activated B cells to the secondary lymph organs and the formation of germinal centres (GCs) (Kaji *et al.*, 2012, Taylor,Pape and Jenkins, 2012). Within GCs, B cells undergo antigen specific clonal expansion, facilitated by an increase in glycolysis, somatic hypermutation and class switch recombination, to generate higher affinity BCR binding (Jellusova *et al.*, 2017). Somatic hypermutation and class switch recombination involve the introduction of mutations into the BCR heavy chain via activation induced cytidine deaminase (AID) which converts cytosine bases to uracil bases, triggering removal via repair pathways and the induction of mutations (Stavnezer and Schrader, 2014). These alterations enable a robust response with less cell death compared to processes that rely on apoptosis. From here, cells with the highest affinity expand and clones with the lowest affinity contract (Victora and Nussenzweig, 2022). Current theories for the development of GC-dependent memory cells are that the B cells with lower affinity either undergo apoptosis or exit the GC as a memory cell and those with the highest affinity differentiate into plasma cells (Viant *et al.*, 2020, Inoue and Kurosaki, 2024); therefore, memory B cells are likely to have undergone fewer replicative episodes than plasma cells.

Long-lived plasma cells migrate to the bone marrow where they persist, continuously secreting antibodies. These cells are not replenished and can persist for decades, as demonstrated by prolonged antibody titres years from vaccination. It has been postulated that this is due to fine-tuning of survival factors within these cells (Hammarlund *et al.*, 2017, Simons and Karin, 2024). Interestingly, plasma cells can persist in the absence of memory B cells (Slifka *et al.*, 1998). As with the T cell response, after retraction of the B

cell response, antigen specific B memory cells remain for decades and have the capability of quickly activating upon reinfection.

## 1.10 Aims and objectives.

The decline of m.3243A>G level in blood with age is a well-characterised phenomenon, first documented 26 years ago (Sue *et al.*, 1998). However, the drivers and mechanism behind this are relatively unexplored. Deeper understanding of this decline has the potential to drive research into immune competence in individuals with mitochondrial disease, research into therapeutics to decrease levels of pathogenic mtDNA and delineate metabolic pathways driving immune cell function, which will aid in cancer and autoimmune therapeutics.

The overarching aim of this thesis is to investigate the mechanism behind negative selection of m.3243A>G. To address this, I have divided my research into three parts, each trying to answer the one of the following questions:

1. Which cells of the blood demonstrate the same age-related decline in m.3243A>G?

I first sought to understand the selection patterns across the different cell types making up the blood tissue. To investigate this, I utilised different sequencing technologies to quantify heteroplasmy within bulk populations of cells and single cells isolated via fluorescence activated cell sorting (FACS). These data sets allowed identification of cell types of interest to pursue for further investigation.

2. Does m.3243A>G impact T cell function?

Mitochondrial dysfunction induced by both nuclear and mitochondrial genome variants has been identified as driving dysregulations in immune cell development and thus weakening immune function. In chapter 5 of this thesis, I focus on understanding whether a decline in m.3243A>G level is correlated with T cell divisions while also assessing proliferative competency in response to stimulation. To investigate this, I activated T cells *in vitro*, which allowed measurement of m.3243A>G level as T cells divided and assessed cell proliferation via flow cytometry in m.3243A>G patients compared to controls.

3. Are cells with a high m.3243A>G level transcriptionally distinct from those with a low m.3243A>G level?

The inability to sequence both the transcriptome and the mtDNA heteroplasmy of a single cell has hindered the progression of mtDNA disease research. Here, I adapted protocols optimised for identification and transcriptome sequencing of cells possessing rare cancer genes into identification of cells with differing m.3243A>G levels. Comparison of transcript expression in high and low m.3243A>G cells from the same individual informed how m.3243A>G influences cellular gene expression. For example, disruption of cellular pathways vital for cell survival or function may hint towards a cell death-based mechanism of selection.

# Chapter 2 Methods

## 2.1 Equipment, consumables, and reagents

Detailed lists of the equipment, consumables and reagents used to carry out the protocols outlined in this chapter can be found in **Appendix A - Appendix D**.

## 2.2 Solutions

### 2.2.1 R10

| | |
|---|---|
| Penicillin-Streptomycin | 1% |
| RPMI (without L-glu) | - |
| FBS (foetal bovine serum) | 10% |
| L-glutamine | 1% |

### 2.2.2 RAB10

| | |
|---|---|
| Penicillin-Streptomycin | 1% |
| RPMI (without L-glu) | - |
| Human Ab Serum | 10% |
| L-glutamine | 1% |

### 2.2.3 Cell lysis buffer (500ul)

| | |
|---|---|
| 0.5M Tris-Hcl | 50µl |
| 1% Tween-20 | 250µl |
| Proteinase K | 5µl |
| dH2O | 195µl |

### 2.2.4 RBC lysis buffer

| | |
|---|---|
| EDTA disodium salt solution | 0.1mM |
| Ammonium Chloride | 4.15g |
| Sodium Bicarbonate | 0.5g |
| dH2O | 500µl |

### 2.2.5 Sort Buffer

| | |
|---|---|
| PBS | - |
| EDTA | 0.4% |
| FBS | 0.5% |

## 2.3 Ethical approval

Ethical approval for this project was granted under the Newcastle and North Tyneside Local Research Committee (REC:19/LO/0117; “Understanding the decline in levels of the mitochondrial DNA mutation m.3243A>G within blood cell subtypes”). This granted recruitment, blood draw and phenotype information from 50 individuals carrying m.3243A>G, 25 individuals carrying other heteroplasmic mtDNA variants/ single mtDNA deletions as well as 25 age matched controls. Written informed consent was obtained in accordance with the declaration of Helsinki prior to sample retrieval and all human tissue was stored in accordance to the human tissue act. Retrospective information regarding progression of disease phenotype was obtained from the Wellcome Centre for Mitochondrial Research Patient Cohort (MitoCohort): A Natural History Study and Patient Registry (REC Ref: 13/NE/0326).

Additional control PBMC samples were obtained from the “Dendritic Cell Homeostasis in Health and Disease study” (REC:08/H0906/72) and the “MAGMA study” (REC:17/NE/0015).

## 2.4 Cohorts

### 2.4.1 Newcastle patient cohort

Blood (5-20ml) was donated by 50 individuals carrying m.3243A>G (ages: 18 – 70; Male: 21 Female: 29). Project inclusion criteria stated that recruited individuals must be over 16 years, registered on the MitoCohort and must not, in the opinion of the recruiting investigator, be suffering from an obvious infection at the time of sample retrieval. NHS full blood count data were provided to ensure no elevation of lymphocyte or myeloid cells

as confirmation no infection was present; as well as a full Newcastle Mitochondrial Disease adult scale (NMDAS) assessment to assess current clinical phenotype (Schaefer *et al.*, 2006). Only one individual presented with an abnormal lymphocyte count; samples from this individual were removed from the dataset to assess for any differences throughout. Samples were obtained from 2019 – 2024 from the Newcastle Mitochondrial Disease Clinic for Adults and Children. Cohort demographics are outlined in **Table 2. 1**. Data from nine of these individuals contributed to my Stem Cells and Regenerative MRes in 2019.

| Study ID | Age | Sex | mtDNA variant | Clinical phenotype | Scaled total NMDAS | Most recent tissue level of mtDNA variant (%) | | |
|---|---|---|---|---|---|---|---|---|
| | | | | | | Blood (age) | Muscle | Urine |
| **P01** | 60 | M | m.3243A>G | Deafness, Diabetes mellitus, Cardiovascular involvement, Ptosis, Myopathy, Cerebellar ataxia, End-stage Renal Failure | 24.9 | 24 (57) | 80 | 84 |
| **P02** | 58 | F | m.3243A>G | Deafness, Diabetes mellitus | 16.6 | 21 (58) | N/A | 41 |
| **P03** | 51 | M | m.3243A>G | Diabetes mellitus, mild hearing deficit | 8.3 | 20 (38) | N/A | 67 |
| **P04** | 61 | M | m.3243A>G | Diabetes mellitus, Ptosis, Myopathy, Cerebellar ataxia, Dysphagia | N/A | 18 (59) | N/A | 73 |
| **P05** | 31 | M | m.3243A>G | Deafness | 4.1 | 6 (27) | 25 | 52 |
| **P06** | 51 | F | m.3243A>G | Deafness, chronic constipation | 9.3 | 13 (49) | N/A | 35 |
| **P07** | 56 | F | m.3243A>G | Impaired glucose tolerance, chronic constipation | 9.3 | 10 (55) | N/A | 57 |
| **P08** | 41 | M | m.3243A>G | Deafness, Diabetes mellitus, chronic kidney disease (focal segmental glomerulosclerosis) | 10.4 | 32 (40) | N/A | N/A |
| **P09** | 66 | M | m.3243A>G | Deafness, Diabetes mellitus, Dysphonia/dysarthria, Cerebellar ataxia, Neuropathy | 32.2 | N/A | 67 | 66 |
| **P10** | 24 | M | m.3243A>G | Deafness, Myopathy, Chronic Constipation, Short stature | 17.6 | 59 (22) | N/A | 92 |
| **P11** | 36 | F | m.3243A>G | Diabetes mellitus, Myopathy | 8.3 | 11(36) | 48 | 49 |
| **P12** | 31 | F | m.3243A>G | Deafness, Diabetes mellitus, Cardiovascular involvement, Short Stature, Renal transplant for focal segmental glomerulosclerosis | 18.6 | 36 (31) | N/A | 42 |

| | | | | | | | | |
|---|---|---|---|---|---|---|---|---|
| **P13** | 24 | F | m.3243A>G | Mild hearing deficit | 7.3 | 31 (24) | N/A | 47 |
| **P14** | 60 | F | m.3243A>G | Deafness, CPEO, Cerebellar ataxia | 14.5 | 14 (60) | N/A | 74 |
| **P15** | 45 | M | m.3243A>G | Deafness, Diabetes Mellitus, Cerebellar Ataxia, Myopathy, Cardiovascular involvement | 45.2 | 23 (45) | N/A | 85 |
| **P16** | 43 | F | m.3243A>G | Deafness | 4.1 | 23 (43) | 71 | 76 |
| **P17** | 46 | F | m.3243A>G | Myopathy, Deafness | 17.6 | 9 (46) | N/A | 64 |
| **P18** | 24 | F | m.3243A>G | Deafness, chronic constipation | 14.5 | 36 (24) | N/A | 80 |
| **P19** | 20 | F | m.3243A>G | Deafness, severe psychiatric involvement, migraines, cardiovascular involvement | 24.9 | 59 (20) | N/A | 70 |
| **P20** | 25 | M | m.3243A>G | MELAS syndrome, dementia, chronic constipation | 51.8 | 42 (25) | N/A | N/A |
| **P21** | 65 | M | m.3243A>G | Deafness, Myopathy, Ataxia, Neuropathy | N/A | 12(65) | N/A | 77 |
| **P22** | 18 | F | m.3243A>G | Deafness, Cardiovascular involvement, Myopathy, Short Stature | 24.5 | 60 (18) | N/A | 96 |
| **P23** | 23 | F | m.3243A>G | Diabetes Mellitus, Migraines | 13.5 | 58 (23) | N/A | 74 |
| **P24** | 34 | M | m.3243A>G | Cerebellar Ataxia, Myopathy, Psychiatric involvement, Hearing impairment | N/A | 36 (34) | N/A | 81 |
| **P25** | 50 | F | m.3243A>G | Diabetes Mellitus, | 15 | 24 (50) | N/A | 53 |
| **P26** | 56 | F | m.3243A>G | Deafness, Migraines, Diabetes Mellitus, Myopathy, Cerebellar Ataxia | 23.8 | 19 (56) | 73 | 52 |
| **P27** | 58 | F | m.8344A>G | Asymptomatic | 6.4 | 55 (58) | N/A | N/A |
| **P28** | 24 | M | m.8344A>G | MERRF syndrome, lipomatosis, cerebellar ataxia, deafness | 46.2 | 86 (24) | N/A | N/A |

| | | | | | | | | |
|---|---|---|---|---|---|---|---|---|
| **P29** | 75 | F | m.8344A>G | Myoclonus, Neuropathy, Hearing impairment, cerebellar ataxia | 10.7 | 65 (75) | N/A | 67 |
| **P30** | 35 | F | m.8344A>G | Ataxia, lipomatosis, mild hearing deficit | N/A | 67 (35) | N/A | N/A |
| **P31** | 59 | M | m.5703G>A | Ptosis, CPEO, Myopathy | 39.7 | 28 (59) | 46 | 44 |
| **P32** | 52 | F | m.12258C>A | Diabetes Mellitus, GI disturbance | 34.8 | 48 (52) | N/A | N/A |
| **P33** | 45 | F | m.3252A>G | No NMDAS taken | N/A | 16 (45) | N/A | N/A |
| **P34** | 35 | F | m.14709T>C | Diabetes Mellitus, Severe respiratory muscle weakness, Dysphonia-dysarthria, Myopathy | 34.4 | 96 (35) | N/A | 94 |
| **P35** | 29 | F | m.13051G>A | Blindness | 12.9 | 90 (29) | N/A | N/A |
| **P36** | 58 | F | m.15699G>C | No NMDAS taken, previous reports of cardiovascular involvement | N/A | 5 (58) | N/A | 16 |
| **P37** | 40 | F | m.9185T>C | No NMDAS taken, previously asymptomatic | N/A | 80 (40) | N/A | 88 |
| **P38** | 54 | F | m.9035T>C | No NMDAS taken, history of mild neuropathy | N/A | 89 (54) | N/A | 90 |
| **P39** | 26 | F | m.3243A>G | No NMDAS taken, history of Diabetes Mellitus | N/A | 55 (26) | 86 | 76 |
| **P40** | 61 | M | m.3243A>G | No NMDAS taken, history of diabetes mellitus, ptosis and cerebellar ataxia | N/A | 20 (61) | 67 | 72 |
| **P41** | 48 | F | m.3243A>G | Diabetes Mellitus, cerebellar ataxia and cardiovascular involvement | 35.4 | 18 (48) | N/A | 63 |
| **P42** | 47 | F | m.3243A>G | Myopathy, GI Disturbance | 39.4 | 19 (47) | 92 | 59 |
| **P43** | 50 | M | m.3243A>G | CPEO, Cerebellar ataxia | 29 | 19 (50) | 67 | 89 |

| | | | | | | | | |
|---|---|---|---|---|---|---|---|---|
| **P44** | 55 | F | m.3243A>G | Diabetes Mellitus, mild myopathy | 32.1 | 14 (55) | 67 | 58 |
| **P45** | 61 | F | m.3243A>G | Migraines, impaired glucose tolerance, cardiovascular involvement, cerebellar ataxia | 39.7 | 6 (55) | 55 | 40 |
| **P46** | 66 | F | m.3243A>G | Moderate deafness, diabetes mellitus, respiratory weakness, myopathy, cerebellar ataxia, cardiovascular involvement | 34.4 | 14 (62) | N/A | 64 |
| **P47** | 30 | F | m.3243A>G | Asymptomatic | 2.1 | 33 (27) | N/A | 46 |
| **P48** | 58 | F | m.3243A>G | Deafness, diabetes mellitus, cardiovascular involvement | 24.7 | 23 (54) | 84 | 74 |
| **P49** | 57 | F | m.3243A>G | Moderate deafness, diabetes mellitus, respiratory weakness, | 35.2 | 7 (57) | 73 | 46 |
| **P50** | 42 | F | m.3243A>G | Asymptomatic | 4.1 | 3 (42) | N/A | 18 |
| **P51** | 65 | F | m.3243A>G | Moderate deafness, diabetes mellitus, myopathy, neuropathy | 41.8 | 7 (65) | 38 | 22 |
| **P52** | 26 | M | m.3243A>G | Asymptomatic | 1 | 22 (26) | N/A | 42 |
| **P53** | 40 | M | m.3243A>G | MELAS syndrome, moderate deafness, diabetes mellitus, Cardiovascular involvement | 40.2 | 13 (40) | N/A | 82 |
| **P54** | 38 | M | m.3243A>G | No NMDAS taken, history of deafness, seizures, diabetes mellitus, CPEO, ptosis | N/A | 43 (33) | N/A | 94 |
| **P55** | 29 | F | m.3243A>G | Asymptomatic | 7.5 | 25 (29) | N/A | 61 |
| **P56** | 37 | M | m.3243A>G | Diabetes mellitus, cardiovascular involvement, CPEO | 20.7 | 42 (32) | N/A | 95 |
| **P57** | 51 | M | m.3243A>G | Moderate deafness, diabetes mellitus, cardiovascular involvement, myopathy, cerebellar ataxia | 35.2 | 15 (51) | N/A | 58 |
| **P58** | 36 | F | m.3243A>G | MELAS syndrome, moderate deafness, myopathy, Dysphonia/dysarthria | Insf. | 19 (27) | 77 | 57 |

| | | | | | | | | |
|---|---|---|---|---|---|---|---|---|
| **P59** | 34 | M | m.3243A>G | No NMDAS taken, history of seizures, myopathy and GI disturbance | N/A | 31 (25) | 89 | 87 |

***Table 2. 1 Demographics of patient cohort.*** *CPEO: chronic progressive external ophthalmoplegia; MELAS: mitochondrial encephalomyopathy, lactic acidosis and stroke-like episodes; MERRF: myoclonic epilepsy with ragged red fibers; N/A: measurement not available. Age in brackets of whole blood column denotes the age at which the last whole blood heteroplasmy measurement was taken. Insf. = insufficient marks to calculate score, this is due to aspects of NMDAS not being measured during the appointment*

.

### 2.4.2 Newcastle control cohort

Twenty-one control PBMC samples were obtained, these samples were used in investigations in Chapter 3 and Chapter 5.

| Study ID | Age | Sex |
|---|---|---|
| **C01** | 70 | M |
| **C02** | 50 | M |
| **C03** | 24 | M |
| **C04** | 58 | M |
| **C05** | 54 | M |
| **C06** | 63 | M |
| **C07** | 57 | M |
| **C08** | 69 | M |
| **C09** | 22 | M |
| **C10** | 23 | M |
| **C11** | 23 | F |
| **C12** | 24 | F |
| **C13** | 35 | F |
| **C14** | 40 | F |
| **C15** | 43 | F |
| **C16** | 33 | F |
| **C17** | 40 | M |
| **C18** | 34 | M |
| **C19** | 35 | F |
| **C20** | 48 | M |
| **C21** | 29 | F |
| **C22** | 27 | F |
| **C23** | 50 | M |

***Table 2. 2 Demographics of control cohort***

### 2.4.3 Oxford Cohort

This thesis will outline collaborative investigations which involved sixteen samples obtained by the Mitochondrial Diseases Diagnosis and Management Outpatient Clinic, Oxford (associated data presented in 5.3.4).

| Sample | Age | Sex | Patient or control? |
|---|---|---|---|
| **S1** | 54 | F | P |
| **S2** | 37 | M | P |
| **S3** | 25 | F | C |
| **S4** | 54 | M | P |
| **S5** | 50 | M | P |
| **S6** | 32 | F | P |
| **S7** | 63 | F | P |
| **S8** | 28 | F | C |
| **S9** | 60 | F | C |
| **S10** | 30 | F | C |
| **S11** | 56 | M | C |
| **S12** | 30 | F | C |
| **S13** | 30 | M | C |
| **S14** | 38 | M | C |
| **S15** | 58 | M | C |
| **S16** | 64 | F | C |

***Table 2. 3 Participant information from Oxford cohort***

## 2.5 PBMC Isolation

Whole blood was mixed 1:2 with PBS and layered onto 15ml Lymphoprep (Stem Cell Technologies), this was then centrifuged at 800g for 20 minutes with soft deceleration. Once complete, 4 layers formed: an upper plasma layer containing plasma and platelets, a buffy layer containing peripheral blood mononuclear cells (PBMCs), a clear Lymphoprep layer and a large erythrocyte and granulocyte pellet. The buffy layer was isolated and washed twice with 25ml PBS + 10% FBS followed by centrifugation for 5 minutes at 500g (first wash) or 7minutes at 300g (second wash). The PBMC pellet was then resuspended in freezing media (FBS + 10% DMSO) in aliquots of ~$2x10^6$/ml and transferred to -80ºC. Platelets were isolated from the plasma layer by centrifuging at 800g for 15 minutes, the supernatant was discarded and the pellet frozen at -80ºC. 20ml of RBC lysis buffer was added to the erythrocyte and granulocyte pellet and incubated in the dark for 30 minutes, after this the sample was topped up to 50ml using PBS and washed at 500g for 5 minutes, leaving a white pellet of granulocytes. If the pellet was not white, the pellet was resuspended in 1ml of RBC lysis buffer for 5-minutes before spinning at top speed on a bench top centrifuge and supernatant discarded. Similarly, to the platelets, granulocyte pellets were stored at -80° until use.

## 2.6 DNA Extraction from whole blood

200µl of whole blood per patient was segregated for DNA isolation. This was carried out using the QIAGEN QIAmp mini blood kit as per manufacturer's instructions. 20µl of the protease provided was combined with 200µl blood and 200µl buffer AL then vortexed thoroughly before being incubated at 56° for 10 minutes to lyse the cells. The sample was then removed from the heat and 200µl of 100% ethanol was added before transfer to a QIAamp Mini spin column which was then centrifuged at 8000rpm for 1 minute. Next, 500µl buffer AW1 was added to the column and centrifuged at 8000rpm for another minute, after which all liquid was discarded. A final 500µl of buffer AW2 was added to the column and centrifuged at 14000rpm for 3 minutes. Once all washes were complete, 200µl of buffer AE was added to the filter and incubated at room temperature for 1 minute before a 1 minute, 8000rpm spin to elute the purified DNA.

## 2.7 PBMC Thawing

Cryovials of frozen cells were placed in a bead bath until a small shard of ice remained, 1ml of R10 media was then added dropwise to the cells. The entire contents of the cryovial was then added to 10ml of R10. This was centrifuged at 1400rpm for 7 minutes before the supernatant was removed and the cell pellet resuspended in 5ml of R10 and washed once more at 1400rpm for 5 minutes. Following the second wash, cells were resuspended in 5ml of R10 and incubated at 37ºC for 1 hour before experimental use.

## 2.8 Cell Counting

Samples were resuspended in 1ml of R10, 20µl of this was diluted 1:1 with 20µl of trypan blue and added to a cellometer cell counter slide. The approximate number of cells per ml and sample viability was calculated using a Nexalom cell counter.

## 2.9 Cell sorting and lysis

Cell pellets were resuspended in 1ml sort buffer and transferred to a 5ml round-bottom polystyrene tube (Falcon$^{TM)}$ before centrifuging at 1200rpm for 5 minutes. Approximately 1x$10^6$ cells were incubated per 100µl of antibody mix in the dark, at 4° for 20 minutes, specific antibody panels are outlined in the relevant results chapters. Once staining was complete, each sample was washed with 2ml sort buffer and centrifuged at 1200rpm for 5 minutes. The subsequent stained pellet was resuspended in 500µl sort buffer; in the event of poor resuspension, the sample was passed through a 35µM filter.

Cell sorting was carried out using the BDAria Fusion sorter with a 70µM nozzle. Panel compensation was carried out using BD™ CompBeads Anti-Mouse Ig, κ/Negative Control Compensation Particles Set for mouse derived antibodies and where antibodies are not of mouse origin, AbC compensation beads (Thermofisher) where used.

Populations of ~1000 cells were sorted directly into 1.5ml eppendorfs containing 25µl cell lysis buffer and single cells into 96-well PCR plates (Starlab) containing 15µl cell lysis buffer. Once the sort was complete, samples were centrifuged at 8000rpm for 1.5 minutes before being lysed in an incubation of 56° for 2 hours, followed by 10 minutes at 95°. Lysate was centrifuged at 8000rpm for 1 minute before freezing at -20 until use. Sort gates were generated using BD FACSDiva$^{TM}$ DIVA software and gating strategies can be found in chapter methods, where relevant. Analysis of flow cytometry data was carried out using FCS Express 7.

## 2.10 Pyrosequencing for the detection of mtDNA variant heteroplasmy

### 2.10.1 PCR

The mtDNA sequence flanking the gene of interest was amplified using primer pairs (**Table 2. 4**) in a GoTaq G2 polymerase mastermix (Promega) (**Table 2. 5**) under the cycling conditions in **Table 2. 6**

| *Variant of interest* | *Forward Primer (5'-3')* | *Reverse Primer (5'-3')* | *Amplicon Length* | *Sequencing Primer* | *Reference sequence* |
|---|---|---|---|---|---|
| *m.3243A>G* | /bio/ TAAGGCCTACTT CACAAAGCG | GCGATTAGAATG GGTACAATGAG | 211 | ATGCGATTACCGG GC | T/CCTGCCATCTT |
| *m.8344A>G* | /bio/TTTGAAATAGGGCC CGTATTTACC | CGGTAGTATTTAGTT GGGGCATTT | 148 | ATTTCACTGTAAA GAGGTGT | TGGC/TTCTCTTA |
| *m.5703G>A* | /bio/GCCCTTACTAGACC AATGGGACT | GCGGGAGAAGTAGA TTGAAGC | 90 | GCCAGTTGATTAG GGTG | C/TTTAGCTGTTA |
| *m.3252A>G* | /bio/GGGTTTGTTAAGAT GGCAGAGC | GAATGGGTACAATG AGGAGTAGGA | 123 | AGTTTTAAGTTTTA TGCGA | T/CTACCGGGCTC |
| *m.12258C>A* | /bio/ACAGAGGCTTACG ACCCCTTATT | GAAGTCAGGGTTAG GGTGGTTATA | 198 | TTATCCTTTAAAAG TTGAGA | AAG/TCCATGTTG |
| *m.14709T>C* | CACTCAACAGAAACAA AGCATACA | /bio/TTAGGGGGTTAG TTTTGCGTATT | 132 | AACCACGACCAAT GAT | AT/CGAAAAACCA |
| *m.9185T>C* | CGCCTTAATCCAAGCCT ACGTT | /bio/GTGATTGGTGG GTCATTATGTGTT | 79 | CGTTTTCACACTT CTAGTAA | GCCT/CCTACCTG |
| *m.9035T>C* | CCGTACGCCTAACCGCT AACAT | /bio/AGGGTGGCGCT TCCAATT | 67 | ACTGCAGGCCACC TAC | T/CCATGCACCTA |
| *m.13051G>A* | /bio/TAGGTCTCCACCCC TGACTCC | TTTGGATTAGTGGGC TATTTTCT | 144 | TGAGACTGGGGTG GGGC | C/TTTCTATGGCT |
| *m.15699G>C* | /bio/TCATCCTAGCAATA ATCCCCATC | TGGTAAAAGGGTAG CTTACTGGTT | 150 | ATAAAGTGATTGG CTTAGTGGG | C/GGAAATATTAT |

***Table 2. 4 Primer sequences for PCR amplification and pyrosequencing of pathogenic mtDNA variants.*** *Primers designed using revised Cambridge reference sequence GenBank accession number:NC_012920.1. /bio/ = biotinylated primer*

| *Reagent* | *Volume per reaction (µl)* |
|---|---|
| *GoTaq G2 buffer* | 5 |
| *dNTP (2µM)* | 2.5 |
| *Forward Primer (10µM)* | 1.25 |
| *Reverse Primer (10µM)* | 1.25 |
| *$dH_2O$* | 13.8 |
| *GoTaq G2 polymerase* | 0.2 |
| *DNA sample* | 1 |

***Table 2. 5 Mastermix for per-pyrosequencing PCR***

| *Temp (℃)* | *Time* | *No. of cycles* |
|---|---|---|
| *95* | 2 minutes | 1 |
| *95* | 30 seconds | |
| *63* | 30 seconds | 35 |
| *72* | 30 seconds | |
| *72* | 10 minutes | 1 |
| *4* | ∞ | |

***Table 2. 6 Cycling conditions for pre-pyrosequencing PCR reaction.***

### 2.10.2 Gel Electrophoresis

All amplicons generated for pyrosequencing were <250bps. To ensure amplicons were the correct length and no contamination of the reaction occurred, 5µl of PCR product mixed with 1µl Tritrack dye, was loaded alongside a 100bp ladder into a 2% agarose gel containing 4µl of SYBR safe (Invitrogen). The gel was run for ~40 minutes at 90V while submerged in 1X TAE buffer before imaging on a ChemiDoc. The remaining amplicon pool was stored at 4°C until sequencing.

### 2.10.3 Sample preparation.

Primers used to generate PCR amplicons for pyrosequencing are biotinylated at the 5'; this is to allow binding of target sequences to the streptavidin sepharose beads (cytiva). This is facilitated by a binding reaction in which 40µl of QIAGEN binding buffer, 28µl $dH_2O$ and 2µl streptavidin sepharose beads are combined with 10µl amplicon in each well of a 24-well plate (starlab) and incubated, on a shaker, at room temperature, for 10 minutes.

Following this, a vacuum nozzle with 24 probes was washed twice using $dH_2O$ before placing it into the plate. This extracted any liquid to waste, leaving the streptavidin beads bound with amplicon remaining on each probe. Next, the nozzle was placed into a sequence of baths: 70% Ethanol for 5 seconds, denaturation buffer for 5 seconds and finally, wash buffer for 10 seconds before suction was turned off and the probes were placed into a shallow Pyromark Q24 compatible flat 24-well plate containing 25µl annealing buffer (24.25µl QIAGEN annealing buffer and 0.75µl 10µm sequencing primer (**Table 2. 4**)) which encouraged release of the amplicon bound beads from the probes. The plate containing beads and annealing buffer was then incubated for 2 minutes at 80°C followed by a 5-minute incubation at room temperature. The sequential baths and incubations facilitate the denaturation of the template strand and hybridisation of the sequencing primer.

### 2.10.4 Sequencing

Pyrosequencing uses a sequencing by synthesis format, which requires each nucleotide to be added to the reaction sequentially. To facilitate this, the pyrosequencer requires a cartridge to be loaded with each nucleotide, an enzyme mixture consisting of DNA polymerase, ATP sulfurylase, luciferase and apyrase as well as a substrate mix containing adenosine 5' phosphosulfate (APS) and luciferin.

To begin the sequencing process, each well was incubated with the enzyme and substrate mixes before the addition of the first dNTP (deoxyribonucleotide triphosphate), dNTPs are dispensed according to the order of the reference sequence supplied to the PyroMark

Q24 software (**Table 2. 4**). If this is complementary to the template strand, DNA polymerase catalyses its addition to the strand, which induces the release of pyrophosphate (PPi). PPi + APS are then converted to ATP by ATP sulfurylase, ATP facilitates the formation of oxyluciferin from the substrate luciferin via the action of luciferase. This reaction generates visible light which is detected by a charged couple device camera. If the dNTP is not complementary to the template strand, it is degraded by apyrase. dNTPs are added sequentially until sequencing is completed; if multiples of the same dNTP bind consecutively, more light is released. The amount of light is proportional to PPi release, and this is represented on a trace as a peak (**Figure 2.1**). The ratio of bases at the position of interest (underlined in the reference sequence; **Table 2. 4**) is used to determine heteroplasmy.

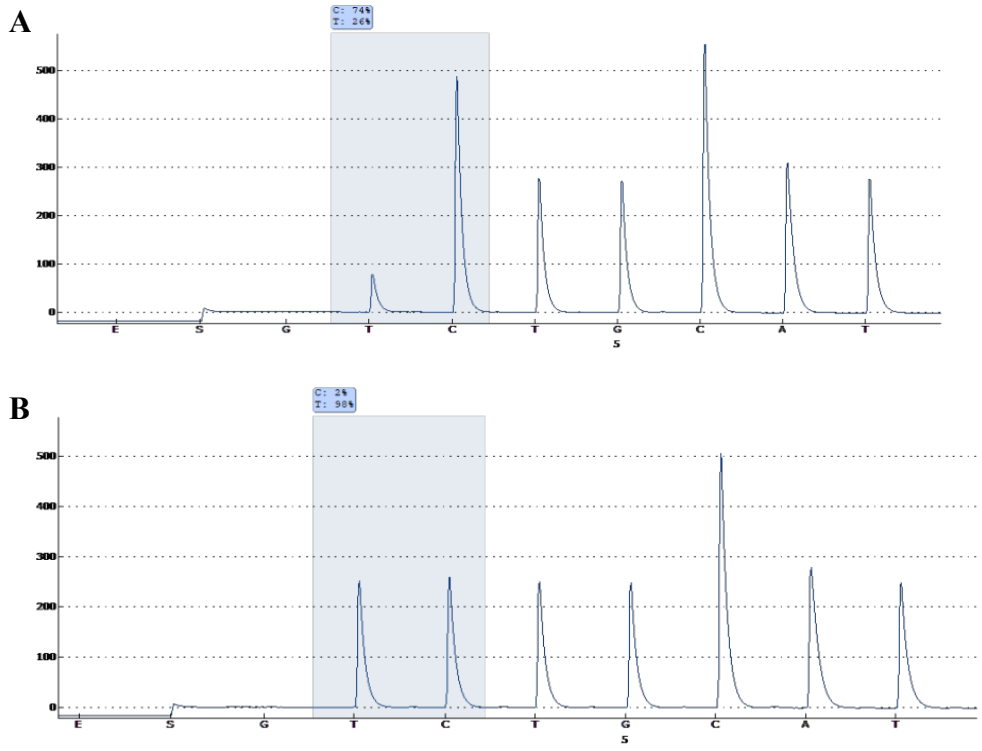


***Figure 2.1 Exemplar pyrogram traces for m.3243A>G.*** *Produced in Pyromark Q24 software. Pyrogram A = 74% m.3243A>G and pyrogram B = 2% (interpreted as wild type as the pyrosequencer sensitivity = ±3%). m.3243A>G reverse sequencing primers were used to sequence both samples according to the reference sequence T/CCTGCCATCTT. Heteroplasmy measurement is calculated as a ratio of T:C values.*

## 2.11 Quantification of mtDNA copy number using real-time PCR

Populations of ~1000 cells isolated via FACS were lysed (section 2.9) and lysate was diluted 1 in 5 with nuclease free $dH_2O$. 5µl of diluted lysate was then combined with a reaction mix which consisted of 10µl TaqMan™ Universal PCR Master Mix (Applied Biosystems), 3.4µl $dH_2O$, 0.4µl VIC-labelled probe (5µM, **Table 2. 7**), 0.6µl forward (10µM, **Table 2. 7**) and reverse primers (10µM, **Table 2. 7**) per well.

This assay uses Taqman chemistry which requires the probe to contain a fluorescent Applied Biosystems FAM or VIC dye on the 5' end and a non-fluorescent quencher bound to a minor grove binder (MGB) at the 3'. The samples were initially heated to 50ºC for 2 minutes before increasing to 90ºC for a further 10 mins followed by 40 cycles of 95ºC for 15 seconds then 60ºC for 1 minute in a StepOnePlus real time thermocycler (Applied Biosystems).

| | **Sequence** | Final conc (nM) |
|---|---|---|
| ND1 Forward Primer | 5'-CCCTAAAACCCGCCACATCT- 3' | 300 |
| ND1 Reverse Primer | 5'-GAGCGATGGTGAGAGCTAAGGT-3' | 300 |
| ND1 Probe | VIC-5'-CCATCACCCTCTACATCACCGCCC-C'-MGB | 100 |

***Table 2. 7 Primer and probe sequences used to estimate mtDNA copy number using real-time PCR. MGB = Minor groove binder***

To calculate mtDNA CN per sample, a standard curve quantifying the copy number of a reference plasmid (p7D1) was used. This plasmid contained the mitochondrial target that was used to determine mtDNA CN, derived from *MT-ND1,* and was of a known molecular weight. The plasmid sample CN/µl was calculated using **Equation 5**.

A ten-fold dilution series of the plasmid sample was used to generate a log10 CN standard curve per run. $R^2$ values of all curves were >0.9992 and gradients fell between −3.264 and −3.449 for all standard curves.

$$\frac{CN}{\mu l} = \frac{g/\mu l}{MW} * (6.03 \times 10^{23})$$

***Equation 5.*** *Plasmid copies per µl*

The equation of the standard curve was then used to calculate absolute copy number (**Equation 5**).$10^x$ was multiplied by the dilution factor to give the number of *ND1* copies in the sample. This was then divided by the number of events sorted via FACS to give an estimate of mtDNA copy number per cell.

$$x = (\frac{mean\ Ct\ of\ sample - y\ intercept\ of\ standard\ curve}{gradient\ of\ standard\ curve})$$

***Equation 6.*** *Using a standard curve to calculate mtDNA CN. Where mean Ct = mean cycle threshold (number of cycles required for the level of fluorescence to exceed a threshold level)*

Each plate contained a control sample which was used to control for inter-plate variation using the following equation:

$$normalised\ value = \left(\frac{\text{absolute mtDNA CN}}{\text{plate control mtDNA CN}}\right) * mean\ control\ mtDNA\ CN$$

***Equation 7.*** *Real-time PCR normalisation*

## 2.12 Determining m.3243A>G level in single cells using a high throughput IonTorrent assay.

15µl of cell lysate was amplified via PCR using a 96-well specific forward primers (**Appendix E**) and a common reverse primer: 5′-GGTTGGCCATGGGTATGTT G-3′. 18µl of mastermix (**Table 2. 8**) was added directly into the 96-well plate containing lysate using a Thermofisher multidrop combi dispenser after the manual addition of 2µl forward primer per well via multichannel pipette. This was then incubated according to cycling

conditions outlined in **Table 2. 9**. 10µl PCR product per well was then pooled per plate prior to sample purification (section 2.12.1) and library preparation (section 2.12.2).

| Reagent | Amount to add (µl) |
|---|---|
| **Platinum SuperFi ii DNA polymerase** | 0.35 |
| **Platinum SuperFi ii 5x buffer** | 7 |
| **Nuclease free $dH_2O$** | 7.95 |
| **10µM dNTPs** | 0.7 |
| **10µM barcoded forward primer** | 2 |
| **10µM reverse primer** | 2 |

***Table 2. 8 PCR mastermix used to amplify mtDNA in single cells.*** *An additional plate of dead volume was added to supplement each batch.*

| Temperature (°C | Time (s) | No of Cycles |
|---|---|---|
| **98** | 30 | 1 |
| **98** | 7 | |
| **60** | 10 | 35 |
| **72** | 30 | |
| **72** | 300 | 1 |
| **4** | ∞ | - |

***Table 2. 9 Cycling conditions required for Platinum Superfi PCR reaction***

### 2.12.1 Sample Purification

200µl from each pooled plate was purified using Ampure XP beads (Beckman Coulter). Room temperature beads were added at 1.8x the sample volume, mixed by pipetting up and down and left to incubate for 5 minutes at 25°. These samples were then placed into a magnetic rack and incubated for a further 3 minutes, until the liquid was clear. The supernatant was then removed from each sample, being careful not to disturb the pellet, followed by the addition of 500µl fresh 70% ethanol. During this, each tube was rotated 360° against the magnet before the ethanol was removed and disposed of and a second ethanol wash was carried out. After the second wash, as much liquid as possible was

removed and each pellet left to airdry on the magnetic rack for 4 minutes. Once almost dry, the pellet was resuspended in 20 - 25µl of nuclease free water and left on the magnetic rack for a further 2 minutes for the DNA to elute. The DNA, now in the nuclease free water was transferred into a separate tube and stored at -20° until use.

### 2.12.2 Library Preparation

An Agilent High sensitivity DNA kit was used to quantify each plate library on the Bioanalyser, as per manufacturer's instructions. Briefly, a gel mixture was added to the chip prior to the addition of buffer to all wells, in conjunction with either the DNA ladder provided or 1µl of purified sample. All libraries produced a strong peak at the expected amplicon size of ~179bp (**Figure 2.2**).

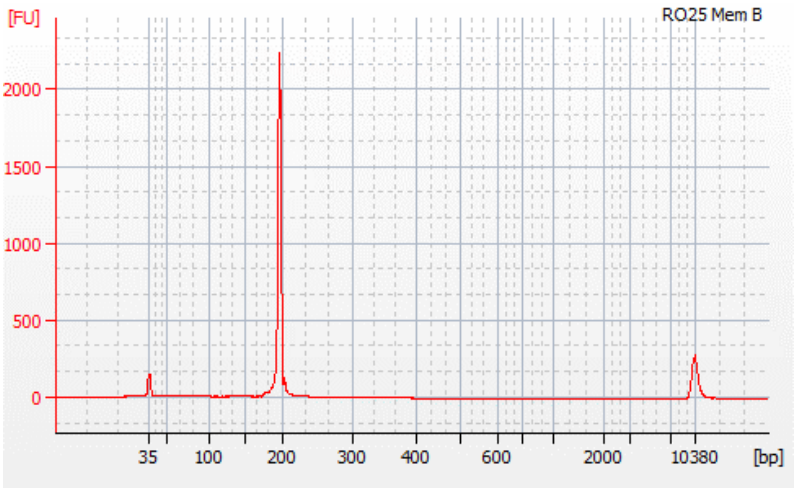


***Figure 2.2 Bioanalyser trace of purified single cell amplicon pool.*** *Expected amplicon length 179bp, represented by a large peak ~180bp. Small peaks at ~35bp and ~10380bp represent the upper and lower size markers.*

### 2.12.3 End repair and adaptor ligation.

100ng amplicon was diluted to a volume of 79µl which was taken forward for use in an end repair reaction. This involved mixing the 100ng samples with 20µl 5X end repair buffer (Ion Plus Fragment Library Kit, life technologies) and 1µl end repair enzyme (Ion Plus Fragment Library Kit, life technologies) followed by a 20-minute incubation at room temperature. This was followed by sample purification, as in section 2.12.1.

Next, plate-specific IonXpress adaptors (Life technologies) were ligated to each purified, end-repaired sample using the mastermix detailed in **Table 2. 10** and incubated for 15 minutes at 25ºC followed by 5 minutes at 72ºC. Consequently, each amplicon contained a unique combination of both plate- and well-specific barcodes which allowed pooling of all plate libraries for sequencing.

| **Reagent** | **Volume (µl)** |
|---|---|
| 10X ligase buffer | 10 |
| Ion P1 adapter | 2 |
| IonXpress barcode | 2 |
| dNTP mix | 2 |
| Nuclease Free water | 49 |
| DNA Ligase | 2 |
| Nick repair polymerase | 8 |
| **Purified Plate Library** | 25 |

***Table 2. 10 IonXpress ligation mastermix.*** *All enzymes derived from Ion Plus Fragment Library Kit, life technologies.*

This was followed immediately by a bead purification which differed slightly from the previous procedures (section 2.12.1) in that the volume of beads added corresponded to the size of the amplicons within the sample (200-300 bp) as per manufacturers instructions. Therefore, rather than the addition of 1.8X the sample volume of beads, 1.2X (120µl) the sample volume was added.

### 2.12.4 Isolation of correct fragment size

The success of adapter ligation was assessed using the bioanalyser (section 2.12.2) (**Figure 2.3**). In the cases which ligation of the barcode was less successful **Figure 2.3B**, fragments of the appropriate length were isolated via size select gel electrophoresis.

Each well of a 2% E-gel™ agarose gel (Invitrogen) was filled with 50µl of $dH_2O$ followed by 25µl of each sample mix (22.5µl of sample + 2.5ul of 10X E-Gel™ sample loading dye) or 50bp ladder (Invitrogen). For ease of interpretation, the ladder was always loaded into the centre well. This gel was then run according to the Sizeselect 2% protocol (~14 minutes), and once bands of the desired length had travelled to the lower wells, they were extracted and re-examined on the Bioanalyser. Equimolar amounts of each plate library were then pooled to form a sequencing library.

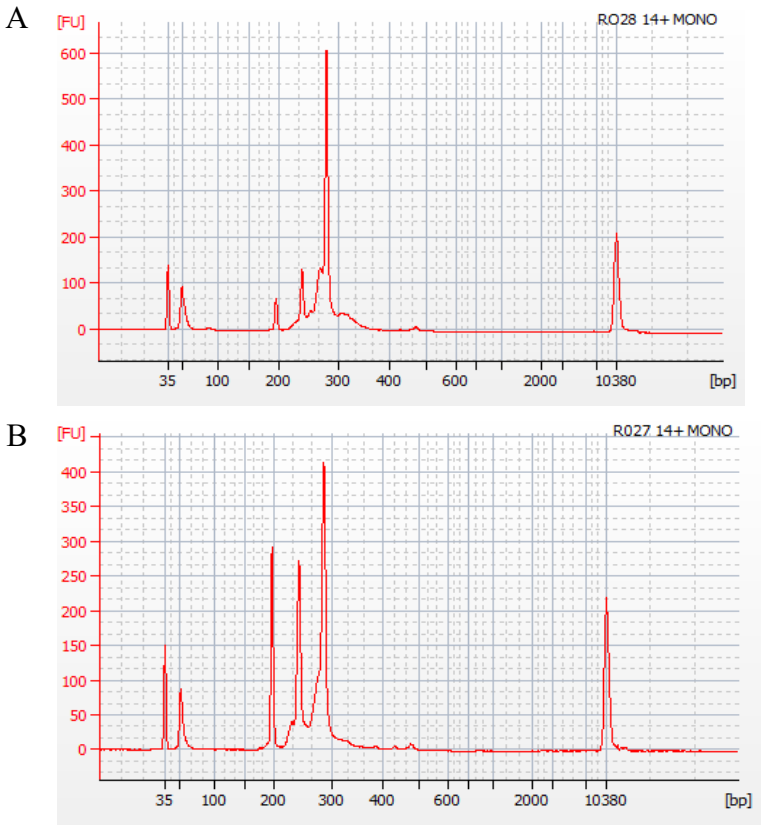


***Figure 2.3 Examples of the variable success of IonXpress adaptor ligation.*** *Successful adaptor ligation is represented by the largest peak at ~280bp in which both adaptors have ligated successfully. Two other peaks smaller in size represent amplicons in which one (~250bp) or no adaptors have bound (~200bp). In the event of similar concentration of different length amplicons, either the adaptor ligation reaction was repeated, or the largest amplicon was isolated via E-Gel size selection.*

### 2.12.5 Template preparation.

Much like in pyrosequencing, IonTorrent systems require the adherence of a sequence to bead like structures named Ion Sphere Particles (ISP). Each ISP will bind an individual sequence and once adhered, these sequences are amplified via ISP bound primers complementary to the IonTorrent adaptors ligated (section 2.12.3*).* This amplification process is automated via the IonChef system: 50µl of library at 80pM was loaded into the reagents cartridge which was loaded in conjunction with a solutions cartridge, provided consumables and an Ion 530 chip. Upon completion of this reaction, the ISP bound, and amplified library was loaded into the sequencing chip. This chip contains microwells which hold a single ISP per well. It was essential that the chip was loaded into the sequencer (S5 system) within 15 minutes of completion of the *template preparation* reaction. Therefore, one hour before completion of this step, the S5 sequencer must be loaded with new reagents and initialised. Once both processes had come to an end, the chip, now loaded with sample, was transferred into the S5 sequencer and the run started.

### 2.12.6 Sequencing

To facilitate sequencing, a Targetseq run template was generated via the Torrent Suite software using the reference sequence derived from the revised Cambridge mtDNA reference sequence (GenBank accession number: NC_012920.1):

5’agctgatNNNNNNNNNNtaaggcctacttcacaaagcgccttcccccgtaaatgatatcatctcaacttagtattatac
ccacacccacccaagaacagggtttgttaagatggcagAgcccggtaatcgcataaaacttaaaactttacagtcagaggttca
attcctcttcttaacaacatacccatggccaacc 3’.

The run settings used were:
Library kit: Ion Xpress Plus Fragment Library Kit
Template kit: Ion 520 & Ion 530 ExT kit-chef
Sequencing kit: Ion S5 ExT Sequencing Kit

Barcode set: IonXpress
All IonXpress barcodes were linked to their corresponding plates as well as the unique identifier code corresponding to the sample in 'Sample Tube Label'.

During the sequencing process, the chip is sequentially flooded with each dNTP (dATP, dGTP, dCTP, dTTP), the incorporation of a complementary nucleotide to the sequence results in the release of a hydrogen ion ($H^+$) and a change in pH. The hydrogen ion release is detected by an ion-sensitive field-effect transistor (ISFET) sensor as an electrical signal. This is followed by a wash to remove any unincorporated dNTPs before being flushed with the next dNTP. This process is repeated until sequence completion.

### 2.12.7 Bioinformatics

BAM files corresponding to each plate were exported directly from the Ionsuite software and subsequently converted into fastq files via SAMtools v.112 (Li *et al.*, 2009). Reads were demultiplexed via plate specific barcodes using Sabre (Sabre, 2011) and aligned to the above reference sequence. The generated SAM files were converted to well-specific pileup files and per well variant calling was performed using the mpileup2cns function of Varscan v2.3.9 (Koboldt *et al.*, 2009). The quality thresholds for this were: minimum average quality = 28, minimum variant allele frequency of 0.0001 and a minimum coverage of 1. Read depth quality control procedure is outlined in section 4.3.2.

### 2.12.8 Data Analysis

To determine the proportion of cells with a near 0% m.3243A>G level, a Bayesian mixture model was fitted to the data per cell type, per individual according to the equation devised by Jordan Childs and Dr Conor Lawless (***Equation 8***). This allowed segregation of the data into two populations: a truncated normal distribution capturing cells with a zero or near-zero m.3243A>G and a second, uniform, distribution spanning the entire range of possible m.3243A>G levels.

$$Y \sim \pi N_0^1\ (\mu, \sigma^2) + (1 - \ \pi) U\ (0,1), \pi \sim \pi_0 \delta_0 + (1 - \pi_0) U(0,1)$$

***Equation 8. Bayesian mixture model****. Where* $N_0^1(\mu, \sigma^2)$ *represents a truncated normal distribution between 0 and 1 with mean μ and variance* $\sigma^2$ *and U(0,1) represents a uniform distribution. The model estimates the value of π, which is the proportion of cells within the normal distribution spike (i.e. the cells with a near zero m.3243A>G level).* $\pi_0$ *is the probability of no spike. The prior beliefs for the unknown parameter were:* $\mu \sim U(0,0.2)$, $\sigma \sim Exp(5)$ *and* $\pi_0 \sim U(0,1)$*. The model inference was run in jags (Plummer, 2018) and the output was checked for convergence and there were no issues.* **Figure 2.4** *demonstrates that the posterior predictive distributions fit the experimental data.*

Two estimates of $\pi$ (i.e. for two different cell types) were considered different if 0 lies outside a 95% credible interval for the difference between them.

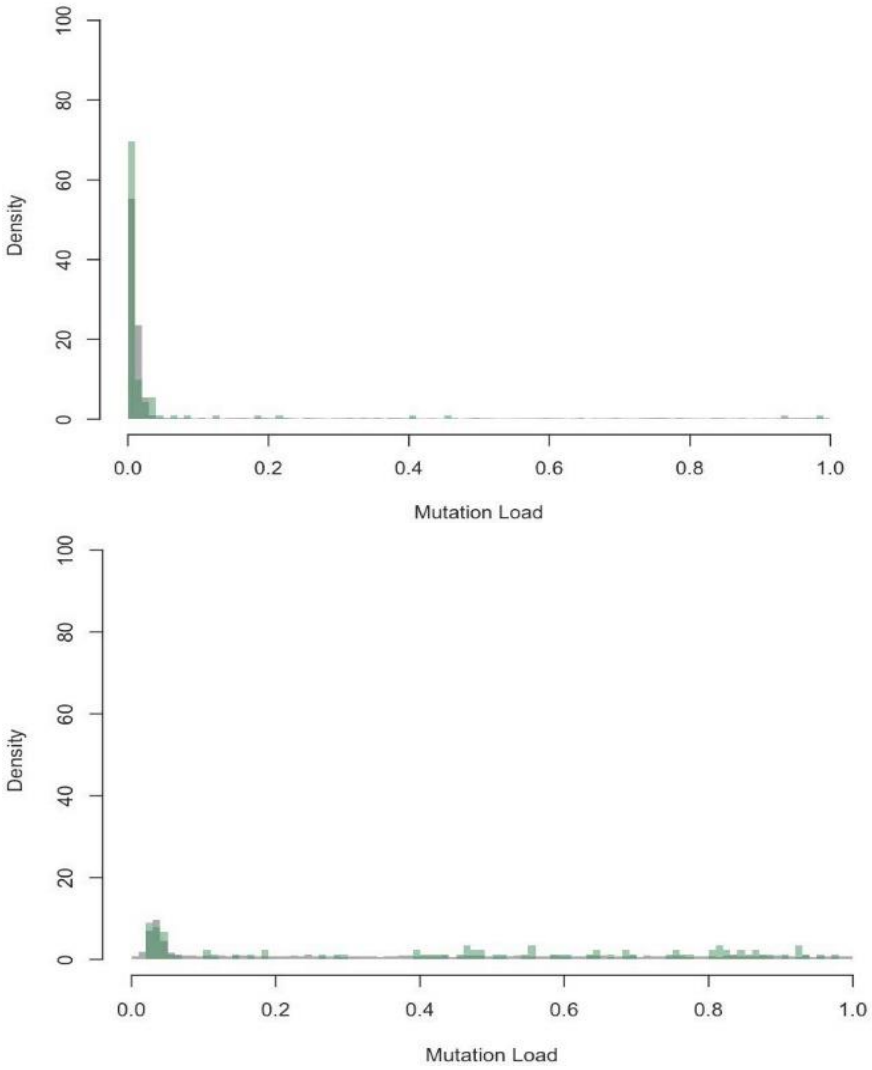


***Figure 2.4 Bayesian posterior predictive reflects experimental data.*** *Exemplar histograms for P18 CD8+ central memory T cell (top) and P22 8+ naïve T cell (bottom). Green bars represent the m.3243A>G distribution in the experimental data and grey is the posterior prediction. Th data on the left shows a large population of cells with near 0% m.3243A>G level and on the right, most cells lie within the uniform distribution.*

## 2.13 T cell functional assessment

### 2.13.1 CTV staining

To track cellular divisions, cells were stained with a Cell Trace Violet (CTV, Invitrogen) dye which binds intracellular proteins and is diluted with divisions. Samples were washed twice in 1ml of sterile PBS before being incubated in 5µM CTV mix (0.5µl CTV/1ml PBS) for 10 minutes at room temperature. The reaction was then quenched by diluting with 4x FBS and incubating for a further 5 minutes at 4ºC. Next the samples were centrifuged at 1500rpm for 5 minutes, resuspended in 5ml R10 and transferred to a clean tube to minimise later CTV infusion as CTV binds plastic easily. This was then incubated at 37ºC for 5 minutes to ensure that excess CTV had diffused out, before cell counting (section 2.8)

### 2.13.2 T cell activation via αCD3 and αCD28

96-well flat-bottomed plates were coated with αCD3 (Biolegend) by adding 100µl of 1µg/ml αCD3 in PBS and sealed tightly before incubating at 4ºC overnight. This was removed and allowed to air dry 10-15 minutes before plating cells.

$1x10^6$ cells per ml were resuspended in activation media (R10 + 10ng/ml IL-2 + 1µg/ml αCD28) or uridine media (R10 + 10ng/ml IL-2 + 1µg/ml αCD28 + 25mg/ml Uridine). 150µl of this cell suspension was then added to each αCD3 coated well and incubated at 37ºC for at least 48 hours. After 48 hours, samples were removed from αCD3 coated wells, underwent a 50% media change, and were returned to incubation. During incubation, cells were visually inspected under a microscope for signs of activation which include the enlargement of cells and cluster formation. From this point, samples were maintained at ~150,000 cells per well, splitting when necessary. On days 5, 7 and 12 post-activation, cells were stained as per section 2.9, fixed via incubation in 4% PFA for 10 minutes before washing with 2ml PBS. The cell pellet was resuspended in 250ul PBS and acquired on the BD Symphony.

### 2.13.3 ELISpot

As in *section 2.13.2,* specialised 96 well plates which possess a PVDF membrane (Millipore) were coated with 50µl 10µg/ml catcher antibody (1-D1K) 8 – 48h before plating cells and incubating at 4ºC overnight. Two hours before plating cells, this solution was removed from wells and 100µl R0 was added to block wells, this was incubated at room temp until addition of cells. Two negative controls, three stimulants and one positive control (ConA) were used for this experiment. The stimulants were cytomegalovirus lysate (CMV), a mix of two Sars-CoV2 spike proteins (S1 + S2) and a mixture of Sars-CoV2 nucleocapsid protein and membrane proteins (M+NP); these peptides were prepared in either DMSO or dH2O before dilution with RAB10 to the initial concentrations in **Table 2. 11**.

| *Stimulant* | *Initial Concentration* | *Final Concentration* |
|---|---|---|
| *S1+S2* | 4µg/ml | 2µg/ml |
| *M+NP* | 4µg/ml | 2µg/ml |
| *ConA* | 10µg/ml | 5µg/ml |

***Table 2. 11 ELISpot stimulant information***

50µl of each 'initial concentration' of stimulant and control were plated in triplicate per patient sample. To this, 50µl of PBMCs ($2x10^5$ cells per 50µl R10) were added. The plate was then incubated for 18 hours at 37ºC, 5% $CO_2$ and 95% humidity. After 18 hours, cells were removed, and each well was washed 6 times using 200µl PBS-Tween (PBS + 0.05% tween) 50µl of 1µg/ml of 7-B6-1-Biotin Ab (mabtech) diluted in PBS was added to each well, followed by a 2-hour incubation at room temperature. After incubation, the Ab solution was removed, cells were washed with PBS-tween wash (x6). Finally, a streptavidin alkaline phosphatase antibody was diluted 1:1000 in PBS and 50µl was added per well and incubated for 1 hour at room temperature. This was followed by a final wash (6x in PBS-tween) before the addition of 50µl of filtered, room temperature BCIP/NBT stock solution to each well. Each plate was wrapped in foil and incubated for 6 minutes, after which the BCIP/NBT solution was flicked out and the plate was washed

3x using $dH_2O$. The purple spots represent cells responding by releasing IFNγ. Plates were air-dried in the dark for a minimum of two days and spots were counted using a CTL ImmunoSpot S6 Ultra-V.

## 2.14 Analysis

All statistical tests were performed in R v.4.4.0. All graphs were produced using the ggplot2 package (Villanueva and Chen, 2019). Linear mixed models were fitted using the nlme package (Pinheiro J, 2019) and included random intercepts for sample ID to account for variation between individuals.

Unless stated otherwise, P-values < 0.05 were considered as significant and, where appropriate, P-values were adjusted for multiple comparisons using the p.adjust function in R using the method = “false discovery rate” option. Comparisons between two groups were performed using the Wilcoxon test. Where shown, box-plots depict the median, and 25th and 75th quantiles and whiskers extend from the hinge to the largest/smallest values no further than 1.5 × IQR from the hinge.

# Chapter 3 Comparison of m.3243A>G level across immune cell populations

## 3.1 Introduction

### 3.1.1 Selection against pathogenic mtDNA variants

Early investigations into the m.3243A>G variant discovered discrepancies between levels in the blood and muscle. In many cases, the m.3243A>G level was prominent in the post mitotic tissue but undetectable in the blood, and when the variant could be detected, it was at consistently reduced levels (Sue *et al.*, 1998). Post mitotic tissues retain a stable m.3243A>G level throughout an individual's lifetime. Longitudinal investigations into this discrepancy lead to the establishment that m.3243A>G demonstrates an age-related decline in mitotic tissues, such as the blood, but not in post mitotic tissues (Rahman *et al.*, 2001, Sue *et al.*, 1998, de Laat *et al.*, 2012, Grady *et al.*, 2018, Veitia, 2018, Langdahl *et al.*, 2018). Estimations of blood m.3243A>G level at birth (age-adjusted blood m.3243A>G level) are similar to levels measured in mitotic tissues (Grady *et al.*, 2018, Pickett *et al.*, 2018). The rate of this decline varies between individuals; some studies suggest that this decline is much more consistent in samples containing only PBMCs (Langdahl *et al.*, 2018) compared to samples of whole blood homogenate which can reach a plateau or increase in rare cases (Grady *et al.*, 2018). Cells present in the whole blood sample that are not present in the PBMC sample, such as platelets, could be contributing to this observed fluctuation.

By building a statistical model simulating the loss of m.3243A>G in the blood tissue, Rajasimha and colleagues provided evidence to support the hypothesis that HSCs are the origin of selection. Inclusion of the asymmetrical cell division required for HSC self-renewal into their simulation model, generated a loss of m.3243A>G level consistent with an aging patient population (Rajasimha,Chinnery and Samuels, 2008a). This is supported by measurement of m.3242A>G level across foetal tissues which demonstrated that all tissues possess the same baseline variant level (Cardaioli *et al.*, 2000, Monnot *et al.*, 2011). A discrepancy between post-mitotic and mitotic tissue heteroplasmy therefore suggests selection and is a common occurrence with m.3243A>G. For example, a reduced level compared to muscle is observed in other mitotic tissues which are replenished via

stem cells, such as the gut epithelium, buccal and cervical tissue (Frederiksen *et al.*, 2006, Su *et al.*, 2018).

### 3.1.2 The relationship between heteroplasmy and mtDNA copy number.

Similar to heteroplasmy, the number of mtDNA molecules (mtDNA copy number (CN)) varies per tissue. Typically, this is linked to the metabolic demand of the tissue, for example smooth and skeletal muscle tissues tend to have a higher mtDNA CN than lung and immune tissues (D'Erchia *et al.*, 2015). A poorly understood mechanism facilitates maintenance of a precise mtDNA level per cell (Berk and Clayton, 1974, Moraes, 2001) which has recently been closely linked to the regulation of the mitochondrial fusion process (Tabara *et al.*, 2024). Each cell is able to sense changes in mtDNA levels and replenish these by replication of existing mtDNA molecules, independently of cell division, in a process known as relaxed replication (Bogenhagen and Clayton, 1977, Kai *et al.*, 2006). Failure of this system can result in severe loss of mtDNA, a phenomenon which is associated with mitochondrial DNA depletion syndrome (MDDS)(Spinazzola *et al.*, 2009). Alterations in mtDNA CN often coincide with disease, for example type 2 diabetes and sepsis (Choi,Kim and Pak, 2001, Pyle *et al.*, 2010). A decrease in blood mtDNA CN is also observed in natural aging and therefore should be taken into account when assessing CN in relation to disease (Mengel-From *et al.*, 2014).

Changes in the mtDNA CN are important to consider when studying selection against m.3243A>G, as a biased increase in either pathogenic or WT DNA within a cell has the potential to modify the relative proportions of each. The literature surrounding a relationship between m.3243A>G level and changes in blood mtDNA CN is conflicting. Pyle and colleagues observed a striking reduction in mtDNA CN in individuals carrying m.3243A>G compared to controls (Pyle *et al.*, 2007) suggesting the presence of pathogenic mtDNA has a large impact on mtDNA levels. However, the majority of the patient samples used in these investigations were aged between 40-70 years and the ages of the controls are not provided. Similar analyses considering age, confirmed the above findings but with the caveat that this phenomenon is isolated to individuals >40 yrs. Interestingly they found an opposing trend in individuals <30 years compared to controls

(Liu *et al.*, 2006), highlighting the importance of stratifying according to age. Analysis of mtDNA copy number in relation to m.3243A>G level is difficult as both are highly dependent on age. Grady, Pickett and team found a weak positive correlation between the two, suggesting an increase in mtDNA CN to compensate for high m.3243A>G levels (Grady *et al.*, 2018). This is consistent with a decline in mtDNA CN as m.3243A<G levels decline in ageing.

*In vitro*, m.3243A>G cybrids have shown a positive correlation between mtDNA copy number and O2 consumption suggesting that an increase in mtDNA CN could alleviate m.3243A>G-related dysfunction (Bentlage and Attardi, 1996). Further to this, Filograna and colleagues found an increase in mtDNA CN ameliorates cardiomyopathy in the m.5024C>T mouse, which can be considered a to be a model of m.3243A>G related disease due to similar tissue specificity and selection patterns in the blood tissue (Filograna *et al.*, 2019). These suggest that modifications in mtDNA CN can impact cell viability and therefore potentially play a role in selection.

This chapter will set out to investigate whether mosaicism can be observed within the blood tissue and if so, is the loss of the m.3243A>G variant driven by a singular or small subset of cell types? I will also examine how selection against the m.3243A>G variant relates to mtDNA copy number and compare trends with other heteroplasmic mtDNA variants (***Table 3. 1***).

| *Variant (gene)* | *Phenotype* | *Biochemical defects* | *Proposed mechanism* | *References* |
|---|---|---|---|---|
| ***m.3252A>G (MT-TL1)*** | MERRF, MELAS, Diabetes Mellitus | Decreased CI activity | Located within the DHU loop of mt-tRNA$^{Leu(UUR)}$ and likely to impact translation. Found within a transcription termination control region therefore may impact MTERF1 binding. | (Morten *et al.*, 1993) |
| ***m.5703G>A (MT-TN)*** | CPEO, MERRF, myopathy | Decreased oxygen consumption, increased lactate production, reduced mitochondrial translation | Destabilised secondary structure of mt-tRNA$^{Asn}$ due to disruption of first base pair in anticodon stem. | (Moraes and Hao, 1997, Moraes *et al.*, 1993, Fu *et al.*, 2019) |
| ***m.8344A>G (MT-TK)*** | MERRF, deafness, lipoma, respiratory dysfunction. | CI & CIV deficiency | Decreased steady-state abundance of mt-tRNALys, reduced aminoacylation of the mt-tRNA, and lack of a post-transcriptional RNA modification of the anticodon wobble base. Resulting in a severe translation defect: | (Richter *et al.*, 2021, Boulet,Karpati and Shoubridge, 1992) |
| ***m.9035T>C (MT-ATP6)*** | Developmental delay, Cerebellar ataxia | Reduced ATP synthase activity, reduced ATP output, increased ROS production | p.Leu170Pro in the A6 subunit of ATP6 | (Sikorska *et al.*, 2009, Saneto and Singh, 2010) |
| ***m.9185T>C (MT-ATP6)*** | Leigh Syndrome, NARP, Motor neuron disease | Reduced ATP synthase activity. | p.Leu220Pro substitution in the fifth transmembrane helix at the inner surface of the outer mitochondrial membrane of ATP6. | (Castagna *et al.*, 2007, Childs *et al.*, 2007, Brum *et al.*, 2014) |
| ***m.13051G>A (MT-ND5)*** | LHON, Leigh syndrome | Fragmented mitochondrial network, increased ROS production, increased mitophagy. | CI instability | (Dombi *et al.*, 2016). |
| ***m.12258C>A (MT-TS2)*** | Deafness, retinitis pigmentosa | Reduced mitochondrial translation | Located within the 3′-end of the aminoacyl acceptor stem of mt-tRNA$^{Ser}$, results in changes to secondary structure, disrupting amino acid-acceptor ability. | (Mansergh *et al.*, 1999) |
| ***m.14709T>C (MT-TE)*** | Diabetes mellitus, myopathy, ataxia, and congenital encephalopathy | Reduced CI & CIV activity, COX deficiency in muscle, overall reduction in protein synthesis | Reduced steady state levels of mt-tRNA$^{Glu}$ result in reduced mitochondrial translation. | (Hanna *et al.*, 1995, McFarland *et al.*, 2004) |
| ***m.15699G>A (MT-CYB)*** | Cerebellar ataxia, hypotonia, peripheral neuropathy, optic atrophy, cerebellar atrophy | CI & CIII deficiency | Inhibits the assembly of CIII | (Blakely *et al.*, 2005, Bannwarth *et al.*, 2013) |

***Table 3. 1 Additional heteroplasmic mtDNA variants investigated in Chapter 3.*** *MERRF, Myoclonic epilepsy with ragged red fibers; MELAS, mitochondrial encephalopathy, lactic acidosis and stroke like episodes; CPEO, Chronic Progressive External Ophthalmoplegia; NARP, Neuropathy, ataxia, retinitis pigmentosa syndrome; LHON, Leber's hereditary optic neuropathy*

## 3.2 Methods

The workflow used to generate the results presented in this chapter is outlined in **Figure 3.1**.

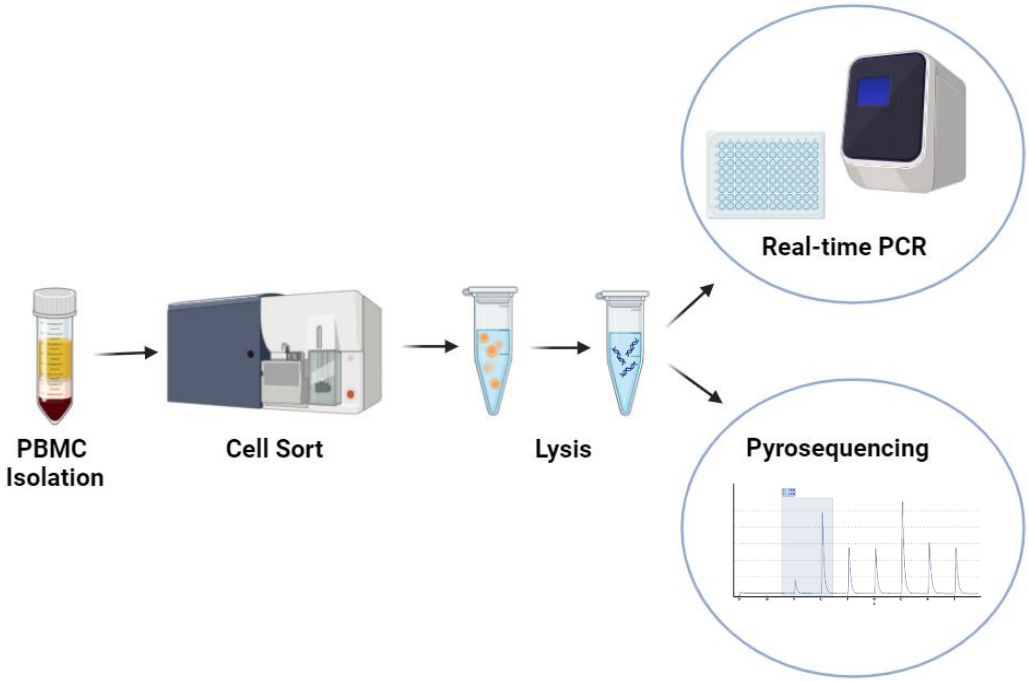


**Figure 3.1** ***The experimental workflow for m.3243A>G and mtDNA CN quantification in PMBC sub-populations.*** *PBMCs were isolated from WB samples via Lymphoprep and sorted into 13 different cell populations consisting of ~1000 cells. These cells were then lysed and mtDNA was subject to amplification via PCR before pyrosequencing to determine heteroplasmy (section 2.10). mtDNA CN was determined using real time PCR (section 2.11). Created using biorender.com.*

### 3.2.1 Cohort

For these analyses, PBMCs from 26/50 recruited individuals carrying m.3243A>G (P01 – P26, *table 2.1)* and 14 age matched controls were investigated (*table 2.2*), alongside PBMCs from 12/25 individuals with other pathogenic mtDNA variants (P27 – P38, *table 2.1*). The demographics of these cohorts are summarised in **Table 3.2**.

| | **Total** | **Sex (M:F)** | **Age (years) [SD]** | **Whole blood het range (%)** |
|---|---|---|---|---|
| ***m.3243A>G*** | 26 | 11:15 | 42.1 [15.24] | 9-60<br>Mean:25.06<br>SD:18.38 |
| ***Non m.3243A>G mtDNA variant*** | 12 | 2:10 | 47.06 [14.38] | 5-96<br>Mean: 60.25<br>SD: 30.63 |
| ***Control*** | 14 | 8:6 | 37.5 [14.43] | NA |

***Table 3. 2 Summary of chapter 3 cohort demographics.*** *Age represented as a mean with standard deviation in square brackets.*

### 3.2.2 Isolation of immune populations via FACS

An antibody panel, designed in collaboration with Dr Paul Milne, combines 16 fluorescent stains to isolate 13 different immune cell populations (**Table 3. 3**); according to the gating strategy outlined in **Figure 3.2**. Patient samples were limited in volume, so this panel was designed to maximise the number of populations that could be obtained during a single sort. Due to inter-individual variation in population sizes and fluorescence intensity, gating was slightly adjusted per patient according to the location and size of clear populations.

| *Ab/Fluorophore* | *Company* | *Cat no* | *Dilution factor* |
|---|---|---|---|
| *DAPI* | Sigma Aldrich | D9542 | 1000 |
| *CD3 FITC* | BD Biosciences | 345764 | 30 |
| *CD19 PE-CF594* | BD Biosciences | 562294 | 30 |
| *CD56 APC* | BD Biosciences | 555518 | 30 |
| *CD11c BUV395* | BD Biosciences | 563787 | 30 |
| *CD123 BV711* | BioLegend | 306030 | 30 |
| *CD4 PE* | BD Biosciences | 345769 | 30 |
| *CD34 PE-Cy7* | BioLegend | 343516 | 30 |
| *CD45 AF700* | BioLegend | 304024 | 100 |
| *CD45RA APC-Cy7* | BioLegend | 304127 | 30 |
| *CD27 BV421* | BioLegend | 302823 | 30 |
| *CD38 BV605* | BD Biosciences | 562665 | 30 |
| *CD14 BV650* | BD Biosciences | 563419 | 30 |
| *HLA-DR BV785* | BioLegend | 307642 | 30 |
| *CD8 PerCP-Cy5.5 (clone HIT8a)* | BioLegend | 344708 | 30 |
| *CD16 V500* | BD Biosciences | 561394 | 30 |

***Table 3. 3 Antibody information for bulk FACS panel***

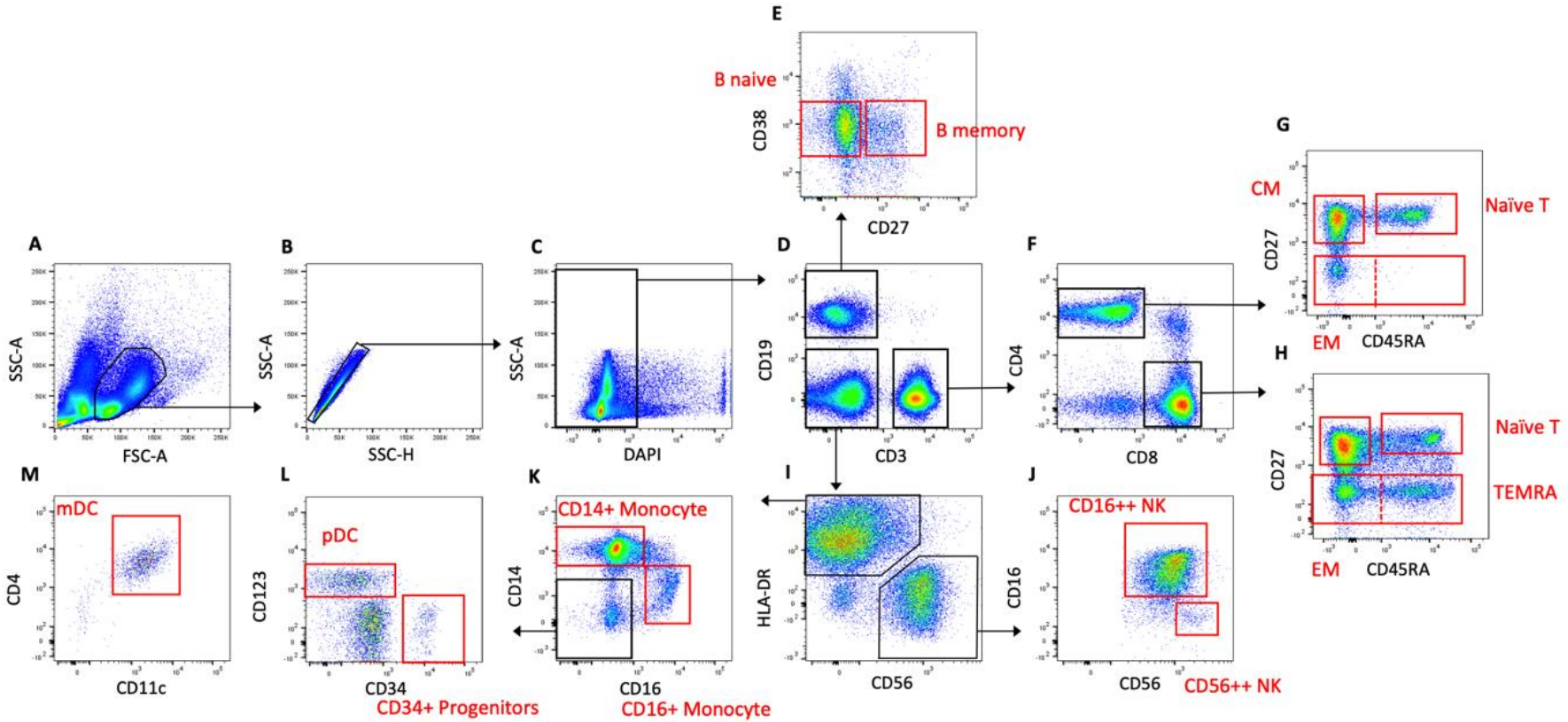


***Figure 3.2 Gating strategy for bulk sort***. *All gates used for sorting are outlined in red. A) Leukocytes are isolated according to forward and side scatter. B) Doublets are removed from leukocyte gate C) live cells D) separation of T cells (CD3+), B cell (CD19+) and all other cell, E) sorting gates for naïve (CD27-) and memory B cells (CD27+), F) Separation of major T cell functional subsets: CD4+ helper and CD8+ cytotoxic T cells. G & H) Isolation of naïve and 3 different T memory cell subsets which make up the memory T cell population I) isolation of NK cells (CD56+) from HLA-DR+ cells. J) Separation of NK cells into mature (CD16++) and immature (CD56++CD16dim), K) isolation of CD14+ monocyte an CD16+ monocytes, CD14-CD16- cells are used as the basis for identification of DC and progenitor cells L) CD34+cells*

## 3.3 Results

### 3.3.1 Cohort Demographics

Before carrying out in-depth investigations, I evaluated the relationship between whole blood m.3243A>G level and age within the cohort (*n=50*) to ensure it is consistent with the literature. Overall, m.3243A>G levels decline with age; where retrospective measurements were available, they show differing rates and directions of change in m.3243A>G level per patient (**Figure 3.3A).** Individuals older than 50 years do not have a m.3243A>G level superseding 24% across the cohort of 50 individuals. The mean level for individuals over 50 is 12.65% (SD = 7.55) and under 25 is 32.45% (SD = 18.8). In the small subset of individuals who have had a muscle biopsy (n=16), m.3243A>G level in blood is consistently lower than in muscle **(Figure 3.3B**); these findings are consistent with the literature outlining negative selection of m.3243A>G within the blood.

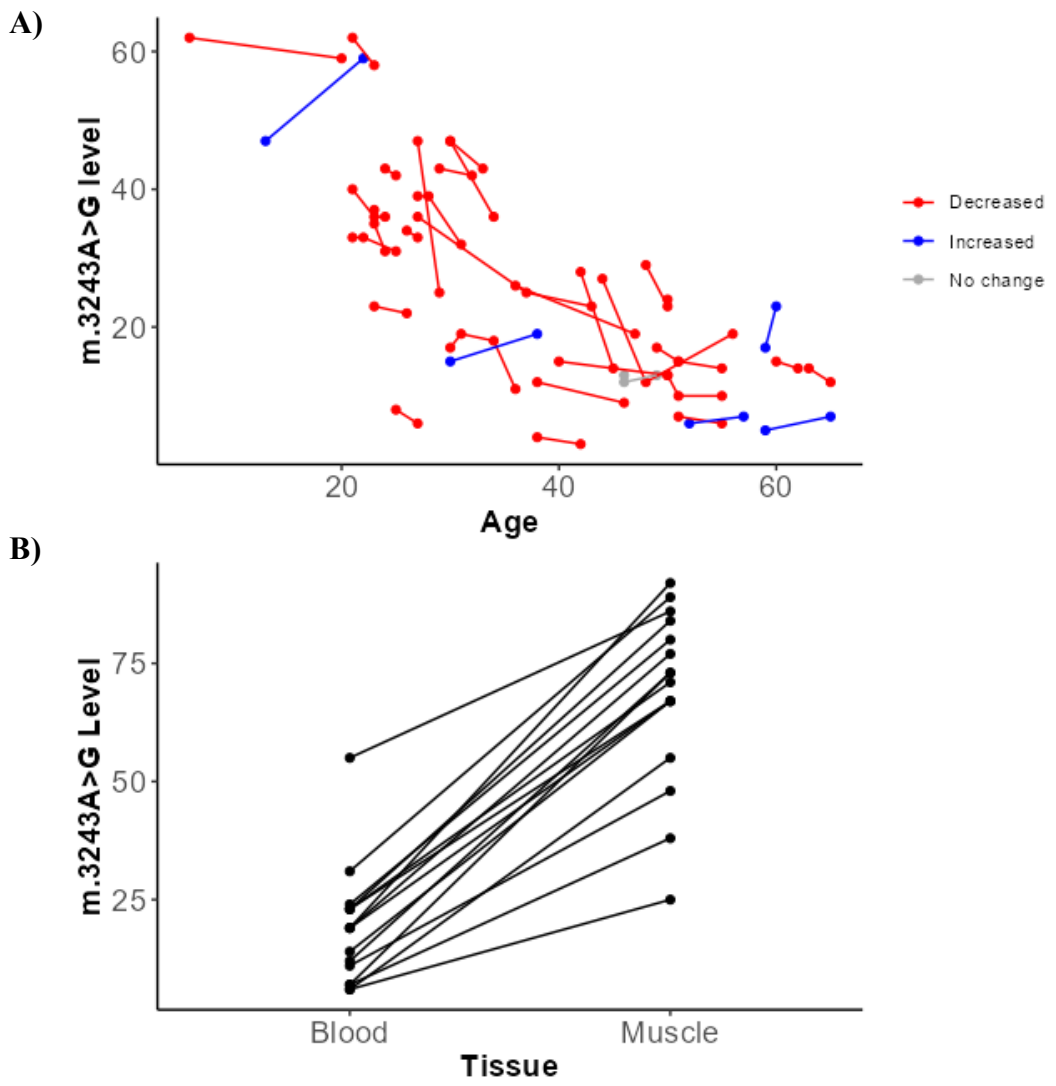


***Figure 3.3 m.3243A>G trends in Newcastle cohort*** *A) m.3243A>G level decreases with age (Linear mixed model; p<0.001, β=-0.675, SE = 0.102). Longitudinal data from 35/50 recruited individuals carrying the m.3243A>G variant. Lines connect heteroplasmy measurements taken from the same individual at different time points. Red = a decrease in variant level with age, blue = an increase in variant level with age, grey = no change. Retrospective measurements obtained from the UK Mitochondrial Patient Cohort. B) Discrepancy between muscle and blood m.3243A>G levels in 16/50 recruited individuals. Muscle m.3243A>G levels are significantly higher than blood (Linear mixed model; p<0.001, β=49.563, SE=3.59). Lines connect measurements from the same individual.*

### 3.3.2 Measurement of m.3243A>G level in haematopoietic cell types

To establish whether m.3243A>G mosaicism can be observed between different cell populations in the blood, I measured m.3243A>G level in 15 different cell populations. This revealed a range of m.3243A>G levels across different cell types per individual, with a clear difference between lymphoid and myeloid cells. When compared to the variant level of the most immature cell type investigated, the CD34+ progenitor cell, six populations had a significantly reduced m.3243A>G level: Memory B cells, Naïve CD4+ T cells, Memory CD4+ T cells, Naïve CD8+ T cells, Memory CD8+ T cells and granulocytes (**Figure 3.4)**. This includes a large proportion of lymphoid cells particularly, all cells of the T cell compartment (linear mixed model; reduction range = 11.51–19.05%, P-values < 0.0001). As many of the cell types investigated had a m.3243A>G level similar to that of the whole blood measurement, these results suggest that the decline in variant level with age was occurring in all cell types investigated and may be enhanced in the T cells.

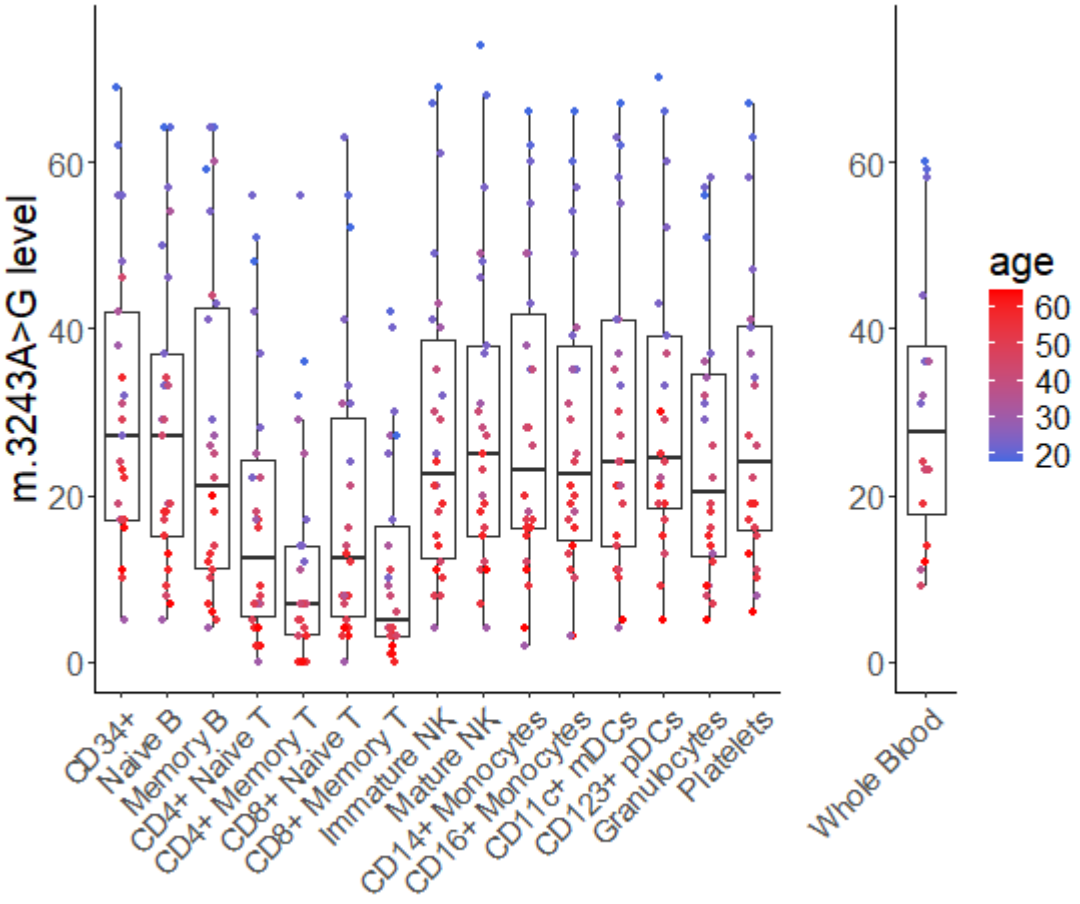


***Figure 3.4 The T cell compartment has significantly decreased m.3243A>G levels***. *Each point represents ~1000 cells per individual (n=26). Points are coloured according to patient age. Comparisons relative to CD34+ progenitor population via linear mixed model (accounting for patient as a fixed effect) identify 6 populations as having a significantly lower m.3243A>G level to this population. CD4+ memory: $\beta = -18.62$, SE = 1.63, $P < 0.0001$; CD8+ memory: $\beta = -19.05$, SE = 1.63, $P < 0.0001$; CD4+ naïve: $\beta = 12.66$, SE = 1.63, $P < 0.0001$; CD8+ naïve: $\beta = -11.51$, SE = 1.63, $P < 0.0001$, memory B cells: $\beta = -3.55$, SE = 1.63, $P = 0.0303$ and granulocytes: $\beta = -5.58$, SE = 1.67, $P = 0.0009$.*

### 3.3.3 Selection enhanced in the T cell compartment.

m.3243A>G level was consistently decreased in T cells; 25/26 donors exhibited this trend. (**Figure 3.4**). P18 naïve T cells were the only to deviate from this (WB = 36%, CD34+ = 27%, CD4+ naïve T = 28%, CD8+ naïve. = 31%,**Figure 3.5**). This phenomenon is consistent across both CD4+ and CD8+ T cells, suggesting that selection against m.3243A>G may be enhanced within the T cell compartment and arise before the generation of single positive cells. Further to this, the heteroplasmy of m.3243A>G as measured in the naïve cells is significantly higher than in their memory counterparts (CD4+: P = 0.0069; CD8+: P = 0.0001), indicating that the transition from naïve to memory states further enhances selection against the m.3243A>G variant. Remarkably, in 50% of individuals the m.3243A>G variant was almost undetectable in memory T cells (<5%).

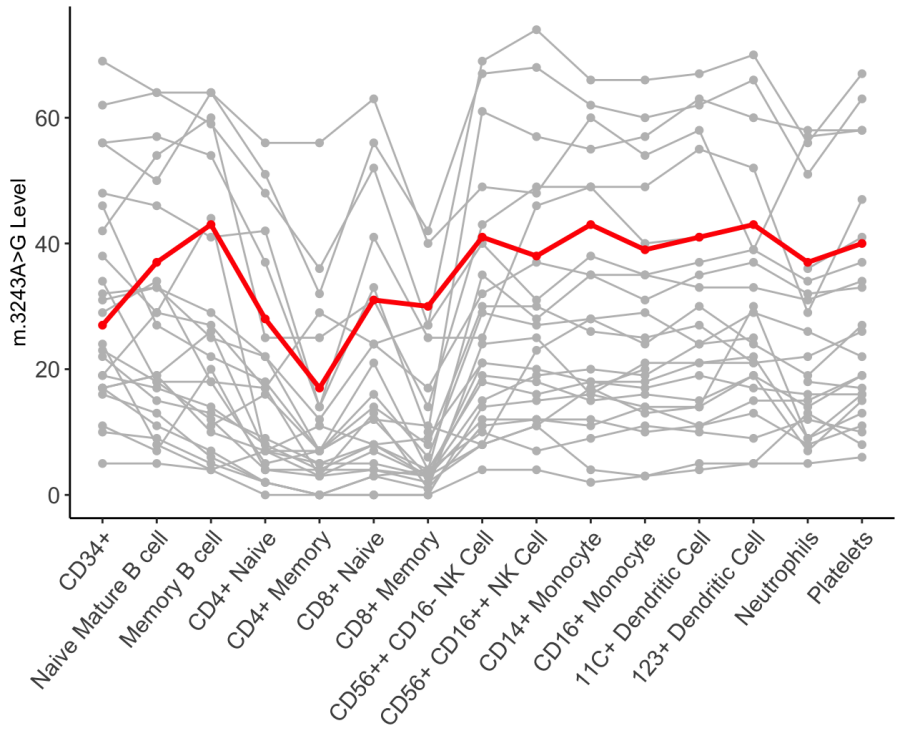


**Figure 3.5** ***Only one individual did not show a reduced m.3243A>G level in naive T cells.*** *Samples from the same individual joined by a line, P18 highlighted in red.*

To understand how this related to the age-related decline observed at a whole blood level, I examined the trends with age stratified by cell type. This analysis exhibited a clear negative relationship with age in all populations investigated (P-value range = <0.0001–0.0002; **Figure 3.6**), demonstrating that all cell types show evidence of negative selection. These data demonstrate a differing gradient between memory and naïve cells when compared to age. m.3243A>G levels are typically lower in memory cells indicating that selection pressures remain at low m.3243A>G levels, albeit at a weaker intensity. These data, combined with those presented in **Figure 3.4**, indicate that the whole blood decline in m.3243A>G level is occurring in all cell types and is not being driven by a single cell type. T cells are decreased compared to CD34+ cells but the remaining cell types have a variant level consistent with whole blood measurements.

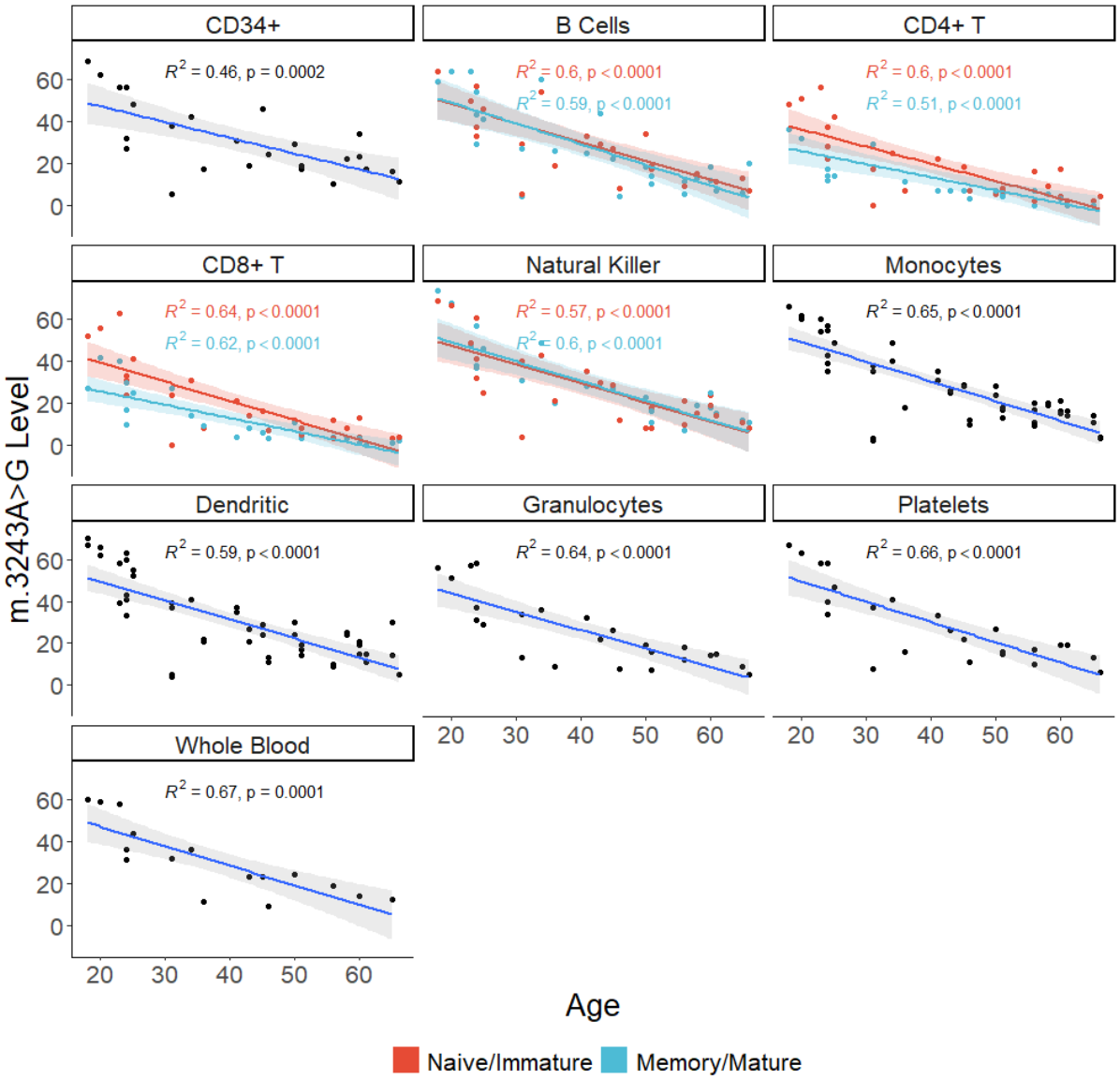


**Figure 3.6** ***m.3243A>G levels in all haematopoietic populations show a negative correlation with age***. *Each point in populations. CD34+ - dendritic represents measurements taken from ~1000 cells from a single donor (n=26), granulocytes and platelet measurements are taken from a large pellet isolated during density centrifugation and whole blood from DNA extracted from 200ul of whole blood. Lines according to linear models with 95% confidence intervals; adjusted R2 and P-values are shown per population, blue lines represent immature subsets and red, mature.*

### 3.3.4 Investigations into a relationship between m.3243A>G level and mtDNA copy number.

Data presented in 3.3.2 indicate that the T and memory B cells are responding differently to the other immune subsets to m.3243A>G. To understand if this was related to changes in mtDNA CN, I compared the mtDNA CN to m.3243A>G level in each cell type investigated. These comparisons show no relationship between m.3243A>G level and mtDNA CN in the CD34+ progenitor cells and myeloid cells. There are strong positive correlations in the B cells ($p = 0.0085$), CD4+ T cells ($p = 0.0005$), CD8 + T cells ($p = 0.0001$) and NK cells ($p = 0.017$) (**Figure 3.7**). This correlation is restricted to cells of the lymphoid lineage, suggesting these cells may be responding to m.3243A>G differently to the myeloid cells.

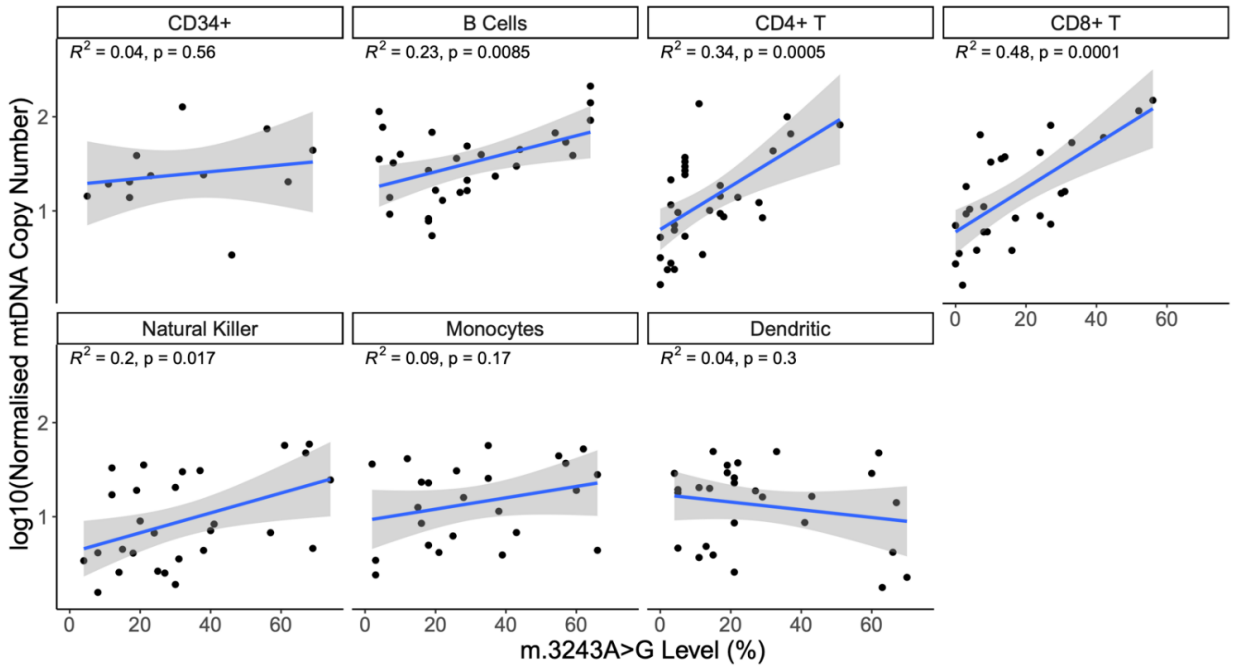


***Figure 3.7 Relationship between m.3243A>G level and mtDNA CN.*** *Patient lymphoid cells show a positive relationship with m.3243A>G level. (linear mixed model; B cells: β=0.0096, SE=0.0034, p=0.0085; CD4+ T cells: β=0.0229, SE=0.0059, p=0.0005; CD8+ T cells: β=0.0234, SE=0.0049, p=0.0001; NK cells: β=0.0106, SE=0.0041, p=0.0169). Each point represents ~1000 cells isolated via FACS.*

This led me to investigate if the above resulted in a deviation in mtDNA CN from control levels by comparing mtDNA CN per cell type in patients and controls. I detected no significant difference between mtDNA CN in patients and controls across the immune populations analysed (**Figure 3.8**; FDR adjusted P>0.05). The CD11c+ mDCs initially had a mtDNA CN which was significantly different between patients and controls (p = 0.0186), however this did not remain significant after correcting for multiple testing.

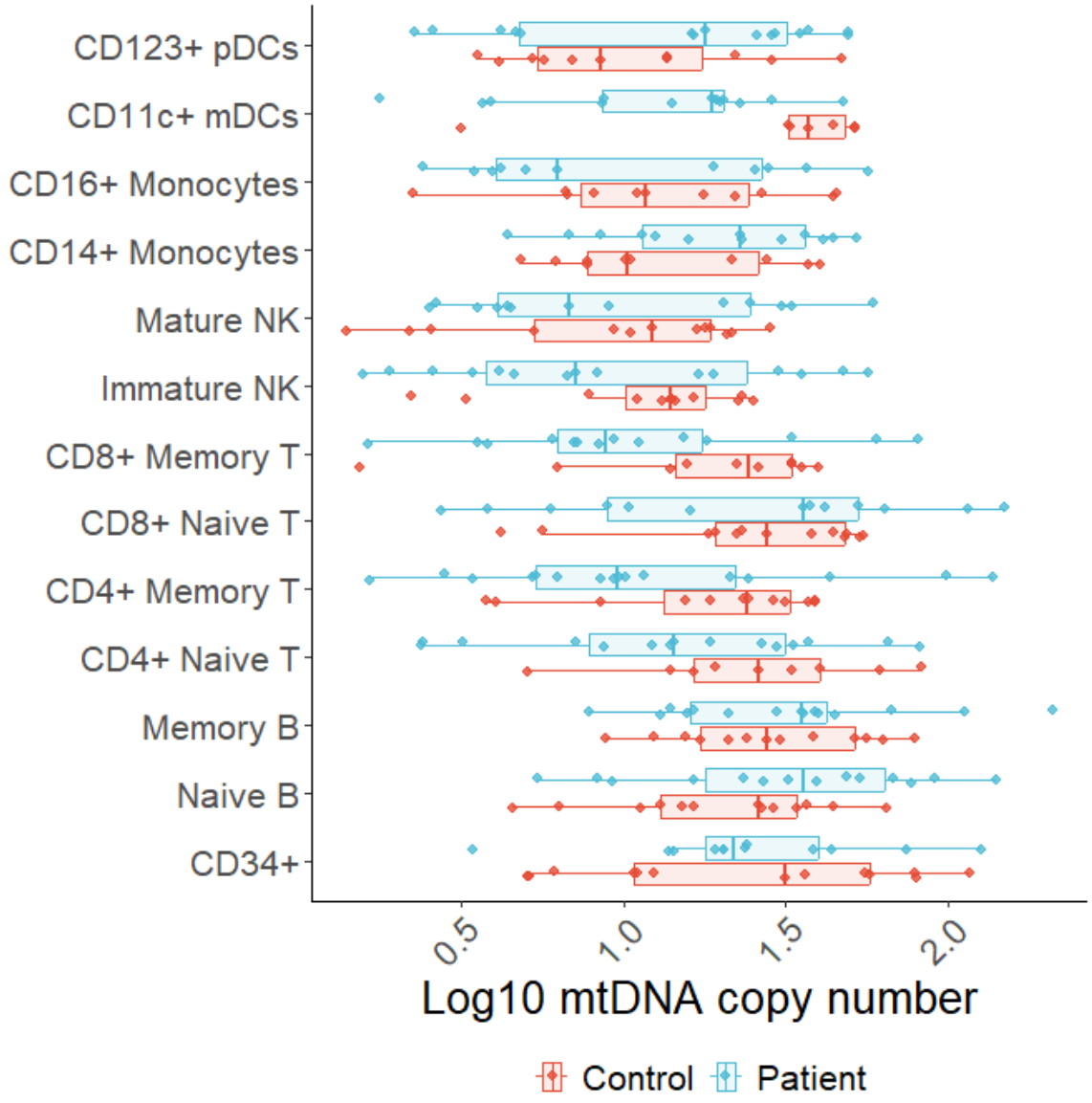


**Figure 3.8** ***mtDNA copy number in patients (blue) and controls (red).*** *Each point represents the mtDNA CN calculated from lysate of ~1000 cells per sample. The control and patient samples in each cell type were compared via Wilcoxon test, patient CD11C+ mDCs had a mtDNA CN significantly lower than controls (P = 0.0186), however, there was no significant differences between the two in all cell types when adjusted for multiple tests (P = 0.2418).*

As mentioned above, mtDNA CN is known to alter with age, therefore it was important to understand this relationship in the control population to determine whether m.3243A>G was driving these cell specific trends. Within my control cohort there was no relationship between mtDNA CN and age (linear mixed model, P = 0.2133; **Figure 3.9A**), however in the patient cohort, there was a clear negative relationship (linear mixed model; β = −0.0121, SE = 0.0031, P = 0.0017). This was consistent with a significant increase in mtDNA CN with m.3243A>G level (**Figure 3.9B**; P = 0.0263). As m.3243A>G level decreases with age, these findings further support the idea that the presence of m.3243A>G alters mtDNA CN; younger individuals with higher m.3243A>G levels have a high mtDNA CN. This may be due to cells compensating for m.3243A>G induced dysfunction by increasing mtDNA CN.

To investigate this further, I stratified the data according to cell type and compared changes with age in cases and controls. Consistent with the combined data in **Figure 3.9**, 7/8 lymphocyte populations did not show a relationship with age in controls. The eighth population: CD8+ T cells, show a positive relationship with age (**Figure 3.10**; linear mixed model, p = 0.0100). This contrasts with patient lymphocytes, which all show a significant negative relationship with age (**Figure 3.10**; CD4+ T: β=0.0229, P = 0.005. CD8+ T: β = 0.234, p=0.0001. B Cell: β=0.0096, p=0.0085. NK cell: β=0.0106, p=0.0169*),* indicating that m.3243A>G is influencing mtDNA copy number. Segregation of the lymphoid and myeloid lineages may suggest that cells from these lineages respond differently to the m.3243A>G variant and lymphoid lineages may require more compensation.

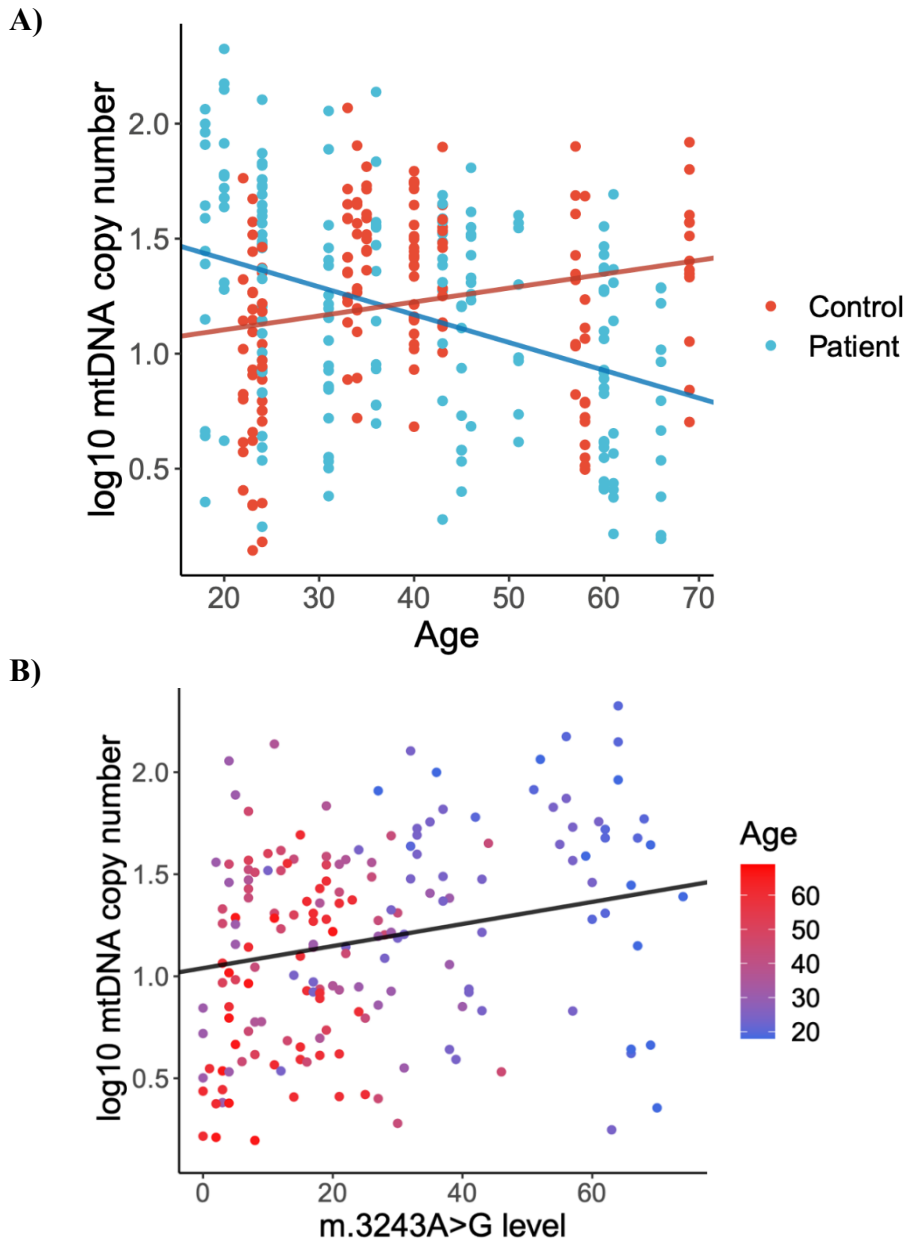


***Figure 3.9 Absolute mtDNA CN increase with age in patients but not controls***. *Each point represents mtDNA CN calculated from lysate of ~1000 cells. A) Comparison of log10 mtDNA CN and age in patients (blue) and controls (orange). Patient samples show a negative correlation with age (linear mixed model; β = −0.0121, SE = 0.0031, P = 0.0017), whereas samples from controls show no significant relationship (P = 0.2133). B) log10 mtDNA CN is positively correlated with mtDNA CN (linear mixed model; β = 0.0054, SE = 0.0024, P = 0.0263). Points are coloured by age.*

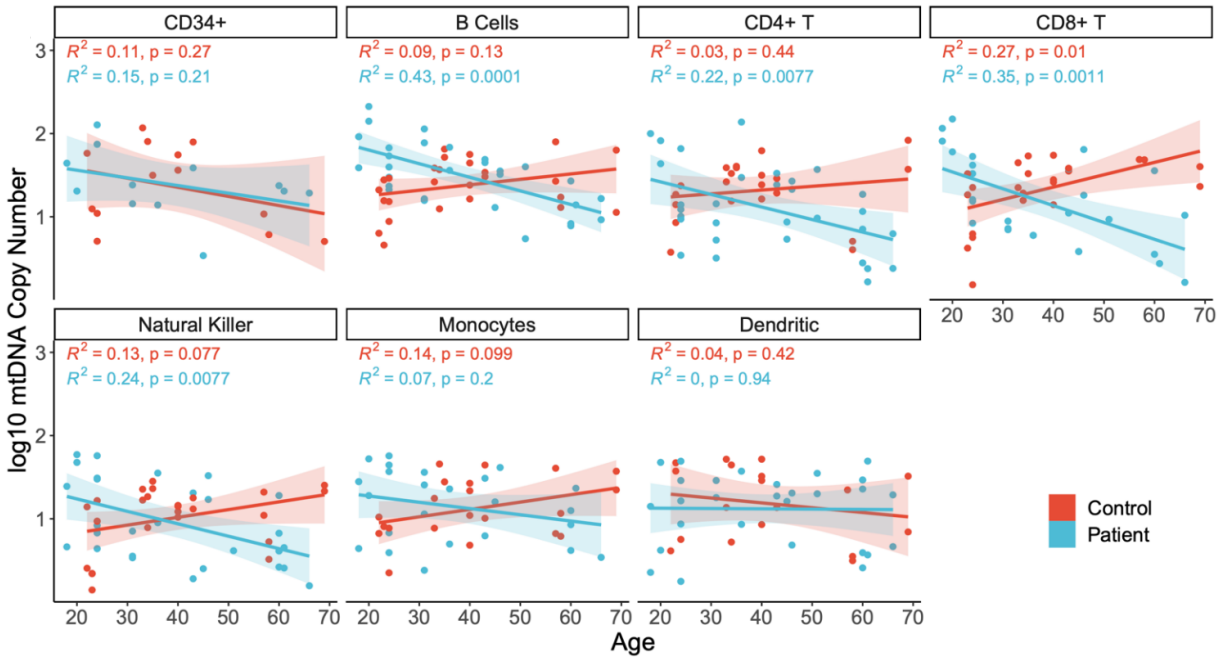


***Figure 3.10 Strong positive correlation between age and mtDNA CN in lymphoid cells from patients***. *Each point represents ~1000 cells isolated via FACS. Lymphoid cells show a negative correlation with age in patients (blue) as determined by linear mixed model (B cells: β=-0.0163, SE=0.0036, p=0.0001, CD4+ T cells: β=-0.0151, SE=0.0053, p=0.0077, CD8+ T cells: β=- 0.0202, SE=0.0055, p=0.0011 and NK cells: β=-0.0149, SE=0.0052, p=0.0077) but not in controls (orange). CD8+ T-cells show the opposite trend in controls (β=0.0149, SE=0.0053, p=0.0102).*

### 3.3.5 Comparisons with other heteroplasmic mtDNA variants

Due to the consistency in the trends seen across T cells carrying m.3243A>G, I sought to understand if this was unique to m.3243A>G or a cell-specific response to any pathogenic mtDNA.

#### 3.3.4.1 tRNA variants

##### 3.3.5.1.1 m.8344A>G

Unlike m.3243A>G, levels of m.8344A>G are thought to remain stable in blood as individuals age. Therefore, m.8344A>G was chosen as a comparison in which no selection was anticipated. Surprisingly, memory T cells displayed a reduced level of m.8344A>G pathogenic mtDNA relative to the CD34+ cells (**Figure 3.11**; linear mixed model accounting for patient as a fixed effect; CD4 memory: $\beta = -20.25$, SE = 3.63, $P < 0.0001$; CD8 memory T: $\beta = -29.5$, SE = 3.63, $P < 0.0001$). As did the memory B cells ($\beta = -11.25$, SE = 3.63, $P = 0.0038$) and granulocytes ($\beta = -7.75$, SE = 3.63, $P = 0.0400$), two cell types of interest which were also highlighted as showing enhanced selection in m.3243A>G investigations.

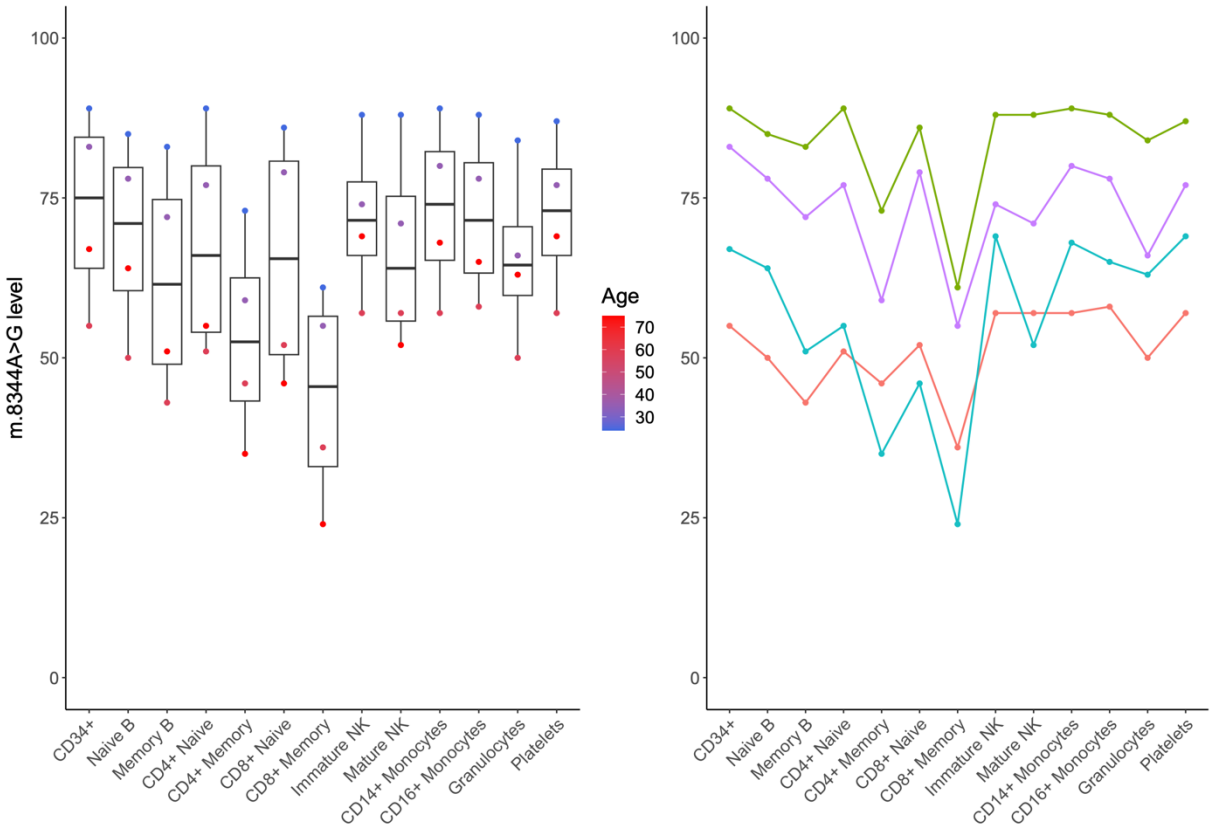


***Figure 3.11 Memory T cells have reduced m.8344A>G levels relative to CD34+ progenitor cells***. *Each point in cell types CD34+ - CD16+ monocytes represent m.8344A>G level measured from lysate of 1000 sorted cells per patient (n=4). m.8344A>G level of granulocytes and platelets determined from lysate of pellets isolated via density centrifugation of whole blood. A) Memory lymphoid cells and granulocytes possess a m.8344A>G-level significantly reduced from the CD34+ precursor cells (linear mixed model accounting for patient as a fixed effect; CD4 memory: $\beta = -20.25$, SE = 3.63, $P < 0.0001$; CD8 memory T: $\beta = -29.5$, SE = 3.63, $P < 0.0001$; memory B cells: $\beta = -11.25$, SE = 3.63, $P = 0.0038$; granulocytes: $\beta = -7.75$, SE = 3.63, $P = 0.0400$). B) Each population joined per patient to demonstrate consistent decline in memory T m.8344A>G across all samples.*

#### 3.3.5.1.2 Other tRNA Variants

Together, the m.8344A>G and m.3243A>G data suggest a cell specific response to pathogenic mt-tRNA variants. To determine whether enhanced negative selection in T cells is a property of all pathogenic mt-tRNA variants I sequenced cells from samples with the following variants: m.12258C>A (mt-tRNA$^{Ser}$/*MT-TS2*), m.14709T>C (mt-tRNA$^{Glu}$/*MT-TE*), m.3252A>G (mt-tRNA$^{Leu(UUR)}$/*MT-TL1*) and m.5703G>A (mt-tRNA$^{Asn}$/*MT-TN*). Many of these variants are incredibly rare, meaning that recruitment of more than a single individual is difficult, however, some interesting observations can be made.

Only one of the four additional variants displayed a decreased variant level within the memory T cells: m.5703G>A (**Figure 3.12;** *purple*). This sample was more consistent with the trends observed within m.8344A>G as we do not see a significant reduction in m.8344A>G level in the naïve T cells, unlike m.3243A>G. This could be a consequence of the reduced power of the m.8344A>G and m.5703G>A investigations.

m.3252A>G is found within the same gene as m.3243A>G, therefore there was an expectation that negative selection would be observed. However, this was not the case; both CD8+ and CD4+ memory cells presented with a variant level higher than their naïve counterparts (**Figure 3.12**, *orange*). It is possible that this is unique to this individual or timepoint; recruiting additional individuals with m.3252A>G would be required to understand this further.

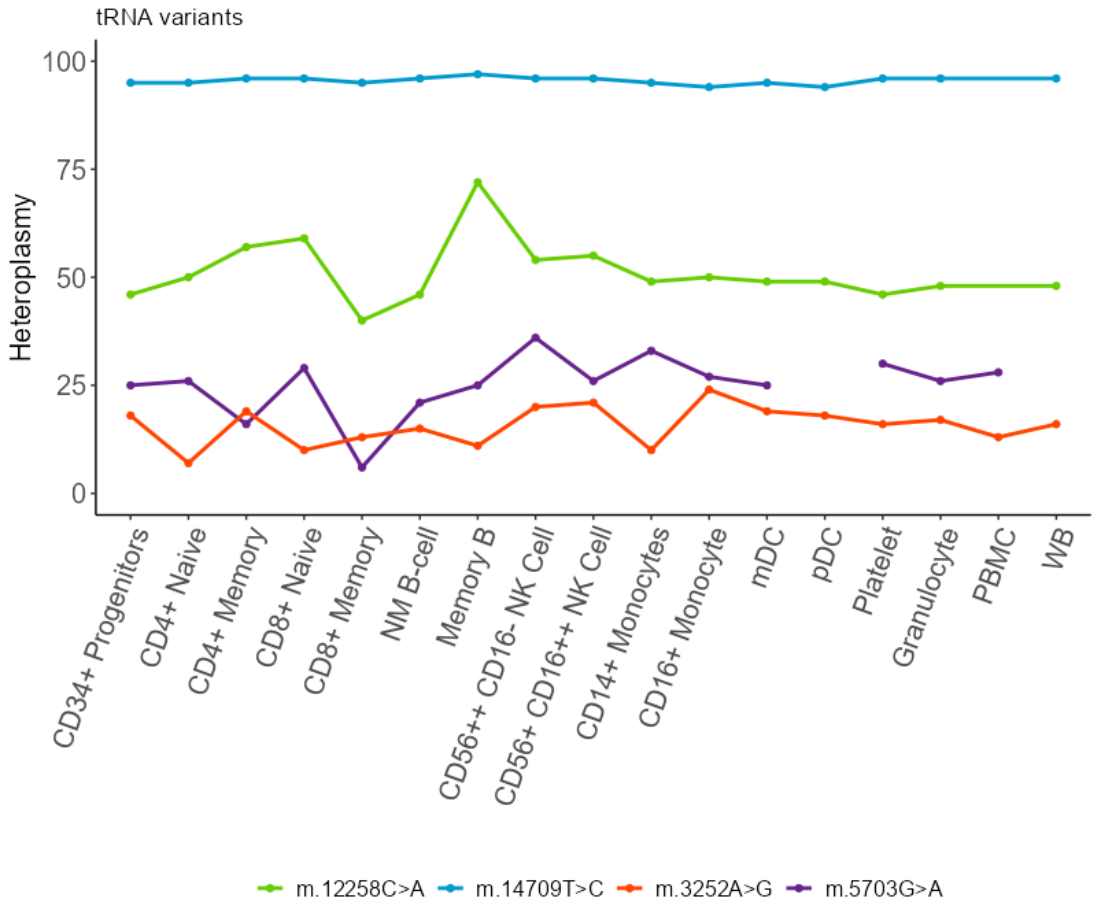


***Figure 3.12 Cell-type specific selection is not observed in all mt-tRNA variants investigated***. *Each point in cell types CD34+ - CD16+ monocytes represent variant level measured from lysate of 1000 sorted cells per patient (n=4). heteroplasmy of PBMC, granulocytes and platelets were determined from lysate of pellets isolated via density centrifugation of whole blood. Whole blood (WB) heteroplasmy is determined from DNA extracted from 200ul whole blood. Points from the same individual are joined and coloured according to individual and variant. Reduced levels in memory T cells are only observed in m.5703G>A.*

### 3.3.5.2 Protein coding variants

Building on this, I investigated the following protein-encoding variants: m.13051G>A (*MT-ND5*), m.15699G>A (*MT-CYB*), m.9035T>C (*MT-ATP6)*, m.9185T>C (*MT-ATP6).* Heteroplasmy of all variants remained similar between different cell types and no T cell specific effect was observed. The average observed variation between cell types was much lower in protein coding variants (+/- 9%) than tRNA variants (+/- 45%) (**Figure 3.12 & Figure 3.13**). This suggests that the investigated protein coding variants may be less impactful than mt-tRNA variants on cell viability or mitochondrial function and therefore are under less selection pressure.

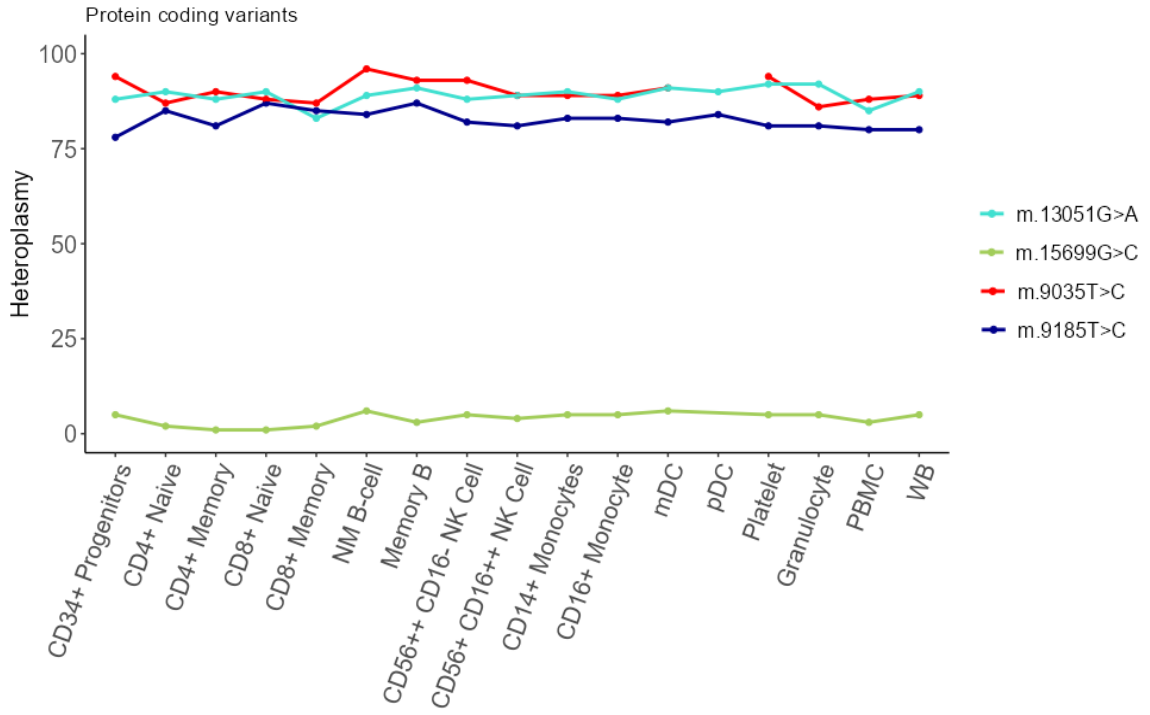


***Figure 3.13 Heteroplasmy in different immune cell populations is consistent in protein-coding mtDNA variants****. Each point in cell types CD34+ - CD16+ monocytes represent variant level measured from lysate of 1000 sorted cells per patient/variant. Heteroplasmy of PBMC, granulocytes and platelets were determined from lysate of pellets isolated via density centrifugation of whole blood. Whole blood (WB) heteroplasmy is determined from DNA extracted from 200ul whole blood. Points from the same individual are joined and coloured according to variant.*

Though the range of variants is limited, and the sample size is small, therefore this requires further exploration. Protein coding variants generally remain stable in the blood tissue, with stable longitudinal measurements and blood tissue levels that are concordant with muscle. Retrospective data from P36 (m.15699G>C) is indicative of negative selection as measurements taken 19 years apart demonstrate an 8% decline (13% at 39 years and 5% at 58 years). Analysis of measurements taken from four tissues in 2003 demonstrate highly disparate values between muscle and three mitotic tissues, 90% of mtDNA in muscle was affected by m.15.699G>C compared to 13% in blood and 14% in hair follicles (**Table 3.4**). Recruitment of further individuals with this variant would aid in the understanding of a potential segregation mechanism here as it is possible this phenomenon is restricted to a single individual.

| ***Variant*** | ***Tissue Heteroplasmy (%)*** | | | | |
|---|---|---|---|---|---|
| | **Muscle** | **Blood** | **Urine** | **Buccal** | **Hair Follicle** |
| ***m.15699G>C*** | 90 | 13 | 16 | | 14 |
| ***m.5703G>A*** | 46 | 30 | 44 | 57 | |
| ***m.8344A>G*** | 90 | 71 | 78 | | |
| ***m.9185T>C*** | 98 | 100 | | | |

***Table 3. 4 Heteroplasmy readings in mitotic and post mitotic tissues in tRNA and protein coding variants****. Each line represents multiple tissue sample taken from the same individual. Post mitotic and mitotic tissues are similar in m.9185T>C a protein coding variant, but lower in the mitotic tissues of tRNA variants showing negative selection in the T cell compartment (m.5703G>A and m.8344A>G). m.15699G>C is a protein coding variant which shows highly disparate mitotic and post mitotic heteroplasmy values, suggesting selection.*

## 3.4 Discussion

In this chapter, I have shown that m.3243A>G levels decline in blood cell subsets with age, indicating that selection is taking place in all cells investigated. Cells of the T cell compartment, memory B cells and granulocytes have a significantly lower m.3243A>G level relative to the CD34+ progenitor cells, which is further enhanced in the memory T cells. A decrease in m.3243A>G level in T cells with age was accompanied by a lower mtDNA copy number than in younger individuals with a higher variant level, an alteration with age that was not observed in individuals who do not harbour m.3243A>G. These data are consistent with the literature which demonstrate 'purifying selection' of the m.3243A>G variant in T cells (Walker *et al.*, 2020).

When compared to other heteroplasmic mtDNA variants, selection in the T cell compartment was identified in two tRNA variants which do not show a decline with age on a tissue level as opposed to protein coding variants which remained consistent across all cell types. This could be indicative of some mt-tRNA molecules being key in T cell fitness.

### 3.4.1 Selection observed in all cell types.

The CD34+ cells are multipotent cells found in the peripheral blood. This mixed population contains both lymphoid and myeloid progenitor cells. Interestingly, the CD34+ m.3243A>G level observed was not significantly different from the majority of immune cells. This result is consistent with the modelling proposed by Rajashima and colleagues (Rajasimha,Chinnery and Samuels, 2008a) which suggests an exponential loss of pathogenic mtDNA originating at the HSC. This model highlights the importance of asymmetric cell division in driving this loss, as when based on symmetrical divisions, the model did not produce a decline in m.3243A>G consistent with longitudinal patient data. Some lymphoid populations, in addition to stem cells, are capable of undergoing asymmetric cell division (Borsa *et al.*, 2019). This could explain the enhanced loss observed in T cells.

### 3.4.2 Unique trends in T cells

Unlike the other cells investigated, T cell precursors mature in the thymus before being released into the peripheral blood. As mentioned in the introduction, these cells are subject to a rigorous central tolerance process which involves high levels of cell proliferation and cell death (Anderton *et al.*, 1999). As selection is isolated to mitotic cells, it is likely that the observed selection is related to proliferative episodes and the metabolic changes required to transition from one cell state to another. Central tolerance could explain the reduced level of the variant in naïve cells with infection being responsible for the further loss from naïve to memory states. Only a subset of effector T cells differentiate into long-lived memory cells; their survival and function are dependent upon spare respiratory capacity, facilitated by enhanced fatty acid oxidation, and higher expression of complex I (Windt *et al.*, 2012). As a result, the transition from effector to memory cell could be a stage in which T cells with a high proportion m.3243A>G are vulnerable.

Recent research has identified asymmetric cell division to be prominent in T cells and key in the generation of memory cells (Chang *et al.*, 2007, Ciocca *et al.*, 2012, Borsa *et al.*, 2019). Using murine models, Borsa and colleagues have found that only naïve and memory cells are able to undergo asymmetric cell division and that the highly replicative effector cells and other more terminally differentiated cells divide symmetrically (Borsa *et al.*, 2019). The generation of one cell primed to become a memory cell and the other an effector cell, two cells with different metabolic need, via asymmetric cell division would require different loads of mitochondria/mtDNA. An unequal distribution of mtDNA to daughter cells has the potential to alter heteroplasmy, as discussed in section 1.5.3, a very low proportion of mtDNA can induce a bottleneck effect, producing mature cells with drastically different m.3243A>G level than the parent cell.

Preferential distribution of mitochondria upon division has been demonstrated by Adams *et al.* (2016) in which mother cells distribute mitochondria according to age. They found that one daughter cell tended to contain the majority of the ‘aged’ mitochondria (the effector cell) and the other, a more stem-like cell, contained the ‘new’ mitochondria. Aged mitochondria are likely to have endured more ROS induced damage and may be less efficient, increased ROS has also been observed in cells from individuals with

m.3243A>G (Chung *et al.*, 2021). It is possible that high heteroplasmy mitochondria are distributed in the same way as 'aged' mitochondria, leading to a memory population with low heteroplasmy. In a subsequent preprint these findings were corroborated in T cells (Borsa et al. 2024). This study utilizes a mouse model which allows specific labelling of mitochondria before and after cell division which demonstrated daughter cells with newer mitochondria were memory-like and in an autophagy deficient mouse model, the proportion of cells which lost old mitochondria dropped from 23% to 3.6%. This highlights autophagy as a key factor in asymmetric cell division and potentially, clearance of pathogenic mtDNA from the population via death of effector old cells with 'old' mitochondria (Borsa *et al.*, 2024).

Further to this, Borsa *et al.* (2019) show that the incidence of asymmetric cell division could be manipulated by modulating mTOR signaling. Transient inhibition of mTOR increased asymmetric cell division in naïve and memory states. Interestingly, enforcing asymmetric cell division in terminally differentiated cells increased cells' memory potential indicating that T cell fate is highly reliant on metabolism. Similar transitions into a more stemlike memory state can be observed when manipulating mitochondrial fusion protein, OPA1 (Buck *et al.*, 2016). Pharmacological mTOR inhibition has also been proven to decrease m.3243A>G heteroplasmy in fibroblasts, perhaps through a similar mechanism (Chung *et al.*, 2021).

### 3.4.3 m.3243A>G influences mtDNA CN

Mengel-Fron *et al* demonstrate that loss of mtDNA in the blood begins midway through life (~50yrs), and using longitudinal data, reported an average loss of 12.7 mtDNA copies over 10 years in a cohort of 108 individuals (Mengel-From *et al.*, 2014). The majority of participants and controls in my investigations are <50, therefore I am unlikely to see a similar relationship. They also found that a decrease in mtDNA levels coincides with worsening health outcomes: lower mtDNA CN was associated with high mortality. mtDNA CN measurements in the m.3243A>G cohort have a strong relationship with age, driven by cells of lymphocyte lineage (T, B & NK cells). It is possible that the high variant level, common in younger individuals, induces a compensatory increase in mtDNA CN specific to cells of this lineage. A higher mtDNA CN in skeletal muscle

coincides with a lower NMDAS in patients and higher oxygen consumption in cybrid cells, giving support to the notion that an increase in mtDNA copy number improves m.3243A>G-induced defects (Bentlage and Attardi, 1996, Grady *et al.*, 2018). Lymphocytes were also highlighted as efficient at selecting against m.3243A>G; the strong response of these cells to the presence of the variant implies a different mechanism of selection, perhaps due to a vulnerability to the effects of the pathogenic mtDNA and the high proliferative demand.

Like the lymphocytes, the granulocytes showed consistently reduced variant levels in both m.3243A>G and m.8344A>G samples but are not cells of the lymphoid lineage. As granulocytes were isolated directly at the lymphoprep stage, rather than via FACS, cell number could not be estimated using the number of cells sorted. mtDNA CN estimations would not be comparable as a different methodology would have to be used. This isolation procedure also means that the granulocyte population is a mixed population which has the potential to be contaminated with other cell types such as lymphoid cells. Further research into pure neutrophil, basophil and eosinophil populations are important to gauge whether there is enhanced selection within this population and a similar relationship between mtDNA CN and age.

### 3.4.4 Selection is not universal.

This chapter has demonstrated that not all mtDNA variants show negative selection in the T cells. It is possible that the variants showing selection are having an impact on cell function, a cell's ability to proliferate or a cell's ability to switch between different forms of metabolism.

Upon antigen stimulation, a shift to glycolysis is key to efficient T cell activation, however, OXPHOS still plays a role to maintain the adaptive response. Deficiency of complexes I and IV, as observed in m.3243A>G, impairs T cell activation/proliferation (Yi *et al.*, 2006b, Tarasenko *et al.*, 2017b, Vardhana *et al.*, 2020b). As m.3243A>G is theorised to result in the misincorporation of amino acids in mitochondrially encoded proteins, it has the potential to cause instability in all OXPHOS complexes aside from

complex II (Sasarman,Antonicka and Shoubridge, 2008). A high cellular replicative demand, such as that seen during T cell activation would induce high levels of mitochondrial protein synthesis to generate viable daughter cells. High levels of unstable complexes could explain why selective pressures are stronger in pathogenic tRNA variants as these are likely to have global effect whereas protein-coding variants are restricted to a single molecule. This is supported by the notion that many of the protein coding variants investigated occur in a homoplasmic state within blood, something that has not been reported with m.3243A>G.

The notion of a global impact also supports a reduction in m.3243A>G level from naïve to memory T cell state as, in their effector cell state, T cells are highly glycolytic and are not primed to become memory cells (Borsa *et al.*, 2024). The shift to OXPHOS required to differentiate into a memory T cell could result in these cells becoming apoptotic.

## 3.5 Concluding Remarks

The investigations outlined in this chapter have identified that negative selection of m.3243A>G is occurring in all PBMC subsets. I have identified T cells to have a significantly lower variant level than progenitor cells, a phenomenon which is consistent with ATAC-seq data described by Walker and colleagues (Walker *et al.*, 2020). This research is the first to identify that this reduction is enhanced in the memory T cells and to identify a similar phenomenon in T cells carrying m.8344A>G. Further to this, I have identified a strong relationship between mtDNA CN and age in lymphoid cells but not myeloid cells, indicative of differing mechanisms of selection within these lineages.

As whole tissue m.3243A>G level does not fully represent levels within individual cells, it is important to investigate the variant level in single cells. The distribution of heteroplasmies within each cell population will help to understand the process of negative selection, for example, the absence of any memory T cells with a high m.3243A>G level would support findings by Borsa *et al.* (2019).To understand the level of variability further and understand the dynamics of selection, I chose to investigate the m.3243A>G level within these populations by sequencing the mtDNA of single cells.

# Chapter 4 Distribution of m.3243A>G levels within immune cell populations

## 4.1 Introduction

### 4.1.1 m.3243A>G mosaicism

Different tissues within the same individual possessing m.3243A>G present with diverse levels of pathogenic mtDNA. This difference can be stark, as evident in the large variation between muscle and blood heteroplasmy (de Laat *et al.*, 2012, Grady *et al.*, 2018). Post-mortem studies investigating m.3243A>G levels in a multitude of tissues reveal huge variation across these, for example, Scholle and colleagues recorded a near 27% difference in m.3243A>G measurement between kidney and tissues of the nervous system (Hamazaki,Koshiba and Sugiyama, 1993, Scholle *et al.*, 2020).

This mosaicism extends further, within the tissues themselves, where different cells making up a tissue can possess vastly different proportions of pathogenic mtDNA. Investigations into individual skeletal muscle fibres have demonstrated that fibres within the same muscle can differ in m.3243A>G level (Karppa *et al.*, 2005). This is reflected in the respiratory capacity of the fibre as measured by COX-SDH staining; a number of studies have observed a higher m.3243A>G level in fibres with COX deficiency (Petruzzella *et al.*, 1994, Tokunaga *et al.*, 1994, Karppa *et al.*, 2005).

Mosaicism can also be observed in murine models of mtDNA disease. There are few *in vivo* models of mt-tRNA disease, the most comparable to m.3243A>G is a murine model presenting with a variant at m.5024C>T ($tRNA^{Ala}$). Similar to m.3243A>G patients, these mice tend to have mild cardiomyopathy and an inability to gain weight (Kauppila *et al.*, 2016) and like the m.3243A>G variant, the m.5024C>T variant in the mouse exhibits purifying selection in the T cells (Zhang *et al.*, 2023). An elegant study into the single cell m.5024C>T heteroplasmy of a post mitotic tissue: the brain, and a mitotic tissue: the spleen, revealed a wide range of m.5024C>T level cells in both (interquartile range (IQR): 40.5 to 75% for the brain and 35.75 to 67% for the spleen). There was an increase in variance with a shift towards cells with 0% as the mice aged in both tissues consistent with a decrease in bulk tissue m.5024C>T level with age (Glynos *et al.*, 2023).

### 4.1.2 Theories behind changes in heteroplasmy

There is debate as to whether the decline in pathogenic mtDNA levels with age is occurring intracellularly; for example, via a mechanism which actively degrades or

releases pathogenic mtDNA or at the level of the cell, i.e., the loss of cells with a high load of pathogenic mtDNA.

A main contributor to changes in pathogenic mtDNA load is the aforementioned distribution of mtDNA upon cell division. The production of daughter cells with differing heteroplasmy can occur as a result of random segregation of mtDNA molecules as well as the asymmetric mechanisms outlined by Borsa *et al.* (2019). The Osman group used a yeast model to trace the distribution of two fluorescently labelled mtDNA molecules, and concluded that a main driver in alterations in heteroplasmy during cell division is the transmission of a limited number of mtDNA copies to daughter cells (Roussou *et al.*, 2024). This effect was particularly prevalent in cells with low mtDNA CN, while an increased mtDNA CN resulted in slower establishment of homoplasmy. When crossed with DNM1 knockout (KO) strains, they found that the absence of fission induced increased the occurrence of homoplasmic cells supporting the notion of asymmetric distribution of mtDNA distribution drives heteroplasmy. As discussed in section 1.5.3, the mitochondrial genetic bottleneck is highly dependent on a decrease in mtDNA CN.

Recent work by Kotrys and colleagues into understanding negative selection of CI variants (both silent and missense) in DdCBE edited HEK293T cells, revealed that selection of a variant *in vitro* depends on the environment. Maintenance of a high population heteroplasmy could be induced by placing cells in a hypoxic environment, however proliferation of these cells was limited. Placing cells in a glucose rich environment was accompanied by high levels of proliferation and a decline in variant levels; galactose mimicked this selection, albeit with higher levels of cell death. This research also identified the loss of high variant level lineages as the driver of overall decline in heteroplasmy, rather than intracellular selection against pathogenic mtDNA (Kotrys *et al.*, 2024). They observed no selection of the silent variant strongly suggesting a fitness advantage driving selection.

The research above focuses on mechanisms of mtDNA segregation which are dependent on cellular division. However, a number of intracellular mechanisms have also been implicated in selection against pathogenic mtDNA molecules, this includes destruction of dysfunction mitochondria which contain a high proportion of pathogenic mtDNA via mitophagy (Narendra *et al.*, 2010). PINK1 has been proposed to identify damaged mitochondria and enable parkin binding which facilitates destruction of the organelle

(Chen and Dorn II, 2013). Loss of mitochondria with high levels of pathogenic mtDNA could drive the cellular heteroplasmy down.

In addition, the presence of a pathogenic mtDNA has the potential to impact mtDNA replication, for example ATP synthase deficiency has been found to increase ROS which activates mitochondrial transcription (Fukuoh *et al.*, 2014). During relaxed replication, (Chinnery and Samuels, 1999) a differing rate of replication between WT and pathogenic mtDNA molecules could alter sub cellular heteroplasmy as is observed in the case of large deletions (Diaz *et al.*, 2002b). Although, this differing rate is likely due to the smaller size of the molecule. As immune cells have a low copy number a slight bias toward one type of mtDNA can shift heteroplasmy rapidly. Reduction of mtDNA CN to low levels in primordial germ cells has been theorised to drive the large discrepancies in inheritance of pathogenic heteroplasmic variants known as 'the mtDNA genetic bottleneck' (Floros *et al.*, 2018). The mitochondria distributed to each oocyte then replicates to levels of ~400,000 copies to facilitate embryonic expansion, thereby generating offspring with heteroplasmy levels vastly different from parent (de Laat *et al.*, 2013, Chiang *et al.*, 2020). This is consistent with Roussou *et al.* (2024) findings in which a low CN drives stark differences in heteroplasmy between parent and daughter cells.

In this chapter I will outline optimisation and implementation of a novel, high throughput sequencing assay used to estimate m.3243A>G heteroplasmy in 5,732 single cells from six patients (ages 18 – 46). Interrogation of m.3243A>G level in single cells allowed deeper understanding of the dynamics of the decline in m.3243A>G and how this differs between lymphoid and myeloid cells. Using single cell analyses I aimed to answer the following questions:

- Is negative selection a result of a gradual loss of m.3243A>G in all cells or do some cells retain a high level of m.3243A>G, as suggested with asymmetric cell division leading to cell death?
- Is there a difference between the distribution of m.3243A>G in lymphoid and myeloid cells?
- Could selection be related to cellular activity in high m.3243A>G level cells as is suggested by the Kortys *et al.* study?

## 4.2 Methods

### 4.2.1 Cohort

PBMCs from six individuals were chosen for these investigations (**Table 4. 1**); full information found in *methods (table 2.1*). Participant samples were selected to cover a range of ages and mtDNA levels, with individuals under 30 being prioritised as strong selection is still likely to be taking place.

| ***Patient ID*** | ***Age*** | ***Sex*** | ***Blood m.3243A>G level (%)*** |
|---|---|---|---|
| P22 | 18 | F | 60 |
| P19 | 20 | F | 59 |
| P10 | 24 | M | 47 |
| P18 | 24 | F | 36 |
| P15 | 45 | M | 14 |
| P17 | 46 | F | 9 |

***Table 4. 1. Samples used in single cell investigations.*** *Full demographic information presented in Table 2.1.*

### 4.2.2 Sort Strategy

Naïve and memory T cells showed a reduced m.3243A>G level when compared to the progenitor cells (Section 3.3.3). The term 'Memory' describes a mixed population of cells which includes $T_{CM}$, $T_{EM}$ and $T_{EMRA}$ cells. Each of these cell types has a different metabolism and consequently, may respond differently to the presence of m.3243A>G. Therefore, for these investigations, I chose to investigate each of these memory subsets separately, according to the gating strategy outlined in Figure 4.1.

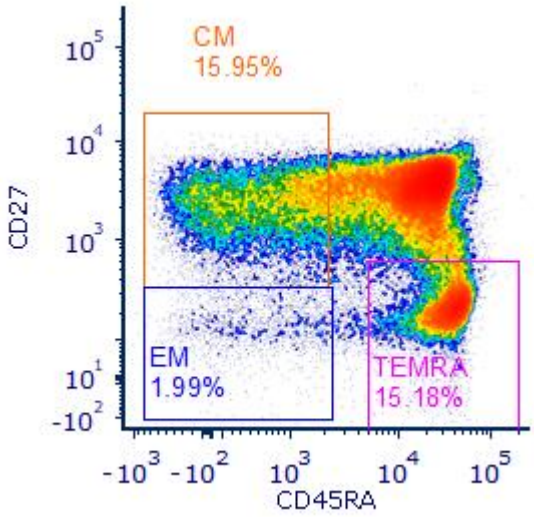


*Figure 4.1* ***Modified memory T cell gating strategy.*** *Density plot where red represents the highest density of cells and blue the lowest. Squares represent sorting gates. Orange = Central memory T cell gate, blue = effector memory T cell sorting gate and pink = T effector memory cell re-expressing CD45RA (TEMRA) sorting gate*

To give a broad understanding as to how the presence of m.3243A>G may influence cell function, Dr Paul Milne helped to design a FACS panel targeting a number of additional functional markers, chosen to identify cells exhibiting signs of activation, senescence and exhaustion. The expression or absence of these markers, combined with index sort data enabled an investigation of the relationship between m.3243A>G level and cellular activity. To maximise the number of functional and/or subset markers that could be included, each sample was split into two. All T and B subsets were isolated using panel A (**Table 4. 2**) and monocytes and CD34+ progenitor cells were isolated using panel B (**Table 4. 3**), before sequencing according to the methods summary in **Figure 4.2**.

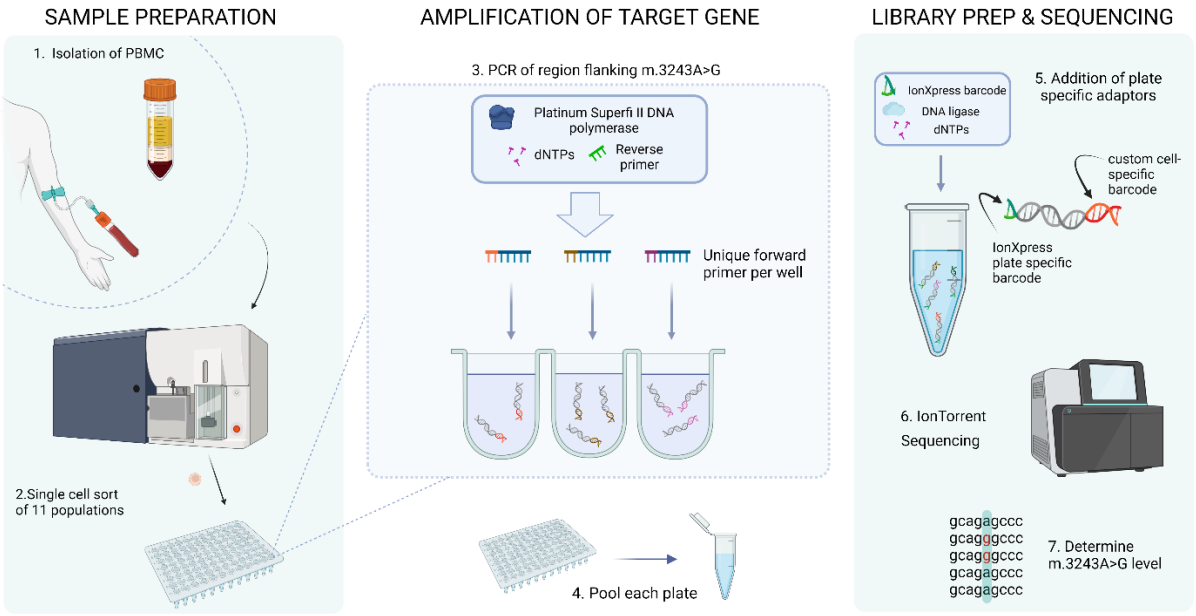


***Figure 4.2 Protocol summary for methods utilised in chapter 4.*** *PBMCs were isolated from patient samples via Lymphoprep before being stained and a single cell was sorted per well of a 96-well plate via FACS. Unique barcoded primers were used in the amplification of the MT-TL1 gene to allow identification of reads from individual cells. Each plate was pooled before plate specific adaptors were ligated and all samples were combined to form the sequencing library. This was diluted to 80pM and sequenced using the Ion S5 semiconductor sequencer. Figure generated using biorender.com.*

**Panel A: Lymphocytes**

| ***Antibody*** | *Company* | *Cat no* |
|---|---|---|
| *CD45RO FITC* | BD | 555492 |
| *CD19 PerCP-Cy5.5* | BD | 332780 |
| *CD95/FAS PE* | BioLegend | 305608 |
| *CCR7 PE-CF594* | BioLegend | 353236 |
| *CD62L PE-Cy7* | BioLegend | 304821 |
| *CD56 APC* | BD | 555518 |
| *PD-1 A700* | BioLegend | 329952 |
| *CD8 APC-Cy7* | BD | 557834 |
| *CD27 BV421* | BioLegend | 302823 |
| *CD45RA V500* | BD | 561640 |
| *CD57 BV605* | BioLegend | 393304 |
| *CD25 BV650* | Biolegend | 302633 |
| *CD4 BV711* | BioLegend | 317439 |
| *HLA-DR BV786* | BioLegend | 307642 |
| *CD3 BUV395* | BD | 563546 |
| *CD38 BUV737* | BD | 612824 |

***Table 4. 2 Ab panel used to sort single lymphoid cells.*** *3.5µl per antibody was added to a 100µl antibody mix with sort buffer.*

**Panel B: Progenitor and Monocytes**

| *Antibody* | *Company* | *Cat no* |
|---|---|---|
| *CD3 7 19 20 FITC* | BD | 345763<br>347483<br>345776<br>345792 |
| *CD141 PerCP-Cy5.5* | BioLegend | 344112 |
| *CD49F PE* | BioLegend | 313611 |
| *CD16 PE-Dazzle* | Biolegend | 302053 |
| *CD1c PE-Cy7* | Biolegend | 331516 |
| *CD34 APC* | BD | 555824 |
| *CD90 A700* | BioLegend | 328120 |
| *CD14 APC-Cy7* | BD | 557831 |
| *CD123 BV421* | BioLegend | 306018 |
| *CD45RA BV510* | Biolegend | 304142 |
| *CD117 BV605* | BD | 562687 |
| *CD10 BV650* | BD | 563734 |
| *CD33 BV711* | BD | 563171 |
| *HLA-DR BV786* | BioLegend | 307642 |
| *CD11c BUV 395* | BD | 563787 |
| *CD38 BUV 737* | BD | 612824 |

***Table 4. 3 Ab panel used to isolate CD34+ progenitor cells and monocytes.*** *3.5µl per antibody was added to a 100µl antibody mix with sort buffer.*

From this panel, progenitor subsets were identified using the antigen combinations outlined below (**Table 4. 4**):

| ***Cell subset*** | ***Markers*** |
|---|---|
| *Haematopoietic Stem Cell (HSC)* | Lin-, CD34+, CD38-, CD45RA-, CD90+, CD49f+ |
| *Multipotent progenitor (MPP)* | Lin-, CD34+, CD38-, CD45RA-, CD90-, CD49f- |
| *Lymphoid progenitor (CLP)* | Lin-, CD34+, CD38-CD45RA+, CD90- |
| *Common Myeloid progenitor (CMP)* | Lin-, CD34+, CD38+, CD45RA- |
| *Granulocyte-Macrophage Progenitor (GMP)* | Lin-, CD34+, CD38+, CD45RA+ |

***Table 4. 4 Marker expression combinations used to identify 5 different CD34+ progenitor cell subsets.***

## 4.3 Results

### 4.3.1 Protocol Optimisation

The current gold standard for estimation of m.3243A>G percentage is pyrosequencing. In section 3.3, I utilised the Qiagen pyromark Q24, a system which can sequence 24 samples per run, however, the use of this system for sequencing a large number of samples is time consuming and expensive. To negate this, I optimised a high throughput sequencing protocol on the IonTorrent Ion S5 using barcoded m.3243A>G primers designed by Dr Oliver Russell.

The basis of this experiment relied on sufficient and faithful expansion of the *MT-TL1* gene. Amplification of mtDNA from a single cell, although more abundant than nDNA, often requires two rounds of amplification using nested primers. Subjecting amplicons to more than one PCR increases the likelihood of sequencing errors, non-specific binding and carryover contamination, further to this, it significantly increases hands-on time. Amplification using a nested technique gave inconsistent results which sometimes produced long off-target amplicons or poor amplification depending on the efficacy of the first reaction (**Figure 4.3**).

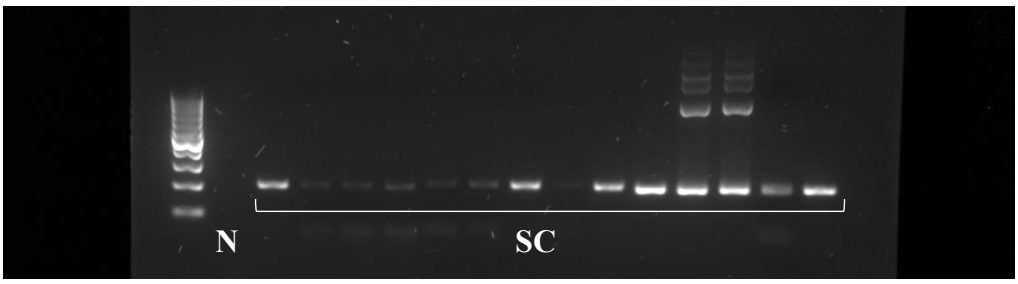


***Figure 4.3 Electrophoresis image showing the range of amplification success using a nested approach to amplify MT-TL1.****Lane one contains a 100bp ladder, N = DNA free negative control, SC = lysate from single cells*

To increase the efficacy and time efficiency, I used a high fidelity taq polymerase: Platinum superfi II taq polymerase in a 20 µl reaction (**Table 4. 5**, *original reaction*). I began by optimising polymerase concentration, cycling conditions and lysate concentration. To investigate the optimal but also most cost-effective concentration of

polymerase required to amplify mtDNA from single cells I used a serial dilution, halving the concentration of the enzyme each time, beginning with 1x unit (0.4 µl). These investigations revealed sufficient amplification of control DNA with half a unit (0.2 µl) of polymerase at 30 cycles of the conditions outlined in section 2.12. These cycling conditions, however, were not sufficient to amplify mtDNA from single cell lysate, at minimum, 35 cycles were required to produce detectable bands on an agarose gel from 5µl of cell lysate.

| ***Reagent*** | ***Original reaction x1 (µl)*** | ***Optimised reaction x1 (µl)*** |
|---|---|---|
| *Buffer* | 4 | 7 |
| *Barcoded Forward Primer* | 5 (2µM) | 2 (10µM) |
| *Reverse Primer (10µM)* | 1 | 2 |
| *dNTP (10µM)* | 0.4 | 0.7 |
| *Platinum superfi II Taq Polymerase* | 0.2 | 0.35 |
| *dH2O* | 4.4 | 7.95 |
| *lysate* | 5 | 15 |

***Table 4. 5 Original and optimised PCR mastermix used to amplify MT-TL1 gene in sequencing run 1.***

Sequencing of the amplicons using the Ion S5 system was successful. To validate the given heteroplasmy estimates, a second 5µl aliquot from the same lysate was sequenced via pyrosequencing; unfortunately, this highlighted large discrepancies between the two measurements (**Figure 4.4A**). Such inconsistencies were not observed in the positive controls which contain ~100 cells. From this, I concluded that using a small fraction of the cell lysate rather than the entire single cell induced a sampling bias, akin to a bottleneck effect, and that a 5µl sample was not representative of the whole cell. This is likely due to the low mtDNA copy number of immune cells, as demonstrated in section 3.3.4.

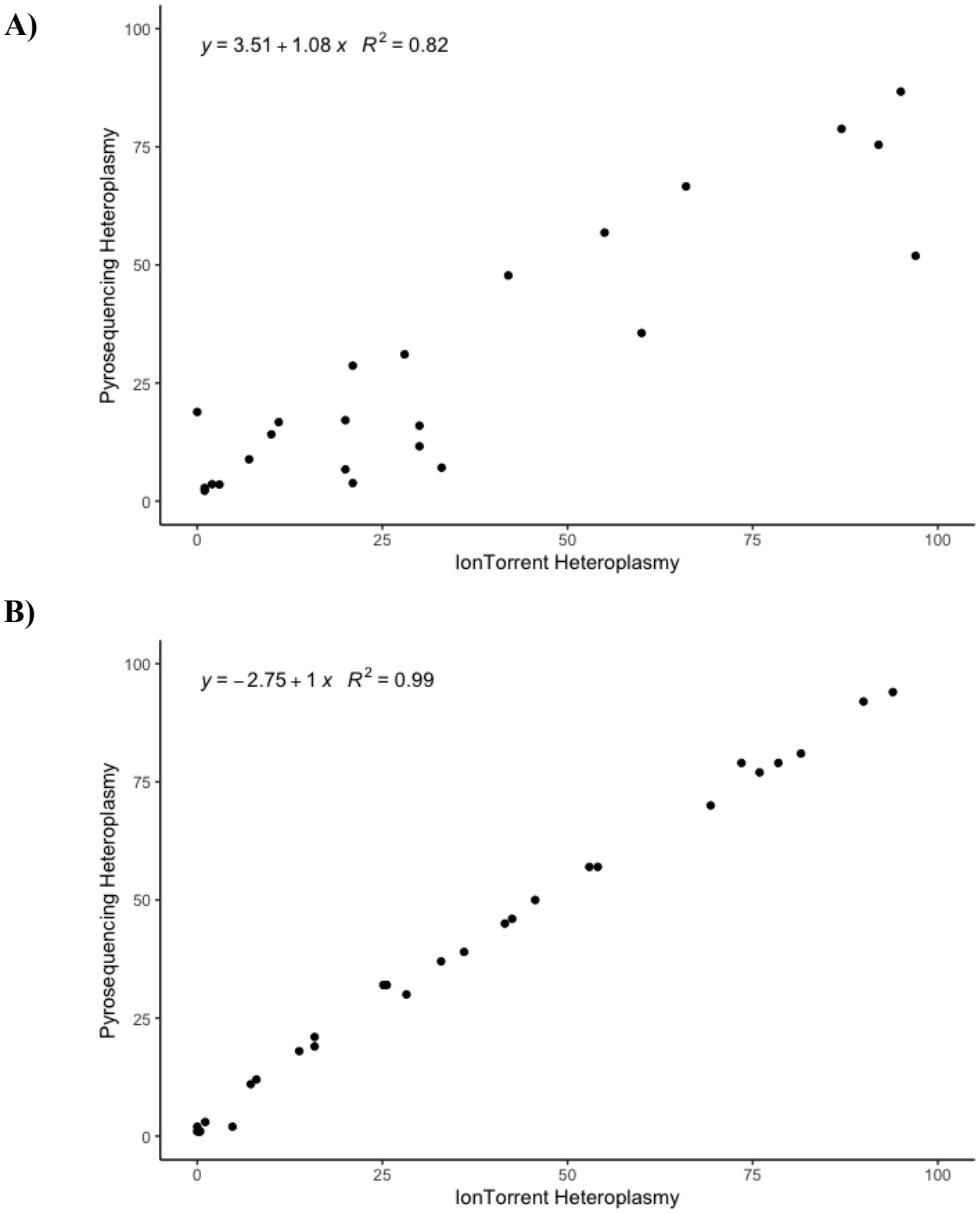


***Figure 4.4 Comparison of single cell m.3243A>G measurements obtained from pyrosequencing and Ion Torrent sequencing using 2 amplification protocols.*** *A) amplified using a 20µl mastermix containing 5µl of cell lysate. High levels of variance between the two sequencing technologies were observed when only a portion of the cell lysate is used. B) Amplified using 35µl mastermix containing full 15µl cell lysate. High concordance between the two measurements was observed. Each point represents measurements of a 210bp product from a single cell.*

To determine whether amplifying the full 15µl single cell lysate would produce more consistent results, I increased the reaction volume from 20µl to 35µl to account for the increased volume of lysis buffer that needed to be incorporated. To maintain similar ratios of key components, the volumes of buffer, dNTPs and polymerase were scaled up by 1.75x (**Table 4. 5**, *optimised reaction*). This reaction produced visible bands on an electrophoresis image when the full cell lysate was added (**Figure 4.5**). This reaction was then used for the following four PCR batches before being sequenced using IonTorrent technology.

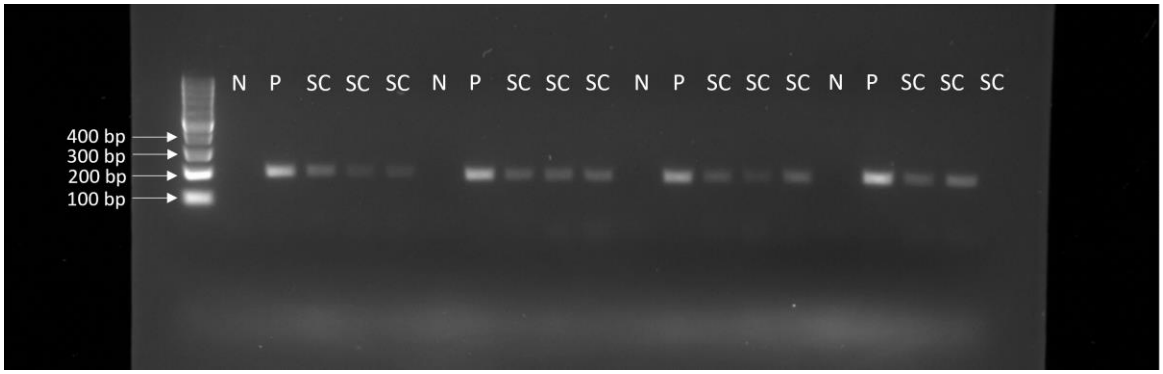


***Figure 4.5 Electrophoresis image of single cell PCR product using Platinum Superfi II DNA polymerase 35µl reaction.*** *Lane one contains a 100bp ladder, the following lanes are labelled according to contents N = Negative control, P = positive control (~100 cells) and SC = single cells. Three single cells were randomly selected from the same plate. This was repeated for four plates on the image shown. Expected amplicon length = 196bp.*

Pyrosequencing of 1µl from the same amplicon pool used for S5 sequencing gave highly correlated heteroplasmy measurements to the IonTorrent (mean difference = 2.86%, median = 2.95%; with an overall difference in the range of 0.07–6.87%), demonstrating that this is a robust method of determining m.3243A>G level from a single mononuclear cell (**Figure 4.4**). This protocol was then used to sequence 5,732 cells from 6 patients (**Table 4. 1**) in 4 sequencing batches using the IonTorrent S5 sequencer.

### 4.3.2 Data quality control

First, I established read depth cut offs to remove doublets and empty wells from investigations. A read depth histogram of the of the library revealed two peaks (**Figure 4.6A**), one clustering above zero, made up of wells which do not contain an intact cell, and another at a larger read depth which is made up of data obtained from single cells. Wells at the upper periphery of this second peak are more likely to contain multiple cells; these were removed if they had a read depth over 1.5x the upper quartile. This threshold was determined for each plate, to account for any read depth differences per plate (**Figure 4.6B**). The lower cut off of 200 in batches one and two and 400 in batches three and four, was determined per run by visual inspection of the histogram (e.g. **Figure 4.6A**). These thresholds resulted in the elimination of 397 (321 lower, 76 upper) cells from batch one, 483 from batch two (474 lower, 9 upper), 90 from batch 3 (89 lower, 1 upper) and 29 from batch 4 (29 lower, 0 upper).

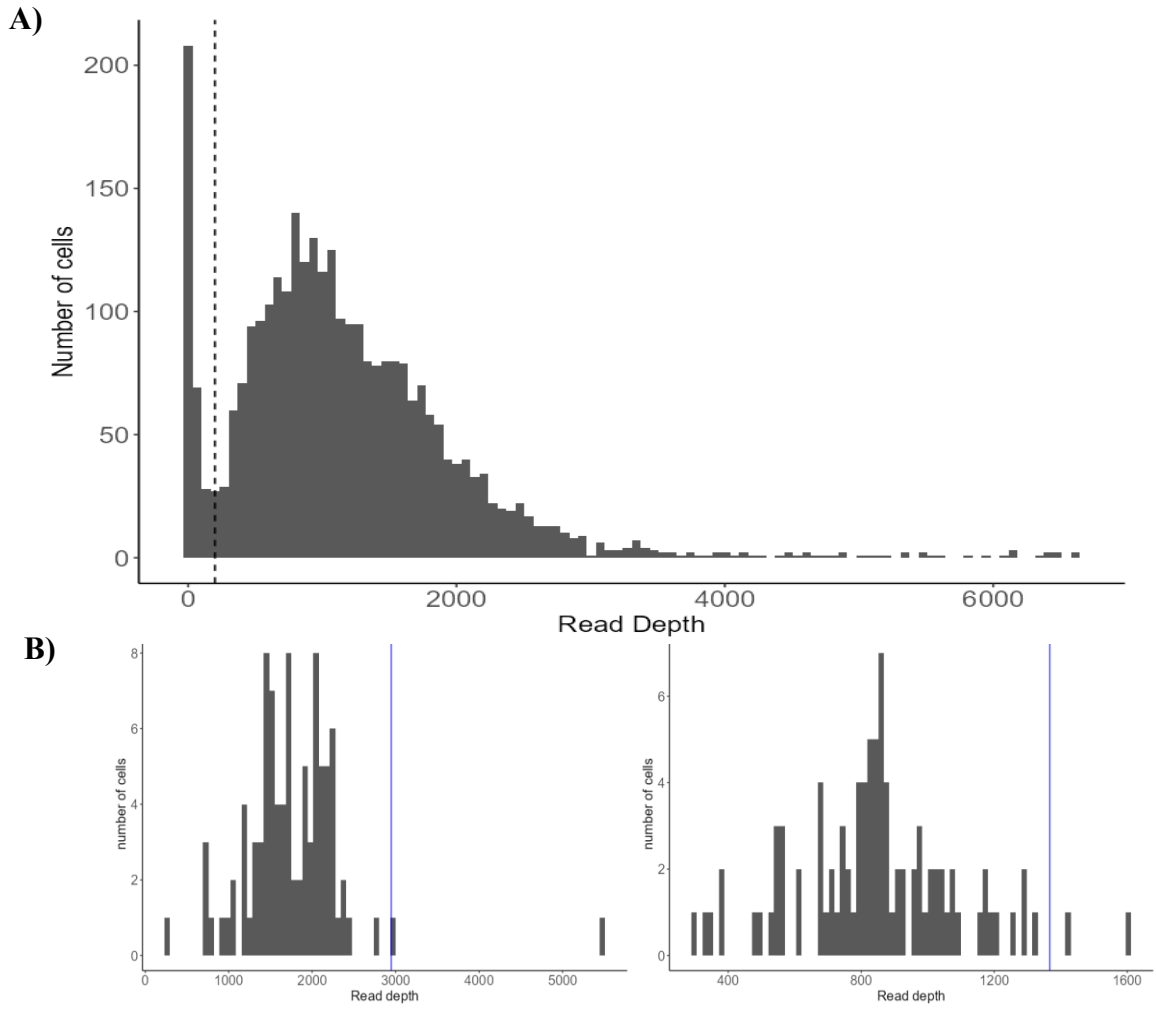


***Figure 4.6 Distribution of read depth per cell from targeted Ion Torrent sequencing***. *A) lower thresholds for read depth were determined per Ion Torrent run (batch) by visual inspection. Data presented are from 3002 cells from batch one. The black dashed line denotes the lower cut off at a read depth of 200. B) Two exemplar plate upper cut offs (P18 CD34+ Progenitor and P18 Monocyte) blue lines represent upper cuts offs as determined by 1.5x plate SD.*

### 4.3.3 Immune cell populations display m.3243A>G mosaicism.

Single cell sequencing revealed the distribution of m.3243A>G levels spans almost the entire possible range in all cell types (0-99.23%) (**Figure 4.7**). Cells from P17 are the only to exhibit a range restricted towards low m.3243A>G levels; this may be due to a low baseline m.3243A>G level or efficient purifying selection of the variant. P17 did possess cells which retained >75% m.3243A>G, but these were found only in the monocyte and CD8+ naïve populations (**Figure 4.7**). Interestingly, an individual of a similar age and m.3243A>G level, P15, possessed cells with >75% m.3243A>G level in every cell group investigated, despite only having a whole blood level of 14%. This highlights the importance of other factors, perhaps environmental or nuclear, which can play a role in this process.

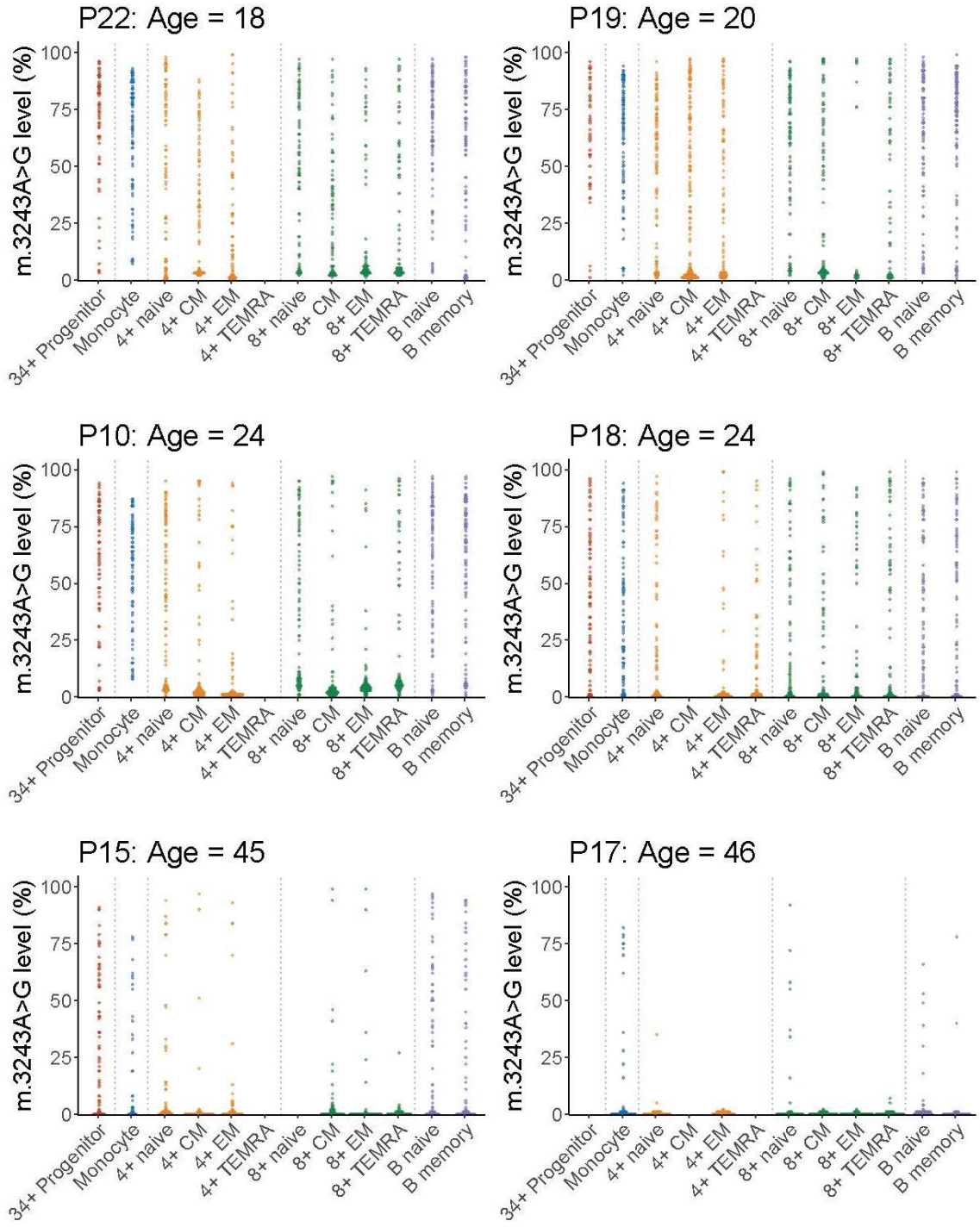


***Figure 4.7 Single cell m.3243A>G analysis reveals mosaicism within all immune cell subsets***. *Each point represents the m.3243A>G level of a single cell from a single individual and is coloured according to wider cell group: Red = progenitor cells, Blue = myeloid cells, yellow = CD4+ T cells, green = CD8+ T cells and purple = B cells. The median number of cells sequenced per subset = 91 cells (IQR = 87, 93; range = 26, 200). Missing data for 4+ TEMRA was due to an absence of this cell type within five patient*

*samples and P15 8+ naïve, P17 34+ progenitors and 4+ CM were removed due to suspected contamination of negative control.*

### 4.3.4 Enhanced negative selection in all subsets of memory T cells

Bayesian modelling of the data, as outlined in 2.12.8, is consistent with the findings of *chapter 3*, which found enhanced selection against m.3243A>G within the T-cell compartment. Throughout this chapter I will described the proportion of cells residing in the 'near 0 % peak' as cells which have cleared the m.3243A>G variant.

Patient T cells have the highest proportion of cells which have cleared the m.3243A>G variant (**Figure 4.8**), this is consistent across both CD4+ and CD8+ T cells. Not only does this increase with patient age, but it also increases with T cell maturity. As represented by a red line joining cell types in **Figure 4.8**. The proportion of cells with near 0% m.3243A>G levels is significantly higher in all memory subsets of both CD4+ and CD8+ T-cells, compared to their naïve counterparts. Consistent with decline in overall population m.3243A>G level recorded in *chapter 3*.

In individuals below 25, the proportion of CD8+ T cells which have cleared the pathogenic mtDNA increases following the current orthodoxy of T cell differentiation (**Figure 4.8**). The increase from $T_{CM}$ to $T_{EM}$ cell states only reaches significance in P22, supporting a non-linear differentiation between these states. Interestingly, the most 'terminally differentiated' memory T cell, the $T_{EMRA}$ cell, fails to follow this trend. In the same individuals, the $T_{EMRA}$ cells exhibit fewer cells which have cleared the variant than the $T_{EM}$ cells. These data confirm that selection against m.3243A>G continues throughout T cell differentiation and cannot be isolated to a single point in cell development.

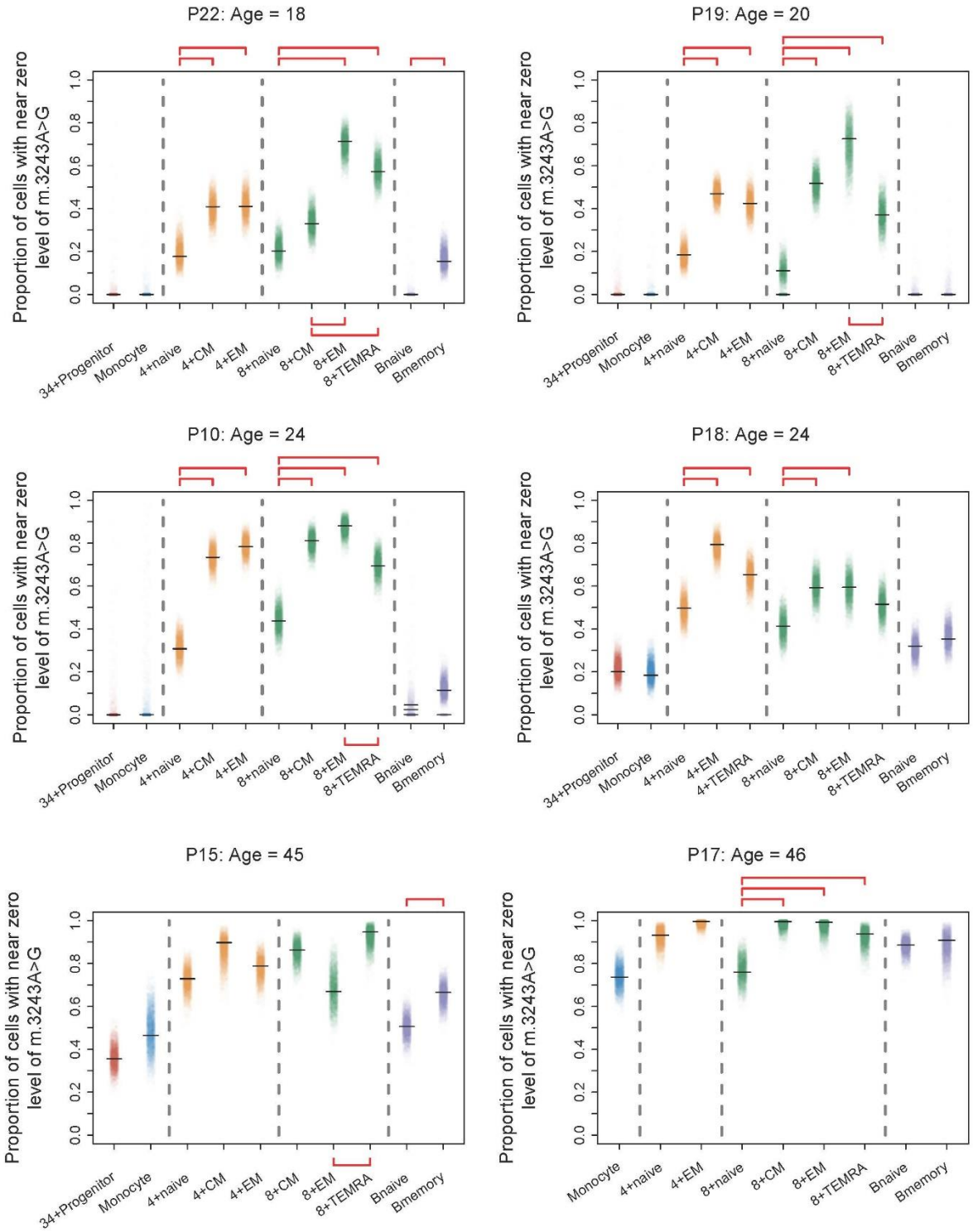


***Figure 4.8 The proportion of cells which have cleared m.3243A>G increases through T cell differentiation.*** *Each point is representative of an estimation from one Bayesian iteration and coloured according to wider cell group: Red = progenitor cells, Blue = myeloid cells, yellow = CD4+ T cells, green = CD8+ T cells and purple = B cells. Peak estimates are represented by a black horizontal line. Red lines join statistically different*

*cell types (zero lies outside the 95% credible interval of the posterior difference between the proportions)*

Data from *chapter 3* suggested a similar mechanism of selection in B and T cells, therefore, it was surprising that naïve and memory B cells retained a large proportion of cells with >50% m.3243A>G. However, memory B cells from 5/6 individuals had a higher proportion of cells that have cleared m.3243A>G, although, this only reached significance in 2/6 individuals. Therefore, a trend with maturity can be observed in B cells, consistent with section 3.3.2, however the effect is much weaker than in T cells.

The myeloid lineage shows a contrasting distribution of m.3243A>G to the T cells. Cells with over 90% m.3243A>G are more common in the progenitor and monocyte populations, consistent with the bulk measurements (**Figure 4.8**). The monocyte and progenitor populations exhibit a remarkably similar m.3243A>G distribution, which shifts towards a m.3243A>G level of over 50% (mean m.3243A>G level: monocyte; P22 74%, P19 73%, P10 61%. progenitor; P22 82%, P19 74%, P10 65%). The proportion of cells with a near 0% heteroplasmy was lowest in these cell types in every participant and there was no difference in the proportion of cells near 0% between monocytes and progenitors. This finding suggests that monocytes are metabolically similar to progenitor cells.

### 4.3.5 Interrogation of progenitor subset profile

I then compared the occurrence of six progenitor subsets (**Table 4. 1**) to evaluate whether increasing whole blood m.3243A>G heteroplasmy affects the proportion of different progenitor subsets. The occurrence of these subsets within the blood is extremely rare and the populations accounting for the highest proportion of CD34+ cells in all patients were granulocyte-macrophage progenitors (GMP) and common myeloid progenitors (CMP) (range 3.21% -40.9%, median = 19.6% and 0.58% - 38.8%, median = 9.02% respectively), likely due to a high turnover of the mature cells (**Figure 4.9**). Lymphoid progenitor (CLP) cells were much less frequent within the CD34+ cells of all patients (median = 0.18%), a level comparable to that of the MPP cells (median = 0.12%) and HSC's (median = 0.38%) (**Figure 4.9**). I was unable to identify any CLPs within samples from P22 and P10. This may explain why myeloid cells have a m.3243A>G distribution

similar to that of the CD34+ cells as the majority of circulating CD34+ characterised were primed to give rise to cells of the myeloid lineage.

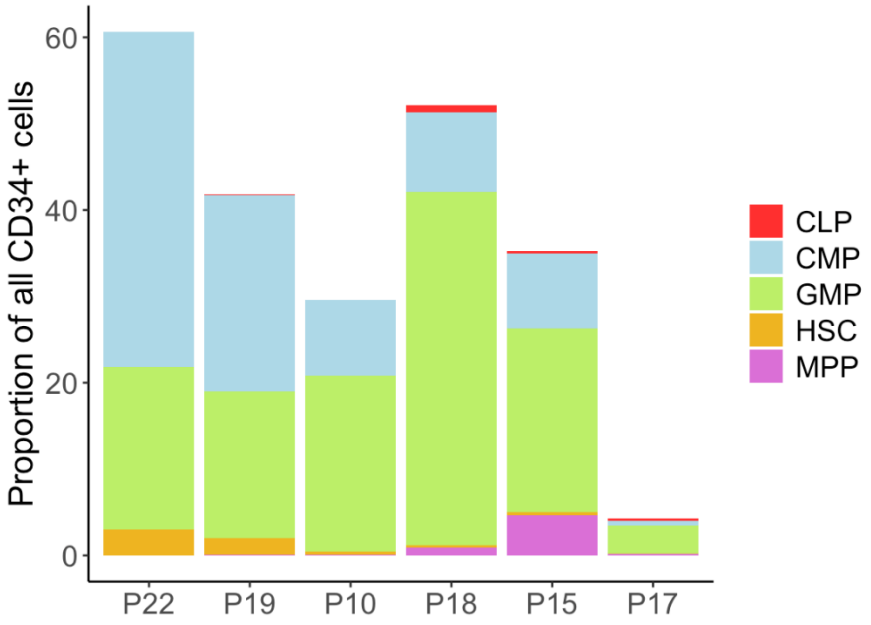


***Figure 4.9 The proportion of different progenitor subsets making up the peripheral blood CD34+ population.*** *Each measurement is derived from flow cytometry data from a single patient. Points are coloured according to the sample they are derived from. CLP were absent from P22 and P10 therefore are not represented on this graph.*

I was unable to detect a relationship between m.3243A>G level and proportions of progenitor cell type in samples from any of the patients investigated. Due to a mixed population of CD34+ cells being sorted, the sample size per subtype is too small to make any conclusions and there is no consistent pattern across patients (**Figure 4.10**). Of note, individuals with a whole blood m.3243A>G level below 45% all had a higher proportion of MPPs than those with >45%. Those above 45% also had a higher proportion of HSCs in the peripheral blood than the those below, a larger cohort is needed to investigate this further.

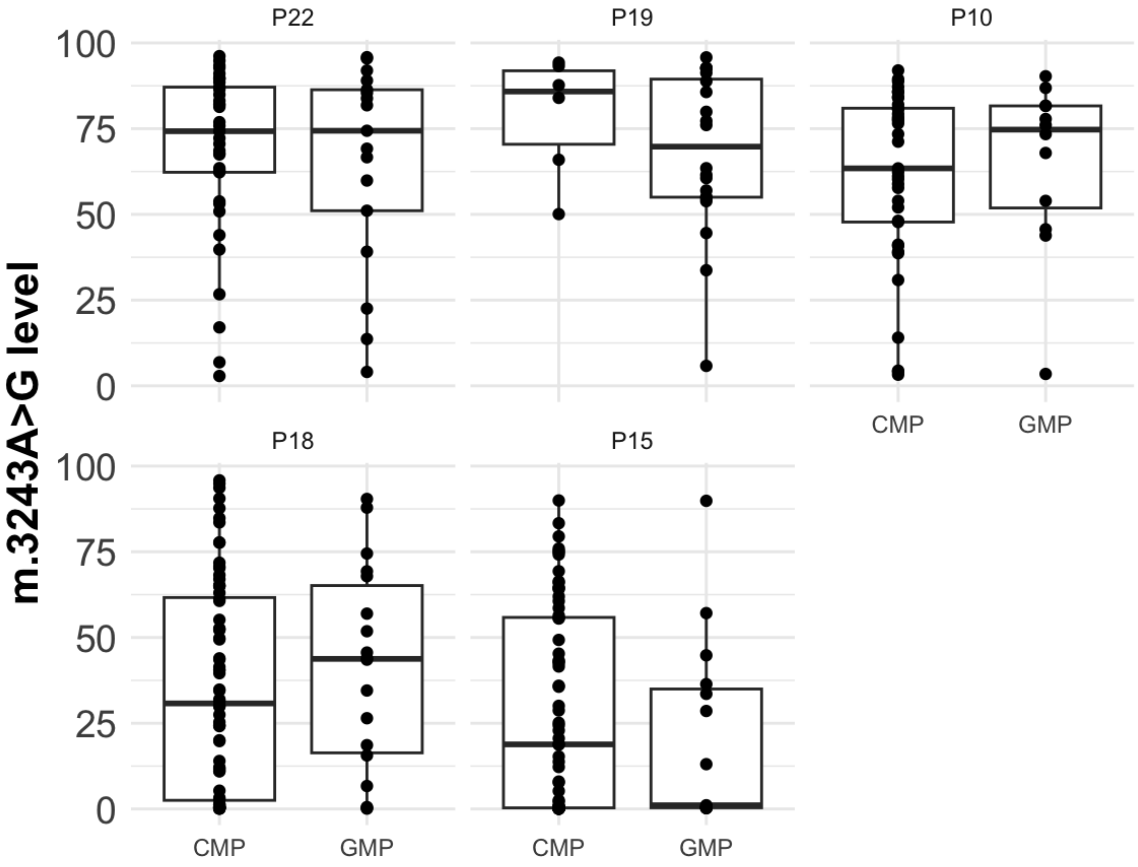


***Figure 4.10 There is no relationship between m.3243A>G level and progenitor subset.*** *Each point represents a single CD34+ cell sorted via FACS. No or very low numbers of CLPs and HSCs were sorted as part of the CD34+ positive population therefore they are excluded from this graph. Linear mixed model, p>0.05.*

### 4.3.6 Analysis of T cell functional markers

To understand whether m.3243A>G levels within a particular cell type are related to cell function, I investigated the expression of five additional cell surface markers (**Table 4. 2** & **Table 4. 3**). These markers were chosen for their association with T cell senescence (CD57), activation (CD56, HLA-DR, CD38) and exhaustion (PD-1). This revealed high expression levels of T cell exhaustion marker, PD-1, in CD4+ T cells from individuals with a whole blood m.3243A>G level >45% but not in those with a whole blood measurement below this threshold (**Figure 4.11**). It is interesting that this was observed primarily in the CD4+ T cells, where over 90% of CD4+ cells from these three patients expressed PD-1. For P10, >99% of CD4+ cells expressed PD-1 and, therefore, could be considered exhausted. Expression on CD8+ T cells was restricted to <30% of cells in P22 and <15% in P19 and P10. High PD-1 expression was observed within all CD4+ T cell subsets investigated, (**Figure 4.12**); it is particularly unusual to see expression of this marker on cells which have not been exposed to antigen such as naïve cells. Interestingly, expression of PD-1 did not appear in conjunction with markers of activation or senescence. P18, who is an identical age to P10 but has a whole blood m.3243A>G level of 36% does not show this this trend, suggesting it is not an age dependent phenomenon.

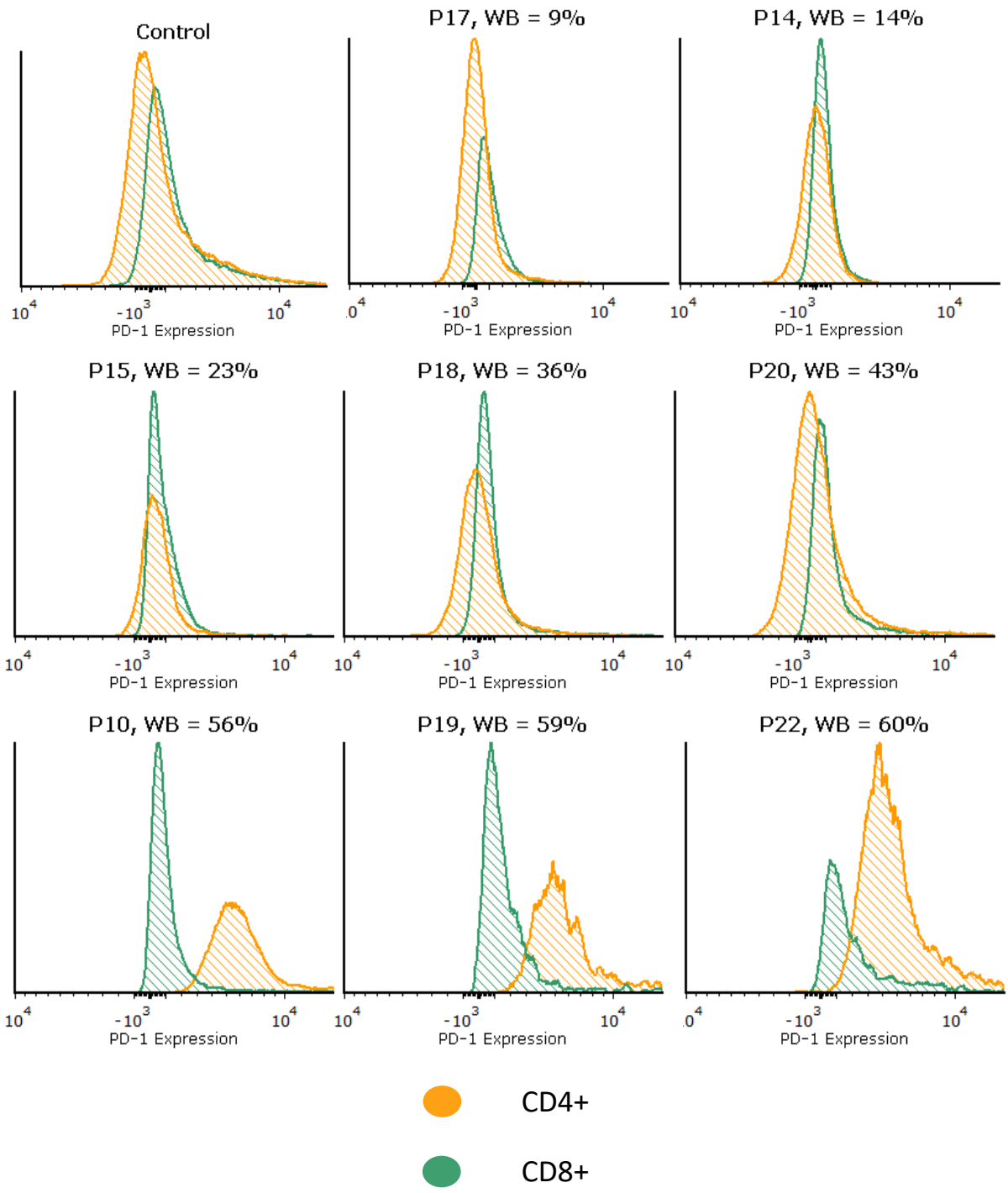


***Figure 4.11 PD-1 expression is restricted to CD4+ T cells in individuals with a whole blood m.3243A>G level above 45%.*** *Histograms represent mean fluorescence index of PD-1 in CD4+ T cells (orange) and CD8+ T cells (green) per patient. Measurements were taken from whole sample recording during FACS of single cells.*

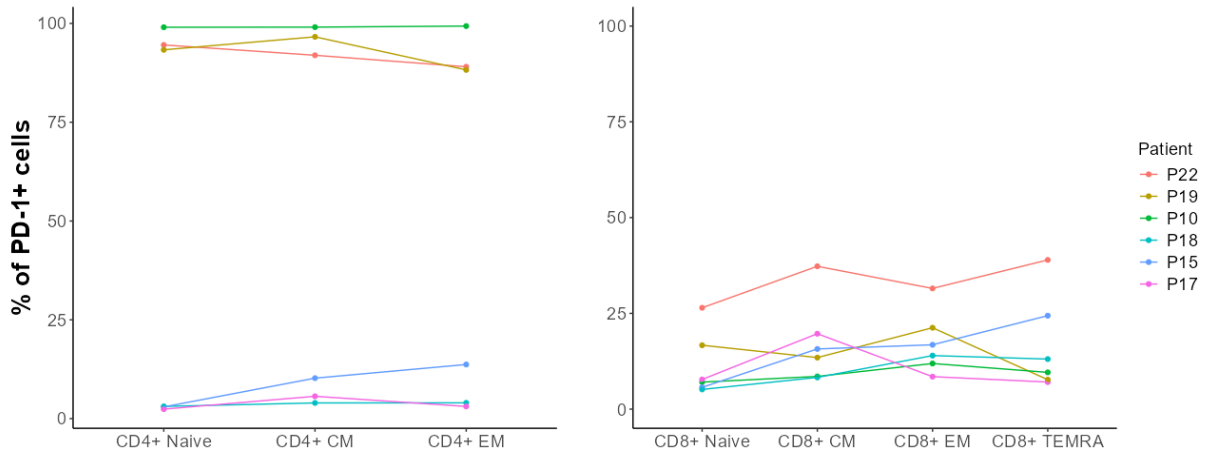


***Figure 4.12 PD-1 expression is present at all stages of CD4+ T cell maturity in individuals with a m.3243A>G level over 45%.*** *A) The proportion of CD4+ cells expressing PD-1 in naïve and memory (CM, EM) cell states. B) The proportion of CD8+ cells expressing PD-1 in naïve and memory (CM, EM, TEMRA) cell states. Measurements from the same patient are joined by a coloured line. Red = P22, yellow = P19, green = P10, turquoise = P18, blue = P15, pink = P17.*

I next asked whether PD-1 expression correlates with m.3243A>G level at a single cell level. There was no relationship between cellular m.3243A>G level and its expression of PD-1 in all patients investigated (**Figure 4.13**; linear model $p>0.05$). Due to the high expression of this marker in individuals with ~45% heteroplasmy and above, few low PD-1 expression cells were sorted to enable comparison. Surprisingly, PD-1+ cells spanned the entire possible range of m.3243A>G levels (0-100%;**Figure 4.13**).

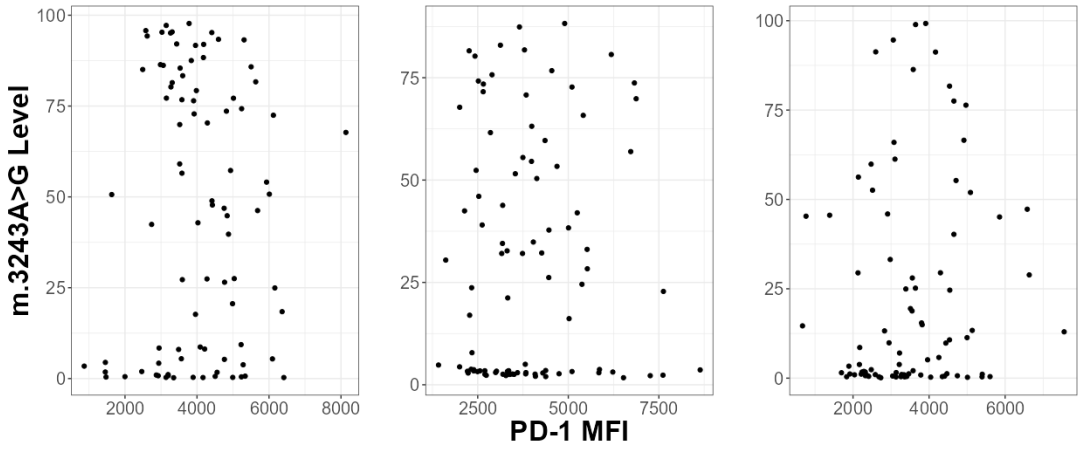


***Figure 4.13 PD-1 expression is not correlated with m.3243A>G level within single cells.*** *Data show PD-1 expression and single cell m.3243A>G level in CD4+ naïve T cells (left), CD4+ CM T cells (middle) and CD4+ EM T cells (right) from P22 as an example. Each point represents a single cell. Linear model p>0.05*

## 4.4 Discussion

The work presented in this chapter demonstrates high variability in m.3243A>G level within cellular subsets and therefore the importance of single cell analyses when investigating the dynamics of negative selection of this variant. These data demonstrate an increase in proportion of cells that have cleared m.3243A>G level with T cell maturity across both CD4+ and CD8+ cells. This observation, that the negative selection we see at the bulk level is the result of the complete clearance of m.3243A>G within a subset of cells, rather than a decline in levels across in all cells, indicates that negative selection is occurring even at low levels. This is in agreement with findings from the Mootha group, who used ATAC-seq to measure m.3243A>G level in single PBMCs and whose results were published during the course of my experiments (Walker *et al.*, 2020).

### 4.4.1 m.3243A>G clearance follows T cell maturation

An accepted consensus for T-cell maturation follows the differentiation series naïve –$T_{CM}$ – $T_{EM}$ – $T_{EMRA}$. $T_{EMRA}$ cells are considered the most terminally differentiated cells due to their reduced proliferative ability supported by their short telomere length, as well as low plasticity. (Hamann *et al.*, 1999, Geginat,Lanzavecchia and Sallusto, 2003, Verma *et al.*, 2017). With this in mind, differentiation through these cell states is unlikely to be a linear process; as a memory cell is capable of reverting to an effector state upon stimulation as well as $T_{CM}$ and $T_{EM}$ cell states. In support of this, only one of six patient-derived samples showed a significant difference between $T_{EM}$ and $T_{CM}$ cells in the proportion of cells that had cleared m.3243A>G. However, an increasing step-like trend in this proportion of cells can be seen following progression from naïve to $T_{CM}$ to $T_{EM}$, suggesting that more cell divisions are required to reach the $T_{EM}$ state.

For all patient samples, with the exception of P15, $T_{EMRA}$ cells do not follow the expected trend of an increased proportion of near 0% m.3243A>G cells with cell maturity (**Figure 4.8**). The number of cells within this population decreases from the CD8+ $T_{EM}$ level, indicating that these cells may not be terminally differentiated and may be a more naïve cell altogether. This is supported by conclusions made by Rufer and colleagues who describe these cells as an intermediate state between naïve and effector T-cells (Rufer *et al.*, 2003). Furthermore, the expression of the long CD45 isoform, CD45RA on $T_{EMRA}$

cells, which is typically expressed by naïve T-cells indicates that these cells are phenotypically similar and are closely related.

An increased proportion of $T_{EMRA}$ cells is often an indicator of age-related immune dysfunction (Verma *et al.*, 2017). This, as well as the differentiation status of a T cell impacts m.3243A>G clearance by increasing the proportion of $T_{EMRA}$ cells; therefore, the age and infection history of an individual has the potential to impact m.3243A>G level. The low m.3243A>G levels observed in P15's single cells may be a result of clonal expansion of $T_{EMRA}$ cells due to immune ageing or recurrent infections; as I do not have the data from naïve CD8+ cells for this patient, it is difficult to gauge if these cells show a more similar profile to their naïve counterparts. Due the rarity of CD4+ $TE_{MRA}$ cells occurring in the natural population, these observations focus on the CD8+ $T_{EMRA}$ cells only.

Recent research has identified two distinct subsets of $T_{EMRA}$ cells, discernible by their differential expression of CD57 (Verma *et al.*, 2017). CD57- 'young' $T_{EMRA}$ cells have a high proliferative capacity, more representative of the intermediate state proposed by Rufer et al and CD57+ 'old' $T_{EMRA}$ cells representative of a terminally differentiated T-cell state. Regrouping cells according to these criteria and repeating analysis would be interesting to see if this change in surface marker expression and cell functionality has a relationship with m.3243A>G level.

### 4.4.2 B cells show weak selection between naïve and memory

Results from *chapter 3* suggest B cells to have similar selection behaviour to T cells, however, the single cell analyses revealed a much lower proportion of near 0% cells in T cells. This goes against the idea that selection at the naïve cell state is a result of thymic central tolerance as B cells also undergo central tolerance (Schwartz, 2012).

Moderately self-reactive B cells have the ability to undergo receptor editing rather than immediate apoptosis, which likely reduces the number of replications required by the common lymphoid progenitor to reach the naïve-mature B cell stage and perhaps offering an explanation as to why naïve B cells retain higher m.3243A>G levels (Tiegs,Russell and Nemazee, 2011, Nemazee, 2017). A limitation of this study is that I was unable to investigate the 'true' B memory cell: the plasma cell, which is of a more comparable cell age to the memory T cell. A bone marrow sample is required to investigate these cells which is far more invasive to obtain, therefore their collection was not specified on the

ethics application for this project. Investigating these, as well as immature immune cells which reside in the marrow would be a positive next step for this project. Measurement of the m.3243A>G level in immature cells from the marrow would allow for an accurate lymphoid progenitor measurement as well as HSC measurement which could elucidate the origin of selection in this tissue.

### 4.4.3 Cellular activity may be driving selection.

A m.3243A>G level surpassing 90% is rarely observed in patient tissue samples and m.3243A>G homoplasmy has been considered incompatible with cellular survival, therefore the presence of near homoplasmic cells within populations with a low m.3243A>G level such as the immune cells was unexpected. The in vitro functionality of these cells would be interesting to investigate in relation to this, as there was no direct relationship between any of the functional markers investigated in this chapter and m.3243A>G level.

High levels of the exhaustion marker PD-1 were expressed on CD4+ cells in samples derived from patients with a whole blood m.3243A>G level above 45%. Interestingly, this expression was not limited to cells with high m.3243A>G levels; high expression was observed in cells across the full possible range of heteroplasmy. These data suggest that the increased proportion of 'high' mutation level cells within these groups could be inducing the expression of PD-1 via extracellular factors. m.3243A>G levels within the CD34+ population were skewed towards >50% in these patients, whereas for P15 and P18, the distributions were either normal or skewed towards 0%, indicative that a predisposition to PD-1 expression could originate in the CD34+ progenitor cell. Research by the Picard group has identified that the presence of m.3243A>G or a single, large-scale deletion of mtDNA can alter the cytokine response to LPS. Leukocytes derived from individuals with m.3243A>G exhibited a slightly increased IL-1β response (Karan *et al.*, 2022). IL-1β likely influences the expression of PD-L1, the ligand for PD-1, as the two are highly correlated in a number of cancers (Bar *et al.*, 2020, Takahashi *et al.*, 2021) and silencing of IL-1β has also been shown to decrease PD-L1 expression (Chen *et al.*, 2019). An increase in the expression of the PD-L1 by APCs could drive the high expression of PD-1 on patient CD4+ T cells. Why only CD4+ T cells are impacted in m.3243A>G patients is unknown, but CD4+PD-1+ T cells have been implicated in the pathogenesis of primary immune thrombocytopaenia. Li and colleagues found that these cells have

increased levels of ROS and treatment with mitoQ decreased PD-1 expression, TNF-α and IFNγ secretion. They concluded that these cells were not exhausted but retained their cytotoxic abilities and were regulated by ROS. Perhaps, CD4+ T cells are more sensitive to ROS, inducing this phenotype (Li *et al.*, 2023).

## 4.5 Concluding Remarks

Consistent with the findings of Kotrys *et al.* (2024), this data shows that the selection against m.3243A>G in T cells can be explained by an increased proportion of cells with near-zero levels of mutation, as opposed to a consistent decline in levels across all cells. This is compelling evidence that selection against the pathogenic mtDNA continues to occur even at very low levels. To further understanding of the mechanism behind this process, it would be beneficial to carry out transcriptome analyses to assess differentially expressed pathways between cells with low and high variant levels alongside in vitro assessments of T cell function. These experiments could shed further light on whether decreased cellular fitness in cells with high m.3243A>G level is a driver of selection against pathogenic mtDNA.

# Chapter 5 Analysis of the effect of m.3243A>G on T cell function

## 5.1 Introduction

As cellular fitness has been implicated as a driver of selection in the literature (Kotrys *et al.*, 2024), this chapter will explore the possibility of m.3243A>G being related to a functional defect in T cells. A T cell's function and survival can be dictated by its ability to proliferate in response to TCR stimulation and its ability to produce and respond to cytokines (Chopp *et al.*, 2023).

Upon encounter of a cognate antigen, naïve and memory T cells rapidly exit a quiescent state and transition into an active effector state before undergoing mass clonal expansion (Chopp *et al.*, 2023). This process is facilitated by a metabolic switch from glucose oxidation through the TCA cycle or β oxidation of fatty acids to glycolytic and pentose phosphate pathways in activated T cells (Wang *et al.*, 2011). Known as the Warburg effect, this flux occurs before the first division and facilitates the high levels of synthesis required to proliferate at such a substantial rate (Warburg, 1956). Metabolic reprogramming of these cells is regulated by master signalling pathways mTOR and c-myc (Tan *et al.*, 2017, Wang *et al.*, 2011, Yang *et al.*, 2013). It is also at this point of quiescence exit that the fate of a naïve T cell is believed to be established, i.e. whether it is primed to become an effector or a memory T cell (Verbist *et al.*, 2016, Pollizzi *et al.*, 2016).

Interestingly, the mitoribosome and mitochondrial proteins including COX-10 have been implicated in playing a role in quiescence exit. Tan et al identify coordinated upregulation of both cytoplasmic and mitochondrial ribosomes in WT mice following TCR stimulation, which they hypothesise to be under the control of mTOR (Tan *et al.*, 2017). The use of cells deficient in Raptor, a key component in the mTOR pathway, resulted in a reduction of mitochondrial biogenesis and decreased expression of mitochondrial ribosomal proteins MRPS16 and MRPL20 post TCR stimulation. Further to this, treatment with mitoribosome inhibitors minimised cell division but did not alter expression of activation markers highlighting mitochondrial translation as involved in quiescent exit. Being a tRNA variant, m.3243A>G is intrinsic to mitochondrial translation and known to impact CIV activity. Investigations into TCR response in COX-10 (CIV assembly factor) deficient mice revealed increased cell death and inhibited proliferation

in surviving cells, indicating a role for OXPHOS in cell cycle/quiescent exit (Tan *et al.*, 2017). COX-10 deficient mice were found to have altered T cell homeostasis in the form of a reduced level of splenic T cells and a defective differentiation of naive CD4+ T cells into Th1 cells. Given that m.3243A>G is known to induce a mitochondrial translation defect and decrease CIV activity, there may be a proliferation defect in T cells carrying m.3243A>G.

T cell proliferative abnormalities have been identified in other mtDNA diseases. Lareau and colleagues used single cell sequencing of PBMCs to trace single deletion selection behaviours (Lareau *et al.*, 2023). In young individuals with Pearson syndrome, the authors identified purifying selection against deletion-carrying mtDNA molecules in mucosal associated invariant T cells (MAIT) and CD8+ EM cells, similar to our observations for m.3243A>G. Stimulation of patient T cells with αCD3/αCD28 unveiled reduced expansion compared to controls, particularly of CD8+ cells. A 52% increase in cells with 0% deletion mtDNA was observed in a 21-day expansion culture. This supports cellular fitness as a driver of selection against pathogenic mtDNA. The speed at which the sideroblastic anaemia and disturbed maturation of the myeloid lineage are resolved in Pearsons syndrome cases, coinciding with the loss of deleted mtDNA from all haematopoietic populations, suggests the selection pressure is high (Yoshimi *et al.*, 2021). A milder immune phenotype for m.3243A>G could lead to the moderate selection pressures observed for this variant.

If selection is related to cellular fitness during proliferation, there are two points at which it could be occurring; at the point of quiescent exit during selection in the thymus and naïve cell activation or during the mass cell proliferation that follows these events. The above research suggests that some high heteroplasmy cells may not be able to transition from a quiescent state and therefore either do not proliferate or exhibit inhibited proliferation. It is possible that selection is isolated to cells primed to become memory cells due to their need to self-renew, preferential reliance on OXPHOS and long-life span. This could be in the form of asymmetric distribution (Borsa *et al.*, 2019) of pathogenic mitochondria to daughter effector cells only or via an intrinsic mechanism. This could explain the low incidence of high m.3243A>G memory cells. The other possibility is that cells with high m.3243A>G levels are able to exit quiescence and the loss of m.3243A>G is simply a result of random distribution of mitochondria during cell division. The high

level of proliferation in such a small timeframe after TCR stimulation could accelerate the ‘dilution’ of pathogenic mtDNA.

To explore these possibilities, I will carry out preliminary investigations to guide the design of future experiments. These investigations will focus on the following questions:

- Does activation of T cells result in a decrease in m.3243A>G level?
- Do m.3243A>G patients exhibit an altered response to αCD3/αCD28 stimulation compared to controls?
- Do m.3243A>G patients exhibit an altered response to specific antigen stimulation compared to controls?

## 5.2 Methods

### 5.2.1 Investigating T cell response to artificial stimuli

To assess the competence of T cell proliferative ability, two patient samples and two aged-matched control samples (**Table 5. 1**) were stimulated to divide *in vitro* using αCD3 and αCD28 antibodies (2.13.2). These individuals were chosen to represent a range of ages and m.3243A>G levels.

| | | | **m.3243A>G level (%)** | | |
|---|---|---|---|---|---|
| | Age (years) | Sex | Whole blood | CD4+ Naïve/memory | CD8+ naïve/memory |
| **P24** | 34 | M | 36 | 25/25 | 31/14 |
| **P26** | 56 | F | 19 | 16/7 | 12/3 |
| **C20** | 48 | M | NA | NA | NA |
| **C21** | 29 | F | NA | NA | NA |

***Table 5. 1 Participant information for T cell proliferation investigations.***

Before stimulation, the cells were incubated with cell trace violet (CTV) (section 2.13.1), a dye which diffuses into cells and covalently binds intracellular proteins via an amine group. Upon division, the stained proteins are distributed between daughter cells, diluting the fluorescent signal by 50%; thus, the strength of the signal corresponds to the number of divisions a cell has undertaken. This can be visualised on a histogram, where individual peaks represent cells which have undergone the same number of divisions (**Figure 5.1**). When changing media or splitting wells, at least 100,000 cells were taken forward for flow cytometry analysis on days 2, 5, 7, 10 and 12 post stimulation. Measurements taken at these timepoints include the CD4+ to CD8+ ratio, m.3243A>G level (section 2.10), the number of live cells (section 2.8) and the percentage of dividing CD4+ and CD8+ cells. Analysis of cellular divisions was carried out using the FCS Express 7 proliferation fit feature on days 2, 5 and 7 post-stimulation (**Table 5. 2**;**Figure** 5.2). The maximum number of peaks was set as 10 and the same coefficient of variation was applied to all peaks. If the undivided peak was not automatically detected, a fixed

starting generation was applied according to values derived from an unstimulated control. The CTV had diluted beyond reliable measurement by day 10, therefore this analysis was restricted to a period of 7 days.

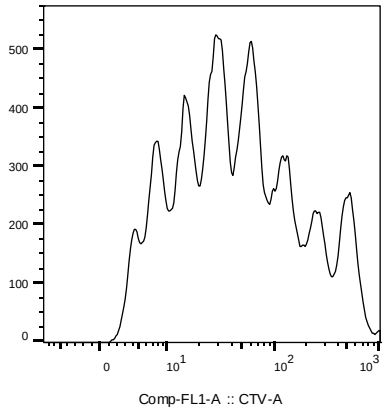


***Figure 5.1 Histogram demonstrating CTV dilution peaks.*** *The peak with the highest CTV fluorescence (~103) represents undivided cells and as peaks shift to the left, they represent different generations of daughter cells. Data obtained using 200,000 control PBMCs stimulated for 5 days using αCD3/αCD28.*

| **Antibody/stain** | **Company** | **Cat No.** | **Final concentration** |
|---|---|---|---|
| **LD NiR** | Life Technologies | L34976 | As per manufacturer's instructions |
| **CD3 FITC** | BD | 345763 | 3.5ug/ml |
| **CD4 APC** | Biolegend | 300514 | 0.25ug/ml |
| **CD8 PerCp-Cy5.5** | Biolegend | 300924 | 1.4ug/ml |
| **CTV** | Invitrogen | C34571 | 5uM |

***Table 5. 2 Antibody panel used to isolate CTV stained CD4+ and CD8+ T cells.***

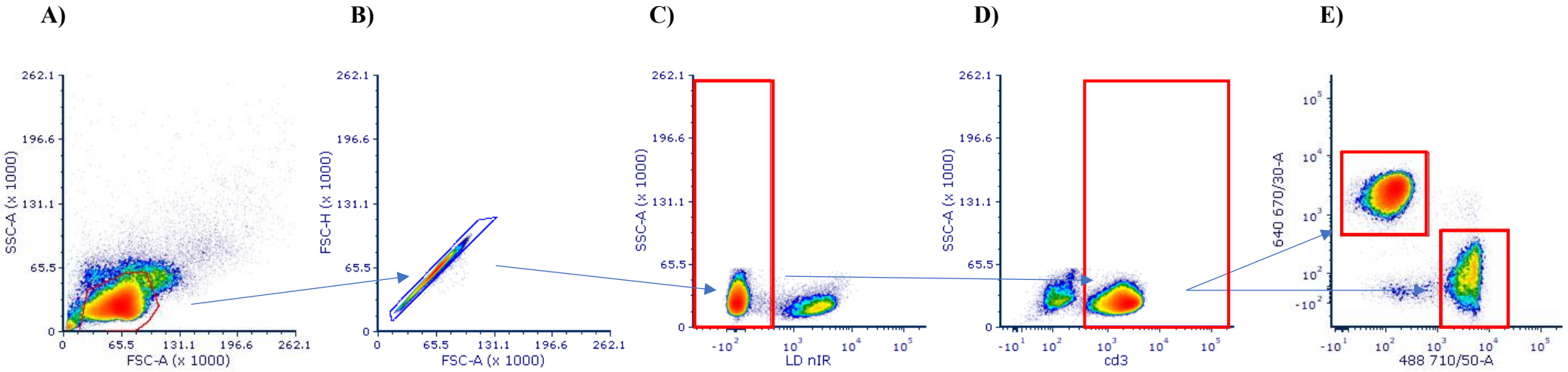


***Figure 5.2 Gating strategy for CTV analysis.*** *Density plots representing flow cytometry data obtained from C20. Coloured lines surrounding populations are gates which isolate the following populations A) Lymphocytes B)Singlet C) Live cells C) T cells D) CD4+ and CD8+ T cells day 0*

### 5.2.2 ELISpot

Response to Sars-CoV2 and CMV peptides was assessed using an enzyme linked immunospot assay (ELISpot) (Siota *et al.*, 2011). Therefore, only individuals recruited February 2021 onwards, who had received the COVID-19 vaccination could be included (P24, P39, P26, P40, P41, P42, P23, P43, C22, C23; *Table 2.1*). These investigations were carried out, in part, on a cohort of individuals recruited by researchers from The University of Oxford (**Table 2. 3**) in collaboration with Dr Ana Victoria Lechuga-Vieco (The Kennedy Institute of Rheumatology, The University of Oxford). A summary of all participants used in the ELISpot investigations is outlined below (**Table 5. 3**).

| | **Total** | **Age (years)** | | **Sex (F:M)** | | **Het (%)** |
|---|---|---|---|---|---|---|
| | Patient: Control | Patient | Control | Patient | Control | Patient |
| **Oxford** | 5:9 | 48 (13) | 41.9 (14.4) | 3:2 | 5:4 | NA |
| **Newcastle** | 8:2 | 43.1 (13.9) | 38.5(16.3) | 5:3 | 1:1 | 12-60 31.25 (19.3) |

***Table 5. 3 Summary of participant cohort for ELISpot investigations.*** *Patient = individual with m.3243A>G. Mean age given with SD represented in brackets. Heteroplasmy (Het) represented as range, mean and SD.*

The ELISpot is a highly sensitive assay designed to detect individual cells secreting specific cytokines, in this case, IFNγ. This is facilitated by plate-bound antibodies which capture IFNγ secreted in the immediate vicinity of the cell. The addition of a chromatic substrate produces spots which allow quantification of each spot forming unit (SFU) (**Figure 5.3**). For these analyses I chose to investigate the response to the Sars-CoV2 (COVID-19) vaccination as this was recently undertaken by both patients and control groups and was likely to generate a strong and comparable response. All individuals included had received at least one vaccination; currently, I only have access to exact dates

of vaccination from the Newcastle cohort therefore these dates will not be used in analysis. I also chose to examine the response to a pathogen which is relatively common in the population and so chose cytomegalovirus (CMV), which is well controlled by the immune system and invokes a strong IFNγ response (Klenerman and Oxenius, 2016).

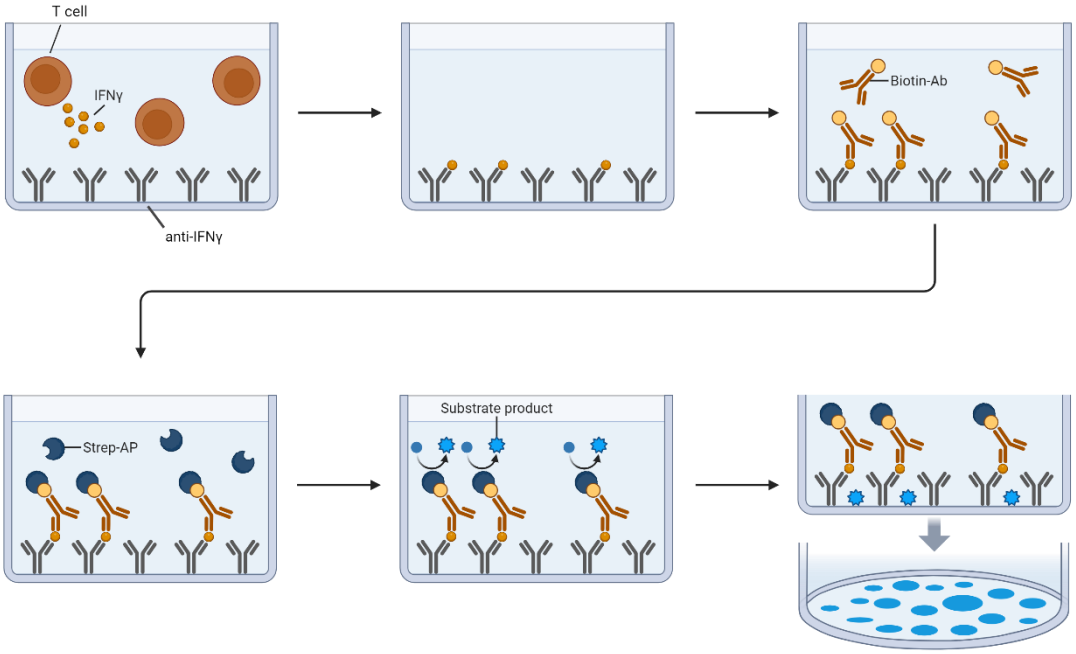


***Figure 5.3 Schematic of ELISpot protocol.*** *200,000 PBMCs and antigen stimulus are incubated in a plate coated with an anti IFNγ antibody. Secreted IFNγ is captured by adjacent antibodies. Cells are removed and the plate is washed before incubating with a biotin labelled secondary antibody. This is removed before the addition of streptavidin ab which binds the biotin. The enzyme substrate is added which induces a colour change, exposing the 'spots. Figure adapted from biorender template.*

### 5.2.3 mtDNA Copy number measurements

The protocol outlined in section 2.11 utilises events sorted as a cell number proxy. In section 5.3.2, a nuclear housekeeping gene B2M is used to estimated cell number per sample via division of the B2M copy number by two (Grady *et al.*, 2014).

## 5.3 Results

### 5.3.1 m.3243A>G alters PBMC composition.

First, to determine whether there was an alteration in the cellular composition of blood in individuals carrying m.3243A>G, I used flow cytometry data obtained in chapter 3 (cohort information in section 2.4) to compare the proportion of each immune cell type within the PBMC fraction. This revealed a reduced proportion of T cells (Wilcoxon test; p = 0.0001), which was accompanied by an increased proportion of B (p = 0.0045) and HLA-DR+ cells (p = 0.0001), a population largely made up of monocytes *(***Figure 5.4***)*. Interestingly, although the proportion of T cells was reduced overall, the ratio of CD4+ to CD8+ T cells remained similar as well as the ratio of naïve T to memory T cells (p>0.05). However, there was a trend towards patients possessing a lower proportion of memory T cells than controls (**Figure 5.4***)*.

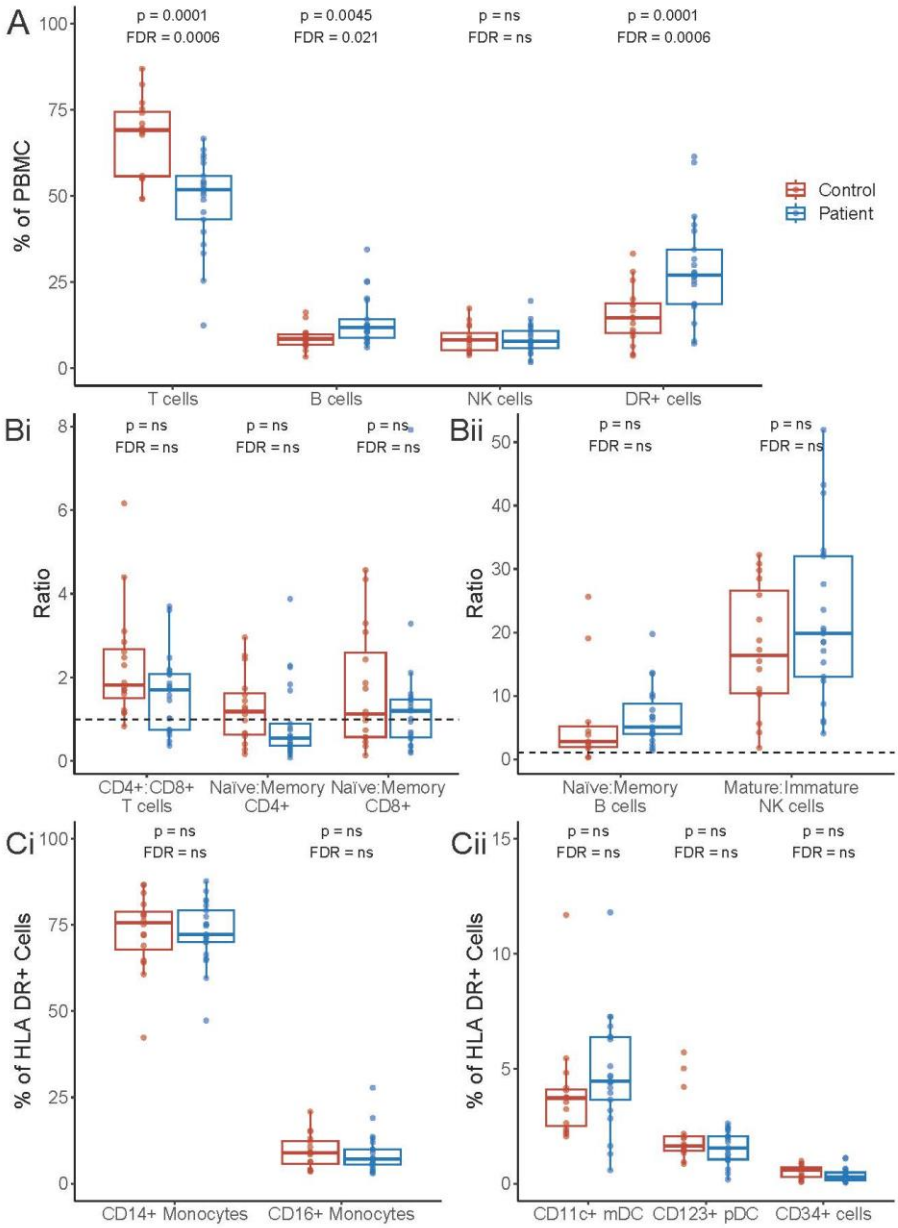


***Figure 5.4 Comparison of the proportions of cell types making up the PBMC fraction in patients and controls.*** *Percentage proportion calculated using flow cytometry data obtained in chapter 3, consisting of 21 patients (blue) and 14 (controls). FDR adjusted P values were generated using linear regression to compare patients and controls in each cell type/ cell subset and are displayed above each comparison. ns= not significant (p>0.05). (A) Proportion of T, B, NK, and HLA DR+ cells. (B) Ratio of CD4+:CD8+ T cells, and naïve:memory CD4+ and CD8+ T cells, B cells, and NK cells; a ratio of 1 is represented with a dotted line. (Ci) Proportion of subsets of CD3- HLA DR+ cells. CD34+: precursor cells; NK, natural killer cells; CD11c+ mDCs: CD11c+ myeloid dendritic cells; CD123+ pDCs: CD123+ plasmacytoid dendritic cells; PBMC, peripheral blood mononuclear cells.*

### 5.3.2 Proliferation in response to artificial stimuli

To understand whether m.3243A>G impacts cell proliferation, as is observed with COX-10 deficiency and Pearsons Syndrome, I stimulated PBMC samples using αCD3 and αCD28 *in vitro.* Cell count fold change throughout a 12-day period following activation did not differ between patient and control samples (**Figure 5.5A**). A higher proportion of cells appear to die in the patient samples at day 2 post activation, as demonstrated by a decrease in fold change from day 0, however this was not significantly different from controls (t test, $p > 0.05$). Further interrogation of this via flow cytometry analysis using a live/dead dye confirmed an average increase of 13.1% dead cells in patient samples compared to controls (**Figure 5.5B**).

Age appears to be a bigger factor in post-stimulation expansion; younger individuals (29-34) have a higher fold change by day 12 than those over 45 years. Although this doesn't reach statistical significance ($p>0.05$), likely due to small sample size, this highlights the importance of age matching for experiments that investigate the impact of m.3243A>G on cellular function.

A)

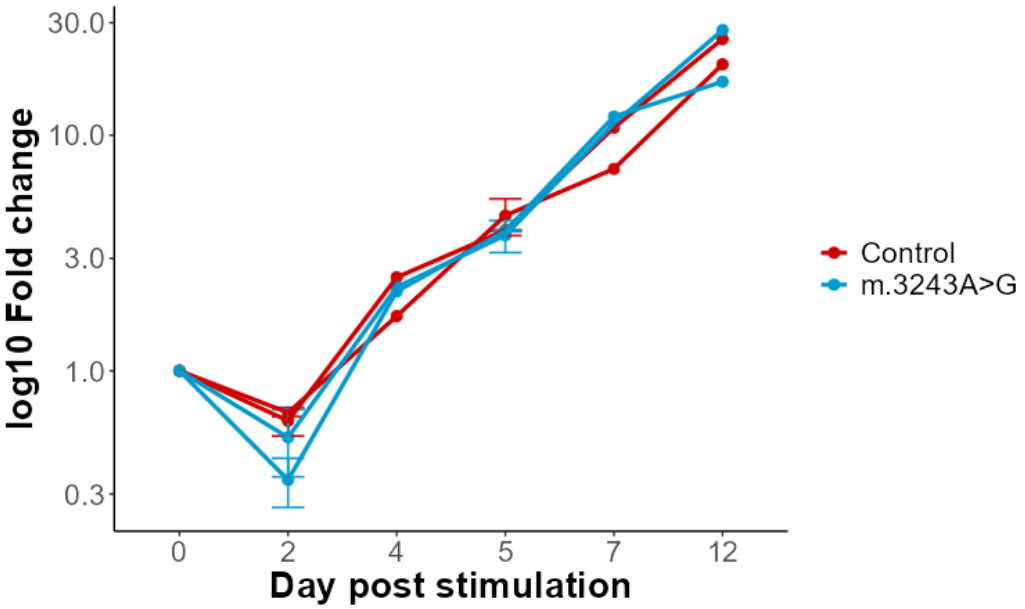


B)

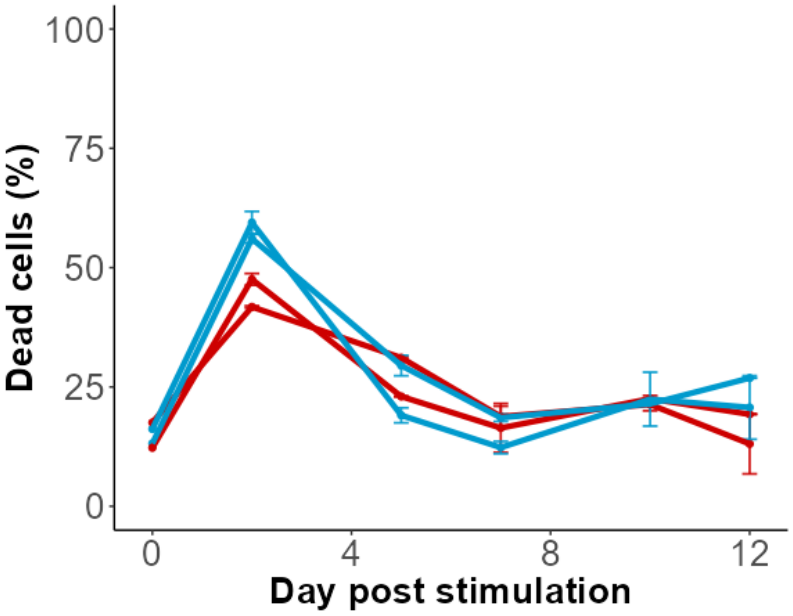


***Figure 5.5 Fold change after T cell stimulation with αCD28 and αCD3 in patient and control samples.*** *A) Viable Cells were measured using trypan blue exclusion on a haemocytometer. Measurements per individual are connected; red lines demonstrate control and blue lines m.3243A>G samples. Points with error bars represent an average of two technical replicates B). Error bars represent sd of percentage of dead cells as determined via flow cytometry using a live/dead stain from two technical replicates.*

Next, I used the above cell count and the proportions of CD3+ cells determined by flow cytometry to calculate the proportion of dead cells that were T cells. Both patient and control samples exhibited a high proportion of CD3+ T cells within the dead cell population (**Figure 5.6A**). Further investigation revealed a loss of over 60% of CD8+ cells in both patient samples. Although not significantly different to controls (t-test, $p < 0.05$), this result warrants further investigation in a larger sample size.

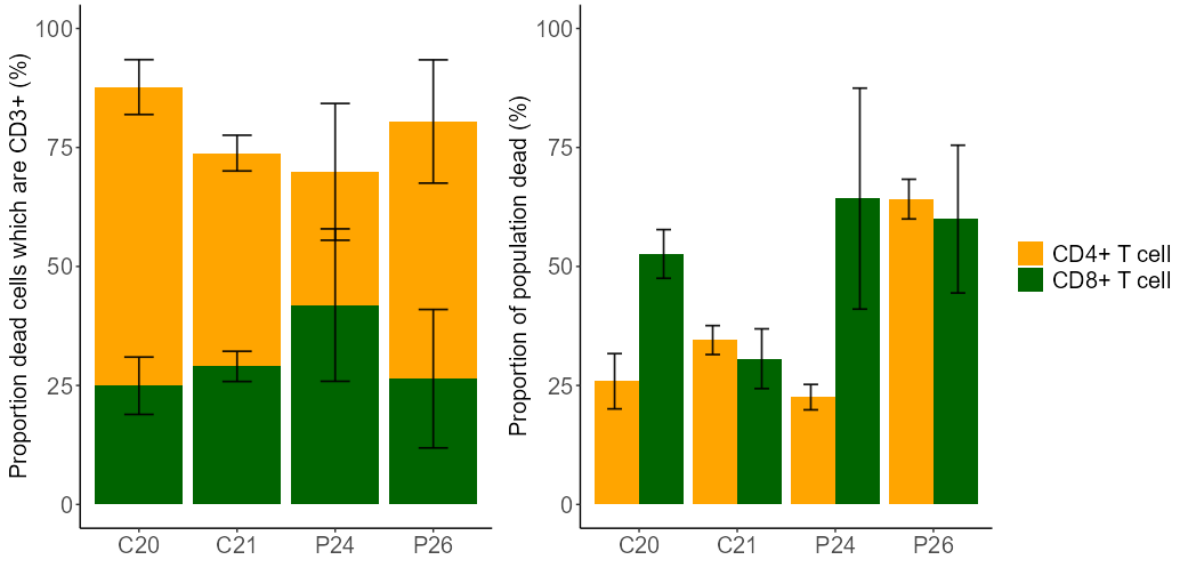


***Figure 5.6 T cell contribution to cell death at day 2 post stimulation*** *A) The proportion of dead cells that are CD3+ T cells. B) The proportion of CD8+ and CD4+ T cells which are dead at day 2 for CD4+ (yellow) and CD8+ (green) cells. Bar charts represent an average from two technical replicates per individual. Standard deviation represented by black bars. T cell death determined via flow cytometry using live cell dye and the proportion of T cells determined via flow cytometry.*

Increased CD8+ T cell death in patient samples at day 2 is reflected in the changes in CD4+ to CD8+ T cell ratio. In patient samples, there is a delayed progression into a CD8+ dominated response (**Figure 5.7**). Control samples switched from a CD4+ dominated response to a CD8+ dominated response on day five whereas in patient samples, this did not occur until days 7-12 These data suggest a vulnerability of CD8+ T cells to activation induced cell death resulting in a longer recovery period.

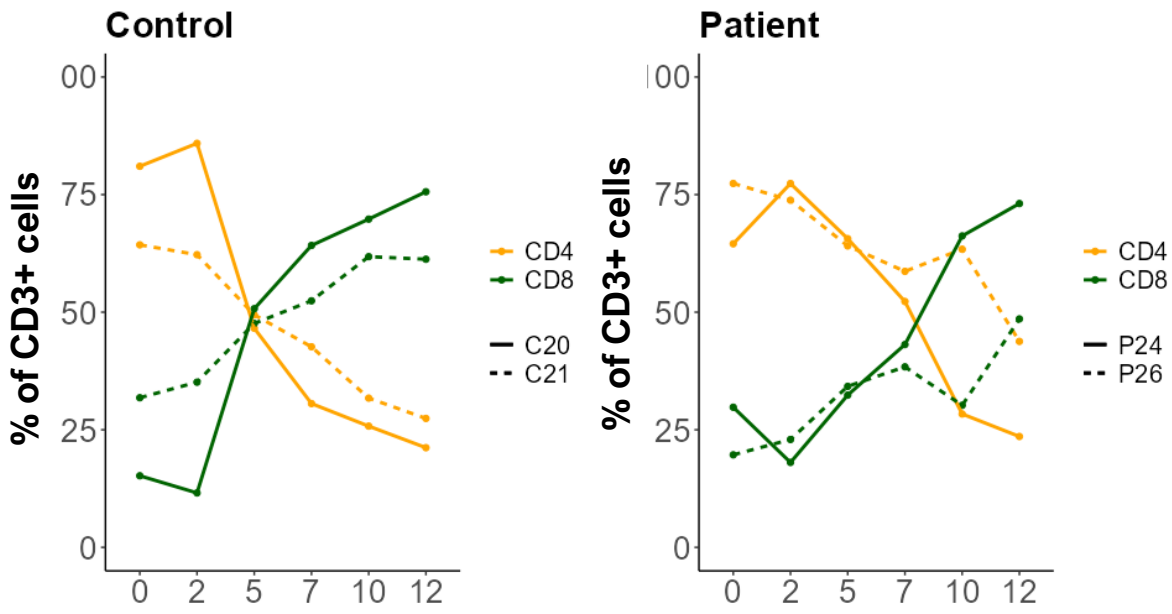


***Figure 5.7 CD4:CD8 ratio in controls and patients during 12-days following CD3/CD28 stimulation.*** *Patients exhibit a delayed response trajectory compared to controls. Each point represents the proportion of T cells made up of single positive CD8+ cells (green) or CD4+ cells (yellow) in control samples (C20 or C21) or patient samples (P24 or P26).*

To understand if the delayed transition to a CD8+ dominated response was driven by alterations in proliferation, I used CTV concentration to assess the proliferative index and the proportion of cells which have undergone at least one division from day two until day seven post stimulation. Patient T cells demonstrated a proliferative index similar to controls in surviving CD4+ and CD8+T cells (**Figure 5.8Ai & Bi**). In both groups the proliferative index was higher in CD8+ T cells. The percentage of dividing CD4+ T cells was mildly decreased in m.3243A>G samples at day 7; as the proliferative index was normal, this may suggest a decreased proportion of CD4+ are dividing at this point (**Figure 5.8Aii**).

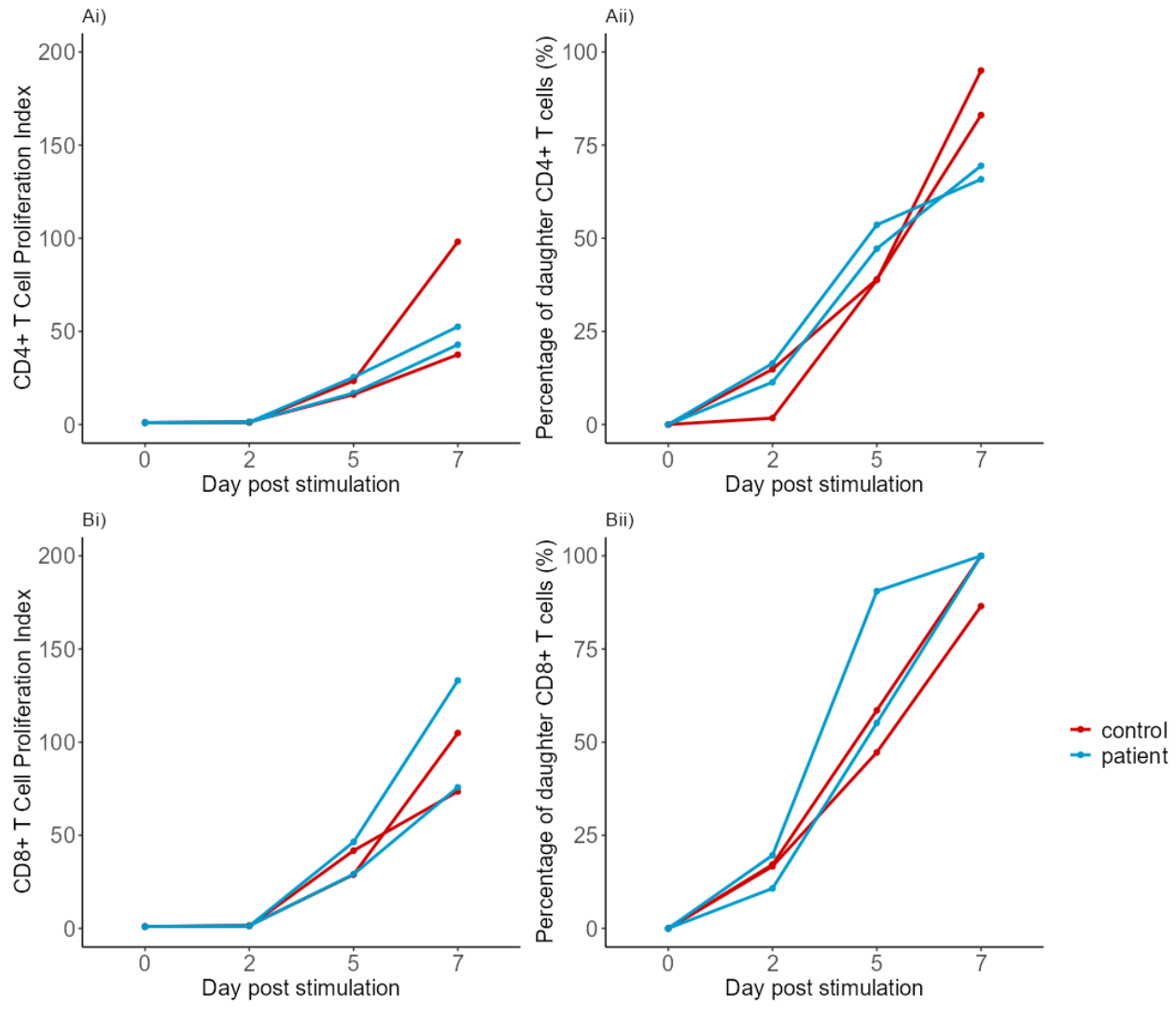


***Figure 5.8 Proliferative index and percentage of dividing cells in patients and controls***. *Ai) The proliferation index of CD4+ cells at days 0 to 7 is not different to controls (t-test, p>0.05) Aii) The proportion of CD4+ T cells which have undergone at least one division. There is no significant difference between patients and controls at day 7 (t-test p > 0. 05) Bi) The proliferation index of CD8+ cells at days 0 to 7 is not different to controls. Bii) The proportion of CD8+ cells which have undergone at least one division on days 0-7. Proliferation index and percentage of daughter cells were quantified using the proliferation fit feature on FCS Express 7.*

Further investigation of proliferation via assessment of the contents of each proliferative generation revealed similar progression through the response in patients and controls, supporting the notion that surviving T cells have a proliferative potential comparable to controls. However, although not significant (t-test, $p>0.05$), the proportion of original CD4+ cells which had not undergone a division by day 7 was higher in patient samples compared to controls (**Figure 5.9**), consistent with the decreased proportion of CD4+ cells dividing identified in **Figure 5.8Ai**.

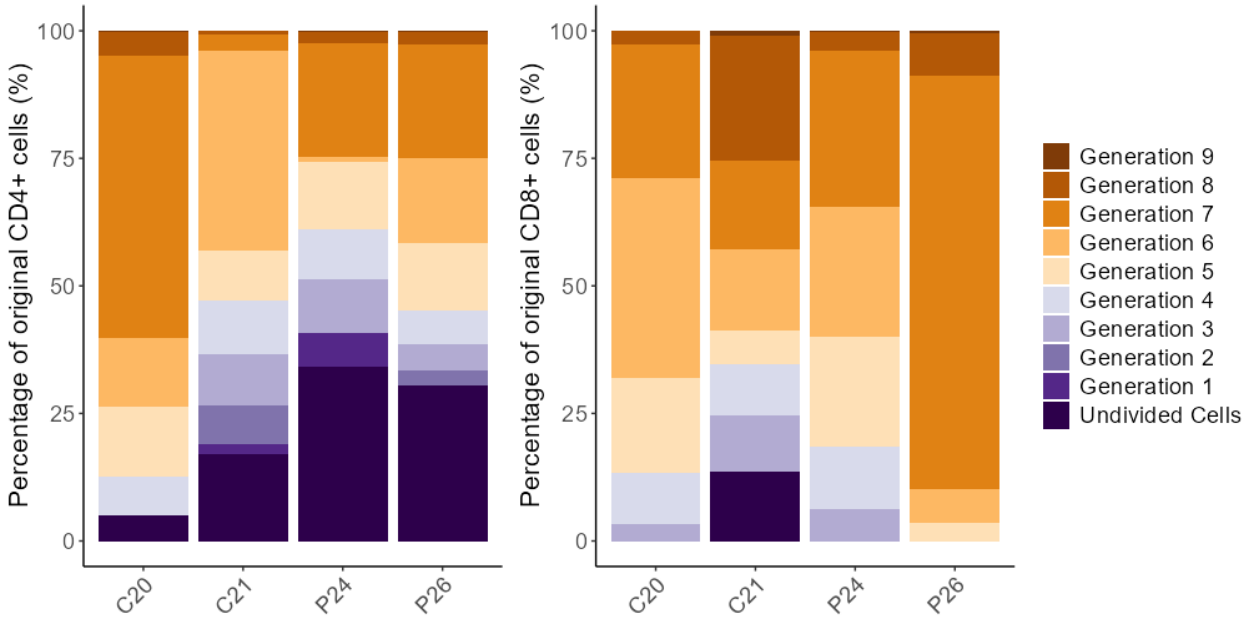


***Figure 5.9 The proportion of original cells contributing to each peak in CD4+ and CD8+ T cells at day 7 post stimulation in patient and control samples.*** *The proliferation fit feature on FCS Express 7 was used to calculate the number of proliferative episodes undergone by the original cells stimulated on day 0. Each generation signifies the number of divisions a cell has undergone.*

In the early stages of T cell activation following TCR stimulation, T cells undergo increased mitochondrial biogenesis (Ron-Harel *et al.*, 2016). To understand whether this is affected by m.3243A>G, I compared absolute mtDNA copy number in patient and control samples. There was a large increase in mtDNA CN in both patient and control sample (**Figure 5.10**). The sample with the smallest increase in mtDNA CN was from

P24, the individual with the highest heteroplasmy (36%). This suggests that higher levels of m.3243A>G may impede mitochondrial biogenesis associated with T cell activation and warrants further investigation in a larger number of samples.

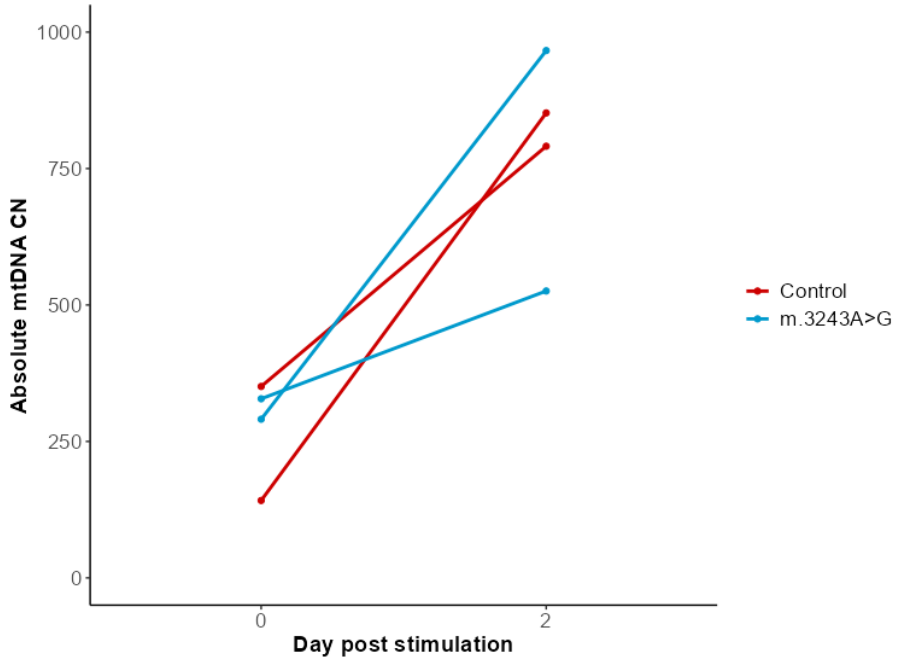


***Figure 5.10 Changes in absolute mtDNA copy number following anti-CD3/anti-CD28 stimulation.*** *All samples show an increase in mtDNA CN two days post stimulation. CN represented as a mean of triplicate measurements.*

### 5.3.3 Interrogation of negative selection of m.3243A>G during expansion

To investigate whether m.3243A>G level changed with cell division, I compared m.3243A>G levels throughout the T cell expansion. As a mixed population of cells was stimulated on day 0, this would not be representative of a change in only T cells. Data presented in section 3.3.2 show that T cells typically have a lower m.3243A>G than a mixed population, therefore I compared m.3243A>G level at day 5, when the population is >95% T cells (**Figure 5.11**), to day 12. Interestingly, a decline in m.3243A>G level in T cells was restricted to the sample from P24, in which a measurement of 22% was taken on day 5 and 17% on day 12 (**Figure 5.11**). The level in the sample from P26 altered within the limits of the pyrosequencing sensitivity (±3%), therefore, there was no change

within this sample. The steeper decline observed with P24 is consistent with a steeper decline in m.3243A>G in the whole blood with age in those with a higher heteroplasmy.

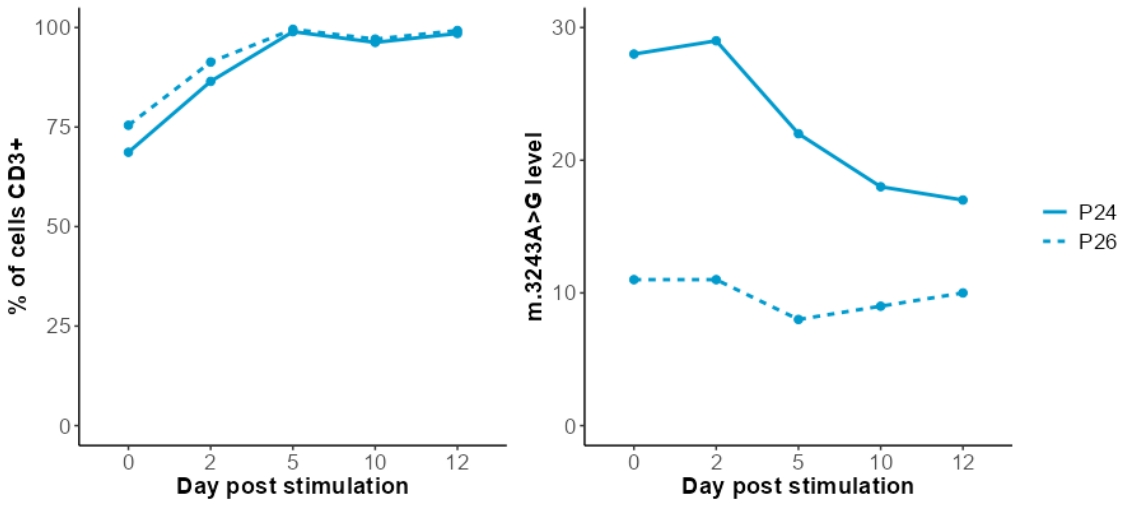


***Figure 5.11 Proportion of T cells and their m.3243A>G at different timepoints post activation*** *Left) The percentage of T cells in each sample reaches ~95% at day 5 in all samples. Right) A decline in m.3243A>G level occurs in cells from P24 but not P25 or P26 between days 5 and 12. Lines join measurements from the same sample.*

I then compared these measurements to samples stimulated in media enriched with uridine, a ribonucleoside which is synthesised in the mitochondria and essential for pyrimidine synthesis. Enrichment of media with uridine and pyruvate maintains survival of cells with mitochondrial dysfunction in culture (King and Attardi, 1989). Addition of uridine into the culture did not change the fold change in patient or control samples, however, it did result in a small increase in viability in the patient cells when compared to media without uridine (**Table 5. 4**), suggesting that some cells may be succumbing to mitochondrial dysfunction in the non-uridine cultures. After 7 days the m.3243A>G level in the cultures containing uridine supplemented media were comparable (within the limits of pyrosequencing sensitivity) to those with no supplementation (**Table 5. 4**). However, this was only run as a single experiment, and will necessitate repeat experiments to confirm these findings.

| Patient | Day 0 | | Day 10 viability (%) | | Day 10 Het (%) | |
|---|---|---|---|---|---|---|
| **No.** | **Viability (%)** | **Het (%)** | **R10** | **Uridine** | **R10** | **Uridine** |
| **P24** | 86.8 | 28 | -13.7 | -6.2 | -10 | -7 |
| **P26** | 83.8 | 11 | -10.2 | -2.3 | -2 | -4 |
| **C20** | 87.7 | NA | -9.2 | -10.7 | NA | NA |
| **C21** | 82.5 | NA | -2.9 | -4.6 | NA | NA |

***Table 5. 4 A comparison of viability and m.3243A>G levels of PBMCs cultured in R10 and uridine supplemented media.*** *Patient samples demonstrated a mild increase in viability in uridine media compared to R10. Viability measurements taken using live/dead dye. Day10 measurements presented as difference between Day 7 and day 0 measurements.*

### 5.3.4 Response to antigen specific stimulus

As αCD3 and αCD28 induce a high proportion of T cells to proliferate, the above investigations are not reflective of a true infection scenario, therefore, I chose to investigate the antigen specific response in m.3243A>G samples to two viral peptides: Sars-CoV2 and CMV.

Patients have a larger range in the proportion of IFN-γ producing cells in response to Sars-CoV2 than controls, however there was no significant difference between the two groups (**Figure 5.12**, *linear mixed model, p=0.165, β=1.449, SD=65.389*). There was also no relationship observed with age or sex and response to Sars-CoV2 (*linear mixed model, age: p=0.658, sex=0.267*). As vaccine response is known to be dependent on age, this suggests more samples are needed to see an effect. Interestingly, this was an opposing effect to that observed in response to CMV, in which a significantly higher number of IFN-γ producing cells were present in controls compared to patients (*linear mixed model; p=0.0253, β=-2.452, SD = 348.69*). These data do not suggest that m.3243A>G specifically inhibits or enhances viral response but the differences in response to the viral peptides could relate to the altered CD4 to CD8 ratio in patient T cells. More information is needed about patient vaccine schedule and CMV serology to understand this fully.

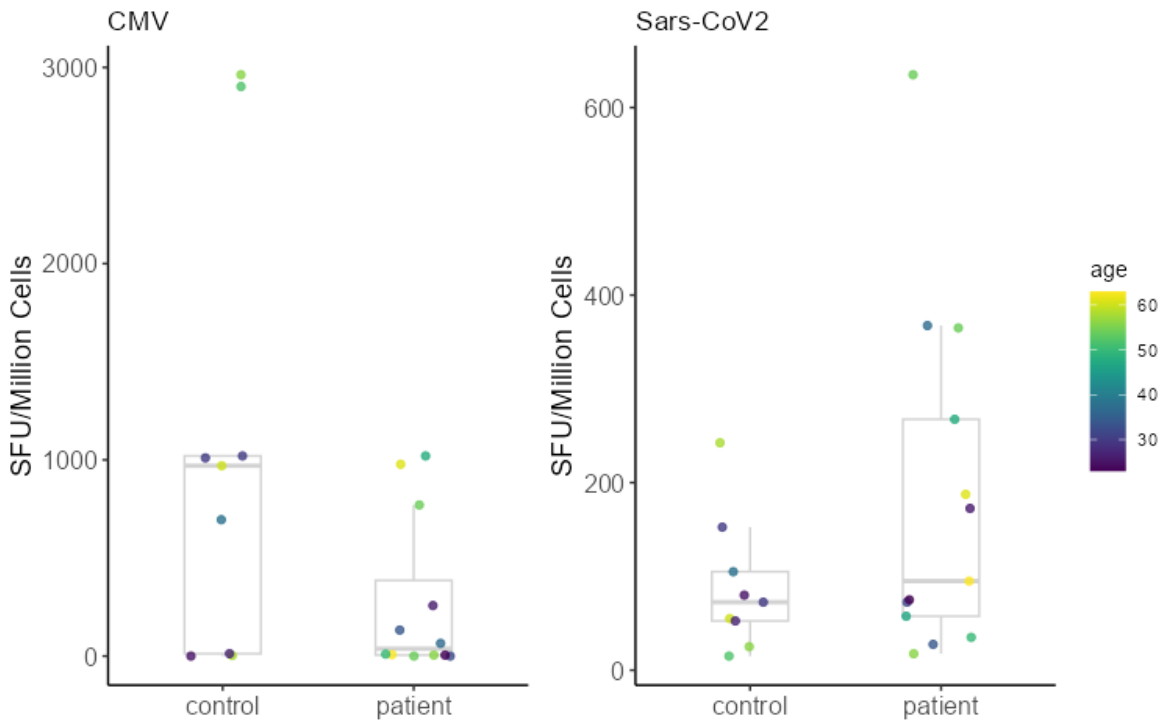


***Figure 5.12 IFNγ response to CMV and Sars-CoV2 in patients and control samples.*** *A) Response to cytomegalovirus lysate B) Response to Sars-CoV2 spike proteins 1 and 2. Each point represents the mean response per individual from 3 technical replicates and is coloured by patient age. SFU, spot forming units.*

## 5.4 Discussion

In this chapter, I have carried out preliminary investigations into the proliferative and cytokine production capabilities of T cells carrying the m.3243A>G pathogenic variant. These investigations identify that individuals with m.3243A>G have a reduced proportion of T cells. In response to stimulation, T cells carrying m.3243A>G expanded at a rate similar to controls in a CD4+ dominated expansion. This differed from control T cells which transitioned to a CD8+ dominated response around day 5 and demonstrated higher levels of CD8+ cell death. This differing response trajectory between patients and controls does not appear to influence viral response, however trends are emerging in IFNγ response which require further investigation. During the expansion of T cells, negative selection of m.3243A>G was observed in one of two patient samples, P24, which had the highest starting m.3243A>G level of the two (28%). It is important to note that these investigations were carried out using a small sample size and should be interpreted with caution; no conclusions can be made until sample size has been increased substantially. These investigations do, however, identify areas that warrant discussion.

### 5.4.1 m.3243A>G impacts blood homeostasis

A decreased proportion of T cells in m.3243A>G patients as well as enhanced selection in these cells (sections 3.3.2 & 4.3.4) suggests that m.3243A>G is impacting T cells in a unique way. The overall reduction in the proportion of T cells suggests that m.3243A>G is having a negative impact early in cell development, perhaps at the thymocyte stage, like that observed in the mutator mouse. This a mouse model with a dysfunctional polymerase γ, generated via a D257A knock-in, which results in the accumulation of mtDNA variants over the mouse's lifetime (Trifunovic *et al.*, 2004). These mice typically have a short lifespan, surviving until just 13-15 months due to the development of megaloblastic anaemia that is associated with both erythrodysplasia and impaired lymphopoiesis (Chen *et al.*, 2009). Lymphoid abnormalities originate early in development, as indicated by their decreased thymic mass (Kujoth *et al.*, 2005), total number of viable thymocytes and defects in generation in pro-B and pre-B cells. As mentioned already, this may be a consequence of the enormous metabolic demand thymocytes undergo in the generation of single positive cells.

The same signalling pathways highlighted as key regulators of quiescence exit, c-myc and mTOR, are also involved in the transition from DN to DP in murine thymocytes (Yang *et al.*, 2013). The mitochondrial fusion protein OPA1 (discussed in section 1.2) has been found to be important at the DN3 stage (Corrado *et al.*, 2021), as is the induction of fusion in the transition from naïve to memory (Buck *et al.*, 2016), indicating the same mechanism of selection at the naive to memory stage could be occurring at the thymocyte stage, driving the observed loss of cells. Memory T cells have been demonstrated to display a fused mitochondrial network, whereas effector T cells have a highly fragmented network (Buck *et al.*, 2016). Infection of OPA1 knock out mice with Listeria monocytogenes expressing ovalbumin (LmOVA) revealed a normal effector response but drastically impaired memory cell development. This discovery lead authors to induce fusion in effector T cells via culturing cells with the 'fusion promotor' M1 and fission inhibitor 'Mdivi-1' resulting in the formation of cells morphologically similar to memory cells as demonstrated by a fused network, increased mitochondrial mass and increased OXPHOS activity (Buck *et al.*, 2016). Exposure of human effector T cells to M1 and Mdivi-1 *in vitro* displayed an increase in memory cell external marker expression suggesting fusion drives changes in metabolism which induce cell differentiation. A more fragmented mitochondrial network has been observed in patient fibroblasts suggesting the fusion process may be affected by m.3243A>G and may inhibit memory formation in highly pathogenic cells (Lin *et al.*, 2023, Tokuyama *et al.*, 2020).

### 5.4.2 Emerging trends in m.3243A>G cell death

The experiments outlined in this chapter have suggested that there may be increased CD8+ T cell death in patients compared to controls but does not identify a difference in overall fold change. As the proliferative indices stay largely the same, this suggests that surviving populations are able to respond at a rate comparable to controls. This presents an avenue of further investigation, which requires a larger sample size. High levels of activation induced cell death could present a bottleneck which drives the selection observed between T naïve and memory states. Activation induced cell death is utilised highly during negative selection in the thymus as well as being a key form of peripheral

tolerance, therefore this could also be applied to the reduced m.3243A>G levels in naïve T cells (Badovinac,Tvinnereim and Harty, 2000, Dadamio,Awad and Reinherz, 1993). This is supported by research into large single deletions which indicated CD8+ memory cells are more sensitive to selection than their CD4+ counterparts (Lareau *et al.*, 2023). Characterisation of the cell death further, for example by using an antibody panel which identifies apoptotic naïve (CCR7+) and memory CD8+ T cells (CD45RO+) using markers such caspase 3 (late) and caspase 7 (early), will allow the investigation of whether cell death is restricted to a specific cell state. In addition to this, sorting of, single, apoptotic cells via FACS and measurement of the m.3243A>G level would enable assessment of whether a high proportion of these have a high m.3243A>G level.

Interestingly, selection against m.3243A>G was only identified in one of two patient samples *in vitro*. This is consistent with an experiment carried out by Walker and colleagues earlier this year, who showed that CD4+ T cells from one of four patient samples do not exhibit selection as a result of αCD3, αCD28 stimulation (Walker *et al.*, 2024). As selection at a whole blood level seems to be highest at high heteroplasmy, it was surprising that in Walker et al's study the sample which did not show selection had a m.3243A>G level of 33%, whereas other samples with 13% m.3243A>G declined by ~10%. This suggests that selection is not solely dictated by m.3243A>G level and number of divisions, supporting findings from *chapter 4* which suggest purifying selection is occurring even at low heteroplasmy. Walker et al's (2024) work focused on bulk measurements; comparison of single cell m.3243A>G level in samples showing selection and those remaining the same would improve this study and give insight into differing selection behaviours. The authors of this study also found that m.3243A>G carriers have higher levels of oligoclonality than controls. They suggest that T cells with high m.3243A>G levels die upon activation, resulting in enrichment of the T cell pool with clonal cells; this is consistent with the CD8+ T cell death data presented in this chapter and Kotrys *et al.* (2024)'s proposed theory of selection. But this cannot explain why samples from some individuals do not display selection after activation, suggesting that other factors, such as nuclear cofactors play a role.

Increased death of CD8+ cells was supported by the altered CD4:CD8 ratio observed in patients compared to controls. A delay in generation of a robust cytotoxic response could

increase incidence of infection. If m.3243A>G is driving an immune phenotype, the effects would be more apparent in paediatric cases as at a younger age, individuals will possess the highest m.3243A>G level. Few investigations into m.3243A>G in childhood have been carried out as it is typically a disease presenting in adulthood, therefore the presence of a mild, self-resolving, paediatric immune deficiency in m.3243A>G may be overlooked. In the future, monitoring paediatric cases in families carrying the variant would be the most informative pathway for investigating this.

### 5.4.3 Limitations

Research into the long-term response to the Sars-CoV2 vaccination has identified periods of waning after vaccination. Following the rise of the delta variant, Andrews et al investigated vaccine responsiveness in a 20-week period following vaccination with two doses of the ChAdOx1 (AstraZeneca) and BNT162b2 (Pfizer–BioNTech) vaccinations (Andrews *et al.*, 2022). This revealed BNT162b2 to have a higher effectiveness 1 week following the second dose (92.3% compared to 64.8%) and both vaccinations exhibit significant waning by 20 weeks. A decrease in effectiveness of 20.5% to 44.3% was identified in those inoculated with ChAdOx1 and a 26% decline with Pfizer–BioNTech, which even with this period of waning retains a high response. This research highlights the importance of considering the period post-inoculation as well as the form of vaccination received in order to interpret the IFNγ ELISpot data. There is the potential that patients and controls may be on different vaccination schedules which may be driving the trend observed in **Figure 5.12**. Therefore, in the future, each group needs to be further stratified according to the number of vaccinations they have received as well as the period since inoculation.

A caveat to comparing CMV and Sars-CoV2 data is that there is the potential that Sars-CoV2 vaccination and latent CMV infection could impact one another. Assessment of serology from 143 nursing home residents and 107 healthcare workers revealed CMV seropositive status can negatively impact vaccine response (Freeman *et al.*, 2023). This is most prominent when the Sars-CoV2 antigen has not been encountered before and is ameliorated after booster infection. As these participants were recruited in 2021/2022, they have had either 1 or 2 vaccinations before recruitment. It is possible that the higher

incidence of CMV infection in controls is driving the lower proportion of cells responding to Sars-CoV2.

### 5.4.4 Future Directions

As proliferation data from this chapter demonstrated negative selection of m.3243A>G in one sample and not the other, it has highlighted the importance of using a larger number of m.3243A>G samples to understand the heterogeneity of this process. In addition to this, cells underwent five days of expansion before heteroplasmy comparisons could be made; further experiments should involve isolation of a pure population of T cells before stimulation to avoid indirect effects of B cells and myeloid cells. Naïve T cells typically have a higher m.3243A>G level than memory T cells (sections 3.3.3 & 4.3.4) therefore isolation of these cells and stimulation with αCD3/αCD28 may give a clearer picture of selection as these cells are antigen naïve and have not previously undergone mass proliferation outside of the thymus. The use of a pure population will alleviate the variability added by non-T cells within the activated PBMC population in these investigations. Measurement of m.3243A>G in single cells from individual proliferation peaks before and after activation will also improve this protocol as the change in distribution across the population can hint towards the mechanism of selection. Perhaps coupling this with investigations into the TCR, to understand which T lineages survive and populate the effector population and how the heteroplasmy has changed within this lineage. It would also be interesting to repeat this experiment with other mtDNA variants to understand if it is occurring randomly during proliferative episodes in tRNA variants or is truly restricted to variants demonstrating selection in the memory cells such as m.3243A>G, m.8344A>G and m.5703G>A.

Capturing the media during media changes and quantifying the production of cytokines such as IFNγ, IL-10, IL-2 and IL-4 throughout the response and comparing this to control samples would elucidate discrepancies between the two. Assessment of cytokine release in this way may be more informative than the use of ELISpot as there are fewer confounding variables. As yet, cytokine release has not been assessed in patient T cells, only whole leukocyte response to LPS (*data discussed in section 4.4.3*)(Karan *et al.*, 2022).

## 5.5 Concluding Remarks

This chapter has outlined exploratory investigations into the possibility of a function defect in T cells carrying m.3243A>G. I have identified a disruption in T cell homeostasis and the possibility of increased CD8+ T cell death in those with m.3243A>G. This was accompanied by negative selection in one of two patient samples, indicating that further and more refined investigations focusing on a single subset of T cells such as the naïve T cells would be beneficial for understanding of this process. To build on this, investigation into any alterations in c-myc and mTOR pathways by sequencing of the cellular transcriptome would elucidate understanding of the cells ability to exit quiescence and whether it is dependent on m.3243A>G level. The following chapter will outline the optimisation of a protocol to investigate this.

# Chapter 6 Using parallel mtDNA and transcriptome sequencing to understand the impact of m.3243A>G in single cells.

## 6.1 Introduction

Single cell data presented in chapter 4 demonstrates high levels of heterogeneity between individual cells within the same cell population, while also showing an increase in cells which have cleared the m.3243A>G variant. In order to understand selection, it's important to be able to determine cellular phenotype of cells with different m.3243A>G levels. To date, this has been an unexplored area, due to the difficulties involved in sequencing both the *MT-TL1* gene and transcriptome within the same cell. *MT-TL1* encodes a tRNA which is not poly-adenylated and undergoes immediate post transcriptional modifications; as a result, it does not sequence to the depth required to determine heteroplasmy via RNA sequencing (Zheng *et al.*, 2015). Therefore, traditional scRNA sequencing protocols would not be appropriate. In this chapter I will use an alternate method to assess mtDNA and the transcriptome in the same cell.

### 6.1.1 Interrogations of changes in the transcriptome with m.3243A>G level

Due to the difficulties in sequencing m.3243A>G level and RNA in the same cell, many investigations into m.3243A>G-related changes in the transcriptome rely on bulk RNA sequencing of cell lines/cybrid cells lines with known m.3243A>G level. Picard and colleagues generated cybrids of varying m.3243A>G level and found alterations to the bulk transcriptome at different m.3243A>G levels (Picard *et al.*, 2014). They describe an upregulation of pathways involved in transcriptional regulation, cytoplasmic translation, mitochondrial protein import and OXPHOS with an increasing m.3243A>G level. Dysregulation of some pathways did not show a linear relationship to m.3243A>G level for example, an upregulation in glycolytic pathways was observed between 60 and 90% m.3243A>G. As this seems to increase with m.3243A>G level, it was surprising that this was not seen at 100% heteroplasmy or in Rho0 cells. mTOR signalling, a major signalling pathway involved in cell proliferation and autophagy regulation, was also identified as being highly dysregulated: at 20-30% m.3243A>G mTOR was downregulated compared to 0%, followed by a steep upregulation at m.3243A>G levels between 50 and 90% and another downregulation at 100% and Rho0. As outlined in section 1.6.1, transmitochondrial cybrids are not a reliable model for m.3243A>G related dysfunction;

particularly in this case as treatment of cells with ethidium bromide can vastly alter the transcriptome, particularly the mitochondrial transcripts (Danielson *et al.*, 2005).

Recently, a different group compared the transcriptome of two populations of iPSC derived neurons (iNeurons) each with 0% and 60% m.3243A>G levels respectively, which produced contrasting results in terms of OXPHOS gene expression (Klein Gunnewiek *et al.*, 2021). In iNeurons with 60% m.3243A>G, five of the top ten downregulated pathways were related to OXPHOS; cell specific pathways such as neurotransmitter secretion were also downregulated. The discrepancies between these two studies could reflect cell-type specific effects; perhaps iNeurons and 143B.TK- cybrids have different thresholds for OXPHOS dysfunction, however, their contrasting results could also reflect differences between their experimental cellular models.

As I and others have demonstrated, there is heterogeneity in the blood tissue (Franklin *et al.*, 2023, Walker *et al.*, 2020) and therefore bulk RNA sequencing, as with bulk mtDNA sequencing, would not capture the distribution within the population, only an average. Parallel RNA sequencing and mtDNA genotyping within the same cell is likely to be a more powerful tool to understand the relationship between gene expression and m.3243A>G level. This chapter introduces a novel technique for sequencing the transcriptome and mtDNA in the same cell and aims to identify genes and pathways which differ between high and low heteroplasmy cells to pursue for further analysis. The identification of affected pathways will allow deeper understanding on the mechanism by which m.3243A>G is affecting T cell proliferation rates and homeostasis (sections 5.3.1 & 5.3.2).

## 6.2 Methods

The protocol used in this chapter was adapted from one developed by Rodriguez-Meira and colleagues (Rodriguez-Meira *et al.*, 2020) and allows for sequencing of the cellular transcriptome alongside simultaneous targeted sequencing of the region surrounding m.3243A>G within the mitochondrial genome (**Figure 6.1**). As mentioned above, it is unlikely that I would be able to sequence the region flanking m.3243A>G directly from RNA; therefore, I chose not to carry out targeted sequencing of the cDNA as the original protocol suggests.

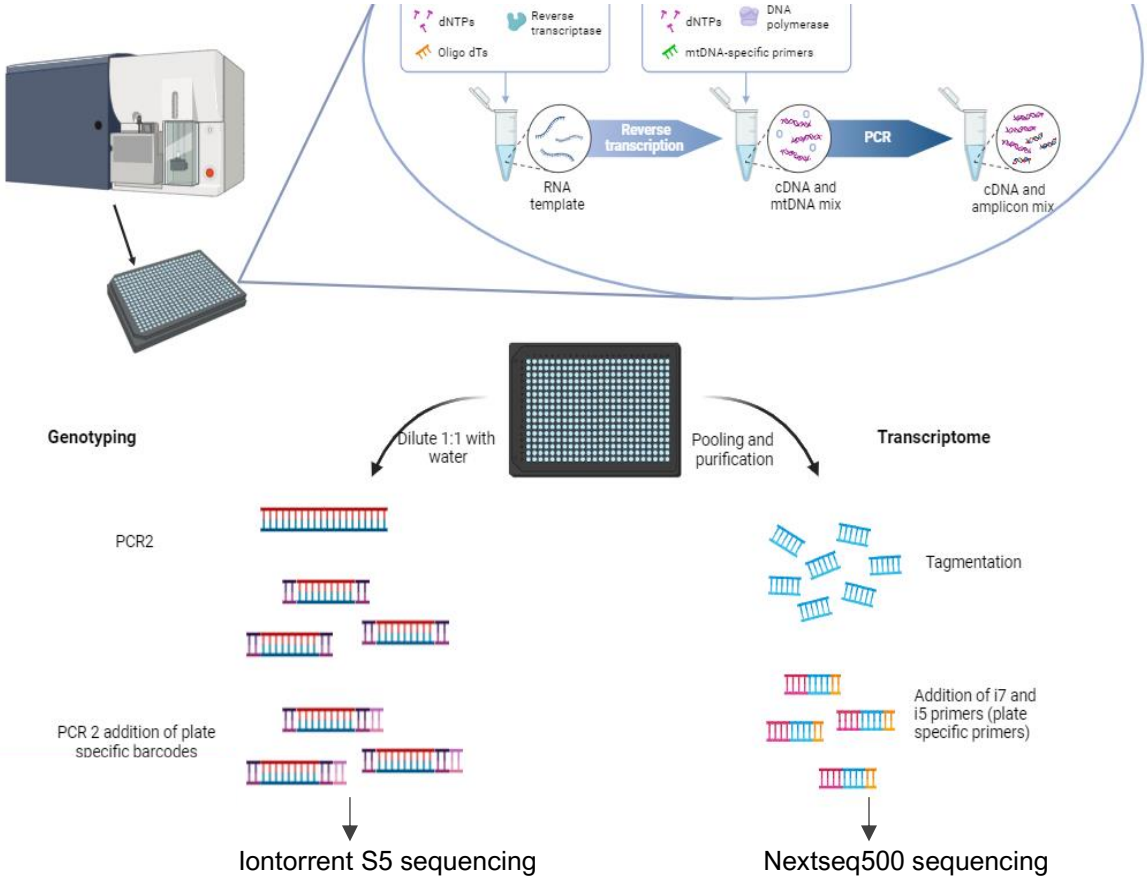


***Figure 6.1 Schematic of modified Targetseq protocol.*** *Single cells were sorted per well of a 384-well plate. Each lysed cell was subject to an oligo(dT) primed RT reaction immediately followed by a PCR amplifying a 496bp region of the mtDNA. This amplicon/cDNA mix was then split for transcriptome and mtDNA sequencing library preparation. Figure made using biorender.com*

### 6.2.1 Sample

PBMCs from a single individual, P23, were used for these investigations. P23 is a female aged 23, who has a whole blood m.3243A>G level of 58% and a urine m.3243A>G level of 74%. Her phenotype is relatively mild, presenting with diabetes mellitus and migraines only. A large number of both high and low m.3243A>G level cells are required for the following analysis therefore, this patient was selected as they are likely to possess a high proportion of cells with a high m.3243A>G level in all selected cell types (**Table 6. 1**).

| Cell Type | m.3243A>G level (%) |
|---|---|
| CD4+ Naïve | 56 |
| CD4+ Memory | 56 |
| CD8+ Naïve | 63 |
| CD8+ Memory | 40 |
| CD14+ Monocyte | 60 |
| CD34+ Progenitor | 53 |

***Table 6. 1 P23 m.3243A>G level in bulk populations***.

### 6.2.2 Cell sort & Lysis

3.5 million PBMCs were sorted into five different cell populations: CD34+ progenitor cells, Monocytes, CD8+ naïve and memory T cells and CD4+ naïve and memory cells using an identical sorting strategy to section 3.2.2. These cell types were chosen as the T cells have been highlighted as a cell type of interest in chapters 3,4, and 5. Monocytes were chosen as a myeloid comparison as I have previous identified differences in the response of lymphoid and myeloid lineages to m.3243A>G (section 3.3 & section 4.3). As the most immature cells in the blood, CD34+ progenitors will help to identify how the variant is influencing development of mature immune cells.

Individual cells were sorted into wells of a 384-well plate containing 2µl of Targetseq single cell lysis buffer (**Table 6. 2**) which preserved RNA by allowing lysis at a moderate temperature as well as containing reagents for downstream reactions, for example oligo(dT) primers and dNTPs. Each plate contained cells of single type; cell types were

not mixed as low and high m.3243A>G level cells of the same cell type were compared. Once sorted, plates were immediately snap frozen in dry ice before storing at -80ºC for up to 3 months.

| ***Reagent*** | ***X1 well (µl)*** |
|---|---|
| *0.43% Triton* | 0.88 |
| *RNase Inhibitor* | 0.05 |
| *10µm dNTPs* | 0.5 |
| *1.09AU/ml Protease* | 0.05 |
| *ERCC RNA spike in mix* | 0.02 |
| *10um Barcoded Oligo(dT)-ISPCR* | 0.5 |

***Table 6. 2 Targetseq single cell lysis buffer.*** *List of oligo(dT) primers can be found in the appendix (**Appendix F**).*

### 6.2.3 Heat inactivation and reverse transcription.

Plates were removed from -80ºC and incubated at 72°C for 15 minutes to inactivate the lysis enzymes. During this, the RT master mix was made on ice, according to the specifications in **Table 6. 3**. 3µl per well was added, on ice, immediately after the completion of the incubation via an INTEGRA MINI 96. Each plate was then incubated in a 384-well thermocycler (**Table 6. 4**)

| *Reagent* | *X1 reaction (µl)* |
|---|---|
| *5X Buffer* | 1.00 |
| *Nuclease free $dH_2O$* | 1.33 |
| *RNase Inhibitor* | 0.125 |
| *TSO-LNA (100 µM)* | 0.050 |
| *SMARTScribe enzyme* | 0.5 |

***Table 6. 3 Targetseq reverse transcription master mix***

| *Temperature* | *Time* | *Cycles* |
|---|---|---|
| *42°C* | 90 min | 1 |
| *50°C*<br>*42°C* | 2 min<br>2 min | 10 cycles |
| *70°C* | 15 min | 1 |
| *4°C* | ∞ | - |

***Table 6. 4 Targetseq reverse transcription thermocycling conditions***

Upon completion of the RT reaction, 8µl of PCR mastermix (**Table 6. 5**) was added per well using an INTEGRA MINI 96 and placed back in a thermocycler (**Table 6. 6**).

| *PCR Master Mix* | *X1 (µl)* |
|---|---|
| *2X Buffer* | 6.50 |
| *ISPCR primer (10 µM) AAGCAGTGGTATCAACGCAGAGT* | 0.07 |
| *RT-PCR Grade Water* | 0.99 |
| *SeqAMP PCR enzyme* | 0.25 |
| *Forward primer (100 µM) CGATGGTGCAGCCGCTATTA* | 0.05 |
| *Reverse primer (100 µM) AGATGTGGCGGGTTTTAGGG* | 0.05 |

***Table 6. 5 Targetseq PCR Master Mix.*** *Forward and reverse primers are derived from revised Cambridge mtDNA reference sequence GenBank accession number: NC_012920.1 Expected amplicon length is 496bp of the region flanking MT-TL1.*

| *Temperature* | *Time* | *Cycles* |
|---|---|---|
| *98°C* | 3 min | 1 |
| *98°C* | 00:15 | 24 cycles |
| *67°C* | 00:20 | |
| *72°C* | 6 min | |
| *72°C* | 5 min | 1 |
| *4°C* | HOLD | 1 |

***Table 6. 6 Targetseq PCR cycling conditions***.

The cDNA / amplicon mix generated was then split for downstream investigations. Each well was diluted 1 in 20 in water and transferred into four 96-well plates; this was used as the stock for mtDNA sequencing. 1.3µl per well was pooled to form a transcriptome library for each plate. Preparation of the mtDNA sequencing library was carried out as a nested reaction from the 496bp PCR product generated in this section 2.12.

### 6.2.4 Transcriptome library preparation

Individual libraries were generated per plate (cell type). 66 µl from each pooled library was purified twice via ampure XP beads (section 2.12.1*)* and resuspended in 25µl EB buffer, before checking library read length distribution on the bioanalyser (section 2.12.2) and quantifying library concentration on the qubit. The libraries produced had an average size of 4277bps (**Figure 6.2**) and the library concentrations were 6.27ng/µl monocyte, 25.2 ng/µl CD8+ memory and 18.6ng/µl CD8+ naïve.

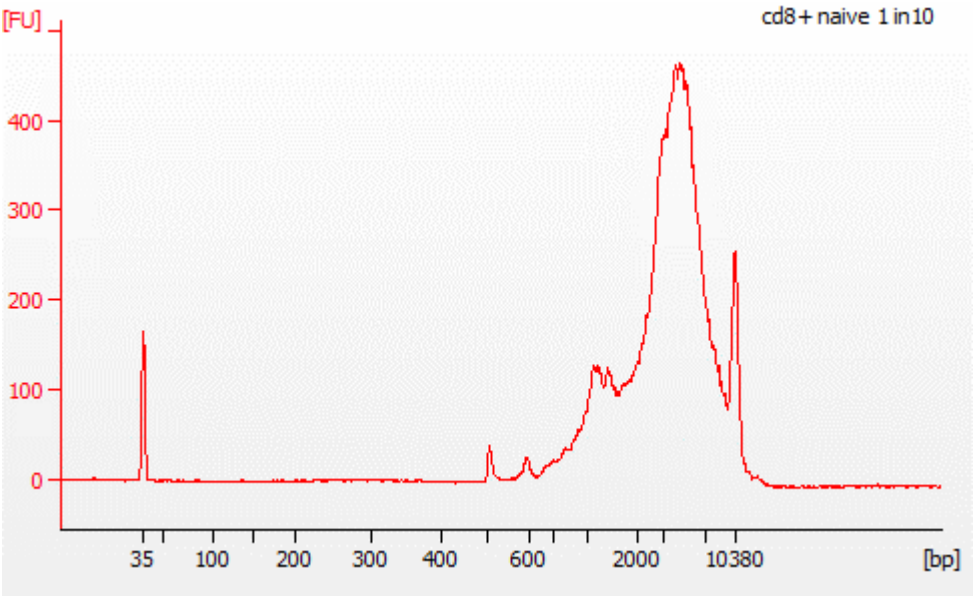


***Figure 6.2 Transcriptome bioanalyser trace before tagmentation.*** *A 1:10 dilution of the pre-tagmented CD8+ naïve library has a mean library size of ~5096bp as represented by a large peak >2000bp. The peak at 35bp and 10380bp are reference peaks which allow determination of the library size.*

### 6.2.5Tagmentation

5ul of purified library was then combined, on ice, with 10µl of tagmentation buffer and 5µl of amplicon tagment mix (Nextera XT Kit). This mixture was vortexed before incubating at 55º for 6 minutes. Immediately upon cessation of the 6 minutes the neutralisation buffer was added to quench the reaction.

### 6.2.6 Addition of sequencing indexes

To facilitate sequencing of the tagmented libraries, Nextseq compatible sequences (N702, N703, N704, *Illumina Nextera i7 adaptors*) and a custom P5_index primer (**Table 6. 7**) were ligated to the cDNA molecule. Ligation was achieved by adding 5µl of each primer plus 15µl NPM master mix to the above mix, incubating as per **Table 6. 8** and purifying, as in section section 2.12.1.

| *Index type* | *Sequence* |
|---|---|
| *P5_Index* | AATGATACGGCGACCACCGAGATCTACACGCCTGTCCGCGGAA GCAGTGGTATCAACGCAGAGT*T*G |

***Table 6. 7 P5_index sequence for Nextseq***

| *Temp (°C)* | *Time* | *Cycles* |
|---|---|---|
| *95* | 30s | 1 |
| *95* | 10s | |
| *55* | 30s | 14 |
| *72* | 30s | |
| *72* | 5 min | 1 |
| *4* | ∞ | - |

***Table 6. 8 Cycling conditions for ligation of Nextseq compatible adaptors.***

Tagmented and indexed libraries were then quantified using the bioanalyser and qubit. Libraries had average size and concentrations of 591bps & 7.56ng/µl (CD8+ Naïve; **Figure 6.3**), 519 & 2.92g/µl (CD8+ Memory) and 555 & 3.25 ng/µl (Monocyte). The concentration as determined by the qubit was used to estimate library molarity using the calculation below (**Equation 9**):

$$Molarity\ (nM) = \left( \frac{concntration\ \left(\frac{ng}{\mu l}\right)}{660 * average\ library\ size} \right) * 1x10^{6}$$

***Equation 9.*** *Calculating molarity from qubit concentration*

Equimolar quantities of each library were combined to form a final library.

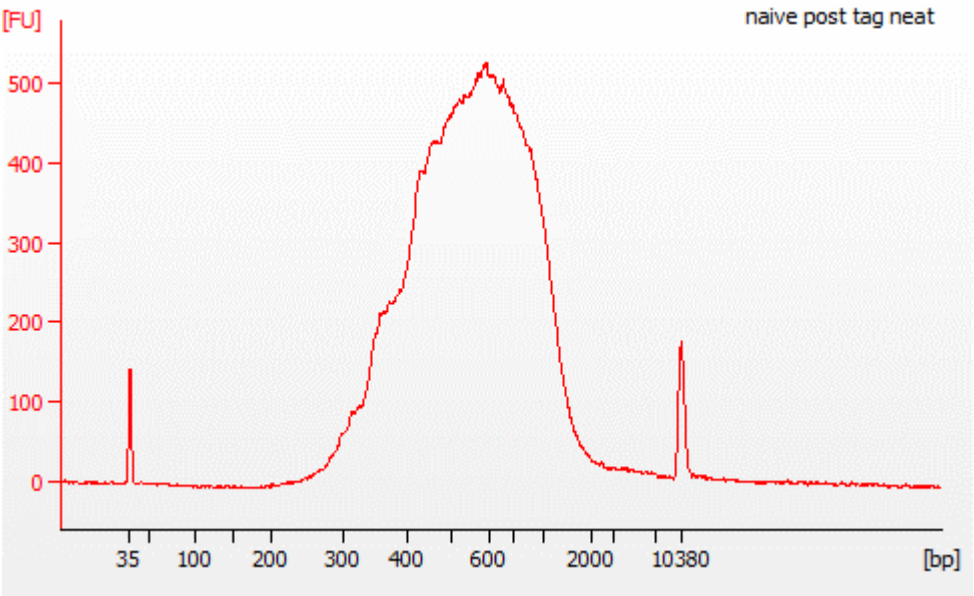


***Figure 6.3 Bioanalyser trace of a tagmented library.*** *The CD8+ naïve T cell library has an average length of 591bps post tagmentation as represented by a bell-shaped curve with the highest point at ~591bp. The peak at 35bp and 10380bp are reference peaks which allow determination of the library size.*

### 6.2.7 Nextseq sequencing

1.8pM of transcriptome library was loaded with 15% PhiX and sequenced on the Illumina NextSeq500 using a 75-cycle flow cell. All plate libraries were sequenced in a single run using paired end sequencing according to the run cycles: read 1 = 26 cycles, index read = 8 cycles and read 2 = 58 cycles.

### 6.2.8 Transcriptome bioinformatics

BCL files were demultiplexed according to both plate and well barcodes using bcl2fastq v2.2.0. Once demultiplexed, polyA tails and reads smaller than 25 bps were trimmed via TrimGalore v0.6.1 (Krueger, 2024). Trimmed fastq files were then aligned to the human genome (GRCh38) in STAR aligner v2.7.0 before quality control in Qualimap v2.2.1 (García-Alcalde *et al.*, 2012). FeatureCounts (Subread v2.0.3) (Liao,Smyth and Shi, 2014) was then utilised to generate a count matrix for downstream analysis in R.

### 6.2.9 Optimisation of mtDNA genotyping sequencing protocol

A major revision made to the Rodriguez-Meira *et al.* (2020) protocol involved adapting the mtDNA genotyping component to be compatible with sequencing using the IonTorrent Ion S5 rather than the Illumina MiSeq. Briefly, the original protocol involves the amplification of a 496bp sequence (PCR1), followed by a second PCR amplifying a 253bp region nested within the larger product (PCR2). The primers used in the second reaction contained CS1 and CS2 tags which facilitated the ligation of well-specific adaptors and sequencing. Miseq sequencing had varying success, which involved over clustering and low-quality reads, particularly at the base of interest (**Figure 6.4**). A number of steps were taken in an attempt to improve sequencing quality:

1. Modifications to PhiX concentration. Due to the library being made up of amplicons of identical length, it was important to dilute the sample with PhiX to prevent over clustering. The PhiX concentration was increased to 40% before the cluster density reached an acceptable level (734±18 K/mm2)
2. Repeat purification steps to ensure no ethanol or PCR1 (496bp) contamination. Ethanol can reduce the efficiency of DNA polymerase, as Miseq relies on a sequencing by synthesis format, it is important the enzyme is working well.
3. Repeat ligation of well-specific barcodes. To ensure that the low quality was not a result of a failure of the sequence binding to the flow cell, I repeated PCR2 and the adaptor ligation. The average library size increased by ~115bps, consistent with the adaptor size.
4. Sanger sequencing of mtDNA from P23 to exclude the presence of any alternate variants in the primer region which may impact sequencing. The only variant identified was m.3243A>G.


***Figure 6.4 Poor sequencing quality using Miseq. A)*** *The average Phred score per base per sample in reads 1 and 2 of monocyte cell library sequenced using the miseq. Green represents a high confidence base call, orange, represents a poor phred score and red have failed. The location of m.3243A>G is indicated by an arrow; a high incidence of reads with the mutant allele had a phred score of 17 and therefore did not pass the pipeline phred threshold of 28.* ***B)*** *The average Phred score per base per sample in reads 1 and 2 of plate 50 (monocytes) sequenced using the IonTorrent S5. The quality is much more consistent and surpasses quality threshold at location of m.3243A>G (indicated by an arrow).*

mtDNA genotyping was successful for just one run using the MiSeq protocol, therefore, I repeated the second PCR using the barcoded forward primers in 2.12 (and continued with library preparation and sequencing as in section 2.12.1-2.12.5 . This generated a high-quality library (Phred Score>28) (**Figure 6.4B**) with m.3243A>G levels consistent with bulk and an average read depth of 3699 (SD = 1781.043).

### 6.2.10 Data QC and filtering

The RT and PCR steps of each plate were carried out independently, this means that each plate was subject to different periods on ice before the RT reaction and each plate underwent this reaction in a different 384-well thermocycler. Due to these confounding factors, when carrying out the QC steps and data analysis, each plate was normalised individually.

Per cell m.3243A>G heteroplasmy information was merged with the counts matrix in R. Gene names were assigned to ensemble IDs where available, via BiomaRt 2.60 (Durinck *et al.*, 2005). This dataset was then split according to plate and negative wells were checked to ensure no contamination was present.

Quality control thresholds were established via visual inspection of the data in conjunction with standard single cell protocols. Filtering and normalisation of each plate was carried out using Seurat  5.0.3 (Hao *et al.*, 2024), thresholds assigned to the data were: mitochondrial reads <8%, RNA count >800 and Feature counts > 200 & < 2500 (**Figure 6.5**). After filtering, transcriptome and m.3243A>G level data for 212 CD8+ naïve T cells, 206 CD8+ memory T cells and 279 monocytes, were taken forward for analysis.

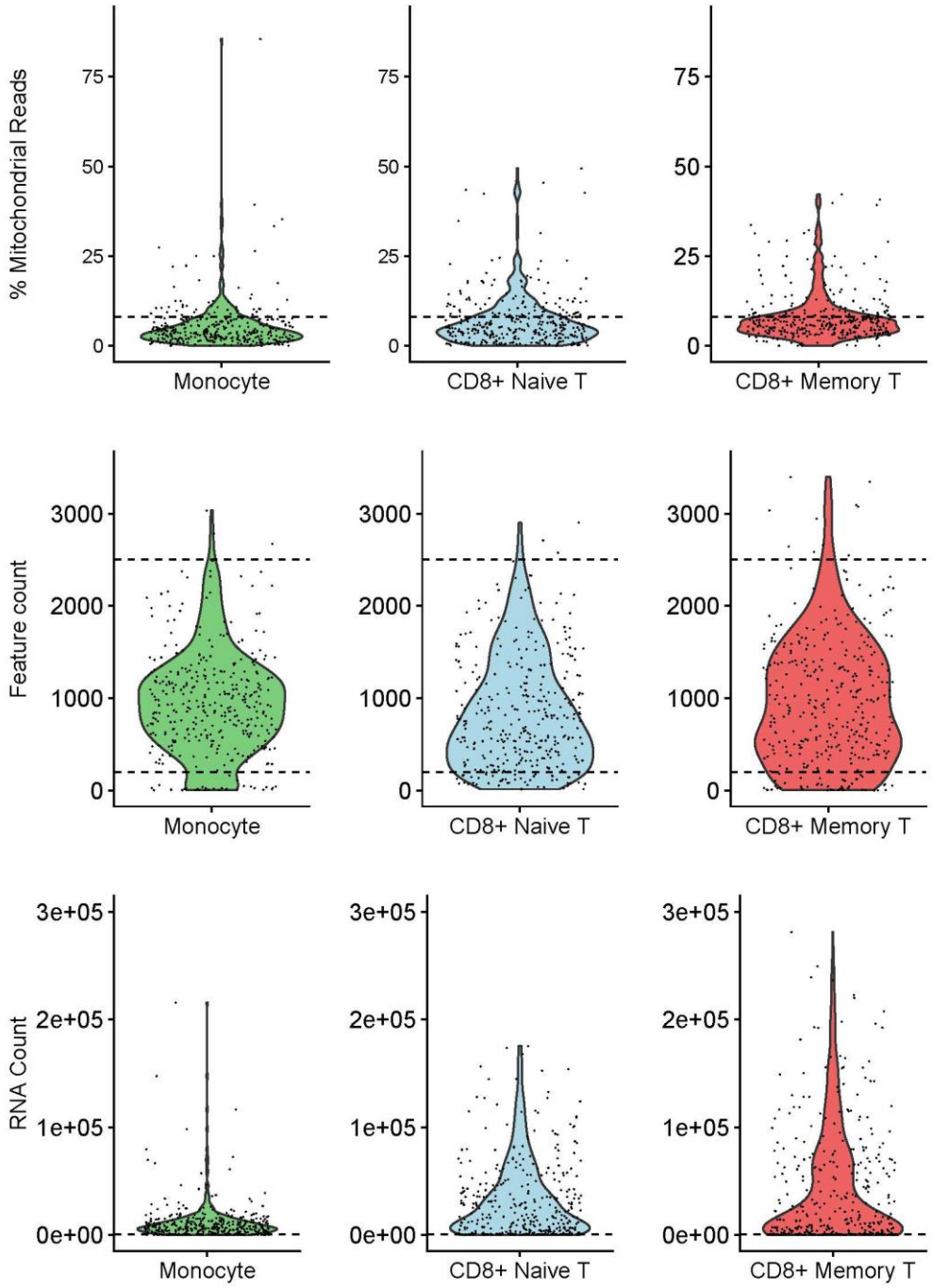


***Figure 6.5 QC thresholds for Targetseq single cell transcriptome analysis***. *The dashed lines represent the thresholds for exclusion of cells according to the percentage of mitochondrial genes (>8% removed), feature count (>2500 and <200 excluded) and RNA count (<800 excluded). Each point is representative of a single cell. 85 monocytes (green), 134 CD8+ naïve (blue), 150 CD8+ memory cells (red) were excluded from analysis according to these thresholds.*

In section 3.3, I identified a relationship between mtDNA CN and m.3243A>G level in lymphocytes, therefore, before confirming the threshold for percentage of mitochondrial reads, it was important to establish there was no relationship between this and m.3243A>G level. There was no relationship in for any cell type (**Figure 6.6**), therefore I proceeded with a threshold of <8%.

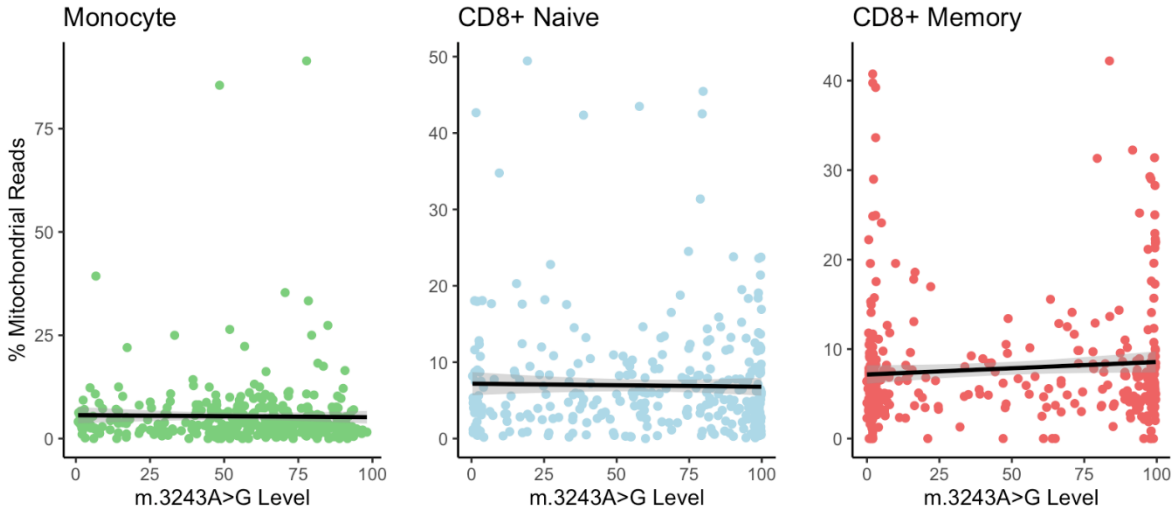


***Figure 6.6 The percentage of mitochondrial reads is not related to m.3243A>G***. *Each point represents the percentage of mitochondrial reads and m.3243A>G level of the same single cell. There was no significant relationship between percentage of mitochondrial reads and m.3243A>G level in any of the 3 cell types (linear model, p>0.05). Green = monocytes, blue = CD8+ Naïve and red = CD8+ memory.*

### 6.2.11 Analysis

Each plate was then normalised individually in Seurat using the 'LogNormalise' function by a scale factor of 10000. To minimise sources of unwanted variation, the data was scaled in Seurat using all genes. The top 2000 variable features were identified and used to perform linear dimensionality reduction. As each plate was analysed individually, clustering as in classical single cell analysis, was not performed and the data was filtered to remove genes with fewer than 10 counts. Each Seurat object was then analysed using DEseq2 1.44.0 (Love,Huber and Anders, 2014) for identification of differentially

expressed genes (DEGs) between high (>75%) and low (<25%) m.3243A>G level cells, with the reference category being low.

The output from DESeq2 analysis was then sorted into descending order according to fold change for use in gene set enrichment analysis (GSEA) using the Reactome data set (Milacic *et al.*, 2024) from the msigdbr 7.5.1 (Dolgalev, 2022) package. Genes with a log2(Foldchange) > 0.5 were used to identify enriched pathways in the gene ontology (GO) database and Human Phenotype Ontology (HPO) (Ashburner *et al.*, 2000, Gene Ontology *et al.*, 2023, Gargano *et al.*, 2023).

## 6.3 Results

### 6.3.1 Heteroplasmy profile

T cells from P23 exhibited an unusual heteroplasmy profile; **Figure 6.7** shows a bimodal distribution, with one peak near 0% m.3243A>G and the other at ~100%. The proportion of cells with a near 0% m.3243A>G level does increase with maturity, consistent with selection, it is unusual however, that such a high proportion of homoplasmic cells are retained. Skewing towards high m.3243A>G level in monocytes is consistent with previous data (section 4.3.4).

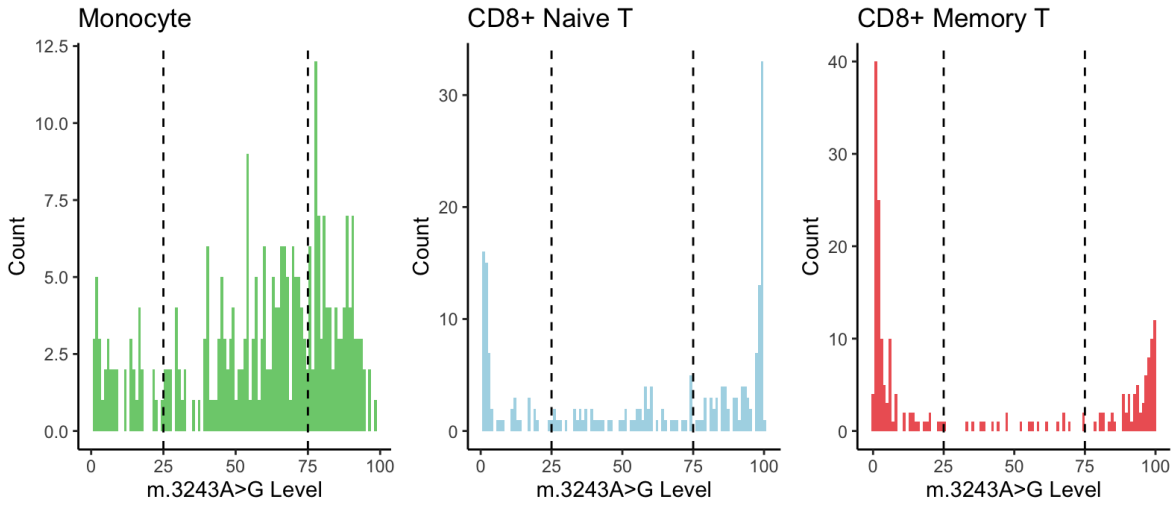


***Figure 6.7 Single cell heteroplasmy distribution in P23.*** *Each histogram represents m.3243A>G level distribution across 279 monocytes (green), 212 CD8+ naïve T cells (blue) and 206 CD8+ memory cells (red) after filtering. Dashed lines represent 25% and 75% thresholds used to categorise cells with 'low' and 'high' m.3243A>G levels.*

A high number of cells existing at these extremes of m.3243A>G is beneficial to this experiment, which will compare the transcriptome in cells with a 'low' m.3243A>G level (<25%) and those with a high m.3243A>G level (>75%).

### 6.3.2 Differential expressed genes can be identified between low and high m.3243A>G level cells.

To be identified as a gene of interest, I set a threshold of -log10(Padj) > 1. Thirty DEGs were identified in the naïve and 80 in the memory CD8+ T cells (**Figure 6.8**). As m.3243A>G is known to disrupt mitochondrial translation leading to mitochondrial dysfunction, it was reassuring to see a number of differentially expressed mitochondrial genes in cells with >75% m.3243A>G: *TOMM7* (memory, logFC = -3.857, FDR adjust p = 0.036), *NDUFS2* (memory, logFC = 4.008, FDR adjust p = 0.015), *NDUFB10* (memory, logFC = 3.689, FDR adjust p = 0.099), *ATP5PO* (memory, logFC = -4.482, FDR adjust p =0.097), *ALDH7A1* (naïve, logFC = -1.443, FDR adjust p =0.100) and *COX4I1* (naïve, logFC = 5.623, FDR adjust p =0.006).

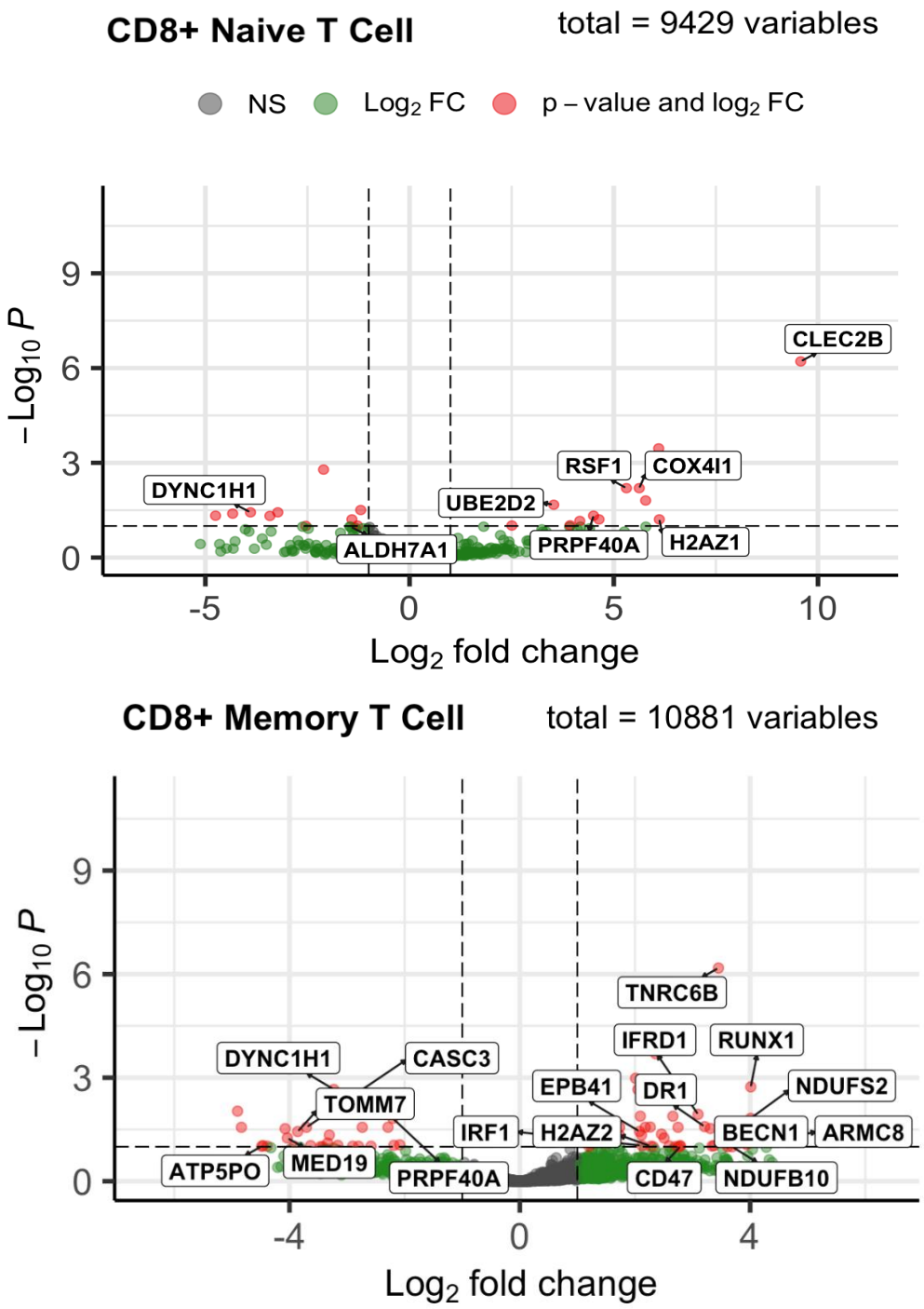


***Figure 6.8 Volcano plots showing over and under expressed genes in naïve and memory CD8+ T cells with a m.3243A>G level >75%.*** *Data generated from a DESeq2 comparison of cells with >75% m.3243A>G level (high) compared to cells from the same individual (P23) with <25% m.3243A>G (low). Top = CD8+ Naïve: n=156 (98 high,58 low); bottom = CD8+ Memory: n=187 (70 high, 117 low). Red points represent DEGs of interest: -log10(Padj) >1 & log2(fold change) > 1, green points have a large fold change but -log10(Padj) <1, black points are not genes of interest. Top hits (genes with lowest p values), mitocarta genes and genes related to cell function are labelled.*

Many related DEGs were identified across the two cell types, particularly those related to RNA Pol II (**Appendix G** *&***Appendix H**), however, only two genes were differentially expressed in both cell states: *DYNC1H1* (Dynein Cytoplasmic 1 Heavy Chain 1) and *PRPF40A* (Pre-MRNA Processing Factor 40 Homolog A).The cellular trafficking gene *DYNC1H1*, which encodes a subunit of the cytoplasmic dynein complex, was downregulated in high m.3243A>G cells of both maturation states (**Figure 6.8**). Interestingly, *PRPF40A*, which is involved in pre-mRNA splicing, was upregulated in naïve but showed an opposing effect in the memory cells; this could hint towards the different metabolism required to tolerate m.3243A>G in each cell state. Upregulation of two H2AZ histone variant genes, which differ by just 3 amino acids (Coon *et al.*, 2005), was seen in both cell subsets: *H2AZ2* in memory and *H2AZ1* in naïve (**Figure 6.8**), perhaps indicating an alteration in transcription in high m.3243A>G level cells, with the different cell states requiring transcription of different genes.

Several genes related to cytokine release were overexpressed in memory T cells, such as Interferon regulatory factor 1 (*IRF1*), Interferon related developmental regulator 1 (*IFRD1*) and erythrocyte membrane protein band 4.1 (*EPB41),* suggesting an immune cell specific effect of the variant. Although these do not reach significance in the naïve T cells, *IRF1* (logFC = 3.4), *IFRD1* (logFC = 2.15) and *EPB41* (logFC = 0.63) show a positive fold change, consistent with the memory cells. This may suggest that the presence of T cells with high m.3243A>G levels promote an inflammatory phenotype.

There were only three overexpressed DEGs identified in the monocytes: *GRK2, BHLHE40* and *KCNJ2 (***Figure 6.9***)*, suggesting high and low m.3243A>G level monocytes are similar, or that this experiment does not have the power to detect changes. Due to this, the following results will largely focus on the CD8+ T cells.

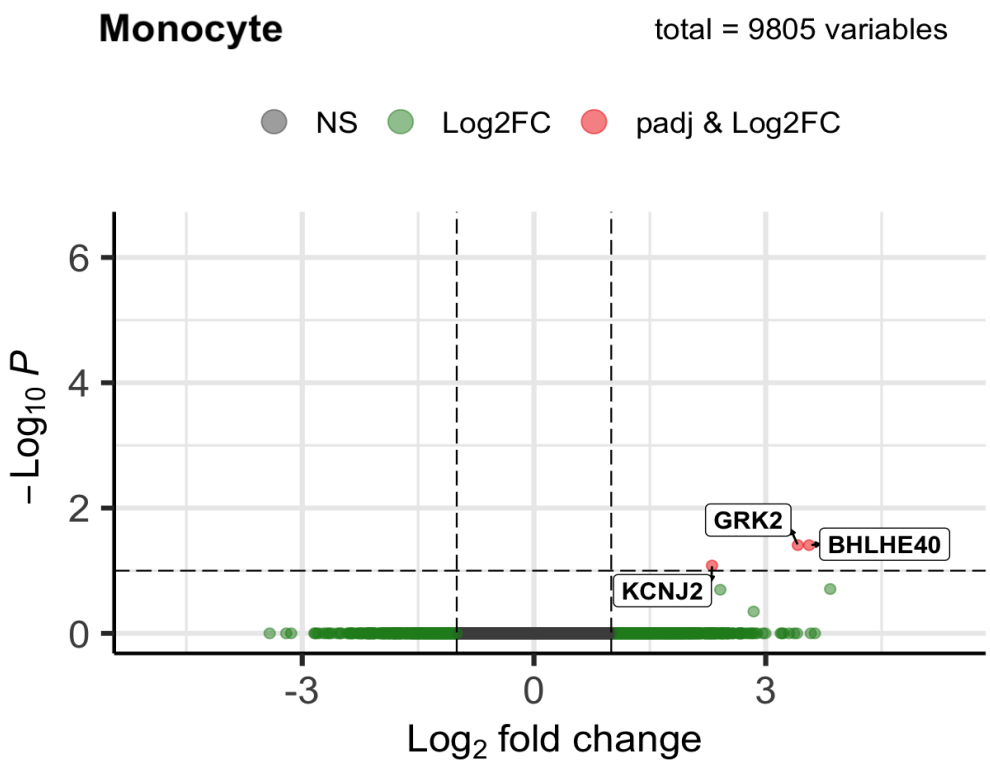


***Figure 6.9 Volcano plot showing genes of interest in P23 Monocytes.*** *N= 134 (93 high, 41 low). Red points represent DEGs of interest: -log10(Padj) >1 & log2(fold change) > 1, green points have a large fold change but -log10(Padj) <1, black points are not genes of interest.*

### 6.3.3 Differentially expressed genes support threshold of dysfunction.

To assess the relationship between m.3243A>G level and the expression of DEGs across the entire range of m.3243A>G levels, I used a linear model. This revealed the expression of some genes to have a significant relationship with m.3243A>G level, this includes *RUNX1, BECN1, DR1, CASC3, ARMC8* and *UBE2D2.* The expression of these genes appears to reach a m.3243A>G level threshold of ~50-70%, after which expression decreases (*CASC3)* or increases (*DR1, BECN1, RUNX1, ARMC8, UBED2B2 (***Figure 6.10***)*. Interestingly, the top hits of *CLEC2B* and *TNRC6B* do not show this trend. The number of cells included in this chapter's investigations are low, therefore a larger sample size is needed to decrease the risk of type I errors and to fully understand how gene expression changes with m.3243A>G level.

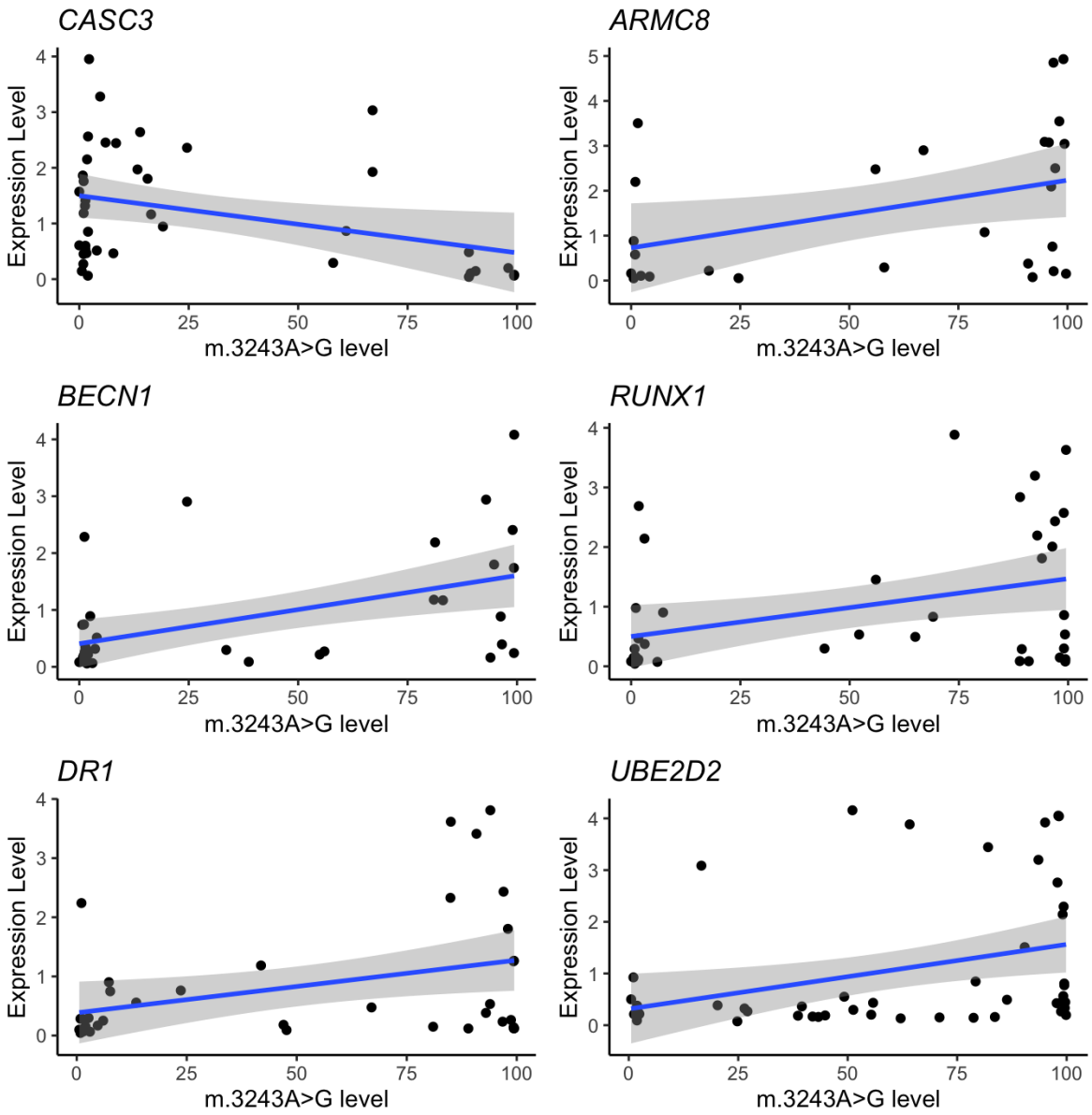


***Figure 6.10 Genes showing a m.3243A>G level dependent expression.*** *Each point represents gene expression in a single CD8+ memory or naïve cell. Blue line represents linear model. CASC3 (p = 0.0004, n=40); ARMC8 (p = 0.0294, n = 27); BENC1 (p =0.0013, n= 35); RUNX1 (p =0.0160, n = 40); DR1 (p = 0.0313, n = 37); UBE2B2 (p=0.0026, n=49).*

### 6.3.4 GO enrichment analysis reveals altered translation in m.3243A>G cells

Single cell sequencing often results in low counts and high feature dropout, which is typically mitigated by sequencing many cells. In this case, where the number of cells is limited, changes in an entire pathway or a significant portion of it are more reliable indicators of the true impact of m.3243A>G than specific DEGs. Therefore, interpretation will focus on these analyses.

To understand whether high m.3243A>G levels induce changes in cellular pathways, I identified pathways that were enriched (logFC>0.5) in high heteroplasmy cells. GO analysis identified an enrichment of pathways associated with oxidative phosphorylation, ribosome biogenesis, cytoplasmic translation, cellular stress, telomere regulation, viral gene expression and increased transcription, particularly via RNA polymerase II in both CD8+ naïve and memory cells with a high m.3243A>G level (***Figure 6.11***; **Appendix I** & **Appendix J**). Twenty pathways associated with cellular stress were highlighted in the naïve cells whereas ten were in the memory cells suggesting naïve cells may be more stressed and therefore are more vulnerable to the effects of m.3243A>G than memory cells (**Figure 6.12**).

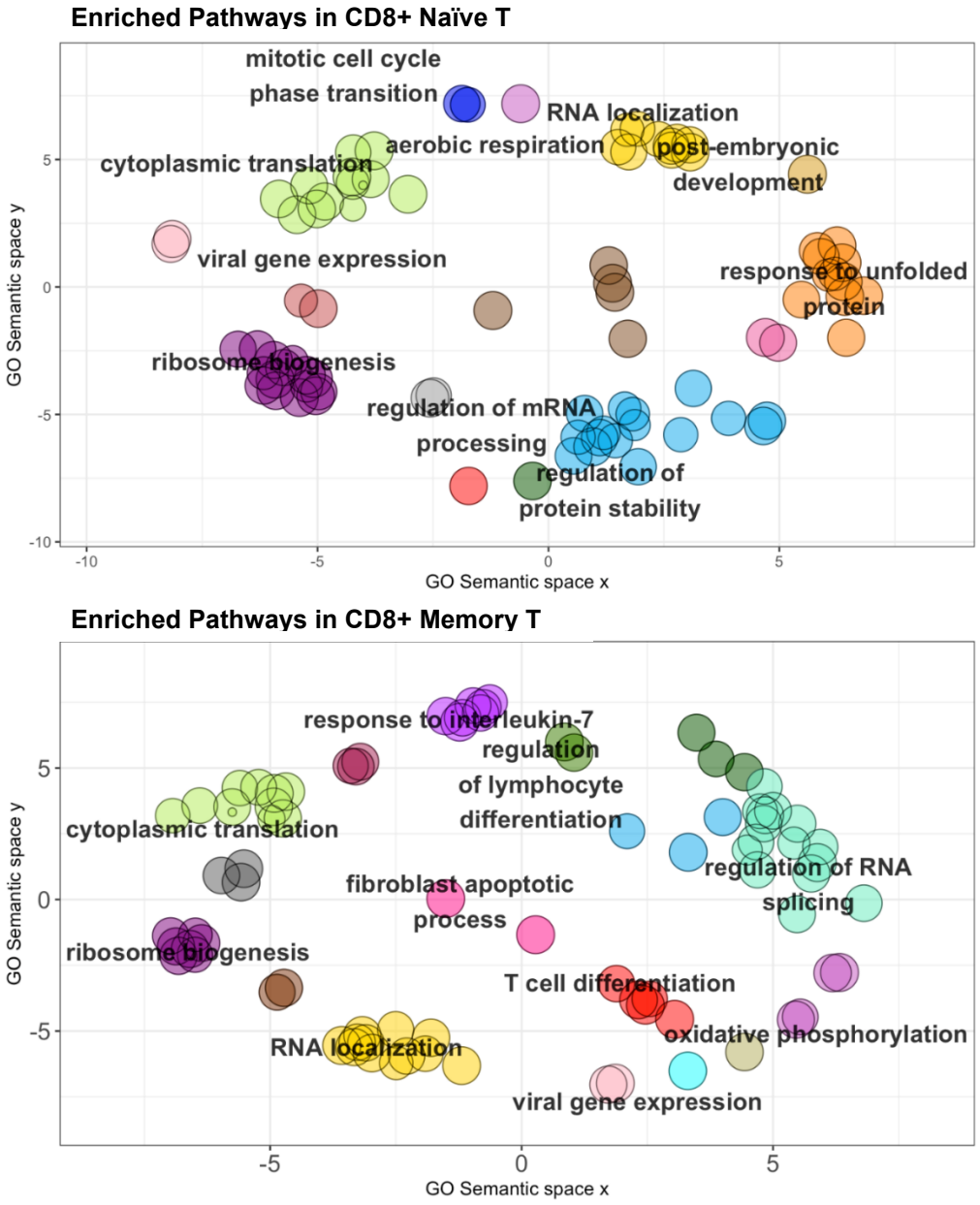


***Figure 6.11 GO BP Enriched pathways in cells with high m.3243A>G levels clustered by semantic similarity.*** *Enriched pathways were identified using genes with a log2(fold change) > 0.5., these were then clustered using Revigo.irb.hr (Supek et al., 2011). Further information on cluster identity can be found in appendix. Clusters identified in CD8+ naïve T cells which are unlabelled include: regulation of embryonic development, apoptosis. Clusters identified in CD8+ memory T cells which are unlabelled include: regulation of protein localisation to cell periphery, positive regulation by host of viral transcription and chromosome segregation. Details of individual pathways making up these clusters can be found in* **Appendix I** *&* **Appendix J**. *The size of the point represents the number of genes in this dataset found in the pathway.*

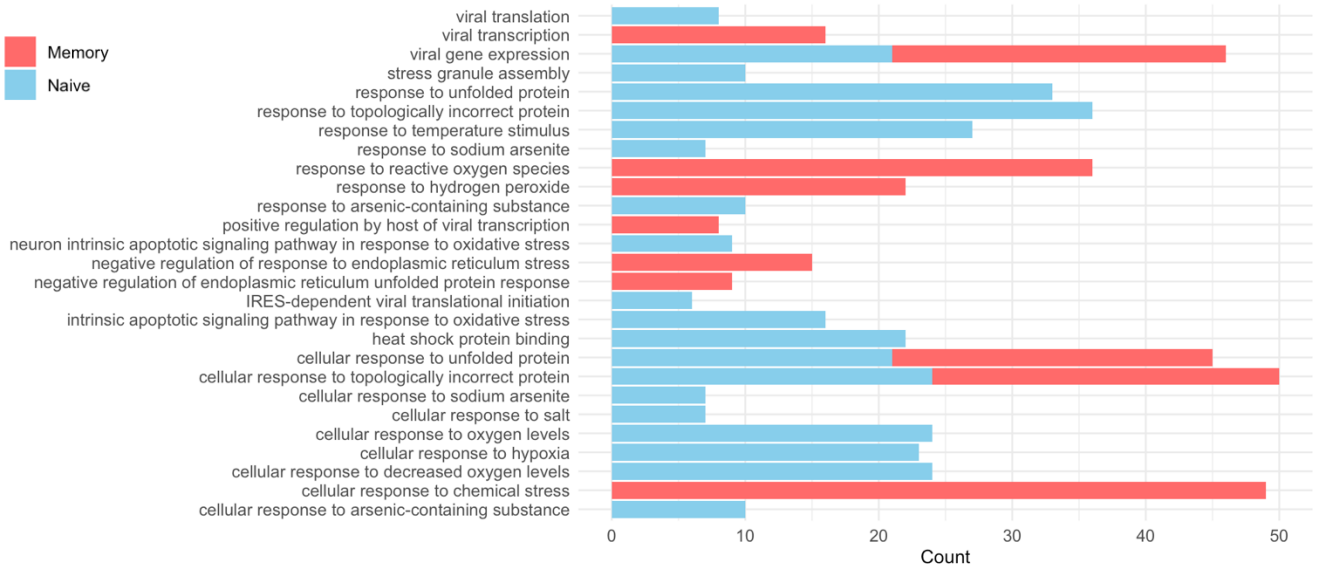


***Figure 6.12 GO comparison of stress pathways enriched in naïve and memory T cells.*** *All significantly enriched (log2(foldchange) >0.5) pathways in memory (red) and naïve (blue) CD8+ T cells (FDR adjusted p < 0.05). Count represents the number of genes identified per pathway.*

To understand how the above enrichment relates to phenotype, I also analysed this data using the Human Phenotype Ontology (HPO) database. Consistent with section 5.3.1, which demonstrated a decrease in the proportion of T cells in patients, *lymphopaenia* and *abnormal leukocyte count* were amongst the most significantly enriched disease pathways (**Figure 6.13**). Interestingly a number of phenotypes associated with mitochondrial disease were highlighted such as *progressive cerebellar ataxia* and *global brain atrophy*. *Recurrent viral infections* was also enriched in both cell types giving support to the m.3243A>G variant being related to an immune deficiency.

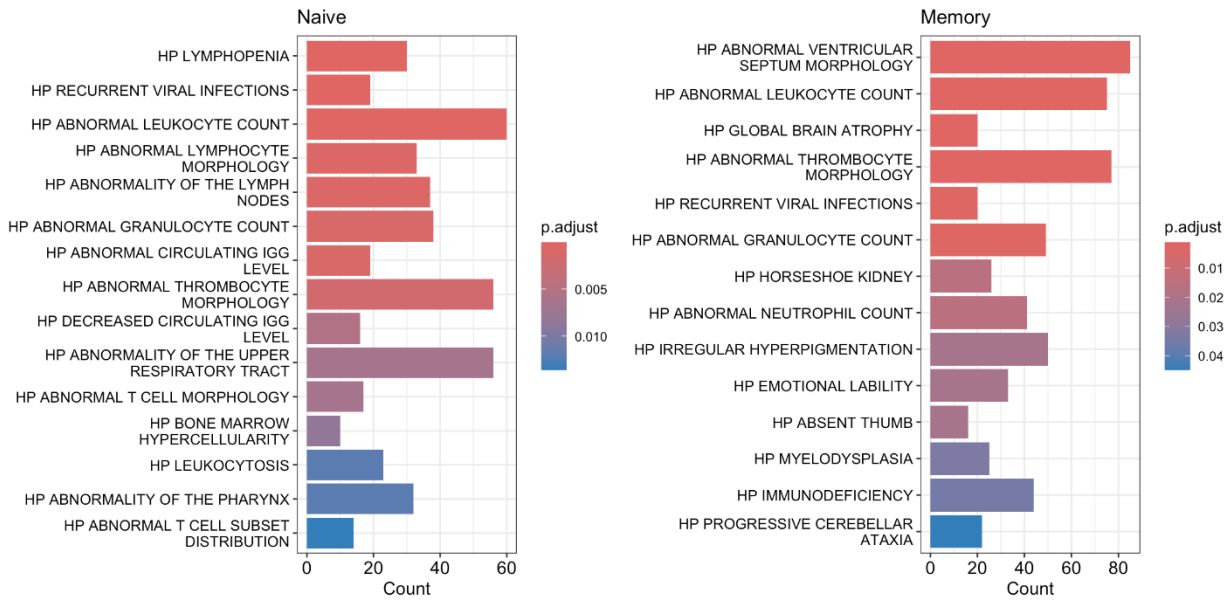


***Figure 6.13 Human Phenotype Ontology Enriched pathways in naïve and memory CD8+ T cell.*** *Enriched pathways are identified using the fold change values of those genes with a log2(fold change) >0.5, the count represents the number of enriched genes within the pathway. FDR adjusted p values are represented by the colour of the bar.*

The enrichment analysis outlined above implicates a number of T cell specific pathways as being upregulated in high m.3243A>G level cells; these include *T cell differentiation*, *regulation of lymphocyte differentiation* and *response to IL-7*. The enriched pathways are largely similar between naïve and memory states, however, IL-7 signalling pathways are isolated to the memory cells.

### 6.3.5 Gene set enrichment analysis reveals an upregulation of interleukin signalling in high m.3243A>G level T cells.

To understand in more depth which intracellular signalling pathways may be driving these changes, I carried out GSEA on the CD8+ naïve and memory cells. This identified 73 differentially expressed reactome pathways in naïve cells and 73 in memory cells, 51 of these were consistent in both. Just seven pathways were downregulated across both cell types: *rRNA modifications in the nucleus and the cytosol, recruitment of numa to mitotic centrosomes, aberrant transition of mitotic G1 S transition, E2F mediated regulation of*

*DNA replication, COPI independent golgi to ER retrograde traffic* and two ATF6α activation of chaperone related pathways (**Figure 6.14**). None of these pathways were significant across both naïve and memory datasets.

The pathways represented in both cell types largely belonged to mitotic cell cycle checkpoints and major signalling pathways such as NFκB, WNT, hedgehog and notch signalling (**Figure 6.14**). These pathways can induce a multitude of downstream signalling events, therefore, it is difficult to interpret the impact of this on T cell function. Interestingly, two IL-1 signalling pathways: *Interleukin 1 signalling* and *interleukin 1 family signalling*, were significantly upregulated in high m.3243A>G T cells, suggesting that the presence of m.3243A>G impacts intrinsic interleukin signalling and responses to these cytokines, which can induce mitosis in T cells.

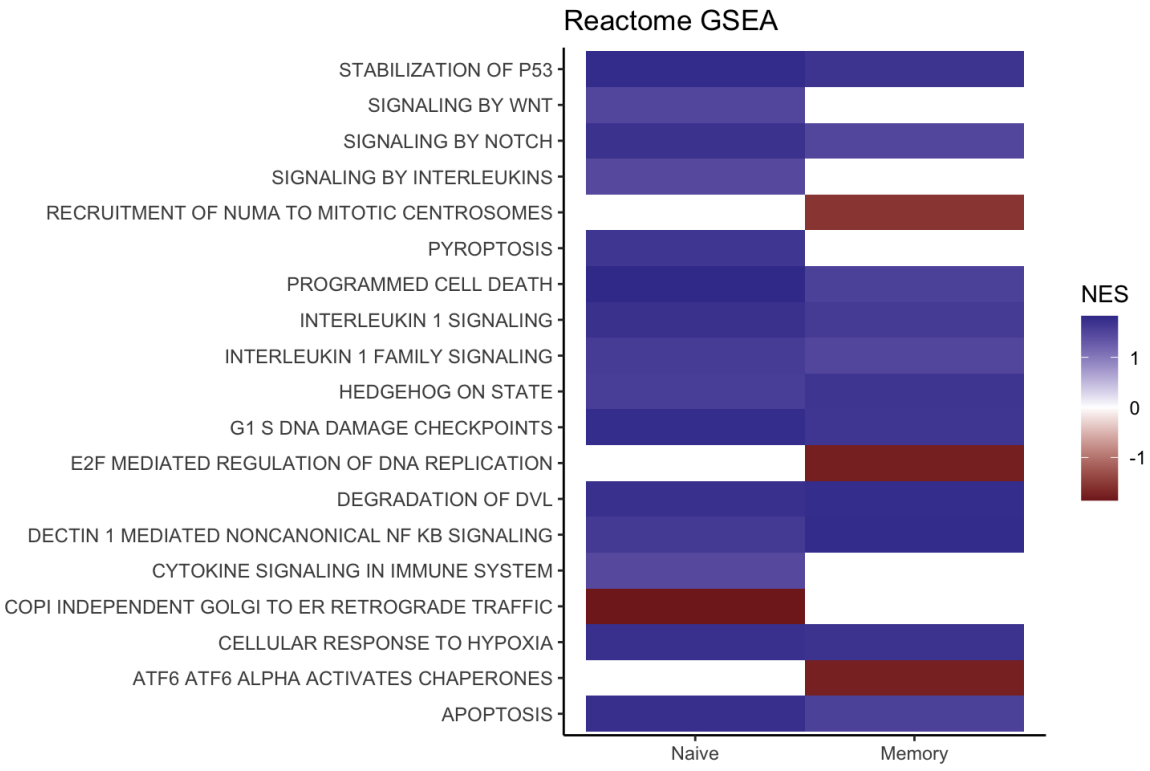


***Figure 6.14 GSEA hits in CD8+ naïve and memory high m.3243A>G cells.*** *94 significantly dysregulated pathways from the Reactome dataset were identified across the two cell types (19 are shown). 51 of these were consistent in both cell states (11 shown). NES = normalised enrichment score. Red represents under expressed pathways and blue represents overexpressed pathways. Details of all pathways and NES score in Appendix K -Appendix M.*

## 6.4 Discussion

This chapter details the first-time m.3243A>G level and the transcriptome have been assessed in single cells. Analysis of 697 immune cells highlighted an enrichment of gene expression related to cytoplasmic transcription and translation, ribosome biogenesis, telomere regulation, OXPHOS, RNA localisation and viral gene expression in cells with high m.3243A>G levels. Alterations in major signalling pathways and a dysregulated cytokine response were also identified which may play a role in driving these changes.

### 6.4.1 Targetseq isolates enriched pathways consistent with the literature.

A comparison to the research by Picard and colleagues (Picard *et al.*, 2014), generates a remarkably similar profile of enriched pathways, much more so than the iNeuron analyses by Gunnewick et al. (Klein Gunnewiek *et al.*, 2021), likely due to similarities between osteosarcoma/lymphoblastoid cells and the patient-derived lymphocytes described here.

The observed upregulation of pathways related to OXPHOS, transcription and translation, alongside the major signalling pathways mTOR, c-myc and NFκB, is consistent between the data described here and that from Picard *et al*. However, there are pathways highlighted in the Picard *et al* study which were not found in this dataset, notably an upregulation in glycolytic pathways as the m.3243A>G level increases. There is no change in glycolytic signalling in P23 CD8+ T cells; this could be due to resting T cells being highly reliant on OXPHOS and FAO for energy generation, whereas cells which have been maintained in culture such as the cybrids have likely adapted to become glycolytic. The majority of the high heteroplasmy cells in my sample are homoplasmic for m.3243A>G; at this level, Picard and colleagues see a drop in glycolytic pathways from cells with 60-90%, therefore, this could be why we don't see an increase. It would be interesting to stratify patient PBMC cells according to the m.3243A>G level groups identified by Picard *et al*. to understand whether these thresholds are consistent in primary cells. However, modification of the protocol to a higher throughput system would be required to collect more cells with mid-range m.3243A>G levels (discussed further in section 6.4.4).

### 6.4.2 m.3243A>G induces cellular stress

The data presented in this chapter highlight the increased level of stress signalling associated with high m.3243A>G levels. *Response to unfolded protein* and *response to topologically incorrect protein* were enriched in both naïve and memory T cells, indicating that m.3243A>G induces responses typically associated with an accumulation of misfolded protein and therefore the unfolded protein response (UPR). The UPR is a form of integrated stress response (ISR), which can also be induced by viral infection and hypoxia (Chen *et al.*, 2014, Zhang *et al.*, 2010), all stress responses enriched in high m.3243A>G level cells. However, the ISR is typically associated with a reduction in translation and ribosome biogenesis, which is not what these data demonstrate. The enrichment of the UPR in high m.3243A>G level cells is perhaps unsurprising given the proposed mechanism of action of m.3243A>G pathogenesis. There is much debate as to the mechanism, Sasarman et al. suggest that the variant results in the misincorporation of amino acids into mitochondrially encoded proteins, resulting in reduced assembly of OXPHOS complexes I, IV and V (Sasarman,Antonicka and Shoubridge, 2008). These data support the notion that free OXPHOS proteins, unbound to a complex may drive the UPR.

Typically, ER stress responses result in the phosphorylation of eIF2α which blocks further translation to reduce stress. ER stress response elements (ERSEs) activate PERK, ATF6 or IRE1 by disassociating from them during ER stress and bind un/misfolded proteins (Shen *et al.*, 2002, Upton *et al.*, 2012, Liu and Kaufman, 2003). Upon activation, ATF6 is chaperoned to the Golgi apparatus, where it is cleaved by S1P and S2P (Ye *et al.*, 2000), this forms a transcription factor responsible for transcribing genes involved in ER-associated degradation (ERAD) and chaperones which aid protein folding via their ATPase activity (Haze *et al.*, 1999, Yamamoto *et al.*, 2007). Chronic activation of the UPR induces apoptosis via CHOP (Xiong *et al.*, 2017).

It is possible that the insufficiency of ATP produced in cells harbouring high levels of m.3243A>G results in a deficiency in the activity of these chaperones, further enhancing the UPR signalling. This is supported by GSEA results which demonstrate an under expression of genes in pathways related to ATF6α activation of chaperone genes. Why cellular translation is not halted is intriguing, however, as this is not an induced ER stress

but a response to dysfunction which has been present for the cell's lifetime, it is likely the cells have adapted to maintain translation in order to survive. Investigating any changes in the size of the ER would be beneficial to understand how these cells are reacting to this ER stress. Immune cells such as plasma cells are able to increase the size of the ER considerably in preparation for the ER stress induced by antibody synthesis, therefore, these cells may respond in a similar way (Zhu *et al.*, 2019).

These data indicate that cells with high m.3243A>G levels are under a high level of cellular stress, which could be a driver of selection against the pathogenic variant. These cells may undergo UPR initiated apoptosis leaving a population of cells with low m.3243A>G levels. This is consistent with the cellular fitness theory of selection suggested by Kotrys et al. (2024). As this patient doesn't exhibit the typical purifying selection in memory T cells demonstrated in 6.3.1, the expression profile may differ. The heteroplasmy profile in the CD8+ naïve and memory T cells of P23 demonstrated peaks at WT and homoplasmy (**Figure 6.7**) which is characteristic of random genetic drift (Elson *et al.*, 2001). Random genetic drift occurs as a result of vegetative segregation rather than selection, suggestion other mechanisms or multiple mechanisms may be occurring simultaneously in this individual. This highlights the importance of investigating samples from further individuals. The down regulation of ATF6α activation of chaperone genes may have a protective effect, leading to the high incidence of memory T cells with a high m.3243A>G levels. Loss of ATF6 promotes longevity in *C. elegans* as it reduces the cellular calreticulin levels. High calreticulin would sequester $Ca^{2+}$ and result in aberrant ER calcium retention which would result in mitochondrial dysfunction (Burkewitz *et al.*, 2020). Carefully regulated $Ca^{2+}$ levels are required for T cell activation (section 1.4.4), therefore it is possible that only high m.3243A>G level cells which downregulate the activity of ATF6 are able to progress to a memory state. This could be investigated by quantifying cellular calreticulin levels and comparing to m.3243A>G level.

### 6.4.3 Increased cytokine signalling in high m.3243A>G resting T cells.

Cytokines such as IL-1 are released by virally infected cells and APCs to drive T cell response (expansion and cytotoxicity) likewise, surface expression of foreign peptides are

required to induce a TCR based response. As *IL-1 signalling* and *viral gene expression* have been highlighted as enriched pathways in cells with high m.3243A>G levels, it indicates that these cells may be mimicking the effects of a viral infection.

IL-1α and IL-1β are produced by APCs as a result of DAMP or PAMPs in the cytosol which bind NLRP3 and activate the inflammasome. Interferon regulatory factor 1 (*IRF1*) has been suggested to control mtDNA synthesis and therefore a downstream induction of IL-1β signalling via NLRP3 (Zhong *et al.*, 2018). Zhong and colleagues discovered that IRF1 ablation in bone marrow derived macrophages (BMDM) blocked the synthesis of new mtDNA molecules, resulting in less oxidated mtDNA found in both the cytosol and mitochondria, and inhibited IL-1β release. In APCs, oxidised mtDNA molecules in the cytosol serve as DAMPs which bind the NLRP3 leading to inflammasome activation and IL-1β secretion. IL-1β release from APCs is critical for the formation of the CD8+ anti-viral response (Ben-Sasson *et al.*, 2013). IL-1α and β interact with IL-1R on T cells to prime cells for increased proliferation and cytokine release upon T cell activation (Jain *et al.*, 2018).

Interestingly, *IRF1* was an over expressed DEG in the CD8+ memory T cells, suggesting an upregulation of mtDNA synthesis could be occurring in these cells, perhaps driving selection via increased mtDNA biogenesis. This could also be acting as a DAMP, driving an 'activation' phenotype. There is growing evidence for the occurrence of inflammasome activation in T cells. The above mentioned NLRP3-ASC-CASP8-IL-1β axis has been demonstrated to operate within T cells; although this research focuses on CD4+ T cells (Martin *et al.*, 2016), it suggests an intrinsic mechanism for IL-1 signalling. The presence of PAMPs, such as mtDNA, in the cytosol can induce either cytokine signalling or programmed cell death – two of the GO BP enriched pathways. Inflammasome signalling in T cells has been linked to pyroptosis in latent HIV infection and DPP-inhibitor treatment (Monroe *et al.*, 2014, Linder *et al.*, 2020). Another possible trigger for the stress response is a reduction in rRNA modifications in the nucleus and the cytosol identified in the GSEA; unmodified rRNA may act as a DAMP, inducing the signalling cascade outlined above.

In support of increased inflammasome activation, increased IL-1β release has been observed in patient macrophages when stimulated with LPS. Although, the observation did not reach significance, it deviated from control measurements much more so than

TNFα and IL-6, which are not involved in an inflammasome response (Karan *et al.*, 2022). To investigate this further, examination of the cytosol for mtDNA using immunofluorescence or qPCR of the cytosolic fraction would allow further understanding of the origin of the IL-1 signalling pathway in high m.3243A>G level cells. It could be that these cells are more responsive to extracellular IL-1, rather than an intrinsic mechanism, perhaps due to higher expression of the IL-1R receptor, something that could be investigated using flow cytometry or immunofluorescence.

These data in combination with the increased abundance of enriched mitotic pathways suggests increased activation/cytotoxicity of high m.3243A>G level cells, similar to that seen with a viral infection, which is indicative of sterile inflammation. Inflammasome activation in CD4+ T cells could be involved in the expression of PD-1 expression (section 4.3.6) as studies have found it to be critical in the differentiation of Th1, Th17 and Th2 cells (Arbore *et al.*, 2016, Bruchard *et al.*, 2015, Gao *et al.*, 2020).

### 6.4.4 Improvements to protocol

To both improve and build on the work carried out in this chapter, it is crucial that the scRNA and mtDNA genotyping is carried out on a range of patient samples to check for consistencies. As P23 has an unusual m.3243A>G distribution, it is important to include more individuals who exhibit a purifying selection profile in the T cells to ensure the pathways highlighted here aren't an anomaly. It is a possibility that this patient possesses a nuclear modifier which allows memory T cells to tolerate high m.3243A>G levels, which in turn could impact the cellular gene expression.

One of the major limitations to the use of targetseq is that it is relatively low throughput. A high throughput methodology effective in determining mtDNA heteroplasmy is ATAC-seq (Assay for Transposase-Accessible Chromatin with high-throughput sequencing) (Buenrostro *et al.*, 2013). This assay utilises the Tn5 transposase to isolate open chromatin regions for sequencing, meaning it allows for deeper understanding into the genes which are undergoing active transcription. As the mtDNA is not associated to chromatin, it is enriched within the sequencing libraries generated.

Using this in conjunction with the 10x genomics chromium platform allows for efficient, high throughput sequencing of chromatin accessible regions in single cells. This protocol involves the incorporation of barcoded gel beads and transposed nuclei into an individual oil droplet per nuclei know as GEMs (Gel Beads in-emulsion) using a microfluidics system. Once a GEM is formed, the gel bead is dissolved releasing Illumina compatible barcoded sequencing adaptors which bind before amplification of the open chromatin regions via PCR. The Illumina adaptors are then utilised in the final sequencing reaction (Satpathy *et al.*, 2019).

However, as the 10x platform is nuclei based, and minimises mtDNA contamination, modification to this protocol to maximise inclusion of mitochondria was developed by Lareau et al in 2021. This modification results in a ~20-fold increase in mtDNA coverage by cell fixation using 1% formaldehyde, followed by a mild cell lysis before incorporation into the oil droplet (Lareau *et al.*, 2021). This technique has been used to trace cell lineage according to the presence of somatic mtDNA mutations (Ludwig *et al.*, 2019). Recently, 10x have introduced the multiome kit, which with the modifications mentioned above could enable the sequencing of RNA, open chromatin regions and mtDNA all within the same cell. Future investigations will be carried out using this platform, which will also allow sequencing of all PBMC cell types, rather than being limited to a number of selected cell types.

## 6.5 Concluding Remarks

This chapter presents a proof of concept, detailing a technique which can determine the m.3243A>G level and gene expression within the same single cell. This technique although imperfect, has identified enrichment in pathways related to translation, transcription, mitosis, OXPHOS, cytokine response and stress in high m.3243A>G level cells. In the future, it will be beneficial to validate these findings using the 10x platform and expand the cohort to see if these findings are consistent across m.3243A>G samples from different patients.

# Chapter 7 Final Discussion

Since m.3243A>G was first reported, 34 years ago (Goto,Nonaka and Horai, 1990), there has been limited progress in the understanding of m.3243A>G selection, nor the development of curative treatment for m.3243A>G-related disease. This field has been challenged by the complexities underlying heteroplasmy such as tissue mosaicism (demonstrated in **Figure 3.4** and **Figure 4.7**) and high levels of phenotypic diversity in those presenting with m.3243A>G related disease. Negative selection against pathogenic mtDNA is not observed with all heteroplasmic mtDNA single nucleotide variants; data in section 3.3.5 indicates it is likely restricted to certain tRNA variants. An understanding of similarities between variants displaying a T cell effect can give new insight into disease mechanism and cellular response to the presence of pathogenic mtDNA.

In this thesis, I set out to understand negative selection of m.3243A>G in the blood. In doing so, I have identified a difference in selection patterns between cells of the lymphoid and myeloid lineage. T cells demonstrated remarkable 'purifying selection' at both bulk and single cell levels, a finding which has been corroborated by groups in the US and Sweden (Walker *et al.*, 2020, Lareau *et al.*, 2023, Zhang *et al.*, 2023). Further interrogation revealed phenotypic differences in CD4+ T cells such as increased PD-1 expression and increased early proliferation following TCR stimulation, both of which require further investigation in a larger sample size to confirm. Transcriptional differences between cells with high and low m.3243A>G levels from the same individual suggest T cells with a m.3243A>G level >75% are under increased ER and oxidative stress while also displaying increased activation of the IL-1 signalling pathway.

While these data give valuable insight into the complexity of selection patterns between different tissues and even individual cells, they have raised a number of further questions which will require further work to answer.

## 7.1 The mechanism of purifying selection

Analysis of m.3243A>G level in bulk (Chapter 3) and single cell (Chapter 4) samples revealed that negative selection is enhanced in T cells and that the proportion of cells that have cleared the variant increases with T cell maturity. These data also indicate that selection occurs beyond levels of m.3243A>G that are typically associated with biochemical dysfunction (60-80%), indicating the driver of selection may not be survival

in one cell state but differentiation between cell states, perhaps associated with metabolic challenge after activation. Recently, activation of the mTOR signalling pathway in patient fibroblasts has been implicated in sustaining m.3243A>G heteroplasmy (Chung *et al.*, 2021). mTOR signalling drives glycolytic metabolism and, therefore, sustained activation could increase cellular survival via reduced reliance on OXPHOS. GO enrichment analysis data from section 6.3.4, in which mTOR signalling is enriched in T cells with high m.3243A>G levels, were consistent with these findings. The data presented in section 6.3.5, also identify modifications to the typical UPR, which is usually characterised by a halt of cytoplasmic translation. In P23 high m.3243A>G cells, cytoplasmic translation is maintained in high levels of stress, perhaps facilitating survival of these cells; another finding which is consistent with the literature (Picard *et al.*, 2014). Modification of ATF-6 (**Figure 6.14**) chaperone activity in memory T cells with high heteroplasmy may enable differentiation potential in otherwise apoptotic cells.

Throughout this thesis, I have discussed two possible timepoints at which selection could occur: the point of quiescent exit and during cellular divisions. A quiescent state in T cells can be induced via metabolic reprogramming; this could, for example, be in the form of mTOR inhibition or triggering of mitochondrial fusion (Buck *et al.*, 2016, Chung *et al.*, 2021). Recent advances in single cell technologies such as the 10x mulitome protocol allow analysis of mtDNA genotype, gene expression and open chromatin regions (discussed in section 6.4.4). Assessing gene expression before and in the immediate days following TCR activation would allow assessment of surviving TCR clones, their m.3243A>G levels and allow assessment of the dynamics of these changes in the days following activation. This would allow understanding of which TCR clones are proliferating and which are dying and how this relates to their m.3243A>G heteroplasmy. Incorporation of this protocol and that outlined in section 5.4.4, which involves the activation of T cells incubated with CTV dye to trace cell divisions, would allow for isolation of T cells from the same generation via FACS. Quantification of the difference in m.3243A>G level between cells of the same TCR clone would answer the paramount question raised by the data generated by this project: Is negative selection driven by death of high m.3243A>G level cells resulting from a proliferative bottleneck or are WT mtDNA molecules being preferentially replicated after division?

Just one of the two samples investigated in T cell proliferative investigations (section 5.3.3) exhibited a decrease in m.3243A>G level; it is possible that this is due to the

existence of a threshold of selection. Cells from P26 had a day 0 m.3243A>G level <15%; perhaps this is below the level for which there is a disadvantage, therefore removing the selective pressure in the experiment. These data demonstrate that a decline in m.3243A>G is not a guarantee in all cases, consistent with the longitudinal whole blood m.3243A>G measurements in which a small proportion of individuals demonstrate increases or plateau over time (**Figure 3.3**). Although bulk m.3243A>G levels show a decreased m.3243A>G level in the memory T cells of P23 compared to the naïve, the distribution of m.3243A>G level in P23 shows peaks at ~0% and ~100% heteroplasmy in T cell subsets (**Figure 6.7**). A heteroplasmy profile which demonstrates fixation at either end of the range is typically associated with random genetic drift, a process in which vegetative segregation of mtDNA results in both homoplasmic WT and variant cells (Elson *et al.*, 2001). Therefore, it is important to consider random genetic drift as a factor when discussing selective pressure as well as the likelihood that a threshold effect results in no selection against the variant in some individuals.

In order to understand if a decline of m.3243A>G in haematopoietic cell subsets is driven by selective pressures only or also influenced by random genetic drift, mtDNA heteroplasmy and TCR data generated from single cell investigations could be used to carry out computational modelling of heteroplasmy dynamics. Previous models rely on longitudinal whole blood m.3243A>G measurements and do not account for a potential lineage bias (Rajasimha,Chinnery and Samuels, 2008a, Veitia, 2018). These models postulate that selection originates at the level of the HSC, which data presented in section 3.3.2, showing a similar trend in CD34+ cells as mature immune cells, supports. Due to the self-renewal capabilities of naïve and memory T cells, modelling of m.3243A>G dynamics may be similar to stem cell behaviours but as these are functionally different cells, this cannot be assumed. As the spectrum of heteroplasmy within cell populations is so diverse, the use of rich, single cell datasets to guide modelling of T cell mtDNA dynamics is likely to be more informative than the use of bulk measurements. Rest and restimulation of the same T cell population coupled with single cell sequencing would provide interesting insight into whether selective pressures remain the same upon/during each mass proliferative event and could be incorporated into this model.

Understanding the mechanism driving selection against m.3243A>G has the capability of benefitting both the mitochondrial disease and immunometabolism fields. Unveiling the cellular pathways associated with a decrease in m.3243A>G level would allow further

investigation into which pathway components are involved in selection and whether disruption of or activation of this signalling can drive selection *in vitro*. In the future this could allow the development of pharmacological interventions which drive a decline in symptomatic tissues such as the skeletal or cardiac muscle and the brain as well as having the potential to reduce m.3243A>G transmission to offspring in mothers with high m.3243A>G levels.

### 7.2 Irregular T cell behaviour

Another important avenue for further investigation is the relationship of irregular T cell behaviour to disease phenotype. Reports of the induction of neurological phenotypes such as ataxia and encephalopathy after infection are commonly reported in cases of m.3243A>G (de Laat *et al.*, 2016) and broader mitochondrial disease (Al-Zubeidi *et al.*, 2014, Wei *et al.*, 2018). Disruption of cellular signalling pathways as a result of mitochondrial dysfunction can either enhance or inhibit activity of the immune system (West *et al.*, 2015, Tan *et al.*, 2017, Luo *et al.*, 2019). Enhanced activity of immune tissues triggered by an incorrect recognition of self-antigens as foreign results in autoimmune diseases, which can bear a remarkably similar phenotype to mitochondrial diseases, for example autoimmune encephalitis (Marina *et al.*, 2022).

Inflammation in the brain and muscle tissues has been linked to mitochondrial dysfunction (Mathew *et al.*, 2012, Wilkins *et al.*, 2015, Irazoki *et al.*, 2023). T cell infiltration in the muscle of an individual with m.3251A>G, also in the *MT-TL1* gene, has been reported (Mancuso *et al.*, 2013). While the metabolic stress of post-mitotic cells may have been the trigger for immune infiltration, it has been suggested that the immune system plays a substantial role in the disease progression in a murine model of Leigh syndrome (Stokes *et al.*, 2022). This is supported by numerous case studies demonstrating the improvement of phenotype in response to corticosteroids in individuals with m.3243A>G (Gubbay *et al.*, 1989, Rossi *et al.*, 2002, Walcott *et al.*, 2012), suggesting a link between the response of high m.3243A>G level immune cells to tissues in metabolic stress, to severity of disease phenotype.

While limited in sample size, the studies outlined in chapters 5 and 6 identified sterile inflammation as an area worthy of further investigation. Sterile inflammation is

characterised by the activation of the NLRP3 inflammasome in the absence of external stimuli (reviewed in Huang *et al.* (2024)). As discussed earlier, this process generates inflammatory cytokine IL-1, which stimulates T cells. The IL-1 signalling pathway was upregulated in P23 T cells (**Figure 6.14**) and PD-1 expression was higher in individuals with a blood level >45%, indicating chronic signalling in these cells (**Figure 4.11**). Chronic IL-1 signalling can inhibit murine HSC differentiation into lymphoid and erythroid lineages (Pietras *et al.*, 2016), a possible explanation for the reduced proportion of T cells in patient PBMC samples and regular incidence of anaemias across mitochondrial disease (Barth *et al.*, 1983, Rotig *et al.*, 1995, Bykhovskaya *et al.*, 2004, Broomfield *et al.*, 2015, Farruggia *et al.*, 2016, Pronman *et al.*, 2019, Yoshimi *et al.*, 2021).

One of the most commonly affected tissues in m.3243A>G related disease is skeletal muscle. Chronic inflammation in the muscle has been found to impair muscle repair (reviewed in Perandini *et al.* (2018)). Muscle resident Treg cells secrete anti-inflammatory cytokines, therefore, it is possible that aberrant mitochondria inhibit beneficial immune activity within affected tissues (Lewkowicz *et al.*, 2013). There is substantial evidence that inflammatory cytokines regulate the proliferation and differentiation of muscle stem cells (Dumke and Lees, 2011, Al-Dabbagh *et al.*, 2015), therefore, the increased rate of damage due to metabolic stress, in conjunction with reduced repair, may drive the induction of symptoms. Or perhaps overactive Tregs inhibit the early inflammation that is key in muscle repair (Panduro,Benoist and Mathis, 2018).

Tissue stress or damage is known to induce the release of IL-1 cytokine family member IL-33 and the release of this cytokine from muscle is believed to encourage the accumulation of Treg cells (Milovanovic *et al.*, 2012, Kuswanto *et al.*, 2016, Panduro,Benoist and Mathis, 2018). It is possible that cells with high m.3243A>G release this stress signal, activating both the innate and adaptive immune systems. The question remains as to why high m.3243A>G level T cells have a higher incidence of IL-1 family signalling. Perhaps due to their altered metabolic capabilities, they are more primed to respond to lower affinity stimulation signals.

There is a gap in the research investigating tissue inflammation. Access to patient muscle biopsies and post-mortem brain tissue may help to elucidate whether there is any immune infiltration. A comparison of control and m.3243A>G muscle, with and without muscle-

related phenotypes, such as myopathy, could aid in deciphering whether the existence of an abnormal immune presence is associated with a symptomatic presentation.

## 7.3 Haematopoietic cell lineage tracing

Individuals with mitochondrial diseases such as Pearsons syndrome, POLG disease and Mitochondrial Myopathy, Lactic Acidosis, and Sideroblastic Anaemia (MLASA) can present with anaemias and other abnormal haematopoietic development (Rotig *et al.*, 1995, Bykhovskaya *et al.*, 2004, Broomfield *et al.*, 2015, Farruggia *et al.*, 2016, Pronman *et al.*, 2019, Yoshimi *et al.*, 2021, Hikmat *et al.*, 2017). This has been theorised to be due to premature arrest in cell development. Impairment of erythroid differentiation and proliferation has been demonstrated in bone marrow mononuclear cells from individuals with Pearsons syndrome (single, large-scale deletion of mtDNA) coinciding with a downregulation of heam and cholesterol biosynthesis; it was speculated by the authors that this was a result of high OXPHOS demand in erythroblasts (Lareau *et al.*, 2023). These studies indicate that mitochondrial dysfunction can alter the trajectory of haematopoietic differentiation.

The results outlined in Chapter 4 demonstrate a relationship between negative selection of m.3243A>G and cellular differentiation state (**Figure 4.8**). Although it is well established that $T_{eff}$ cells are highly glycolytic, a functional OXPHOS system, particularly CI, is essential for T cell activation in vivo and in vitro (Yi *et al.*, 2006b, Tarasenko *et al.*, 2017b, Vardhana *et al.*, 2020b). T cells are vulnerable to decreased CI function more so than other blood cell populations (Milasta *et al.*, 2016). This is observed with deficiency of the mitochondrial flavoprotein apoptosis inducing factor (AIF); which is required for efficient assembly of CI (Vahsen *et al.*, 2004). Decreasing AIF expression by 80% resulted in T cell deficiency in mice, likely due to interference of cell development (Banerjee *et al.*, 2012). Similar responses can be seen in patients with DOCK2-deficiency. DOCK2 a guanine nucleotide exchange factor, plays a critical role in the activation of Rac GTPases, which are important in mitochondrial homeostasis (Alosaimi *et al.*, 2019). In this study, all patient PBMCs lack expression of *DOCK2*, however, only a T cell lymphopaenia is observed. Consistent with this, I observed a decrease in the proportion of T cells in individuals with m.3243A>G (section 5.3.1). The exact role that OXPHOS

plays in effector function and T cell differentiation is incompletely understood, however ROS generated by OXPHOS are used to stabilise transcription factors, such as NFAT, involved in effector function (Sena *et al.*, 2013).

Previous research in haematopoietic development relied on assessment of the colony forming potential of cells upon transplantation and there have been considerable advances in this field in recent years due to the advent of high throughput single cell technologies (Ye,Huang and Guo, 2017). The presence of unique somatic mutations in the mtDNA of individual lineages can be used to trace progenitor cells and their progeny (He *et al.*, 2003). As mtDNA is replicated, further somatic mutations are acquired and heteroplasmy changes. Interrogation of mtDNA genotypes via scATAC-seq presents an opportunity to trace clonal relationships in individual cells; comparisons of lineage tracing using the current gold standard approach involving lentiviral barcodes and the mtDNA method found them to correlate (Ludwig *et al.*, 2019). This methodology combined with scRNA seq (as with the multiome) allows for deeper lineage relationships than TCR sequencing. Using a combination of ATAC and RNA sequencing technologies, authors were able to further subgroup cells of the same TCR clone but also traced which T cells originated from the same progenitor prior to V(D)J recombination (Ludwig *et al.*, 2019). It would be interesting to use this technology to understand whether heteroplasmy is consistent in T cells from the same progenitors, suggesting stability during proliferation and to also interrogate whether those primed to become $T_{CM}$, $T_{EM}$ or $T_{EMRA}$ memory cells share a common progenitor.

## 7.4 Limitations

### 7.4.1 Complete understanding of selection involves thymic selection.

As demonstrated by the decreased m.3243A>G level in naïve T cells compared to the CD34+ progenitors (**Figure 3.4**, **Figure 4.8**), negative selection has occurred before the cells reach the naïve state. This means that a true reflection of selection begins in the thymus, at the HSC or early progenitor cell level. The m.3243A>G level of CD34+ progenitor cells in the blood were similar to the whole blood level and the majority of myeloid cells (**Figure 3.4**). Given that blood levels decline with age, this indicates that

selection has already occurred and originates before release into the periphery. The availability of thymus and bone marrow tissue is scarce, and in the case where a sample can be taken, it is invasive and the relevance of the cells obtained is debatable; although a LMPP has the capability of differentiating into a T cell, it is not a guarantee *in vivo.* A reliable mouse model of m.3243A>G disease would be needed to investigate this. Although it doesn't capitulate the entire phenotypic spectrum, the m.5024T>C mouse displays a similar negative selection in the blood and shows a relationship with T cell maturity, therefore this model may be the best starting point for such investigations (Kauppila *et al.*, 2016, Zhang *et al.*, 2023).

### 7.4.2 Inability to isolate cells according to m.3243A>G level

Currently, the only reliable method of measuring m.3243A>G level is cell lysis followed by sequencing of mtDNA, therefore heteroplasmy cannot be directly measured in live cells. This means that *in vitro* investigations into patient samples are often complicated by intercellular variability in heteroplasmy. Wild type cells can compensate for highly dysfunctional cells in a population and make it difficult to understand how cell phenotype relates to heteroplasmy, particularly in haematopoietic cells where high m.3243A>G cells are the minority. This makes functional experiments such as those carried out in 0 difficult as isolation of a population of cells with a high heteroplasmy before culture is near impossible. Recently, the Mootha group have suggested that TMRM intensity correlates to OXPHOS activity and may be able to be used as a proxy heteroplasmy measurement (To *et al.*, 2024). Further to this, the identification of a DEG whose corresponding protein expression increases with m.3243A>G, such as those in **Figure 6.10**, could be used as a proxy. This would allow for isolation of cells with high m.3243A>G levels and, therefore, better profiling of m.3243A>G-induced dysfunction. For example, to confirm IL-1 signalling in T cells with high heteroplasmy.

### 7.4.3 Rare disease

The study of complex rare disease is challenging due to the difficulty in generating studies with high enough statistical power. m.3243A>G has a disease prevalence of

3.5/100,000. The cohort and samples obtained for these investigations is the largest of its kind and took 3.5 years to compile. Large cohort studies are required to study the immune system due to the high levels of variability dependent on age, sex and lifestyle (Calabro *et al.*, 2023), therefore it is incredibly difficult to investigate this in the case of m.3243A>G, particularly with the caveat of incomplete penetrance of m.3243A>G disease. A global effort needs to be undertaken to recruit a large cohort for investigations into immune irregularities in m.3243A>G related disease. A number of global initiatives investigating mitochondrial disease exist such as GENOMIT, however, the focus of these tends to be on phenotypes traditionally associated with mitochondrial disease such as myopathy and neurological presentations. Haematopoietic dysregulation in m.3243A>G is an underexplored area; therefore, the current data being obtained does not pertain to the questions posed in this discussion. Information regarding infection history, onset of symptoms in relation to infection history and longitudinal blood samples, would allow investigation into cytokine release and infection as a driver of m.3243A>G phenotype.

## 7.5 Conclusion

The work presented in this thesis lays the foundations of an understanding of the complex relationship between pathogenic mt-tRNA and blood cell differenitation. This work supports theories which state that selection originates before the progenitor stage, perhaps in the marrow progenitors or the HSC. The differing trajectorys of selection and potential compensatory mechanisms observed in myeloid and lymphoid cells suggests this may originate at the point of lineage splitting. I have pursued T cells for further investigation due to enhanced selection in this lineage; their long lifespan and reliance on metabolic changes for differentiation are likely the best model for investigaiton. Early investigations into T cells hint towards modified activity which warrants further investigation in the form of i*n vitro* activation followed by single cell omics. Such investigations have the potential to guide future treatment management strategies for affected individuals as well as an understanding of the role of mitochondrial function in T cell biology.

# Chapter 8 Appendix

## *Appendix A. Equiptment list*

| | |
|---|---|
| 2100 Bioanalyser | Agilent |
| Benchtop Centrifuge 5418 | Eppendorf |
| Cellometer Auto 1000 Bright Field Cell Counter | Nexcelom |
| Dynal rack (magnetic rack) | Fisherbrand |
| E1-cliptip pipette | ThermoScientific |
| E-gel safe imager real time transilluminator | Life Technologies |
| Electrophoresis Unit, HU10 Mini-Plus Horizontal Unit | Scie-Plas |
| FACS Fusion | BD |
| Heraeus megacentrifuge 8 | ThermoScientific |
| Imaging System, ChemiDoc MP | Bio-Rad |
| ImmunoSpot S6 Ultra-V | ImmunoSpot |
| Ion S5 semiconductor sequencer | IonTorrent by Thermofisher |
| IonTorrent Ion Chef System | Thermofisher |
| MINI 96 (12.5) | Integra biosciences |
| Nextseq 500 | Illumina |
| Pyromark Q24 | Qiagen |
| Qubit 4 fluorometer | Thermofisher |
| S380-5000 microcentrifuge | Starlab |
| Stepone Plus Real time PCR system | Applied Biosystems |
| Symphony A5 flow cytometer | BD |
| Thermal Cycler, Veriti 96 Well | Applied Biosystems |
| Thermomixer C | Eppendorf |
| VeritiPro™ Thermal Cycler, 384-well | Applied Biosystems |
| VOYAGER (8 channel) | Integra Biosciences |

## *Appendix B. List of consumables*

| | |
|---|---|
| 96 Well PCR Plate, Semi-skirted, Clear | StarLab |
| Cell Star Disposable Tubes (15 ml) | Greiner Bio-One |
| Cell Star Falcon Tubes (50 ml) | Greiner Bio-One |
| 0.2ml thin-walled PCR tubes | StarLab |
| 8-Strip PCR caps, Domed | StarLab |
| Certified Thin Wall 24 x 0.2ml PCR Plates – Elevated Wells | StarLab |
| PyroMark Q24 Plate | Qiagen |
| CryoPure tubes, 2ml | Starstedt |
| 0.2µM syringe filter | Starlab |
| Serological pipette (10ml, 25ml, 50ml) | Thermofisher |
| cellometer cell counter slide | Nexcelom as Revvity |
| 5ml polystyrene round-bottom tubes | Falcon |
| MicroAmp fast optical 96-well reaction plate with barcode | Applied biosystems |
| 0.2ml 96 well PCR plate, semi skirted | Starlab |
| Ionchef consumables | Life Technologies |
| ION 530 chip | Life Technologies |
| E-Gel$^{TM}$ sizeselect II 2% agarose gel | Invitrogen |
| Bioanalyser chip | Agilent |
| 384 well plates | Framestar |
| Cell culture plate, 96 well, surface: Suspension, round base | Sarstedt |
| Cell culture plate, 96 well, surface: Suspension, flat base | Sarstedt |
| Multiscreen-I 96 ELISpot plates | Millipore |
| Qubit assay tubes | Invitrogen |
| Nextseq flow cell (75-cycle high output kit) | Illumina |

*Appendix C. Chemicals and reagents*

**Cell lysis and DNA extraction**

| | |
|---|---|
| QIAmp mini blood kit | Qiagen |
| Tween 20 | Acros Organics |
| Trisma base | Sigma-Aldrich |
| Proteinase K | Invitrogen |
| Ambion™ Nuclease Free water | Invitrogen |

**Flow cytometry.**

| | |
|---|---|
| ArC Amine Reactive Compensation Bead Kit | Life Technologies |
| AbC Total Antibody Compensation Bead kit | Thermofisher |
| BD™ CompBeads Anti-Mouse Ig, κ/Negative Control Compensation Particles Set | BD Biosciences |

**PCR**

| | |
|---|---|
| GoTaq® G2 DNA Polymerase (5u/µl) | Promega |
| 5X Colorless GoTaq® Reaction Buffer | Promega |
| 10µM dNTPs | Life Technologies |
| Platinum SuperFi. ii DNA polymerase | Life Technologies |
| Platinum SuperFi ii 5x buffer | Life Technologies |

**Gel Electrophoresis**

| | |
|---|---|
| Agarose (Molecular grade) | Bioline Reagents |
| Tris Acetate EDTA (TAE) buffer | Sigma-Aldrich |
| SYBR Safe DNA Gel Stain, 10000x | Invitrogen |
| GeneRuler 100bp Plus DNA Ladder | ThermoFisher |
| Blue/Orange 6X Loading Dye | Promega |

**Pyrosequencing**

| | |
|---|---|
| Streptavidin Sepharose High Performance beads | Cytiva |
| PyroMark Binding Buffer | Qiagen |
| PyroMark Annealing Buffer | Qiagen |
| PyroMark Wash Buffer Concentrate | Qiagen |
| 100% Ethanol | Fisher chemicals |
| PyroMark Enzyme mixture | Qiagen |
| PyroMark Substrate mixture | Qiagen |
| Sodium Hydroxide Pellets | VWR |
| PyroMark dATP | Qiagen |
| PyroMark dCTP | Qiagen |
| PyroMark dGTP | Qiagen |
| PyroMark dTTP | Qiagen |

**Real time PCR**

| | |
|---|---|
| Taqman universal PCR mastermix | Thermofisher |

**Sequencing**

| | |
|---|---|
| Bioanalyser high sensitivity DNA reagents | Agilent |
| Ion Plus Fragment Library Kit<br>- Nick repair polymerase<br>- Ion P1 adaptor<br>- DNA ligase<br>- 10x DNA ligase buffer<br>- dNTP mix | Life Technologies |
| IonXpress Barcodes | Life Technologies |
| Ampure XP beads | Fisher Scientific |
| IonChef Solutions Cartridge | Life Technologies |
| IonChef reagents cartridge | Life Technologies |
| Ion S5 sequencing solutions | Life Technologies |

| | |
|---|---|
| Qubit high sensitivity DNA kit | Thermofisher |
| E-Gel™ 50bp ladder | Invitrogen |
| 10X E-Gel™ Sample loading buffer | Invitrogen |

**Tissue Culture**

| | |
|---|---|
| Lymphoprep™ | Stem cell technologies |
| L-Glutamine 200mM | Life Technologies |
| FBS (foetal bovine serum) | Sigma-Aldrich |
| DMSO | Sigma-Aldrich |
| Phosphate buffered saline (PBS) tablets | Fisher |
| RPMI (without L-glu) | Sigma-Aldrich |
| Penicillin-Streptomycin (10,000 U/mL) | Thermo Fisher Scientific |
| Human Ab serum | Sigma Aldrich |
| EDTA disodium salt solution | Sigma-Aldrich |
| Trypan blue | Sigma Aldrich |
| αCD3 coating Ab | Biolegend |
| αCD28 Ab | Biolegend |
| Cell Trace Violet (CTV) | Life Technologies |
| Uridine | Sigma-Aldrich |

**ELISpot**

| | |
|---|---|
| IFN-γ human ELISpot antibody clone 1-D1K | Mabtech |
| IFN-γ human biotinylated antibody clone 7-B6-1 | Mabtech |
| Streptavidin ALP | Mabtech |
| BCIP/NBT | Life Technologies |
| Carbonate/bicarbonate capsules | Sigma Aldrich |
| SARS-CoV2 peptides (S1S2 and M+NP) | Mimotopes |
| Concanavalin A | Merck |

**Targetseq**

| | |
|---|---|
| Triton X-100 | Sigma-Aldrich |
| Rnase inhibitor | Takara clontech |
| Protease | Qiagen |
| ERCC RNA spike-in mix | Life Technologies |
| SMARTScribe enzyme | Takara clontech |
| seqAMP | Takara clontech |
| Nextera XT library prep kit | Illumina |
| Nextera XT Index kit | Illumina |

## *Appendix D Details of software used.*

FCS Express 7
BD FACSDiva
R (v4.4.0)
Image Lab (version 6.1)

***Appendix E. Custom barcoded MT-TL1 primer sequences used for single cell sequencing on the ion s5***

| **Well** | **Barcode + forward** |
|---|---|
| A01 | ACGATCGTGATAA GGC CTA CTT CAC AAA GCG |
| B01 | CTAGATCGTGTAA GGC CTA CTT CAC AAA GCG |
| C01 | GACTCGATCATAA GGC CTA CTT CAC AAA GCG |
| D01 | TGACTAGCTCTAA GGC CTA CTT CAC AAA GCG |
| E01 | ATGCTCAGCATAA GGC CTA CTT CAC AAA GCG |
| F01 | CGATCTGCATTAA GGC CTA CTT CAC AAA GCG |
| G01 | GATAGCTGACTAA GGC CTA CTT CAC AAA GCG |
| H01 | TCAGCTACGTTAA GGC CTA CTT CAC AAA GCG |
| A02 | AGTACGCATGTAA GGC CTA CTT CAC AAA GCG |
| B02 | CACGTCGATATAA GGC CTA CTT CAC AAA GCG |
| C02 | GTATCACGACTAA GGC CTA CTT CAC AAA GCG |
| D02 | TCGCAGTACTTAA GGC CTA CTT CAC AAA GCG |
| E02 | AGCGTCTGATTAA GGC CTA CTT CAC AAA GCG |
| F02 | CAGCATGTCTTAA GGC CTA CTT CAC AAA GCG |
| G02 | GTACTCATCGTAA GGC CTA CTT CAC AAA GCG |
| H02 | TCTGCAGCTATAA GGC CTA CTT CAC AAA GCG |
| A03 | ACTGTACTCGTAA GGC CTA CTT CAC AAA GCG |
| B03 | CGACAGCTATTAA GGC CTA CTT CAC AAA GCG |
| C03 | GTCATGCGTATAA GGC CTA CTT CAC AAA GCG |
| D03 | TAGTCGCATGTAA GGC CTA CTT CAC AAA GCG |
| E03 | ATCGATGACGTAA GGC CTA CTT CAC AAA GCG |
| F03 | CGATAGTCGTTAA GGC CTA CTT CAC AAA GCG |
| G03 | GAGCTGTATCTAA GGC CTA CTT CAC AAA GCG |
| H03 | TCTGATCGCATAA GGC CTA CTT CAC AAA GCG |
| A04 | AGCATCGTCTTAA GGC CTA CTT CAC AAA GCG |
| B04 | CTACGTCTAGTAA GGC CTA CTT CAC AAA GCG |
| C04 | GCTAGATGCTTAA GGC CTA CTT CAC AAA GCG |
| D04 | TCGAGTGCATTAA GGC CTA CTT CAC AAA GCG |
| E04 | ACGCTGACATTAA GGC CTA CTT CAC AAA GCG |
| F04 | CATACAGTGCTAA GGC CTA CTT CAC AAA GCG |
| G04 | GAGCACTAGTTAA GGC CTA CTT CAC AAA GCG |
| H04 | TGCATGTAGCTAA GGC CTA CTT CAC AAA GCG |
| A05 | AGTGATCGACTAA GGC CTA CTT CAC AAA GCG |
| B05 | CTGACATGCATAA GGC CTA CTT CAC AAA GCG |
| C05 | GTAGCAGATCTAA GGC CTA CTT CAC AAA GCG |

| | |
|---|---|
| D05 | TCACTATGCGTAA GGC CTA CTT CAC AAA GCG |
| E05 | ACTCGATACGTAA GGC CTA CTT CAC AAA GCG |
| F05 | CGCATGATCATAA GGC CTA CTT CAC AAA GCG |
| G05 | GCAGATCACTTAA GGC CTA CTT CAC AAA GCG |
| H05 | TCGACTAGTGTAA GGC CTA CTT CAC AAA GCG |
| A06 | ATCAGCGATGTAA GGC CTA CTT CAC AAA GCG |
| B06 | CTGTATGAGCTAA GGC CTA CTT CAC AAA GCG |
| C06 | GTGACTGTCATAA GGC CTA CTT CAC AAA GCG |
| D06 | TACGCTGCATTAA GGC CTA CTT CAC AAA GCG |
| E06 | AGCTGATGCATAA GGC CTA CTT CAC AAA GCG |
| F06 | CTATGCACTGTAA GGC CTA CTT CAC AAA GCG |
| G06 | GCTCATGTCATAA GGC CTA CTT CAC AAA GCG |
| H06 | TAGCGATCTGTAA GGC CTA CTT CAC AAA GCG |
| A07 | ACGTACTGCTTAA GGC CTA CTT CAC AAA GCG |
| B07 | CATAGCATCGTAA GGC CTA CTT CAC AAA GCG |
| C07 | CTGTGTGTGATAA GGC CTA CTT CAC AAA GCG |
| D07 | CAGTGAGAGCTAA GGC CTA CTT CAC AAA GCG |
| E07 | GTACATATGCTAA GGC CTA CTT CAC AAA GCG |
| F07 | GAGACTAGAGTAA GGC CTA CTT CAC AAA GCG |
| G07 | TACGCGTGTATAA GGC CTA CTT CAC AAA GCG |
| H07 | TGTCACTCATTAA GGC CTA CTT CAC AAA GCG |
| A08 | GCACATACACTAA GGC CTA CTT CAC AAA GCG |
| B08 | GCTCGTCGCGTAA GGC CTA CTT CAC AAA GCG |
| C08 | ACAGTGCGCTTAA GGC CTA CTT CAC AAA GCG |
| D08 | TCACACTCTATAA GGC CTA CTT CAC AAA GCG |
| E08 | TCACATATGTTAA GGC CTA CTT CAC AAA GCG |
| F08 | CGCTGCGAGATAA GGC CTA CTT CAC AAA GCG |
| G08 | ACACACAGACTAA GGC CTA CTT CAC AAA GCG |
| H08 | GCAGACTCTCTAA GGC CTA CTT CAC AAA GCG |
| A09 | TGCTCTCGTGTAA GGC CTA CTT CAC AAA GCG |
| B09 | GTGTGAGATATAA GGC CTA CTT CAC AAA GCG |
| C09 | CTCAGTGTGATAA GGC CTA CTT CAC AAA GCG |
| D09 | TGCGAGCGACTAA GGC CTA CTT CAC AAA GCG |
| E09 | GTCAGCTAGTTAA GGC CTA CTT CAC AAA GCG |
| F09 | AGATATCATCTAA GGC CTA CTT CAC AAA GCG |
| G09 | GTGCAGTGATTAA GGC CTA CTT CAC AAA GCG |
| H09 | TGACTCGCTCTAA GGC CTA CTT CAC AAA GCG |
| A10 | ATGCTGATGATAA GGC CTA CTT CAC AAA GCG |
| B10 | GACAGCATCTTAA GGC CTA CTT CAC AAA GCG |

| | |
|---|---|
| C10 | AGCGTCTGACTAA GGC CTA CTT CAC AAA GCG |
| D10 | TCGATATACGTAA GGC CTA CTT CAC AAA GCG |
| E10 | TCGTCATACGTAA GGC CTA CTT CAC AAA GCG |
| F10 | CGACTACGTATAA GGC CTA CTT CAC AAA GCG |
| G10 | GCGTAGACAGTAA GGC CTA CTT CAC AAA GCG |
| H10 | ACAGTATGATTAA GGC CTA CTT CAC AAA GCG |
| A11 | GTCTGATAGATAA GGC CTA CTT CAC AAA GCG |
| B11 | CTGCGCAGTATAA GGC CTA CTT CAC AAA GCG |
| C11 | TAGATCTCTGTAA GGC CTA CTT CAC AAA GCG |
| D11 | CTGATGCGCGTAA GGC CTA CTT CAC AAA GCG |
| E11 | CACTCGTGCATAA GGC CTA CTT CAC AAA GCG |
| F11 | TGACAGTATCTAA GGC CTA CTT CAC AAA GCG |
| G11 | GAGATACGCTTAA GGC CTA CTT CAC AAA GCG |
| H11 | ACGTGAGCTCTAA GGC CTA CTT CAC AAA GCG |
| A12 | ATAGAGAGTGTAA GGC CTA CTT CAC AAA GCG |
| B12 | CATAGAGAGATAA GGC CTA CTT CAC AAA GCG |
| C12 | ATCTCGAGATTAA GGC CTA CTT CAC AAA GCG |
| D12 | ACGATCACTCTAA GGC CTA CTT CAC AAA GCG |
| E12 | GATCGACTCGTAA GGC CTA CTT CAC AAA GCG |
| F12 | ATGCTCACTATAA GGC CTA CTT CAC AAA GCG |
| G12 | CGTGCACATCTAA GGC CTA CTT CAC AAA GCG |
| H12 | GACTGCACATTAA GGC CTA CTT CAC AAA GCG |

*Appendix F. Oligo(dT) primers used for cDNA synthesis.*

| Oligo_Name | Sequence |
|---|---|
| HT001 | aagcagtggtatcaacgcagagttgctCATATTCCTGGTGGvttttttttttttttttttttttttttttt |
| HT002 | aagcagtggtatcaacgcagagttgctACAACAAGGTTCGGvttttttttttttttttttttttttttttttt |
| HT003 | aagcagtggtatcaacgcagagttgctTCGGTGAGGATTGGvttttttttttttttttttttttttttttt |
| HT004 | aagcagtggtatcaacgcagagttgctGACAACATCAGCGGvttttttttttttttttttttttttttttttt |
| HT005 | aagcagtggtatcaacgcagagttgctATATTGCAACCTGGvttttttttttttttttttttttttttttt |
| HT006 | aagcagtggtatcaacgcagagttgctTTGGAACCTTGCCGvttttttttttttttttttttttttttttt |
| HT007 | aagcagtggtatcaacgcagagttgctGTTATAGCTTGTCGvttttttttttttttttttttttttttttt |
| HT008 | aagcagtggtatcaacgcagagttgctGAGGTATGGTCTTGvttttttttttttttttttttttttttttt |
| HT009 | aagcagtggtatcaacgcagagttgctAGCTCATAAGTGAGvttttttttttttttttttttttttttttt |
| HT010 | aagcagtggtatcaacgcagagttgctGAGAAGTAATCCAGvttttttttttttttttttttttttttttt |
| HT011 | aagcagtggtatcaacgcagagttgctGGAATTCGCTTCGGvttttttttttttttttttttttttttttt |
| HT012 | aagcagtggtatcaacgcagagttgctTGATTCCTAGGCGGvttttttttttttttttttttttttttttt |
| HT013 | aagcagtggtatcaacgcagagttgctCCTTCTCCATCCTGvttttttttttttttttttttttttttttt |
| HT014 | aagcagtggtatcaacgcagagttgctCGCGAATTGATTAGvttttttttttttttttttttttttttttt |
| HT015 | aagcagtggtatcaacgcagagttgctTTAGGCGTTGGTGGvttttttttttttttttttttttttttttt |
| HT016 | aagcagtggtatcaacgcagagttgctACAAGTCTCACGTGvttttttttttttttttttttttttttttt |
| HT017 | aagcagtggtatcaacgcagagttgctAGACGGAGTTGTGGvttttttttttttttttttttttttttttt |
| HT018 | aagcagtggtatcaacgcagagttgctACATGAGTGTTCTGvttttttttttttttttttttttttttttt |
| HT019 | aagcagtggtatcaacgcagagttgctAATCCTTCGTGTGGvttttttttttttttttttttttttttttt |
| HT020 | aagcagtggtatcaacgcagagttgctCTCTCCAAGACTGGvttttttttttttttttttttttttttttt |
| HT021 | aagcagtggtatcaacgcagagttgctCCAAGCGAACCTTGvttttttttttttttttttttttttttttt |
| HT022 | aagcagtggtatcaacgcagagttgctTACTACGGTTACGGvttttttttttttttttttttttttttttt |
| HT023 | aagcagtggtatcaacgcagagttgctCACGTGCATACTGGvttttttttttttttttttttttttttttt |
| HT024 | aagcagtggtatcaacgcagagttgctTATAGGCAACGCGGvttttttttttttttttttttttttttttt |
| HT025 | aagcagtggtatcaacgcagagttgctATATGAAGGCTTGGvttttttttttttttttttttttttttttt |
| HT026 | aagcagtggtatcaacgcagagttgctCCTTAGATCCTCCGvttttttttttttttttttttttttttttt |
| HT027 | aagcagtggtatcaacgcagagttgctTACATAAGCCTTCGvttttttttttttttttttttttttttttt |
| HT028 | aagcagtggtatcaacgcagagttgctGCCAGGAAGTCTTGvttttttttttttttttttttttttttttt |
| HT029 | aagcagtggtatcaacgcagagttgctAGCAAGACTAGCGGvttttttttttttttttttttttttttttt |
| HT030 | aagcagtggtatcaacgcagagttgctAGCCTTGGATCTGGvttttttttttttttttttttttttttttt |
| HT031 | aagcagtggtatcaacgcagagttgctTGAGATCCACCTCGvttttttttttttttttttttttttttttt |
| HT032 | aagcagtggtatcaacgcagagttgctGTCCAGTAGTATGGvttttttttttttttttttttttttttttt |
| HT033 | aagcagtggtatcaacgcagagttgctTTATACTCCTTGCGvttttttttttttttttttttttttttttt |
| HT034 | aagcagtggtatcaacgcagagttgctTCCTTGGTACGTGGvttttttttttttttttttttttttttttt |
| HT035 | aagcagtggtatcaacgcagagttgctAGGCAATCAGGTGGvttttttttttttttttttttttttttttt |
| HT036 | aagcagtggtatcaacgcagagttgctTCTAAGCGGTCTTGvttttttttttttttttttttttttttttt |

| | |
|---|---|
| HT037 | aagcagtggtatcaacgcagagttgctGAGGCTTAACTTGGvttttttttttttttttttttttttttttt |
| HT038 | aagcagtggtatcaacgcagagttgctTGACAGGACTTCGGvttttttttttttttttttttttttttttttt |
| HT039 | aagcagtggtatcaacgcagagttgctGGAGCACTAGCTTGvttttttttttttttttttttttttttttttt |
| HT040 | aagcagtggtatcaacgcagagttgctATGTTATCTCGTGGvttttttttttttttttttttttttttttt |
| HT041 | aagcagtggtatcaacgcagagttgctAGCTAATGTTGTCGvttttttttttttttttttttttttttttt |
| HT042 | aagcagtggtatcaacgcagagttgctGGAACGATATTCAGvttttttttttttttttttttttttttttt |
| HT043 | aagcagtggtatcaacgcagagttgctTATGGTGGACCTGGvttttttttttttttttttttttttttttt |
| HT044 | aagcagtggtatcaacgcagagttgctGCATGTATTACCGGvttttttttttttttttttttttttttttt |
| HT045 | aagcagtggtatcaacgcagagttgctACACGCTACTTCGGvttttttttttttttttttttttttttttt |
| HT046 | aagcagtggtatcaacgcagagttgctTTGTCAAGTGGCGGvttttttttttttttttttttttttttttt |
| HT047 | aagcagtggtatcaacgcagagttgctAGGTATGTATACGGvttttttttttttttttttttttttttttt |
| HT048 | aagcagtggtatcaacgcagagttgctGCAAGTACACATAGvttttttttttttttttttttttttttttt |
| HT049 | aagcagtggtatcaacgcagagttgctTTGCGAGTCTCCTGvttttttttttttttttttttttttttttt |
| HT050 | aagcagtggtatcaacgcagagttgctCAATCCACACTCCGvttttttttttttttttttttttttttttt |
| HT051 | aagcagtggtatcaacgcagagttgctACACTTCGCCTTGGvttttttttttttttttttttttttttttt |
| HT052 | aagcagtggtatcaacgcagagttgctGTATATAACTCCGGvttttttttttttttttttttttttttttt |
| HT053 | aagcagtggtatcaacgcagagttgctCGTCATTCTTGCGGvttttttttttttttttttttttttttttt |
| HT054 | aagcagtggtatcaacgcagagttgctACAGAATCGTCCGGvttttttttttttttttttttttttttttt |
| HT055 | aagcagtggtatcaacgcagagttgctTTACTGGCTAGCGGvttttttttttttttttttttttttttttt |
| HT056 | aagcagtggtatcaacgcagagttgctGTAATGCCGTGTAGvttttttttttttttttttttttttttttt |
| HT057 | aagcagtggtatcaacgcagagttgctCGCGATAACGATCGvttttttttttttttttttttttttttttt |
| HT058 | aagcagtggtatcaacgcagagttgctTCTCTGGTAGCTAGvttttttttttttttttttttttttttttt |
| HT059 | aagcagtggtatcaacgcagagttgctATTGGTTATGACGGvttttttttttttttttttttttttttttt |
| HT060 | aagcagtggtatcaacgcagagttgctCAACCATTGCTTGGvttttttttttttttttttttttttttttt |
| HT061 | aagcagtggtatcaacgcagagttgctGCTAATTCCACTCGvttttttttttttttttttttttttttttt |
| HT062 | aagcagtggtatcaacgcagagttgctACTAGTCCTTGGCGvttttttttttttttttttttttttttttt |
| HT063 | aagcagtggtatcaacgcagagttgctGACAATCTTCTTGGvttttttttttttttttttttttttttttt |
| HT064 | aagcagtggtatcaacgcagagttgctAGGTCACTGCCTTGvttttttttttttttttttttttttttttt |
| HT065 | aagcagtggtatcaacgcagagttgctTTCTGCGCCATTCGvttttttttttttttttttttttttttttt |
| HT066 | aagcagtggtatcaacgcagagttgctCCTCGAGAATGTGGvttttttttttttttttttttttttttttt |
| HT067 | aagcagtggtatcaacgcagagttgctGAGTTCTTGTGCGGvttttttttttttttttttttttttttttt |
| HT068 | aagcagtggtatcaacgcagagttgctACCATGTCGTTCCGvttttttttttttttttttttttttttttt |
| HT069 | aagcagtggtatcaacgcagagttgctTATAATTGCCGCGGvttttttttttttttttttttttttttttt |
| HT070 | aagcagtggtatcaacgcagagttgctTAGAAGATTGTCGGvttttttttttttttttttttttttttttt |
| HT071 | aagcagtggtatcaacgcagagttgctGATGTGGACTTCCGvttttttttttttttttttttttttttttt |
| HT072 | aagcagtggtatcaacgcagagttgctAACCTGGAACGCTGvttttttttttttttttttttttttttttt |
| HT073 | aagcagtggtatcaacgcagagttgctCTGAACGTGGCTTGvttttttttttttttttttttttttttttt |
| HT074 | aagcagtggtatcaacgcagagttgctGAGGATATACTGAGvttttttttttttttttttttttttttttt |
| HT075 | aagcagtggtatcaacgcagagttgctGTTCAACTATACGGvttttttttttttttttttttttttttttt |

| | |
|---|---|
| HT076 | aagcagtggtatcaacgcagagttgctCAGCATTGTACGTGvttttttttttttttttttttttttttttt |
| HT077 | aagcagtggtatcaacgcagagttgctCCAACTTCGGTCTGvttttttttttttttttttttttttttttt |
| HT078 | aagcagtggtatcaacgcagagttgctTCTTGCATCTTCGGvttttttttttttttttttttttttttttt |
| HT079 | aagcagtggtatcaacgcagagttgctTTGCTAAGATACGGvttttttttttttttttttttttttttttt |
| HT080 | aagcagtggtatcaacgcagagttgctAGAACACCATCCGGvttttttttttttttttttttttttttttt |
| HT081 | aagcagtggtatcaacgcagagttgctCAGTCAGAACATGGvttttttttttttttttttttttttttttt |
| HT082 | aagcagtggtatcaacgcagagttgctATTGGCTGCTGTGGvttttttttttttttttttttttttttttt |
| HT083 | aagcagtggtatcaacgcagagttgctAACACCAATTACGGvttttttttttttttttttttttttttttt |
| HT084 | aagcagtggtatcaacgcagagttgctAACAGTACCTGCGGvttttttttttttttttttttttttttttt |
| HT085 | aagcagtggtatcaacgcagagttgctGATAGTTGATACGGvttttttttttttttttttttttttttttt |
| HT086 | aagcagtggtatcaacgcagagttgctATAAGGCATAGTGGvttttttttttttttttttttttttttttt |
| HT087 | aagcagtggtatcaacgcagagttgctTTGTTGACACTTGGvttttttttttttttttttttttttttttt |
| HT088 | aagcagtggtatcaacgcagagttgctCATTACCGCTTCGGvttttttttttttttttttttttttttttt |
| HT089 | aagcagtggtatcaacgcagagttgctGTATCACGCGGTTGvttttttttttttttttttttttttttttt |
| HT090 | aagcagtggtatcaacgcagagttgctAGCATCCAACATGGvttttttttttttttttttttttttttttt |
| HT091 | aagcagtggtatcaacgcagagttgctCGTCTTCGACTTCCvttttttttttttttttttttttttttttt |
| HT092 | aagcagtggtatcaacgcagagttgctTCAACTCGACAGCCvttttttttttttttttttttttttttttt |
| HT093 | aagcagtggtatcaacgcagagttgctAAGGCGACAGTCTCvttttttttttttttttttttttttttttt |
| HT094 | aagcagtggtatcaacgcagagttgctGACTGAAGATCTCCvttttttttttttttttttttttttttttt |
| HT095 | aagcagtggtatcaacgcagagttgctCTAGCTAATGCTCCvttttttttttttttttttttttttttttt |
| HT096 | aagcagtggtatcaacgcagagttgctCAGGTACTTATGTCvttttttttttttttttttttttttttttt |
| HT097 | aagcagtggtatcaacgcagagttgctTGCTGTCAGATTGCvttttttttttttttttttttttttttttt |
| HT098 | aagcagtggtatcaacgcagagttgctCTATTGCCTTCGCCvttttttttttttttttttttttttttttt |
| HT099 | aagcagtggtatcaacgcagagttgctCAGAGGCTGTTGTCvttttttttttttttttttttttttttttt |
| HT100 | aagcagtggtatcaacgcagagttgctATGAGTAGACCTTCvttttttttttttttttttttttttttttt |
| HT101 | aagcagtggtatcaacgcagagttgctACCGTTAAGTCGCCvttttttttttttttttttttttttttttt |
| HT102 | aagcagtggtatcaacgcagagttgctATCTGTGGTTCTACvttttttttttttttttttttttttttttt |
| HT103 | aagcagtggtatcaacgcagagttgctACCAAGGAACATACvttttttttttttttttttttttttttttt |
| HT104 | aagcagtggtatcaacgcagagttgctTTCGTTAACTGTCCvttttttttttttttttttttttttttttt |
| HT105 | aagcagtggtatcaacgcagagttgctATGCTCTAACCTCCvttttttttttttttttttttttttttttt |
| HT106 | aagcagtggtatcaacgcagagttgctTGACTCAAGCGTGCvttttttttttttttttttttttttttttt |
| HT107 | aagcagtggtatcaacgcagagttgctTTAACCGGAGTTCCvttttttttttttttttttttttttttttt |
| HT108 | aagcagtggtatcaacgcagagttgctGACACGTGTTCTCCvttttttttttttttttttttttttttttt |
| HT109 | aagcagtggtatcaacgcagagttgctTGTGCGGTTCGTTCvttttttttttttttttttttttttttttt |
| HT110 | aagcagtggtatcaacgcagagttgctAAGCGCCATGGTTCvttttttttttttttttttttttttttttt |
| HT111 | aagcagtggtatcaacgcagagttgctTCAGAGGTAGTTACvttttttttttttttttttttttttttttt |
| HT112 | aagcagtggtatcaacgcagagttgctGTTGGTTAGTCTTCvttttttttttttttttttttttttttttt |
| HT113 | aagcagtggtatcaacgcagagttgctCATTACTATACCGCvttttttttttttttttttttttttttttt |
| HT114 | aagcagtggtatcaacgcagagttgctCGACAACTACTGCCvttttttttttttttttttttttttttttt |

| | |
|---|---|
| HT115 | aagcagtggtatcaacgcagagttgctATACCTCAAGGTCCvttttttttttttttttttttttttttttt |
| HT116 | aagcagtggtatcaacgcagagttgctCAAGGTCTTCCTCCvttttttttttttttttttttttttttttt |
| HT117 | aagcagtggtatcaacgcagagttgctCCAATTGAGCGCTCvttttttttttttttttttttttttttttt |
| HT118 | aagcagtggtatcaacgcagagttgctACACTACCGTGTCCvttttttttttttttttttttttttttttt |
| HT119 | aagcagtggtatcaacgcagagttgctAATAGTTGCGTTGCvttttttttttttttttttttttttttttt |
| HT120 | aagcagtggtatcaacgcagagttgctCAATTCAGTAGCACvttttttttttttttttttttttttttttt |
| HT121 | aagcagtggtatcaacgcagagttgctAACCACGATAGGCCvttttttttttttttttttttttttttttt |
| HT122 | aagcagtggtatcaacgcagagttgctGCTAGAGACTCTTCvttttttttttttttttttttttttttttt |
| HT123 | aagcagtggtatcaacgcagagttgctGTTAGGAAGTTCACvttttttttttttttttttttttttttttt |
| HT124 | aagcagtggtatcaacgcagagttgctTTGATCCGTTCTTCvttttttttttttttttttttttttttttt |
| HT125 | aagcagtggtatcaacgcagagttgctGGTTAGTAGATTCCvttttttttttttttttttttttttttttt |
| HT126 | aagcagtggtatcaacgcagagttgctCCGGACTAACCTTCvttttttttttttttttttttttttttttt |
| HT127 | aagcagtggtatcaacgcagagttgctTAGTTGGTACCTTCvttttttttttttttttttttttttttttt |
| HT128 | aagcagtggtatcaacgcagagttgctAGAGCGATCGTTGCvttttttttttttttttttttttttttttt |
| HT129 | aagcagtggtatcaacgcagagttgctAAGAGTTCTACCACvttttttttttttttttttttttttttttt |
| HT130 | aagcagtggtatcaacgcagagttgctATAATAAGCACGCCvttttttttttttttttttttttttttttt |
| HT131 | aagcagtggtatcaacgcagagttgctGACCTAACTAGCGCvttttttttttttttttttttttttttttt |
| HT132 | aagcagtggtatcaacgcagagttgctCTTCTAGAGGTTCCvttttttttttttttttttttttttttttt |
| HT133 | aagcagtggtatcaacgcagagttgctAGCATGGACTCTCCvttttttttttttttttttttttttttttt |
| HT134 | aagcagtggtatcaacgcagagttgctTTCCAGATACCTTCvttttttttttttttttttttttttttttt |
| HT135 | aagcagtggtatcaacgcagagttgctATAAGACACTCTGCvttttttttttttttttttttttttttttt |
| HT136 | aagcagtggtatcaacgcagagttgctGAATTCTCGATTCCvttttttttttttttttttttttttttttt |
| HT137 | aagcagtggtatcaacgcagagttgctGTCAATTCACCTACvttttttttttttttttttttttttttttt |
| HT138 | aagcagtggtatcaacgcagagttgctGGTATTAAGACGTCvttttttttttttttttttttttttttttt |
| HT139 | aagcagtggtatcaacgcagagttgctTCTCACTTCACTCCvttttttttttttttttttttttttttttt |
| HT140 | aagcagtggtatcaacgcagagttgctTGTTCACCTGCGTCvttttttttttttttttttttttttttttt |
| HT141 | aagcagtggtatcaacgcagagttgctTGTAACTAGTTGCCvttttttttttttttttttttttttttttt |
| HT142 | aagcagtggtatcaacgcagagttgctGGTCTACTGTTCGCvttttttttttttttttttttttttttttt |
| HT143 | aagcagtggtatcaacgcagagttgctTTCCTCTAATCGACvttttttttttttttttttttttttttttt |
| HT144 | aagcagtggtatcaacgcagagttgctGAGTCCGATCTCTCvttttttttttttttttttttttttttttt |
| HT145 | aagcagtggtatcaacgcagagttgctGGTGGATAAGTTCCvttttttttttttttttttttttttttttt |
| HT146 | aagcagtggtatcaacgcagagttgctCCTCCTGAATAGACvttttttttttttttttttttttttttttt |
| HT147 | aagcagtggtatcaacgcagagttgctTAATTGCAATCCGCvttttttttttttttttttttttttttttt |
| HT148 | aagcagtggtatcaacgcagagttgctAATACTGACGCTCCvttttttttttttttttttttttttttttt |
| HT149 | aagcagtggtatcaacgcagagttgctAAGTATTCCACTCCvttttttttttttttttttttttttttttt |
| HT150 | aagcagtggtatcaacgcagagttgctAGGCAGCTAAGTCCvttttttttttttttttttttttttttttt |
| HT151 | aagcagtggtatcaacgcagagttgctGTATACTCTCAGTCvttttttttttttttttttttttttttttt |
| HT152 | aagcagtggtatcaacgcagagttgctTATCGGTTGCCTCCvttttttttttttttttttttttttttttt |
| HT153 | aagcagtggtatcaacgcagagttgctTGGCCTGTACTGTCvttttttttttttttttttttttttttttt |

| | |
|---|---|
| HT154 | aagcagtggtatcaacgcagagttgctTACACCTTATTGCCvttttttttttttttttttttttttttttt |
| HT155 | aagcagtggtatcaacgcagagttgctATACATGACTTGCCvttttttttttttttttttttttttttttttt |
| HT156 | aagcagtggtatcaacgcagagttgctTCCGCTTGGTTGTCvttttttttttttttttttttttttttttttt |
| HT157 | aagcagtggtatcaacgcagagttgctTCCATGCAATTGTCvttttttttttttttttttttttttttttttt |
| HT158 | aagcagtggtatcaacgcagagttgctTCCATACGGAGTCCvttttttttttttttttttttttttttttttt |
| HT159 | aagcagtggtatcaacgcagagttgctTGACTCTTCTCGCCvttttttttttttttttttttttttttttttt |
| HT160 | aagcagtggtatcaacgcagagttgctACTTCAATTCTGCCvttttttttttttttttttttttttttttttt |
| HT161 | aagcagtggtatcaacgcagagttgctTTCACTATTGAGCCvttttttttttttttttttttttttttttttt |
| HT162 | aagcagtggtatcaacgcagagttgctAGAGGAACCGCTTCvttttttttttttttttttttttttttttttt |
| HT163 | aagcagtggtatcaacgcagagttgctAGAAGTCAAGGCGCvttttttttttttttttttttttttttttttt |
| HT164 | aagcagtggtatcaacgcagagttgctATCGGATAAGATGCvttttttttttttttttttttttttttttttt |
| HT165 | aagcagtggtatcaacgcagagttgctGCGCAATAGTCTCCvttttttttttttttttttttttttttttttt |
| HT166 | aagcagtggtatcaacgcagagttgctAATACGCCATATCCvttttttttttttttttttttttttttttttt |
| HT167 | aagcagtggtatcaacgcagagttgctACCTCGTAGCTCTCvttttttttttttttttttttttttttttttt |
| HT168 | aagcagtggtatcaacgcagagttgctAACCAGACTTCTCCvttttttttttttttttttttttttttttttt |
| HT169 | aagcagtggtatcaacgcagagttgctTAGGTTCGAGCTCCvttttttttttttttttttttttttttttttt |
| HT170 | aagcagtggtatcaacgcagagttgctCGATCGGATCATCCvttttttttttttttttttttttttttttttt |
| HT171 | aagcagtggtatcaacgcagagttgctCGTCAAGCATCTCCvttttttttttttttttttttttttttttttt |
| HT172 | aagcagtggtatcaacgcagagttgctGGATTATTGGCGCCvttttttttttttttttttttttttttttttt |
| HT173 | aagcagtggtatcaacgcagagttgctGCGAGGTCGTATTCvttttttttttttttttttttttttttttttt |
| HT174 | aagcagtggtatcaacgcagagttgctCTGGCGGAACATACvttttttttttttttttttttttttttttttt |
| HT175 | aagcagtggtatcaacgcagagttgctCATGGCCAATAGCCvttttttttttttttttttttttttttttttt |
| HT176 | aagcagtggtatcaacgcagagttgctTCTCGAGGATATTCvttttttttttttttttttttttttttttttt |
| HT177 | aagcagtggtatcaacgcagagttgctCTGTGGACCATGTCvttttttttttttttttttttttttttttttt |
| HT178 | aagcagtggtatcaacgcagagttgctTAACTTAAGACCGCvttttttttttttttttttttttttttttttt |
| HT179 | aagcagtggtatcaacgcagagttgctGTTGCCTTATGGCCvttttttttttttttttttttttttttttttt |
| HT180 | aagcagtggtatcaacgcagagttgctGTGATCAATGCCTCvttttttttttttttttttttttttttttttt |
| HT181 | aagcagtggtatcaacgcagagttgctCAAGGATCTGCGAAvttttttttttttttttttttttttttttttt |
| HT182 | aagcagtggtatcaacgcagagttgctGCTTCACACTCCAAvttttttttttttttttttttttttttttttt |
| HT183 | aagcagtggtatcaacgcagagttgctAGGAAGAACCTTGAvttttttttttttttttttttttttttttttt |
| HT184 | aagcagtggtatcaacgcagagttgctCTCGCTAACAAGAAvttttttttttttttttttttttttttttttt |
| HT185 | aagcagtggtatcaacgcagagttgctTCTGGACTCTGTTAvttttttttttttttttttttttttttttttt |
| HT186 | aagcagtggtatcaacgcagagttgctTATTGAGAGCGGAAvttttttttttttttttttttttttttttttt |
| HT187 | aagcagtggtatcaacgcagagttgctAACTCTCCGGAGAAvttttttttttttttttttttttttttttttt |
| HT188 | aagcagtggtatcaacgcagagttgctGAACAGTGGACCAAvttttttttttttttttttttttttttttttt |
| HT189 | aagcagtggtatcaacgcagagttgctAGGTGTAATGTGGAvttttttttttttttttttttttttttttttt |
| HT190 | aagcagtggtatcaacgcagagttgctGCGCTTGTCGACAAvttttttttttttttttttttttttttttttt |
| HT191 | aagcagtggtatcaacgcagagttgctGCTCCGTCACACAAvttttttttttttttttttttttttttttttt |
| HT192 | aagcagtggtatcaacgcagagttgctGTCATTGGTCCGAAvttttttttttttttttttttttttttttttt |

| | |
|---|---|
| HT193 | aagcagtggtatcaacgcagagttgctAATATCTTCGGCCAvttttttttttttttttttttttttttttt |
| HT194 | aagcagtggtatcaacgcagagttgctAGTGGCGTTAACAAvttttttttttttttttttttttttttttttt |
| HT195 | aagcagtggtatcaacgcagagttgctGTGTCCGGCATTGAvttttttttttttttttttttttttttttttt |
| HT196 | aagcagtggtatcaacgcagagttgctCAACCGGAGAAGAAvttttttttttttttttttttttttttttttt |
| HT197 | aagcagtggtatcaacgcagagttgctCTCAGGACTTAGTAvttttttttttttttttttttttttttttttt |
| HT198 | aagcagtggtatcaacgcagagttgctGCTTAGACTAGCTAvttttttttttttttttttttttttttttttt |
| HT199 | aagcagtggtatcaacgcagagttgctGCAGATTAGTGTCAvttttttttttttttttttttttttttttttt |
| HT200 | aagcagtggtatcaacgcagagttgctGGTTGGTGGCTTAAvttttttttttttttttttttttttttttttt |
| HT201 | aagcagtggtatcaacgcagagttgctCTAAGAACACCGAAvttttttttttttttttttttttttttttttt |
| HT202 | aagcagtggtatcaacgcagagttgctTTAGACGTCTACGAvttttttttttttttttttttttttttttttt |
| HT203 | aagcagtggtatcaacgcagagttgctGGACCTCGTGAGAAvttttttttttttttttttttttttttttttt |
| HT204 | aagcagtggtatcaacgcagagttgctGGAAGTTGAGGTAAvttttttttttttttttttttttttttttttt |
| HT205 | aagcagtggtatcaacgcagagttgctACATTGTCCACCAAvttttttttttttttttttttttttttttttt |
| HT206 | aagcagtggtatcaacgcagagttgctATCGCGCCAACCAAvttttttttttttttttttttttttttttttt |
| HT207 | aagcagtggtatcaacgcagagttgctGCGAAGTCCGAGAAvttttttttttttttttttttttttttttttt |
| HT208 | aagcagtggtatcaacgcagagttgctATTAGGAGCTCGAAvttttttttttttttttttttttttttttttt |
| HT209 | aagcagtggtatcaacgcagagttgctGCGTGACGCAGTAAvttttttttttttttttttttttttttttttt |
| HT210 | aagcagtggtatcaacgcagagttgctGGATCCTTAGACAAvttttttttttttttttttttttttttttttt |
| HT211 | aagcagtggtatcaacgcagagttgctCATCAATGCGGCAAvttttttttttttttttttttttttttttttt |
| HT212 | aagcagtggtatcaacgcagagttgctAAGGCCACTAACAAvttttttttttttttttttttttttttttttt |
| HT213 | aagcagtggtatcaacgcagagttgctGGTACCGAAGAGAAvttttttttttttttttttttttttttttttt |
| HT214 | aagcagtggtatcaacgcagagttgctCGATCAGGTCGGAAvttttttttttttttttttttttttttttttt |
| HT215 | aagcagtggtatcaacgcagagttgctACAACATGCTCCTAvttttttttttttttttttttttttttttttt |
| HT216 | aagcagtggtatcaacgcagagttgctGAGACAAGCGATAAvttttttttttttttttttttttttttttttt |
| HT217 | aagcagtggtatcaacgcagagttgctGAAGCATAGGAGAAvttttttttttttttttttttttttttttttt |
| HT218 | aagcagtggtatcaacgcagagttgctCACCTCCATGTGTAvttttttttttttttttttttttttttttttt |
| HT219 | aagcagtggtatcaacgcagagttgctCGCATGCTATAGAAvttttttttttttttttttttttttttttttt |
| HT220 | aagcagtggtatcaacgcagagttgctTGGTCGATCTTGAAvttttttttttttttttttttttttttttttt |
| HT221 | aagcagtggtatcaacgcagagttgctTAGATCTCGCAGAAvttttttttttttttttttttttttttttttt |
| HT222 | aagcagtggtatcaacgcagagttgctTAGTGAGCTAGTCAvttttttttttttttttttttttttttttttt |
| HT223 | aagcagtggtatcaacgcagagttgctCCTGTGAGCCGTTAvttttttttttttttttttttttttttttttt |
| HT224 | aagcagtggtatcaacgcagagttgctCGACGACTCAGGAAvttttttttttttttttttttttttttttttt |
| HT225 | aagcagtggtatcaacgcagagttgctATCTTGACGGCGAAvttttttttttttttttttttttttttttttt |
| HT226 | aagcagtggtatcaacgcagagttgctCTCTTGGTGTTCAAvttttttttttttttttttttttttttttttt |
| HT227 | aagcagtggtatcaacgcagagttgctTCGGTACTAAGGAAvttttttttttttttttttttttttttttttt |
| HT228 | aagcagtggtatcaacgcagagttgctACCTGGTGATACAAvttttttttttttttttttttttttttttttt |
| HT229 | aagcagtggtatcaacgcagagttgctATGAGCGCATATCAvttttttttttttttttttttttttttttttt |
| HT230 | aagcagtggtatcaacgcagagttgctCTATACAGTGCGTAvttttttttttttttttttttttttttttttt |
| HT231 | aagcagtggtatcaacgcagagttgctGAGAGAAGGTTGTAvttttttttttttttttttttttttttttttt |

| | |
|---|---|
| HT232 | aagcagtggtatcaacgcagagttgctCTGGAGAGGTACAAvttttttttttttttttttttttttttttt |
| HT233 | aagcagtggtatcaacgcagagttgctTTATACGATCGCCAvttttttttttttttttttttttttttttt |
| HT234 | aagcagtggtatcaacgcagagttgctCTCGAATCCTACAAvttttttttttttttttttttttttttttt |
| HT235 | aagcagtggtatcaacgcagagttgctAAGAGGTCGGCTAAvttttttttttttttttttttttttttttt |
| HT236 | aagcagtggtatcaacgcagagttgctAACAAGCTCCGCAAvttttttttttttttttttttttttttttt |
| HT237 | aagcagtggtatcaacgcagagttgctCAGGTCCTGAAGAAvttttttttttttttttttttttttttttt |
| HT238 | aagcagtggtatcaacgcagagttgctATTCTTGCTCCTGAvttttttttttttttttttttttttttttt |
| HT239 | aagcagtggtatcaacgcagagttgctATGAAGGTCTGTGAvttttttttttttttttttttttttttttt |
| HT240 | aagcagtggtatcaacgcagagttgctTTGTCGGCCGAGAAvttttttttttttttttttttttttttttt |
| HT241 | aagcagtggtatcaacgcagagttgctGGCTTAGCGGAGAAvttttttttttttttttttttttttttttt |
| HT242 | aagcagtggtatcaacgcagagttgctTGGACGTCGATTAAvttttttttttttttttttttttttttttt |
| HT243 | aagcagtggtatcaacgcagagttgctGTGGTAGCCTAGAAvttttttttttttttttttttttttttttt |
| HT244 | aagcagtggtatcaacgcagagttgctTCTTCGTATCGCAAvttttttttttttttttttttttttttttt |
| HT245 | aagcagtggtatcaacgcagagttgctAAGTGGTGTTCCTAvttttttttttttttttttttttttttttt |
| HT246 | aagcagtggtatcaacgcagagttgctGGAAGGTCATACAAvttttttttttttttttttttttttttttt |
| HT247 | aagcagtggtatcaacgcagagttgctGATTCGGTCCGCTAvttttttttttttttttttttttttttttt |
| HT248 | aagcagtggtatcaacgcagagttgctACACGTATGTGTGAvttttttttttttttttttttttttttttt |
| HT249 | aagcagtggtatcaacgcagagttgctGCAGTTGCTAGTAAvttttttttttttttttttttttttttttt |
| HT250 | aagcagtggtatcaacgcagagttgctGTGTTGTCGCGGAAvttttttttttttttttttttttttttttt |
| HT251 | aagcagtggtatcaacgcagagttgctCGCTGGTAATGTAAvttttttttttttttttttttttttttttt |
| HT252 | aagcagtggtatcaacgcagagttgctCAGCTGTGAATCAAvttttttttttttttttttttttttttttt |
| HT253 | aagcagtggtatcaacgcagagttgctTCGCGTTGCCAGAAvttttttttttttttttttttttttttttt |
| HT254 | aagcagtggtatcaacgcagagttgctTGCACTCTACCTTAvttttttttttttttttttttttttttttt |
| HT255 | aagcagtggtatcaacgcagagttgctCTGAGCTTGTTCAAvttttttttttttttttttttttttttttt |
| HT256 | aagcagtggtatcaacgcagagttgctTATCGGACGTACAAvttttttttttttttttttttttttttttt |
| HT257 | aagcagtggtatcaacgcagagttgctCAGCCAATAAGGAAvttttttttttttttttttttttttttttt |
| HT258 | aagcagtggtatcaacgcagagttgctGGTTCTATAGCCTAvttttttttttttttttttttttttttttt |
| HT259 | aagcagtggtatcaacgcagagttgctCTTACTGGTGCCAAvttttttttttttttttttttttttttttt |
| HT260 | aagcagtggtatcaacgcagagttgctACATCTTGAGCTGAvttttttttttttttttttttttttttttt |
| HT261 | aagcagtggtatcaacgcagagttgctGATCTAACCGAGAAvttttttttttttttttttttttttttttt |
| HT262 | aagcagtggtatcaacgcagagttgctGAAGCCTAATCCAAvttttttttttttttttttttttttttttt |
| HT263 | aagcagtggtatcaacgcagagttgctAGTAACGGTTGGTAvttttttttttttttttttttttttttttt |
| HT264 | aagcagtggtatcaacgcagagttgctCCTCTTCCTATCAAvttttttttttttttttttttttttttttt |
| HT265 | aagcagtggtatcaacgcagagttgctGAGAGGCGACACAAvttttttttttttttttttttttttttttt |
| HT266 | aagcagtggtatcaacgcagagttgctCGAATCGCAAGGAAvttttttttttttttttttttttttttttt |
| HT267 | aagcagtggtatcaacgcagagttgctTGACTCGTTGGTTAvttttttttttttttttttttttttttttt |
| HT268 | aagcagtggtatcaacgcagagttgctTCCTAGGAGAAGAAvttttttttttttttttttttttttttttt |
| HT269 | aagcagtggtatcaacgcagagttgctTCGTGATGTGTGTAvttttttttttttttttttttttttttttt |
| HT270 | aagcagtggtatcaacgcagagttgctTCTGTGCACCAGAAvttttttttttttttttttttttttttttt |

| | |
|---|---|
| HT271 | aagcagtggtatcaacgcagagttgctGTCTTACGCCGCTAvttttttttttttttttttttttttttttt |
| HT272 | aagcagtggtatcaacgcagagttgctCTTGTACTTCCAGAvttttttttttttttttttttttttttttt |
| HT273 | aagcagtggtatcaacgcagagttgctATAGTGGTCGTAGAvttttttttttttttttttttttttttttt |
| HT274 | aagcagtggtatcaacgcagagttgctGCACAACTTGTAGAvttttttttttttttttttttttttttttt |
| HT275 | aagcagtggtatcaacgcagagttgctAAGAGCCTTGTAGAvttttttttttttttttttttttttttttt |
| HT276 | aagcagtggtatcaacgcagagttgctGACCTGTCATTAGAvttttttttttttttttttttttttttttt |
| HT277 | aagcagtggtatcaacgcagagttgctCTGTCGTAATGACAvttttttttttttttttttttttttttttt |
| HT278 | aagcagtggtatcaacgcagagttgctTATCTCGGTACACAvttttttttttttttttttttttttttttt |
| HT279 | aagcagtggtatcaacgcagagttgctTGATTGCTTGCACAvttttttttttttttttttttttttttttt |
| HT280 | aagcagtggtatcaacgcagagttgctATTACCTCTCCACAvttttttttttttttttttttttttttttt |
| HT281 | aagcagtggtatcaacgcagagttgctGGTATCCAATCACAvttttttttttttttttttttttttttttt |
| HT282 | aagcagtggtatcaacgcagagttgctAGACGAGACTCACAvttttttttttttttttttttttttttttt |
| HT283 | aagcagtggtatcaacgcagagttgctACCTTCTTCTCACAvttttttttttttttttttttttttttttt |
| HT284 | aagcagtggtatcaacgcagagttgctGCATCAAGAGTACAvttttttttttttttttttttttttttttt |
| HT285 | aagcagtggtatcaacgcagagttgctTAGTCCTTCCTACAvttttttttttttttttttttttttttttt |
| HT286 | aagcagtggtatcaacgcagagttgctCTTGGCCTATTACAvttttttttttttttttttttttttttttt |
| HT287 | aagcagtggtatcaacgcagagttgctCGCGACAAGTTACAvttttttttttttttttttttttttttttt |
| HT288 | aagcagtggtatcaacgcagagttgctGTGCTTGAGTTACAvttttttttttttttttttttttttttttt |
| HT289 | aagcagtggtatcaacgcagagttgctAACAGACCGTTACAvttttttttttttttttttttttttttttt |
| HT290 | aagcagtggtatcaacgcagagttgctGTGCCTCACCGATAvttttttttttttttttttttttttttttt |
| HT291 | aagcagtggtatcaacgcagagttgctTTGCGCCTCACATAvttttttttttttttttttttttttttttt |
| HT292 | aagcagtggtatcaacgcagagttgctACCGCGAAGATATAvttttttttttttttttttttttttttttt |
| HT293 | aagcagtggtatcaacgcagagttgctCAGGACCGTATATAvttttttttttttttttttttttttttttt |
| HT294 | aagcagtggtatcaacgcagagttgctTTATCTAGACGAGGvttttttttttttttttttttttttttttt |
| HT295 | aagcagtggtatcaacgcagagttgctTAACCGTAATGAGGvttttttttttttttttttttttttttttt |
| HT296 | aagcagtggtatcaacgcagagttgctACTAAGCTGACAGGvttttttttttttttttttttttttttttt |
| HT297 | aagcagtggtatcaacgcagagttgctGTTATGCTACCAGGvttttttttttttttttttttttttttttt |
| HT298 | aagcagtggtatcaacgcagagttgctCCATGAGTAATAGGvttttttttttttttttttttttttttttt |
| HT299 | aagcagtggtatcaacgcagagttgctACGGTTCAGATAGGvttttttttttttttttttttttttttttt |
| HT300 | aagcagtggtatcaacgcagagttgctTGACGGAGGATAGGvttttttttttttttttttttttttttttt |
| HT301 | aagcagtggtatcaacgcagagttgctACTATCGCGCTAGGvttttttttttttttttttttttttttttt |
| HT302 | aagcagtggtatcaacgcagagttgctATTGGAGCATTAGGvttttttttttttttttttttttttttttt |
| HT303 | aagcagtggtatcaacgcagagttgctATGCAGAGCTGACGvttttttttttttttttttttttttttttt |
| HT304 | aagcagtggtatcaacgcagagttgctATTGTATCACCACGvttttttttttttttttttttttttttttt |
| HT305 | aagcagtggtatcaacgcagagttgctGTAAGTCCTATACGvttttttttttttttttttttttttttttt |
| HT306 | aagcagtggtatcaacgcagagttgctTTCATGACCAGATGvttttttttttttttttttttttttttttt |
| HT307 | aagcagtggtatcaacgcagagttgctACCGACTGATTATGvttttttttttttttttttttttttttttt |
| HT308 | aagcagtggtatcaacgcagagttgctAATAACCTAGCAGCvttttttttttttttttttttttttttttt |
| HT309 | aagcagtggtatcaacgcagagttgctTAAGACAAGACACCvttttttttttttttttttttttttttttt |

| | |
|---|---|
| HT310 | aagcagtggtatcaacgcagagttgctGTATTCTTACCACCvttttttttttttttttttttttttttt |
| HT311 | aagcagtggtatcaacgcagagttgctAGACTTCAGATACCvttttttttttttttttttttttttttttt |
| HT312 | aagcagtggtatcaacgcagagttgctCGAACGCTCACATCvttttttttttttttttttttttttttttt |
| HT313 | aagcagtggtatcaacgcagagttgctGACAGGAGAGAGATvttttttttttttttttttttttttttttt |
| HT314 | aagcagtggtatcaacgcagagttgctCCAGTCCAACAGATvttttttttttttttttttttttttttttt |
| HT315 | aagcagtggtatcaacgcagagttgctCAGAATGGACAGATvttttttttttttttttttttttttttttt |
| HT316 | aagcagtggtatcaacgcagagttgctGTTCGCAGGCAGATvttttttttttttttttttttttttttttt |
| HT317 | aagcagtggtatcaacgcagagttgctCATGCGAGTCGGATvttttttttttttttttttttttttttttt |
| HT318 | aagcagtggtatcaacgcagagttgctGGAACGAGGACGATvttttttttttttttttttttttttttttt |
| HT319 | aagcagtggtatcaacgcagagttgctGTCAGTTCGATGATvttttttttttttttttttttttttttttt |
| HT320 | aagcagtggtatcaacgcagagttgctGGTCGGTCCATCATvttttttttttttttttttttttttttttt |
| HT321 | aagcagtggtatcaacgcagagttgctTCGCTGAACCATATvttttttttttttttttttttttttttttt |
| HT322 | aagcagtggtatcaacgcagagttgctCGCCGGCACTATATvttttttttttttttttttttttttttttt |
| HT323 | aagcagtggtatcaacgcagagttgctGGCACCGCGATTATvttttttttttttttttttttttttttttt |
| HT324 | aagcagtggtatcaacgcagagttgctCTGCATCAGGTTATvttttttttttttttttttttttttttttt |
| HT325 | aagcagtggtatcaacgcagagttgctCGGAAGCCACTTATvttttttttttttttttttttttttttttt |
| HT326 | aagcagtggtatcaacgcagagttgctAGTCCACTAGGCGTvttttttttttttttttttttttttttttt |
| HT327 | aagcagtggtatcaacgcagagttgctTTGGTCTGGTGCGTvttttttttttttttttttttttttttttt |
| HT328 | aagcagtggtatcaacgcagagttgctCTCACCGTGATCGTvttttttttttttttttttttttttttttt |
| HT329 | aagcagtggtatcaacgcagagttgctTAACAAGTGCTCGTvttttttttttttttttttttttttttttt |
| HT330 | aagcagtggtatcaacgcagagttgctGGATTCCAGTTCGTvttttttttttttttttttttttttttttt |
| HT331 | aagcagtggtatcaacgcagagttgctAGTTGATGAGGTGTvttttttttttttttttttttttttttttt |
| HT332 | aagcagtggtatcaacgcagagttgctGCTTGAAGGCGTGTvttttttttttttttttttttttttttttt |
| HT333 | aagcagtggtatcaacgcagagttgctGCCATAGAACCTGTvttttttttttttttttttttttttttttt |
| HT334 | aagcagtggtatcaacgcagagttgctCGAATCTTACCTGTvttttttttttttttttttttttttttttt |
| HT335 | aagcagtggtatcaacgcagagttgctCTGCCAGAAGTTGTvttttttttttttttttttttttttttttt |
| HT336 | aagcagtggtatcaacgcagagttgctGGTCCAACCGTTGTvttttttttttttttttttttttttttttt |
| HT337 | aagcagtggtatcaacgcagagttgctCATTCCTCTGTTGTvttttttttttttttttttttttttttttt |
| HT338 | aagcagtggtatcaacgcagagttgctGCTCCTCGACTTGTvttttttttttttttttttttttttttttt |
| HT339 | aagcagtggtatcaacgcagagttgctCACCAACACCTTGTvttttttttttttttttttttttttttttt |
| HT340 | aagcagtggtatcaacgcagagttgctACACCGGTTCTTGTvttttttttttttttttttttttttttttt |
| HT341 | aagcagtggtatcaacgcagagttgctACAGCAGGCAGACTvttttttttttttttttttttttttttttt |
| HT342 | aagcagtggtatcaacgcagagttgctATGGCGTGATCGCTvttttttttttttttttttttttttttttt |
| HT343 | aagcagtggtatcaacgcagagttgctGTCGTCGTAGTGCTvttttttttttttttttttttttttttttt |
| HT344 | aagcagtggtatcaacgcagagttgctGTGTCGTCACACCTvttttttttttttttttttttttttttttt |
| HT345 | aagcagtggtatcaacgcagagttgctCTTGACGAACGCCTvttttttttttttttttttttttttttttt |
| HT346 | aagcagtggtatcaacgcagagttgctTCTTGAAGCCTCCTvttttttttttttttttttttttttttttt |
| HT347 | aagcagtggtatcaacgcagagttgctCACATAACCAGTCTvttttttttttttttttttttttttttttt |
| HT348 | aagcagtggtatcaacgcagagttgctGAATTGCGGCGTCTvttttttttttttttttttttttttttttt |

| | |
|---|---|
| HT349 | aagcagtggtatcaacgcagagttgctGACGTTCAGCCTCTvttttttttttttttttttttttttttttt |
| HT350 | aagcagtggtatcaacgcagagttgctTTACCGTGGCCTCTvttttttttttttttttttttttttttttt |
| HT351 | aagcagtggtatcaacgcagagttgctGGCATACACGTTCTvttttttttttttttttttttttttttttt |
| HT352 | aagcagtggtatcaacgcagagttgctCGTATCGTTGTTCTvttttttttttttttttttttttttttttt |
| HT353 | aagcagtggtatcaacgcagagttgctCCATGGCCACTTCTvttttttttttttttttttttttttttttt |
| HT354 | aagcagtggtatcaacgcagagttgctCTTCGGTCTCTTCTvttttttttttttttttttttttttttttt |
| HT355 | aagcagtggtatcaacgcagagttgctAGTTGTGCCACATTvttttttttttttttttttttttttttttt |
| HT356 | aagcagtggtatcaacgcagagttgctCCGGCGCCAATATTvttttttttttttttttttttttttttttt |
| HT357 | aagcagtggtatcaacgcagagttgctGGCGAGAGGTTATTvttttttttttttttttttttttttttttt |
| HT358 | aagcagtggtatcaacgcagagttgctCCACCGAAGGAGTTvttttttttttttttttttttttttttttt |
| HT359 | aagcagtggtatcaacgcagagttgctGCCTTCCAATAGTTvttttttttttttttttttttttttttttt |
| HT360 | aagcagtggtatcaacgcagagttgctTTGCCGTACCGGTTvttttttttttttttttttttttttttttt |
| HT361 | aagcagtggtatcaacgcagagttgctGGTAGCCTGTGGTTvttttttttttttttttttttttttttttt |
| HT362 | aagcagtggtatcaacgcagagttgctGCTCGTCATGCGTTvttttttttttttttttttttttttttttt |
| HT363 | aagcagtggtatcaacgcagagttgctGTATTGTAGCCGTTvttttttttttttttttttttttttttttt |
| HT364 | aagcagtggtatcaacgcagagttgctTGGTTCATGTCGTTvttttttttttttttttttttttttttttt |
| HT365 | aagcagtggtatcaacgcagagttgctAGGAGGTGCATGTTvttttttttttttttttttttttttttttt |
| HT366 | aagcagtggtatcaacgcagagttgctAAGGAGCAGGTGTTvttttttttttttttttttttttttttttt |
| HT367 | aagcagtggtatcaacgcagagttgctGAGAACCGTGTGTTvttttttttttttttttttttttttttttt |
| HT368 | aagcagtggtatcaacgcagagttgctCCGGATGCACTGTTvttttttttttttttttttttttttttttt |
| HT369 | aagcagtggtatcaacgcagagttgctGGACGGAGACACTTvttttttttttttttttttttttttttttt |
| HT370 | aagcagtggtatcaacgcagagttgctCCTCACCTACGCTTvttttttttttttttttttttttttttttt |
| HT371 | aagcagtggtatcaacgcagagttgctATTGTGGCGCGCTTvttttttttttttttttttttttttttttt |
| HT372 | aagcagtggtatcaacgcagagttgctAAGTCTGTCTGCTTvttttttttttttttttttttttttttttt |
| HT373 | aagcagtggtatcaacgcagagttgctGGAGTTAACACCTTvttttttttttttttttttttttttttttt |
| HT374 | aagcagtggtatcaacgcagagttgctGCGAGATGTGCCTTvttttttttttttttttttttttttttttt |
| HT375 | aagcagtggtatcaacgcagagttgctTCGAGCACATCCTTvttttttttttttttttttttttttttttt |
| HT376 | aagcagtggtatcaacgcagagttgctGCATCCTTATCCTTvttttttttttttttttttttttttttttt |
| HT377 | aagcagtggtatcaacgcagagttgctCATCCGGAGATCTTvttttttttttttttttttttttttttttt |
| HT378 | aagcagtggtatcaacgcagagttgctGTTACACCGATCTTvttttttttttttttttttttttttttttt |
| HT379 | aagcagtggtatcaacgcagagttgctAGTTGACGCATCTTvttttttttttttttttttttttttttttt |
| HT380 | aagcagtggtatcaacgcagagttgctCTTGTCACAGTCTTvttttttttttttttttttttttttttttt |
| HT381 | aagcagtggtatcaacgcagagttgctGCTGTCGAGGTCTTvttttttttttttttttttttttttttttt |
| HT382 | aagcagtggtatcaacgcagagttgctCTCCACTGACTCTTvttttttttttttttttttttttttttttt |
| HT383 | aagcagtggtatcaacgcagagttgctGAACATTGGCTCTTvttttttttttttttttttttttttttttt |
| HT384 | aagcagtggtatcaacgcagagttgctGGCGAGTACCTCTTvttttttttttttttttttttttttttttt |

***Appendix G DEGs in high m.3243A>G CD8+ naive T cells***

| Gene name | log2FoldChange | pvalue | padj |
|---|---|---|---|
| CLEC2B | 9.577427 | 6.26E-10 | 6.16E-07 |
| SELENOK | 6.099656 | 7.11E-07 | 0.000349 |
| SMC3 | -2.10598 | 5.13E-06 | 0.00164 |
| EIF5 | 4.957919 | 6.68E-06 | 0.00164 |
| RSF1 | 5.3098 | 3.30E-05 | 0.006347 |
| COX4I1 | 5.623055 | 3.87E-05 | 0.006347 |
| MYL12A | 5.780696 | 0.000111 | 0.015628 |
| UBE2D2 | 3.530071 | 0.000173 | 0.021271 |
| LAX1 | -1.19631 | 0.000286 | 0.031246 |
| N4BP2L2 | -3.22621 | 0.000396 | 0.037031 |
| DYNC1H1 | -3.89496 | 0.000414 | 0.037031 |
| RSL1D1 | -4.33196 | 0.000496 | 0.040658 |
| PRPF40A | 4.504432 | 0.000665 | 0.047269 |
| CD96 | -4.75023 | 0.000673 | 0.047269 |
| ANKRD12 | -3.42006 | 0.000733 | 0.048023 |
| H2AZ1 | 6.115168 | 0.001134 | 0.06191 |
| ENSG00000235859 | -1.41227 | 0.001095 | 0.06191 |
| GTF3A | 4.638356 | 0.001043 | 0.06191 |
| COPS6 | 4.167626 | 0.001339 | 0.069294 |
| NEMF | 3.929948 | 0.00194 | 0.095366 |
| GNAS | 2.505087 | 0.002071 | 0.096963 |
| MED23 | -1.27616 | 0.002178 | 0.09731 |
| LINC.PINT | -2.54123 | 0.002328 | 0.099488 |

***Appendix H. DEGs in high m.3243A>G CD8+ memory T cells***

| Gene name | log2FoldChange | pvalue | padj |
|---|---|---|---|
| TNRC6B | 3.450536 | 3.09E-10 | 6.64E-07 |
| ARID5B | 2.359723 | 1.88E-07 | 0.000202 |
| RTF1 | -4.73057 | 4.71E-07 | 0.000337 |
| ATRX | 2.010099 | 1.94E-06 | 0.00104 |
| RUNX1 | 4.010938 | 4.28E-06 | 0.001842 |
| RASGRP2 | 2.050277 | 6.56E-06 | 0.002188 |
| DYNC1H1 | -3.22968 | 7.12E-06 | 0.002188 |
| FBXO7 | -4.90233 | 3.47E-05 | 0.009332 |
| IFRD1 | 3.095656 | 4.82E-05 | 0.011522 |
| ETF1 | 2.659066 | 6.51E-05 | 0.013038 |
| MLXIP | 2.092348 | 6.67E-05 | 0.013038 |
| NDUFS2 | 4.008353 | 8.80E-05 | 0.015081 |
| PRPF40A | -2.20522 | 9.12E-05 | 0.015081 |
| BECN1 | 3.898101 | 0.000141 | 0.021698 |
| DR1 | 3.209249 | 0.000182 | 0.026147 |
| CNOT1 | 2.264927 | 0.0002 | 0.026834 |
| YPEL5 | 1.73304 | 0.000235 | 0.027339 |
| RPS27A | 2.177703 | 0.000264 | 0.027339 |
| CREBBP | -2.28934 | 0.000248 | 0.027339 |
| CASC3 | -3.7059 | 0.000227 | 0.027339 |
| CHD6 | 3.751757 | 0.00028 | 0.027339 |
| MYH9 | -2.73559 | 0.000267 | 0.027339 |
| SEC61B | -4.83499 | 0.000293 | 0.027365 |
| RPS24 | 2.747559 | 0.000306 | 0.027395 |
| RALY | 3.308117 | 0.000344 | 0.029544 |
| UFC1 | -4.07612 | 0.000362 | 0.029918 |
| EPB41 | 2.078815 | 0.000469 | 0.035977 |
| CRYBG1 | 4.395337 | 0.000463 | 0.035977 |
| TOMM7 | -3.8576 | 0.00049 | 0.036315 |
| RNF125 | 2.460965 | 0.000602 | 0.043151 |
| GOLGB1 | 1.567077 | 0.000704 | 0.045928 |
| ENSG00000242588 | 2.112472 | 0.000687 | 0.045928 |
| TIAL1 | 1.729704 | 0.000725 | 0.045928 |

| | | | |
|---|---|---|---|
| RAN | -3.30865 | 0.000726 | 0.045928 |
| IKZF5 | 4.801824 | 0.000826 | 0.050742 |
| ENSG00000274275 | 1.609864 | 0.00091 | 0.054376 |
| SRSF6 | 1.24211 | 0.000942 | 0.054737 |
| CCSER2 | 2.5059 | 0.001014 | 0.055898 |
| MED19 | -4.03755 | 0.000997 | 0.055898 |
| ARMC8 | 4.432767 | 0.001125 | 0.06049 |
| BTG3 | 3.813447 | 0.001477 | 0.077451 |
| NOSIP | -3.3374 | 0.001529 | 0.078246 |
| WSB1 | 3.939433 | 0.001733 | 0.086634 |
| PRDM2 | -2.08501 | 0.001801 | 0.087987 |
| UBAP2L | 1.475561 | 0.001885 | 0.090055 |
| EPS15L1 | -2.18788 | 0.001963 | 0.091004 |
| UBE2G2 | -3.16088 | 0.001989 | 0.091004 |
| IRF1 | 2.121171 | 0.002249 | 0.092972 |
| HBS1L | 3.372114 | 0.002169 | 0.092972 |
| GSTP1 | -4.45862 | 0.002216 | 0.092972 |
| GRB2 | -3.63345 | 0.002155 | 0.092972 |
| CIRBP | 2.783633 | 0.002241 | 0.092972 |
| CUL3 | 2.594318 | 0.002334 | 0.094693 |
| SIVA1 | 3.337838 | 0.002407 | 0.095846 |
| SS18L2 | -4.38565 | 0.002524 | 0.096706 |
| CD47 | 2.788348 | 0.002748 | 0.096706 |
| H2AZ2 | 2.275701 | 0.002654 | 0.096706 |
| ZNHIT1 | -2.90335 | 0.002834 | 0.096706 |
| PCSK7 | -2.80127 | 0.002745 | 0.096706 |
| EAPP | -3.91885 | 0.002821 | 0.096706 |
| NKG7 | -2.58428 | 0.002545 | 0.096706 |
| ATP5PO | -4.48182 | 0.002795 | 0.096706 |
| EIF2S3 | 1.201537 | 0.002686 | 0.096706 |
| ORMDL1 | -3.46035 | 0.00297 | 0.099765 |
| IP6K2 | -3.42507 | 0.003169 | 0.099928 |
| FNBP1 | 2.696522 | 0.003219 | 0.099928 |
| NDUFB10 | 3.688989 | 0.003253 | 0.099928 |
| ZNF331 | 2.317436 | 0.003186 | 0.099928 |

| | | | |
|---|---|---|---|
| BRD1 | 2.747965 | 0.00307 | 0.099928 |
| BEX2 | 3.611259 | 0.003094 | 0.099928 |

***Appendix I GO enrichment cluster output for P23 high m.3243A>G level CD8+ naïve T cells****. 296 pathways with a p adjusted value < 0.01 were input into the Revigo.irb.hr algorithm.*

| Ontology | term_ID | description | Cluster | Colour | p | p.adj |
|---|---|---|---|---|---|---|
| BP | GO:0002181 | cytoplasmic translation | Cytoplasmic translation | Lime | 1.08E-23 | 5.55E-20 |
| BP | GO:0042254 | ribosome biogenesis | Ribosome biogenesis | Dark purple | 2.55E-13 | 2.62E-10 |
| BP | GO:0071826 | protein-RNA complex organization | Ribosome biogenesis | Dark purple | 3.66E-12 | 2.36E-09 |
| BP | GO:0035966 | response to topologically incorrect protein | Response to unfolded protein | Orange | 1.70E-11 | 9.71E-09 |
| BP | GO:0032200 | telomere organization | Ribosome biogenesis | Dark purple | 5.76E-11 | 2.70E-08 |
| BP | GO:0006413 | translational initiation | Cytoplasmic translation | Lime | 7.29E-11 | 3.13E-08 |
| BP | GO:0000723 | telomere maintenance | | dark red | 8.51E-11 | 3.37E-08 |
| BP | GO:0006403 | RNA localization | RNA localisation | Yellow | 1.37E-10 | 4.69E-08 |
| BP | GO:0045727 | positive regulation of translation | regulation of mRNA processing | blue | 4.77E-10 | 1.36E-07 |
| BP | GO:0043484 | regulation of RNA splicing | regulation of mRNA processing | blue | 4.63E-10 | 1.36E-07 |
| BP | GO:0031396 | regulation of protein ubiquitination | regulation of mRNA processing | blue | 3.09E-09 | 6.91E-07 |
| BP | GO:0032204 | regulation of telomere maintenance | regulation of mRNA processing | blue | 3.41E-09 | 7.02E-07 |
| BP | GO:0034250 | positive regulation of amide metabolic process | regulation of mRNA processing | blue | 4.31E-09 | 8.45E-07 |
| BP | GO:0051236 | establishment of RNA localization | RNA localisation | Yellow | 1.17E-08 | 2.15E-06 |

| | | | | | | |
|---|---|---|---|---|---|---|
| BP | GO:0044772 | mitotic cell cycle phase transition | mitotic cell cycle phase transition | Dark blue | 1.52E-08 | 2.70E-06 |
| BP | GO:0072594 | establishment of protein localization to organelle | RNA localisation | Yellow | 2.89E-08 | 4.51E-06 |
| BP | GO:0043161 | proteasome-mediated ubiquitin-dependent protein catabolic process | Cytoplasmic translation | Lime | 7.66E-08 | 1.10E-05 |
| BP | GO:0031507 | heterochromatin formation | epigenetic regulation of gene expression | grey | 8.05E-08 | 1.12E-05 |
| BP | GO:0050657 | nucleic acid transport | RNA localisation | Yellow | 9.65E-08 | 1.27E-05 |
| BP | GO:0070828 | heterochromatin organization | Ribosome biogenesis | Dark Purple | 4.20E-07 | 5.15E-05 |
| BP | GO:0051169 | nuclear transport | RNA localisation | Yellow | 4.46E-07 | 5.22E-05 |
| BP | GO:0006913 | nucleocytoplasmic transport | RNA localisation | Yellow | 4.46E-07 | 5.22E-05 |
| BP | GO:0150115 | cell-substrate junction organization | Ribosome biogenesis | Dark Purple | 5.70E-07 | 6.38E-05 |
| BP | GO:1903936 | cellular response to sodium arsenite | Response to unfolded protein | Orange | 6.69E-07 | 7.33E-05 |
| BP | GO:0071243 | cellular response to arsenic-containing substance | Response to unfolded protein | Orange | 7.34E-07 | 7.71E-05 |
| BP | GO:0006986 | response to unfolded protein | Response to unfolded protein | Orange | 7.50E-07 | 7.72E-05 |
| BP | GO:0140694 | non-membrane-bounded organelle assembly | Ribosome biogenesis | Dark Purple | 7.79E-07 | 7.76E-05 |
| BP | GO:0051303 | establishment of chromosome localization | RNA localisation | Yellow | 9.20E-07 | 8.93E-05 |
| BP | GO:1902369 | negative regulation of RNA catabolic process | regulation of mRNA processing | blue | 1.26E-06 | 0.000117988 |
| BP | GO:0007059 | chromosome segregation | mitotic cell cycle phase transition | Dark blue | 1.42E-06 | 0.000122367 |

| | | | | | | |
|---|---|---|---|---|---|---|
| BP | GO:1901990 | regulation of mitotic cell cycle phase transition | regulation of mRNA processing | blue | 1.36E-06 | 0.000122367 |
| BP | GO:1902074 | response to salt | Response to unfolded protein | Orange | 1.52E-06 | 0.000126539 |
| BP | GO:0060382 | regulation of DNA strand elongation | regulation of mRNA processing | blue | 1.70E-06 | 0.000136677 |
| BP | GO:0097193 | intrinsic apoptotic signaling pathway | intrinsic apoptotic signaling pathway | pink | 2.45E-06 | 0.000191514 |
| BP | GO:0006446 | regulation of translational initiation | regulation of mRNA processing | blue | 2.50E-06 | 0.000191766 |
| BP | GO:0007044 | cell-substrate junction assembly | Ribosome biogenesis | Dark Purple | 3.03E-06 | 0.0002264 |
| BP | GO:0030521 | androgen receptor signaling pathway | Response to unfolded protein | Orange | 3.35E-06 | 0.000246522 |
| BP | GO:1900151 | regulation of nuclear-transcribed mRNA catabolic process, deadenylation-dependent decay | regulation of mRNA processing | blue | 3.62E-06 | 0.000258699 |
| BP | GO:0000398 | mRNA splicing, via spliceosome | Cytoplasmic translation | Lime | 5.24E-06 | 0.000359738 |
| BP | GO:0015986 | proton motive force-driven ATP synthesis | Cytoplasmic translation | Lime | 5.37E-06 | 0.000363864 |
| BP | GO:0002183 | cytoplasmic translational initiation | Cytoplasmic translation | Lime | 8.14E-06 | 0.000517421 |
| BP | GO:0019080 | viral gene expression | viral gene expression | Light pink | 1.05E-05 | 0.000627349 |
| BP | GO:0019081 | viral translation | viral gene expression | Light pink | 1.50E-05 | 0.000886185 |
| BP | GO:0036480 | neuron intrinsic apoptotic signaling pathway in response to oxidative stress | Response to unfolded protein | Orange | 1.54E-05 | 0.000888582 |
| BP | GO:0006997 | nucleus organization | Ribosome biogenesis | Dark Purple | 1.79E-05 | 0.000999266 |
| BP | GO:0034063 | stress granule assembly | Ribosome biogenesis | Dark Purple | 1.80E-05 | 0.000999266 |

| | | | | | | |
|---|---|---|---|---|---|---|
| BP | GO:0032386 | regulation of intracellular transport | regulation of RNA export from nucleus | brown | 2.61E-05 | 0.001412356 |
| BP | GO:0150116 | regulation of cell-substrate junction organization | regulation of mRNA processing | blue | 2.80E-05 | 0.001498313 |
| BP | GO:0006278 | RNA-templated DNA biosynthetic process | Cytoplasmic translation | Lime | 2.89E-05 | 0.001518558 |
| BP | GO:0045995 | regulation of embryonic development | regulation of embryonic development | red | 3.39E-05 | 0.001763715 |
| BP | GO:1903513 | endoplasmic reticulum to cytosol transport | RNA localisation | Yellow | 3.99E-05 | 0.002014271 |
| BP | GO:1903311 | regulation of mRNA metabolic process | regulation of mRNA processing | blue | 4.08E-05 | 0.002038252 |
| BP | GO:0032239 | regulation of nucleobase-containing compound transport | regulation of RNA export from nucleus | brown | 4.47E-05 | 0.002211485 |
| BP | GO:0015931 | nucleobase-containing compound transport | RNA localisation | Yellow | 4.47E-05 | 0.002211485 |
| BP | GO:1903008 | organelle disassembly | Ribosome biogenesis | Dark Purple | 4.80E-05 | 0.002308362 |
| BP | GO:0051893 | regulation of focal adhesion assembly | regulation of mRNA processing | blue | 5.13E-05 | 0.002401861 |
| BP | GO:0065004 | protein-DNA complex assembly | Ribosome biogenesis | Dark Purple | 5.49E-05 | 0.002537872 |
| BP | GO:0006310 | DNA recombination | Cytoplasmic translation | Lime | 5.96E-05 | 0.00267299 |
| BP | GO:0009266 | response to temperature stimulus | Response to unfolded protein | Orange | 6.31E-05 | 0.002803092 |
| BP | GO:1903241 | U2-type prespliceosome assembly | | dark red | 6.43E-05 | 0.002831524 |
| BP | GO:0007034 | vacuolar transport | RNA localisation | Yellow | 6.87E-05 | 0.002998844 |
| BP | GO:0034728 | nucleosome organization | Ribosome biogenesis | Dark Purple | 7.03E-05 | 0.003006642 |
| BP | GO:0031647 | regulation of protein stability | regulation of protein stability | green | 7.07E-05 | 0.003006642 |

| | | | | | | |
|---|---|---|---|---|---|---|
| BP | GO:0071456 | cellular response to hypoxia | Response to unfolded protein | Orange | 7.03E-05 | 0.003006642 |
| BP | GO:0022616 | DNA strand elongation | Cytoplasmic translation | Lime | 7.23E-05 | 0.003050374 |
| BP | GO:0032543 | mitochondrial translation | Cytoplasmic translation | Lime | 7.67E-05 | 0.003211779 |
| BP | GO:0034976 | response to endoplasmic reticulum stress | Response to unfolded protein | Orange | 7.74E-05 | 0.003214389 |
| BP | GO:0009141 | nucleoside triphosphate metabolic process | Cytoplasmic translation | Lime | 8.08E-05 | 0.003303824 |
| BP | GO:0050684 | regulation of mRNA processing | regulation of mRNA processing | blue | 8.43E-05 | 0.003391024 |
| BP | GO:0046685 | response to arsenic-containing substance | Response to unfolded protein | Orange | 8.43E-05 | 0.003391024 |
| BP | GO:0140053 | mitochondrial gene expression | Cytoplasmic translation | Lime | 0.000105345 | 0.00401793 |
| BP | GO:0040029 | epigenetic regulation of gene expression | epigenetic regulation of gene expression | grey | 0.000112231 | 0.0042491 |
| BP | GO:0016050 | vesicle organization | Ribosome biogenesis | Dark Purple | 0.000116672 | 0.004353218 |
| BP | GO:0046831 | regulation of RNA export from nucleus | regulation of RNA export from nucleus | brown | 0.000133748 | 0.004792806 |
| BP | GO:1904152 | regulation of retrograde protein transport, ER to cytosol | regulation of RNA export from nucleus | brown | 0.000133748 | 0.004792806 |
| BP | GO:0006999 | nuclear pore organization | Ribosome biogenesis | Dark Purple | 0.000133748 | 0.004792806 |
| BP | GO:0009060 | aerobic respiration | aerobic respiration | purple | 0.000151377 | 0.005305018 |
| BP | GO:0000209 | protein polyubiquitination | Cytoplasmic translation | Lime | 0.000168776 | 0.005871822 |
| BP | GO:0006334 | nucleosome assembly | Ribosome biogenesis | Dark Purple | 0.000181827 | 0.006200186 |
| BP | GO:2000765 | regulation of cytoplasmic translation | regulation of mRNA processing | blue | 0.000190352 | 0.006448178 |

| | | | | | | |
|---|---|---|---|---|---|---|
| BP | GO:0042770 | signal transduction in response to DNA damage | intrinsic apoptotic signaling pathway | pink | 0.000196939 | 0.00658468 |
| BP | GO:0033044 | regulation of chromosome organization | regulation of mRNA processing | blue | 0.000249891 | 0.007942533 |
| BP | GO:0009791 | post-embryonic development | post-embryonic development | beige | 0.00027668 | 0.00853068 |
| BP | GO:0035196 | miRNA processing | regulation of RNA export from nucleus | brown | 0.000293227 | 0.008881343 |

***Appendix J GO enriched pathways in P23 CD8+ memory T cells.*** *Cluster output after 288 pathways with a p adjusted value < 0.01 were input into the Revigo.irb.hr algorithm.*

| term_ID | description | cluster | colour | p | p.adj |
|---|---|---|---|---|---|
| GO:0002181 | cytoplasmic translation | cytoplasmic translation | Lime | 2.70E-19 | 1.55E-15 |
| GO:0043484 | regulation of RNA splicing | regulation of RNA splicing | Turquoise | 7.15E-12 | 8.20E-09 |
| GO:0050684 | regulation of mRNA processing | regulation of RNA splicing | Turquoise | 2.43E-10 | 2.32E-07 |
| GO:0006403 | RNA localization | RNA localization | Yellow | 3.02E-09 | 2.47E-06 |
| GO:0042254 | ribosome biogenesis | ribosome biogenesis | Dark Purple | 4.63E-09 | 3.31E-06 |
| GO:0043161 | proteasome-mediated ubiquitin-dependent protein catabolic process | cytoplasmic translation | Lime | 2.35E-08 | 1.35E-05 |
| GO:0051054 | positive regulation of DNA metabolic process | regulation of RNA splicing | Turquoise | 4.22E-08 | 2.20E-05 |
| GO:0098760 | response to interleukin-7 | response to interleukin-7 | Purple | 9.77E-08 | 3.59E-05 |
| GO:1903008 | organelle disassembly | ribosome biogenesis | Dark Purple | 1.51E-07 | 4.96E-05 |
| GO:0006302 | double-strand break repair | DNA repair | Dark Pink | 1.56E-07 | 4.96E-05 |
| GO:1900151 | regulation of nuclear-transcribed mRNA catabolic process, deadenylation-dependent decay | regulation of RNA splicing | Turquoise | 2.21E-07 | 6.35E-05 |
| GO:0000398 | mRNA splicing, via spliceosome | cytoplasmic translation | Lime | 2.78E-07 | 7.25E-05 |
| GO:0072522 | purine-containing compound biosynthetic process | cytoplasmic translation | Lime | 3.38E-07 | 7.58E-05 |
| GO:0030217 | T cell differentiation | T cell differentiation | Red | 3.34E-07 | 7.58E-05 |
| GO:0032008 | positive regulation of TOR signaling | regulation of RNA splicing | Turquoise | 3.44E-07 | 7.58E-05 |
| GO:0015931 | nucleobase-containing compound transport | RNA localization | Yellow | 5.10E-07 | 0.000102 |
| GO:0009165 | nucleotide biosynthetic process | cytoplasmic translation | Lime | 6.80E-07 | 0.000118 |
| GO:1903311 | regulation of mRNA metabolic process | regulation of RNA splicing | Turquoise | 6.68E-07 | 0.000118 |
| GO:0098761 | cellular response to interleukin-7 | response to interleukin-7 | Purple | 7.24E-07 | 0.000122 |
| GO:0006497 | protein lipidation | cytoplasmic translation | Lime | 8.55E-07 | 0.000128 |

| | | | | | |
|---|---|---|---|---|---|
| GO:0006119 | oxidative phosphorylation | oxidative phosphorylation | Fuchsia | 8.99E-07 | 0.000129 |
| GO:0006900 | vesicle budding from membrane | vesicle budding from membrane | Brown | 1.57E-06 | 0.000196 |
| GO:1990823 | response to leukemia inhibitory factor | response to interleukin-7 | Purple | 1.62E-06 | 0.000197 |
| GO:0071826 | protein-RNA complex organization | ribosome biogenesis | Dark Purple | 3.25E-06 | 0.00033 |
| GO:1903320 | regulation of protein modification by small protein conjugation or removal | regulation of RNA splicing | Turquoise | 3.30E-06 | 0.00033 |
| GO:1990830 | cellular response to leukemia inhibitory factor | response to interleukin-7 | Purple | 3.82E-06 | 0.000359 |
| GO:0048193 | Golgi vesicle transport | RNA localization | Yellow | 4.06E-06 | 0.000364 |
| GO:0050658 | RNA transport | RNA localization | Yellow | 4.02E-06 | 0.000364 |
| GO:0006913 | nucleocytoplasmic transport | RNA localization | Yellow | 5.78E-06 | 0.000452 |
| GO:0051169 | nuclear transport | RNA localization | Yellow | 5.78E-06 | 0.000452 |
| GO:0048872 | homeostasis of number of cells | T cell differentiation | Red | 5.78E-06 | 0.000452 |
| GO:0045862 | positive regulation of proteolysis | regulation of RNA splicing | Turquoise | 5.84E-06 | 0.000452 |
| GO:0034620 | cellular response to unfolded protein | response to interleukin-7 | Purple | 6.32E-06 | 0.000476 |
| GO:0000723 | telomere maintenance | telomere maintenance | Grey | 8.51E-06 | 0.000595 |
| GO:0000725 | recombinational repair | DNA repair | Dark Pink | 8.51E-06 | 0.000595 |
| GO:1900102 | negative regulation of endoplasmic reticulum unfolded protein response | regulation of RNA splicing | Turquoise | 9.74E-06 | 0.000665 |
| GO:0006413 | translational initiation | cytoplasmic translation | Lime | 1.10E-05 | 0.000718 |
| GO:0140694 | non-membrane-bounded organelle assembly | ribosome biogenesis | Dark Purple | 1.47E-05 | 0.000925 |
| GO:0034250 | positive regulation of amide metabolic process | regulation of RNA splicing | Turquoise | 1.66E-05 | 0.001025 |
| GO:0045619 | regulation of lymphocyte differentiation | regulation of lymphocyte differentiation | Blue | 1.82E-05 | 0.001101 |
| GO:0006303 | double-strand break repair via nonhomologous end joining | DNA repair | Dark Pink | 2.00E-05 | 0.001182 |
| GO:0052547 | regulation of peptidase activity | regulation of RNA splicing | Turquoise | 2.03E-05 | 0.001189 |

| | | | | | |
|---|---|---|---|---|---|
| GO:0032200 | telomere organization | ribosome biogenesis | Dark Purple | 2.38E-05 | 0.001324 |
| GO:1904375 | regulation of protein localization to cell periphery | regulation of protein localization to cell periphery | Dark Green | 2.35E-05 | 0.001324 |
| GO:0031331 | positive regulation of cellular catabolic process | regulation of RNA splicing | Turquoise | 2.37E-05 | 0.001324 |
| GO:0032743 | positive regulation of interleukin-2 production | regulation of lymphocyte differentiation | Blue | 2.54E-05 | 0.001403 |
| GO:0006888 | endoplasmic reticulum to Golgi vesicle-mediated transport | RNA localization | Yellow | 2.90E-05 | 0.001566 |
| GO:1900153 | positive regulation of nuclear-transcribed mRNA catabolic process, deadenylation-dependent decay | regulation of RNA splicing | Turquoise | 3.30E-05 | 0.00172 |
| GO:0007034 | vacuolar transport | RNA localization | Yellow | 3.37E-05 | 0.001739 |
| GO:0006122 | mitochondrial electron transport, ubiquinol to cytochrome c | oxidative phosphorylation | Fuchsia | 3.49E-05 | 0.001771 |
| GO:0019080 | viral gene expression | viral gene expression | Light Pink | 3.52E-05 | 0.001771 |
| GO:0006997 | nucleus organization | ribosome biogenesis | Dark Purple | 4.27E-05 | 0.002102 |
| GO:0033119 | negative regulation of RNA splicing | regulation of RNA splicing | Turquoise | 4.29E-05 | 0.002102 |
| GO:0016050 | vesicle organization | ribosome biogenesis | Dark Purple | 4.48E-05 | 0.002141 |
| GO:0031123 | RNA 3'-end processing | cytoplasmic translation | Lime | 4.48E-05 | 0.002141 |
| GO:0034497 | protein localization to phagophore assembly site | vesicle budding from membrane | Brown | 5.49E-05 | 0.002538 |
| GO:0000302 | response to reactive oxygen species | response to interleukin-7 | Purple | 5.58E-05 | 0.00254 |
| GO:0033044 | regulation of chromosome organization | regulation of protein localization to cell periphery | Dark Green | 5.71E-05 | 0.002576 |
| GO:2001252 | positive regulation of chromosome organization | regulation of protein localization to cell periphery | Dark Green | 5.71E-05 | 0.002576 |
| GO:0031929 | TOR signaling | TOR signaling | Green | 5.82E-05 | 0.002607 |
| GO:0051656 | establishment of organelle localization | RNA localization | Yellow | 8.05E-05 | 0.003444 |
| GO:0006383 | transcription by RNA polymerase III | cytoplasmic translation | Lime | 8.37E-05 | 0.003533 |

| | | | | | |
|---|---|---|---|---|---|
| GO:0006310 | DNA recombination | cytoplasmic translation | Lime | 8.39E-05 | 0.003533 |
| GO:0043923 | positive regulation by host of viral transcription | positive regulation by host of viral transcription | beige | 8.78E-05 | 0.00357 |
| GO:0043462 | regulation of ATP-dependent activity | oxidative phosphorylation | Fuchsia | 8.91E-05 | 0.003596 |
| GO:0007059 | chromosome segregation | chromosome segregation | light Blue | 0.000106 | 0.004231 |
| GO:0034504 | protein localization to nucleus | RNA localization | Yellow | 0.000119 | 0.004654 |
| GO:0000480 | endonucleolytic cleavage in 5'-ETS of tricistronic rRNA transcript (SSU-rRNA, 5.8S rRNA, LSU-rRNA) | telomere maintenance | Grey | 0.00012 | 0.004696 |
| GO:1903241 | U2-type prespliceosome assembly | telomere maintenance | Grey | 0.000134 | 0.005097 |
| GO:0038202 | TORC1 signaling | TOR signaling | Green | 0.000159 | 0.005921 |
| GO:0002520 | immune system development | T cell differentiation | Red | 0.000175 | 0.006424 |
| GO:0032623 | interleukin-2 production | fibroblast apoptotic process | Pink | 0.000181 | 0.00649 |
| GO:0032663 | regulation of interleukin-2 production | regulation of lymphocyte differentiation | Blue | 0.000181 | 0.00649 |
| GO:0036444 | calcium import into the mitochondrion | RNA localization | Yellow | 0.000185 | 0.006546 |
| GO:0044346 | fibroblast apoptotic process | fibroblast apoptotic process | Pink | 0.00019 | 0.006648 |
| GO:0048534 | hematopoietic or lymphoid organ development | T cell differentiation | Red | 0.000196 | 0.006795 |
| GO:0006278 | RNA-templated DNA biosynthetic process | cytoplasmic translation | Lime | 0.000211 | 0.00719 |
| GO:0062197 | cellular response to chemical stress | response to interleukin-7 | Purple | 0.00021 | 0.00719 |
| GO:0007041 | lysosomal transport | RNA localization | Yellow | 0.000246 | 0.008282 |
| GO:0019083 | viral transcription | viral gene expression | Light Pink | 0.000254 | 0.008405 |
| GO:0032781 | positive regulation of ATP-dependent activity | oxidative phosphorylation | Fuchsia | 0.000284 | 0.009312 |
| GO:0072683 | T cell extravasation | T cell differentiation | Red | 0.000291 | 0.009437 |
| GO:0048025 | negative regulation of mRNA splicing, via spliceosome | regulation of RNA splicing | Turquoise | 0.000295 | 0.009458 |

***Appendix K. All under and over expressed pathways in >75% m.3243A>G CD8+ naive T cells from P23.*** *GSEA using reactome dataset, pathways with a FDR adjusted p value <0.05 shown*

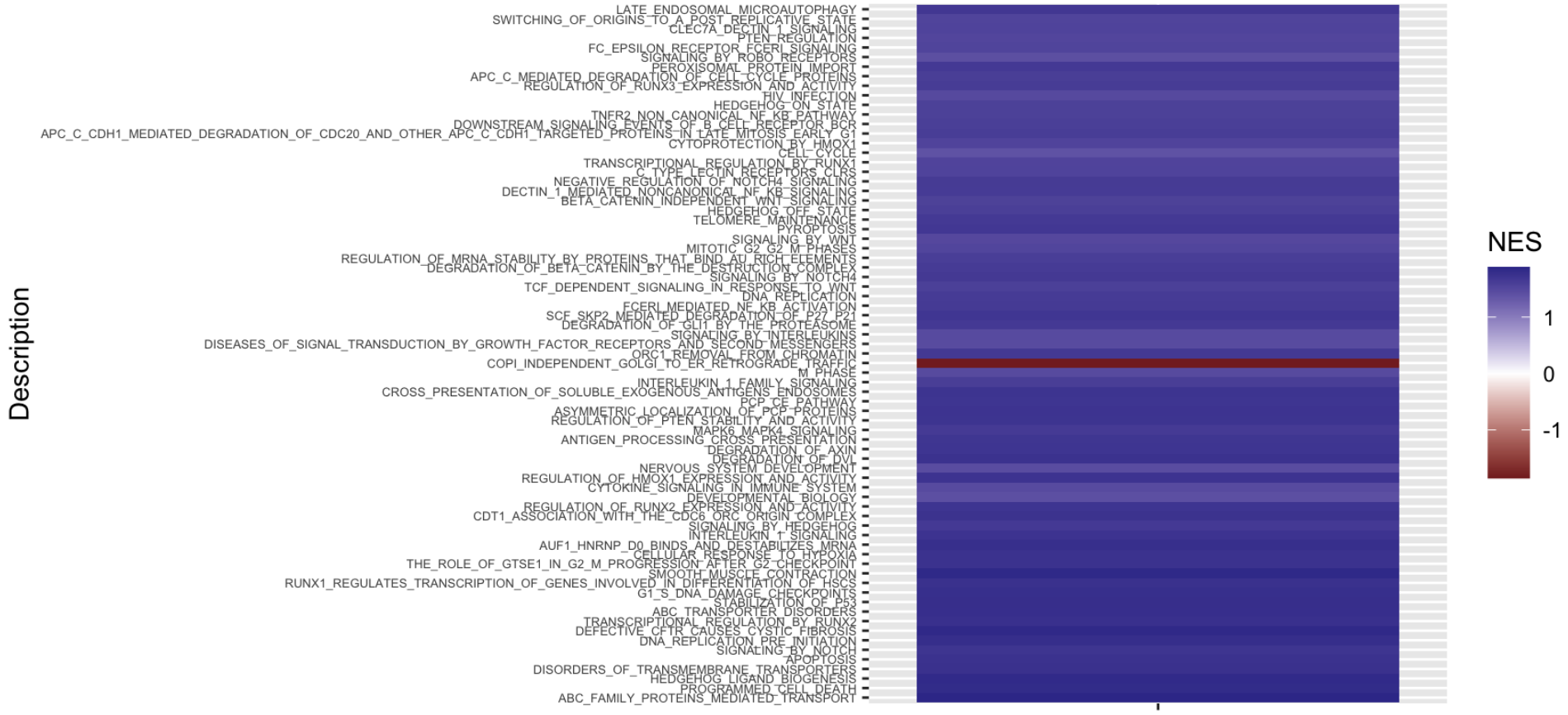

***Appendix L all over and under expressed pathways in P23 high m.3243A>G level memory T cells.*** *GSEA using reactome dataset, pathways with a FDR adjusted p value <0.05 shown*

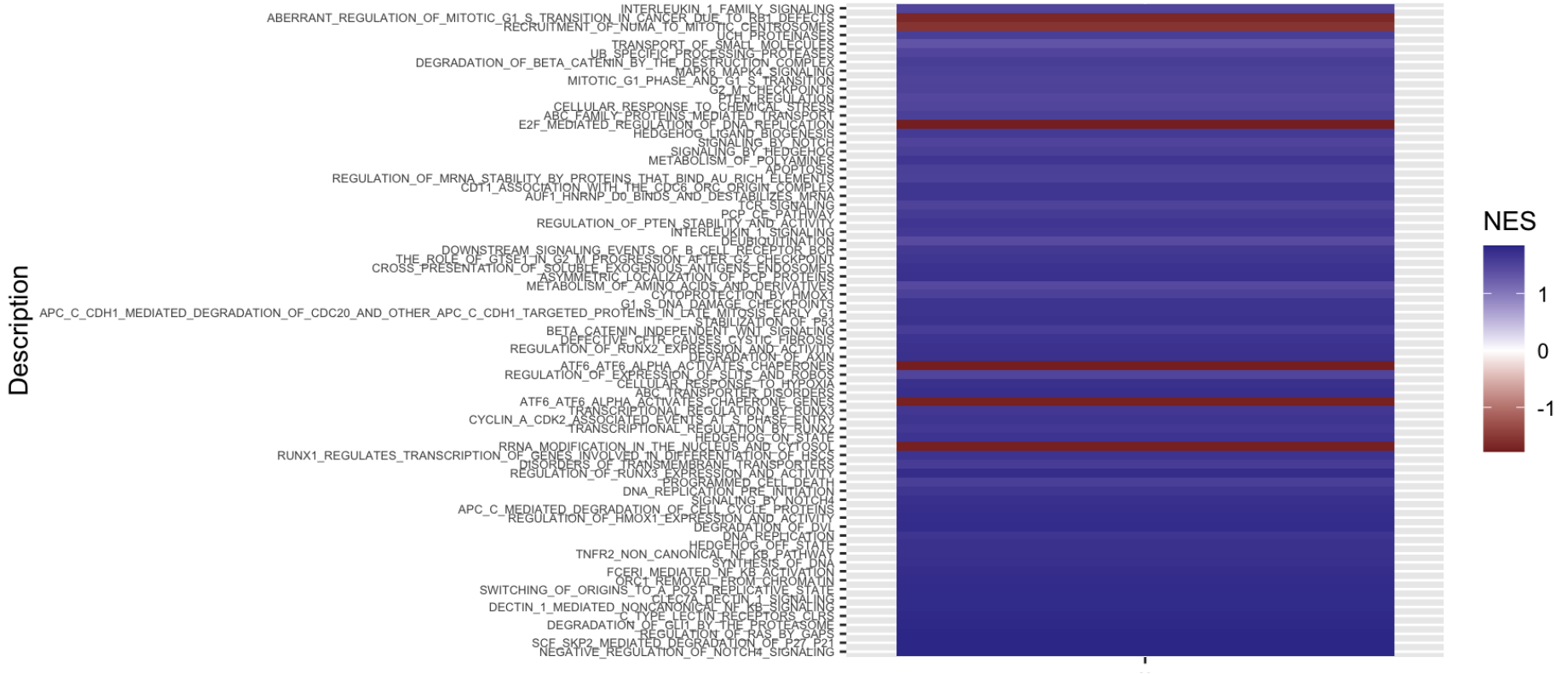

***Appendix M. All significant reactome pathways from GSEA which were common across high heteroplasmy naive and memory T cells***

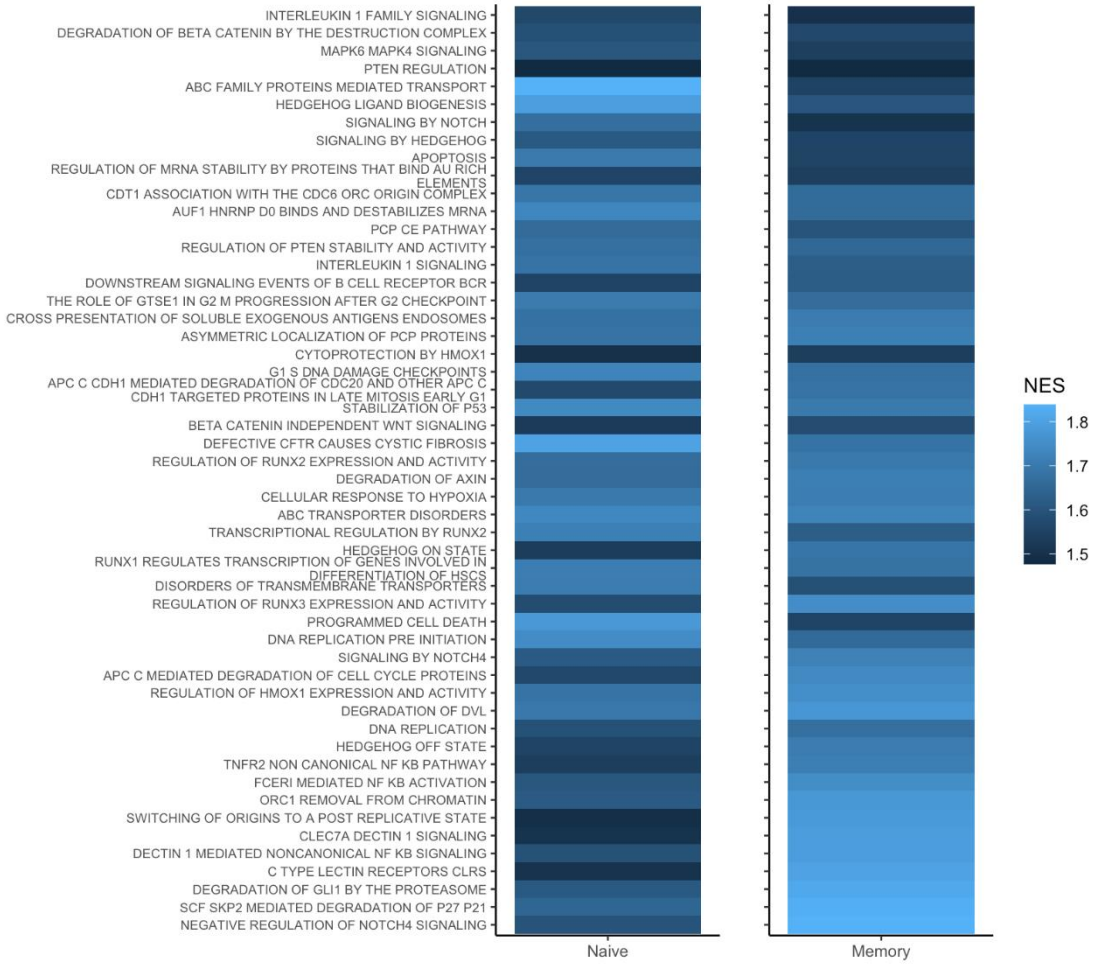

## Chapter 9 References


Abdelsamed, H. A., Moustaki, A., Fan, Y. P., Dogra, P., Ghoneim, H. E., Zebley, C. C., Triplett, B. M., Sekaly, R. P. & Youngblood, B. 2017. Human memory CD8 T cell effector potential is epigenetically preserved during in vivo homeostasis. *Journal of Experimental Medicine,* 214**,** 1593-1606.

Abrahams, J. P., Leslie, A. G. W., Lutter, R. & Walker, J. E. 1994. Structure at 2.8-Angstrom Resolution of F1-Atpase from Bovine Heart-Mitochondria. *Nature,* 370**,** 621-628.

AbuSamra, D. B., Aleisa, F. A., Al-Amoodi, A. S., Jalal Ahmed, H. M., Chin, C. J., Abuelela, A. F., Bergam, P., Sougrat, R. & Merzaban, J. S. 2017. Not just a marker: CD34 on human hematopoietic stem/progenitor cells dominates vascular selectin binding along with CD44. *Blood Advances,* 1.

Acín-Pérez, R., Bayona-Bafaluy, M. P., Fernández-Silva, P., Moreno-Loshuertos, R., Perez-Martos, A., Bruno, C., Moraes, C. T. & Enríquez, J. A. 2004. Respiratory complex III is required to maintain complex I in mammalian mitochondria. *Molecular Cell,* 13**,** 805-815.

Adams, W. C., Chen, Y. H., Kratchmarov, R., Yen, B., Nish, S. A., Lin, W. W., Rothman, N. J., Luchsinger, L. L., Klein, U., Busslinger, M., Rathmell, J. C., Snoeck, H. W. & Reiner, S. L. 2016. Anabolism-Associated Mitochondrial Stasis Driving Lymphocyte Differentiation over Self-Renewal. *Cell Rep,* 17**,** 3142-3152.

Ademokun, A., Wu, Y. C. & Dunn-Walters, D. 2010. The ageing B cell population: Composition and function. *Biogerontology,* 11**,** 125-137.

Akkaya, M., Traba, J., Roesler, A. S., Miozzo, P., Akkaya, B., Theall, B. P., Sohn, H., Pena, M., Smelkinson, M., Kabat, J., Dahlstrom, E., Dorward, D. W., Skinner, J., Sack, M. N. & Pierce, S. K. 2018. Second signals rescue B cells from activation-induced mitochondrial dysfunction and death. *Nature Immunology,* 19**,** 871-+.

Al-Dabbagh, S., McPhee, J. S., Murgatroyd, C., Butler-Browne, G., Stewart, C. E. & Al-Shanti, N. 2015. The lymphocyte secretome from young adults enhances skeletal muscle proliferation and migration, but effects are attenuated in the secretome of older adults. *Physiological Reports,* 3.

Al-Zubeidi, D., Thangarajh, M., Pathak, S., Cai, C., Schlaggar, B. L., Storch, G. A., Grange, D. K. & Watson, M. E. 2014. Fatal Human Herpesvirus 6–Associated Encephalitis in Two Boys With Underlying POLG Mitochondrial Disorders. *Pediatric Neurology,* 51.

Alosaimi, M. F., Shendi, H., Beano, A., Stafstrom, K., El Hawary, R., Meshaal, S., Galal, N., Pai, S. Y., El-Marsafy, A., Geha, R. S. & Chou, J. 2019. T-cell mitochondrial dysfunction and lymphopenia in DOCK2-deficient patients. *Journal of Allergy and Clinical Immunology,* 144**,** 306-+.

Amunts, A., Brown, A., Toots, J., Scheres, S. H. W. & Ramakrishnan, V. 2015. The structure of the human mitochondrial ribosome. *Science,* 348**,** 95-98.

Anderson, S., Bankier, A. T., Barrell, B. G., Debruijn, M. H. L., Coulson, A. R., Drouin, J., Eperon, I. C., Nierlich, D. P., Roe, B. A., Sanger, F., Schreier, P. H., Smith, A. J. H., Staden, R. & Young, I. G. 1981. Sequence and Organization of the Human Mitochondrial Genome. *Nature,* 290**,** 457-465.

Anderton, S., Burkhart, C., Metzler, B. & Wraith, D. 1999. Mechanisms of central and peripheral T-cell tolerance: lessons from experimental models of multiple sclerosis. *Immunol Rev,* 169**,** 123-37.

Andrews, N., Tessier, E., Stowe, J., Gower, C., Kirsebom, F., Simmons, R., Gallagher, E., Thelwall, S., Groves, N., Dabrera, G., Myers, R., Campbell, C. N. J., Amirthalingam, G., Edmunds, M., Zambon, M., Brown, K., Hopkins, S., Chand, M., Ladhani, S. N., Ramsay, M. & Lopez Bernal, J. 2022. Duration of Protection against Mild and Severe Disease by Covid-19 Vaccines. *N Engl J Med,* 386**,** 340-350.

Ansó, E., Weinberg, S. E., Diebold, L. P., Thompson, B. J., Malinge, S., Schumacker, Paul T., Liu, X., Zhang, Y., Shao, Z., Steadman, M., Marsh, K. M., Xu, J., Crispino, John D., Chandel, N. S., Ansó, E., Weinberg, S. E., Diebold, L. P., Thompson, B. J., Malinge, S., Schumacker, Paul T., Liu, X., Zhang, Y., Shao, Z., Steadman, M., Marsh, K. M., Xu, J., Crispino, John D. & Chandel, N. S. 2017. The mitochondrial respiratory chain is essential for haematopoietic stem cell function. *Nature Cell Biology,* 19.

Antolínez-Fernández, A., Esteban-Ramos, P., Fernández-Moreno, M. A. & Clemente, P. 2024. Molecular pathways in mitochondrial disorders due to a defective mitochondrial protein synthesis. *Frontiers in Cell and Developmental Biology,* 12.

Antonicka, H., Sasarman, F., Nishimura, T., Paupe, V. & Shoubridge, E. A. 2013. The Mitochondrial RNA-Binding Protein GRSF1 Localizes to RNA Granules and Is Required for Posttranscriptional Mitochondrial Gene Expression. *Cell Metabolism,* 17**,** 386-398.

Arbore, G., West, E. E., Spolski, R., Robertson, A. A. B., Klos, A., Rheinheimer, C., Dutow, P., Woodruff, T. M., Yu, Z. X., O'Neill, L. A., Coll, R. C., Sher, A., Leonard, W. J., Köhl, J., Monk, P., Cooper, M. A., Arno, M., Afzali, B., Lachmann, H. J., Cope, A. P., Mayer-Barber, K. D. & Kemper, C. 2016. T helper 1 immunity requires complement-driven NLRP3 inflammasome activity in CD4 T cells. *Science,* 352.

Arnberg, A., van Bruggen, E. F. & Borst, P. 1971. The presence of DNA molecules with a displacement loop in standard mitochondrial DNA preparations. *Biochim Biophys Acta,* 246**,** 353-7.

Ashburner, M., Ball, C. A., Blake, J. A., Botstein, D., Butler, H., Cherry, J. M., Davis, A. P., Dolinski, K., Dwight, S. S., Eppig, J. T., Harris, M. A., Hill, D. P., Issel-Tarver, L., Kasarskis, A., Lewis, S., Matese, J. C., Richardson, J. E., Ringwald, M., Rubin, G. M. & Sherlock, G. 2000. Gene ontology: tool for the unification of biology. The Gene Ontology Consortium. *Nat Genet,* 25**,** 25-9.

Ashley, M. V., Laipis, P. J. & Hauswirth, W. W. 1989. Rapid Segregation of Heteroplasmic Bovine Mitochondria. *Nucleic Acids Research,* 17**,** 7325-7331.

Asin-Cayuela, J., Schwend, T., Farge, G. & Gustafsson, C. M. 2005. The human mitochondrial transcription termination factor (mTERF) is fully active in vitro in the non-phosphorylated form. *J Biol Chem,* 280**,** 25499-505.

Athens, J. W., Haab, O. P., Raab, S. O., Mauer, A. M., Ashenbrucker, H., Cartwright, G. E. & Wintrobe, M. M. 1961. Leukokinetic studies. IV. The total blood, circulating and marginal granulocyte pools and the granulocyte turnover rate in normal subjects. *J Clin Invest,* 40**,** 989-95.

Badovinac, V. P., Tvinnereim, A. R. & Harty, J. T. 2000. Regulation of antigen-specific CD8+ T cell homeostasis by perforin and interferon-γ. *Science,* 290**,** 1354-1357.

Bailis, W., Shyer, J. A., Zhao, J., Canaveras, J. C. G., Al Khazal, F. J., Qu, R. H., Steach, H. R., Bielecki, P., Khan, O., Jackson, R., Kluger, Y., Maher, L. J., Rabinowitz, J., Craft, J. & Flavell, R. A. 2019. Distinct modes of mitochondrial metabolism uncouple T cell differentiation and function. *Nature,* 571**,** 403-+.

Bajwa, G., DeBerardinis, R. J., Shao, B., Hall, B., Farrar, J. D. & Gill, M. A. 2016. Cutting Edge: Critical Role of Glycolysis in Human Plasmacytoid Dendritic Cell Antiviral Responses. *Journal of Immunology,* 196**,** 2004-2009.

Banerjee, H., Das, A., Srivastava, S., Mattoo, H. R., Thyagarajan, K., Khalsa, J. K., Tanwar, S., Das, D. S., Majumdar, S. S., George, A., Bal, V., Durdik, J. M. & Rath, S. 2012. A role for apoptosis-inducing factor in T cell development. *Journal of Experimental Medicine,* 209**,** 1641-1653.

Bannwarth, S., Procaccio, V., Lebre, A. S., Jardel, C., Chaussenot, A., Hoarau, C., Maoulida, H., Charrier, N., Gai, X., Xie, H. M., Ferre, M., Fragaki, K., Hardy, G., Mousson de Camaret, B., Marlin, S., Dhaenens, C. M., Slama, A., Rocher, C., Bonnefont, J. P., Rötig, A., Aoutil, N., Gilleron, M., Desquiret-Dumas, V., Reynier, P., Ceresuela, J., Jonard, L., Devos, A., Espil-Taris, C., Martinez, D., Gaignard, P., Le Quan Sang, K., Amati-Bonneau, P., Falk, M. J., Florentz, C., Chabrol, B., Durand-Zaleski, I. & Paquis-Flucklinger, V. 2013. Prevalence of rare mitochondrial DNA mutations in mitochondrial disorders. *Journal of Medical Genetics,* 50.

Bar, N., Costa, F., Das, R., Duffy, A., Samur, M., McCachren, S., Gettinger, S. N., Neparidze, N., Parker, T. L., Bailur, J. K., Pendleton, K., Bajpai, R., Zhang, L., Xu, M. L., Anderson, T., Giuliani, N., Nooka, A., Cho, H. J., Raval, A., Shanmugam, M., Dhodapkar, K. M. & Dhodapkar, M. V. 2020. Differential effects of PD-L1 versus PD-1 blockade on myeloid inflammation in human cancer. *Jci Insight,* 5.

Barth, P. G., Scholte, H. R., Berden, J. A., Van der Klei-Van Moorsel, J. M., Luyt-Houwen, I. E., Van 't Veer-Korthof, E. T., Van der Harten, J. J. & Sobotka-Plojhar, M. A. 1983. An X-linked mitochondrial disease affecting cardiac muscle, skeletal muscle and neutrophil leucocytes. *J Neurol Sci,* 62**,** 327-55.

Battersby, B. J., Loredo-Osti, J. C. & Shoubridge, E. A. 2003. Nuclear genetic control of mitochondrial DNA segregation. *Nature Genetics,* 33**,** 183-186.

Ben-Sasson, S. Z., Hogg, A., Hu-Li, J., Wingfield, P., Chen, X., Crank, M., Caucheteux, S., Ratner-Hurevich, M., Berzofsky, J. A., Nir-Paz, R. & Paul, W. E. 2013. IL-1 enhances expansion, effector function, tissue localization, and memory response of antigen-specific CD8 T cells. *Journal of Experimental Medicine,* 210**,** 491-502.

Bentlage, H. A. & Attardi, G. 1996. Relationship of genotype to phenotype in fibroblast-derived transmitochondrial cell lines carrying the 3243 mutation associated with the MELAS encephalomyopathy: shift towards mutant genotype and role of mtDNA copy number. *Hum Mol Genet,* 5**,** 197-205.

Berk, A. J. & Clayton, D. A. 1974. Mechanism of mitochondrial DNA replication in mouse L-cells: asynchronous replication of strands, segregation of circular daughter molecules, aspects of topology and turnover of an initiation sequence. *J Mol Biol,* 86**,** 801-24.

Bezawork-Geleta, A., Rohlena, J., Dong, L. F., Pacak, K. & Neuzil, J. 2017. Mitochondrial Complex II: At the Crossroads. *Trends in Biochemical Sciences,* 42**,** 312-325.

Bhargava, K. & Spremulli, L. L. 2005. Role of the N- and C-terminal extensions on the activity of mammalian mitochondrial translational initiation factor 3. *Nucleic Acids Research,* 33.

Birky, C. W., Jr. 2001. The inheritance of genes in mitochondria and chloroplasts: laws, mechanisms, and models. *Annu Rev Genet,* 35**,** 125-48.

Blackburn, S. D., Shin, H., Haining, W. N., Zou, T., Workman, C. J., Polley, A., Betts, M. R., Freeman, G. J., Vignali, D. A. A. & Wherry, E. J. 2009. Coregulation of CD8+

T cell exhaustion by multiple inhibitory receptors during chronic viral infection. *Nature Immunology,* 10**,** 29-37.

Blakely, E. L., Mitchell, A. L., Fisher, N., Meunier, B., Nijtmans, L. G., Schaefer, A. M., Jackson, M. J., Turnbull, D. M. & Taylor, R. W. 2005. A mitochondrial cytochrome b mutation causing severe respiratory chain enzyme deficiency in humans and yeast. *The FEBS Journal,* 272.

Blum, T. B., Hahn, A., Meier, T., Davies, K. M. & Kühlbrandt, W. 2019. Dimers of mitochondrial ATP synthase induce membrane curvature and self-assemble into rows. *Proceedings of the National Academy of Sciences of the United States of America,* 116**,** 4250-4255.

Boengler, K., Heusch, G. & Schulz, R. 2011. Nuclear-encoded mitochondrial proteins and their role in cardioprotection. *Biochimica Et Biophysica Acta-Molecular Cell Research,* 1813**,** 1286-1294.

Bogenhagen, D. & Clayton, D. A. 1977. Mouse L-Cell Mitochondrial-DNA Molecules Are Selected Randomly for Replication Throughout Cell-Cycle. *Cell,* 11**,** 719-727.

Bogenhagen, D. F., Rousseau, D. & Burke, S. 2008. The layered structure of human mitochondrial DNA nucleoids. *Journal of Biological Chemistry,* 283**,** 3665-3675.

Borsa, M., Barnstorf, I., Baumann, N. S., Pallmer, K., Yermanos, A., Grabnitz, F., Barandun, N., Hausmann, A., Sandu, I., Barral, Y. & Oxenius, A. 2019. Modulation of asymmetric cell division as a mechanism to boost CD8(+) T cell memory. *Sci Immunol,* 4.

Borsa, M., Lechuga-Vieco, A. V., Kayvanjoo, A. H., Yazicioglu, Y., Compeer, E. B., Richter, F. C., Bui, H., Dustin, M. L., Katajisto, P. & Simon, A. K. 2024. Inheritance of old mitochondria controls early CD8+ T cell fate commitment and is regulated by autophagy. *bioRxiv*.

Boulet, L., Karpati, G. & Shoubridge, E. A. 1992. Distribution and Threshold Expression of the Trans Rnalys Mutation in Skeletal-Muscle of Patients with Myoclonic Epilepsy and Ragged-Red Fibers (Merrf). *American Journal of Human Genetics,* 51**,** 1187-1200.

Bousso, P., Bhakta, N. R., Lewis, R. S. & Robey, E. 2002. Dynamics of thymocyte-stromal cell interactions visualized by two-photon microscopy. *Science,* 296**,** 1876-1880.

Broomfield, A., Sweeney, M. G., Woodward, C. E., Fratter, C., Morris, A. M., Leonard, J. V., Abulhoul, L., Grunewald, S., Clayton, P. T., Hanna, M. G., Poulton, J. & Rahman, S. 2015. Paediatric single mitochondrial DNA deletion disorders: an overlapping spectrum of disease. *J Inherit Metab Dis,* 38**,** 445-57.

Broxmeyer, H. E., Douglas, G. W., Hangoc, G., Cooper, S., Bard, J., English, D., Arny, M., Thomas, L. & Boyse, E. A. 1989. Human Umbilical-Cord Blood as a Potential Source of Transplantable Hematopoietic Stem Progenitor Cells. *Proceedings of the National Academy of Sciences of the United States of America,* 86**,** 3828-3832.

Bruchard, M., Rebé, C., Derangère, V., Togbé, D., Ryffel, B., Boidot, R., Humblin, E., Hamman, A., Chalmin, F., Berger, H., Chevriaux, A., Limagne, E., Apetoh, L., Végran, F. & Ghiringhelli, F. 2015. The receptor NLRP3 is a transcriptional regulator of Th2 differentiation. *Nature Immunology,* 16**,** 859-+.

Brum, M., Semedo, C., Guerreiro, R. & Marques, J. P. 2014. Motor Neuron Syndrome as a New Phenotypic Manifestation of Mutation 9185T>C in Gene MTATP6. *Case Reports in Neurological Medicine,* 2014.

Brzezniak, L. K., Bijata, M., Szczesny, R. J. & Stepien, P. P. 2011. Involvement of human ELAC2 gene product in 3' end processing of mitochondrial tRNAs. *RNA Biol,* 8**,** 616-26.

Buck, M. D., O'Sullivan, D., Klein Geltink, R. I., Curtis, J. D., Chang, C. H., Sanin, D. E., Qiu, J., Kretz, O., Braas, D., van der Windt, G. J., Chen, Q., Huang, S. C., O'Neill, C. M., Edelson, B. T., Pearce, E. J., Sesaki, H., Huber, T. B., Rambold, A. S. & Pearce, E. L. 2016. Mitochondrial Dynamics Controls T Cell Fate through Metabolic Programming. *Cell,* 166**,** 63-76.

Buenrostro, J. D., Giresi, P. G., Zaba, L. C., Chang, H. Y. & Greenleaf, W. J. 2013. Transposition of native chromatin for fast and sensitive epigenomic profiling of open chromatin, DNA-binding proteins and nucleosome position. *Nature Methods,* 10**,** 1213-+.

Burkewitz, K., Feng, G. M., Dutta, S., Kelley, C. A., Steinbaugh, M., Cram, E. J. & Mair, W. B. 2020. Regulates Lifespan through ER-Mitochondrial Calcium Homeostasis. *Cell Reports,* 32.

Bykhovskaya, Y., Casas, K., Mengesha, E., Inbal, A. & Fischel-Ghodsian, N. 2004. Missense mutation in pseudouridine synthase 1 (

) causes mitochondrial myopathy and sideroblastic anemia (MLASA). *American Journal of Human Genetics,* 74**,** 1303-1308.

Cai, Y. C., Bullard, J. M., Thompson, N. L. & Spremulli, L. L. 2000. Interaction of mitochondrial elongation factor Tu with aminoacyl-tRNA and elongation factor Ts - PubMed. *The Journal of biological chemistry,* 275.

Calabro, A., Accardi, G., Aiello, A., Caruso, C. & Candore, G. 2023. Sex and gender affect immune aging. *Front Aging,* 4**,** 1272118.

Cao, Y., Rathmell, J. C. & Macintyre, A. N. 2014. Metabolic Reprogramming towards Aerobic Glycolysis Correlates with Greater Proliferative Ability and Resistance to Metabolic Inhibition in CD8 versus CD4 T Cells. *Plos One,* 9.

Cao, Y. H., Li, H., Liu, H. F., Zheng, C., Ji, H. B. & Liu, X. L. 2010. The serine/threonine kinase LKB1 controls thymocyte survival through regulation of AMPK activation and Bcl-XL expression. *Cell Research,* 20**,** 99-108.

Cao, Y. L., Meng, S. X., Chen, Y., Feng, J. X., Gu, D. D., Yu, B., Li, Y. J., Yang, J. Y., Liao, S., Chan, D. C. & Gao, S. 2017. MFN1 structures reveal nucleotide-triggered dimerization critical for mitochondrial fusion. *Nature,* 542**,** 372-+.

Cardaioli, E., Fabrizi, G. M., Grieco, G. S., Dotti, M. T. & Federico, A. 2000. Heteroplasmy of the A3243G transition of mitochondrial tRNA(Leu(UUR)) in a MELAS case and in a 25-week-old miscarried fetus. *J Neurol,* 247**,** 885-7.

Carroll, J., Fearnley, I. M., Skehel, J. M., Shannon, R. J., Hirst, J. & Walker, J. E. 2006. Bovine complex I is a complex of 45 different subunits. *Journal of Biological Chemistry,* 281**,** 32724-32727.

Cassel, S. L. & Sutterwala, F. S. 2010. Sterile inflammatory responses mediated by the NLRP3 inflammasome. *European Journal of Immunology,* 40**,** 607-611.

Castagna, A. E., Addis, J., McInnes, R. R., Clarke, J. T. R., Ashby, P., Blaser, S. & Robinson, B. H. 2007. Late onset Leigh syndrome and ataxia due to a T to C mutation at bp 9,185 of mitochondrial DNA. *American journal of medical genetics. Part A,* 143A.

Chang, D. D. & Clayton, D. A. 1984. Precise Identification of Individual Promoters for Transcription of Each Strand of Human Mitochondrial-DNA. *Cell,* 36**,** 635-643.

Chang, J. T., Palanivel, V. R., Kinjyo, I., Schambach, F., Intlekofer, A. M., Banerjee, A., Longworth, S. A., Vinup, K. E., Mrass, P., Oliaro, J., Killeen, N., Orange, J. S., Russell, S. M., Weninger, W. & Reiner, S. L. 2007. Asymmetric T lymphocyte division in the initiation of adaptive immune responses. *Science,* 315**,** 1687-91.

Chapman, N. M., Boothby, M. R. & Chi, H. B. 2020. Metabolic coordination of T cell quiescence and activation. *Nature Reviews Immunology,* 20**,** 55-70.
Chen, J. G., Del Valle, L., Lin, H. Y., Plaisance-Bonstaff, K., Forrest, J. C., Post, S. R. & Qin, Z. Q. 2019. Expression of PD-1 and PD-Ls in Kaposi's sarcoma and regulation by oncogenic herpesvirus lytic reactivation. *Virology,* 536**,** 16-19.
Chen, M. L., Logan, T. D., Hochberg, M. L., Shelat, S. G., Yu, X., Wilding, G. E., Tan, W., Kujoth, G. C., Prolla, T. A., Selak, M. A., Kundu, M., Carroll, M. & Thompson, J. E. 2009. Erythroid dysplasia, megaloblastic anemia, and impaired lymphopoiesis arising from mitochondrial dysfunction. *Blood,* 114**,** 4045-53.
Chen, X., Iliopoulos, D., Zhang, Q., Tang, Q. Z., Greenblatt, M. B., Hatziapostolou, M., Lim, E., Tam, W. L., Ni, M., Chen, Y. W., Mai, J. H., Shen, H. F., Hu, D. Z., Adoro, S., Hu, B., Song, M. Y., Tan, C., Landis, M. D., Ferrari, M., Shin, S. J., Brown, M., Chang, J. C., Liu, X. S. & Glimcher, L. H. 2014. XBP1 promotes triple-negative breast cancer by controlling the HIF1α pathway. *Nature,* 508**,** 103-+.
Chen, X., Prosser, R., Simonetti, S., Sadlock, J., Jagiello, G. & Schon, E. A. 1995. Rearranged mitochondrial genomes are present in human oocytes. *Am J Hum Genet,* 57**,** 239-47.
Chen, Y. & Dorn II, G. W. 2013. PINK1-Phosphorylated Mitofusin 2 Is a Parkin Receptor for Culling Damaged Mitochondria. *Science,* 340.
Chesnut, R. W. & Grey, H. M. 1981. Studies on the Capacity of B-Cells to Serve as Antigen-Presenting Cells. *Journal of Immunology,* 126**,** 1075-1079.
Chiang, J. L., Shukla, P., Pagidas, K., Ahmed, N. S., Karri, S., Gunn, D. D., Hurd, W. W. & Singh, K. K. 2020. Mitochondria in Ovarian Aging and Reproductive Longevity. *Ageing Res Rev,* 63**,** 101168.
Childs, A. M., Hutchin, T., Pysden, K., Highet, L., Bamford, J., Livingston, J. & Crow, Y. J. 2007. Variable Phenotype Including Leigh Syndrome with a 9185T>C Mutation in the MTATP6 Gene. *Neuropediatrics,* 38.
Chinnery, P. F., DiMauro, S., Shanske, S., Schon, E. A., Zeviani, M., Mariotti, C., Carrara, F., Lombes, A., Laforet, P., Ogier, H., Jaksch, M., Lochmüller, H., Horvath, R., Deschauer, M., Thorburn, D. R., Bindoff, L. A., Poulton, J., Taylor, R. W., Matthews, J. N. S. & Turnbull, D. M. 2004. Risk of developing a mitochondrial DNA deletion disorder. *Lancet,* 364**,** 592-596.
Chinnery, P. F. & Samuels, D. C. 1999. Relaxed replication of mtDNA: A model with implications for the expression of disease. *American Journal of Human Genetics,* 64**,** 1158-1165.
Choi, Y. S., Kim, S. & Pak, Y. K. 2001. Mitochondrial transcription factor A (mtTFA) and diabetes. *Diabetes Research and Clinical Practice,* 54**,** S3-S9.
Chomyn, A., Enriquez, J. A., Micol, V., Fernandez-Silva, P. & Attardi, G. 2000. The mitochondrial myopathy, encephalopathy, lactic acidosis, and stroke-like episode syndrome-associated human mitochondrial tRNALeu(UUR) mutation causes aminoacylation deficiency and concomitant reduced association of mRNA with ribosomes. *J Biol Chem,* 275**,** 19198-209.
Chomyn, A., Martinuzzi, A., Yoneda, M., Daga, A., Hurko, O., Johns, D., Lai, S. T., Nonaka, I., Angelini, C. & Attardi, G. 1992. Melas Mutation in Mtdna Binding-Site for Transcription Termination Factor Causes Defects in Protein-Synthesis and in Respiration but No Change in Levels of Upstream and Downstream Mature Transcripts. *Proceedings of the National Academy of Sciences of the United States of America,* 89**,** 4221-4225.

Chopp, L., Redmond, C., O'Shea, J. J. & Schwartz, D. M. 2023. From thymus to tissues and tumors: A review of T-cell biology. *Journal of Allergy and Clinical Immunology,* 151**,** 81-97.

Chung, C. Y., Singh, K., Kotiadis, V. N., Valdebenito, G. E., Ahn, J. H., Topley, E., Tan, J., Andrews, W. D., Bilanges, B., Pitceathly, R. D. S., Szabadkai, G., Yuneva, M. & Duchen, M. R. 2021. Constitutive activation of the PI3K-Akt-mTORC1 pathway sustains the m.3243 A > G mtDNA mutation. *Nat Commun,* 12**,** 6409.

Ciocca, M. L., Barnett, B. E., Burkhardt, J. K., Chang, J. T. & Reiner, S. L. 2012. Cutting edge: Asymmetric memory T cell division in response to rechallenge. *J Immunol,* 188**,** 4145-8.

Clark, K. A., Howe, D. K., Gafner, K., Kusuma, D., Ping, S., Estes, S. & Denver, D. R. 2012. Selfish Little Circles: Transmission Bias and Evolution of Large Deletion-Bearing Mitochondrial DNA in

Nematodes. *Plos One,* 7.

Coon, J. J., Ueberheide, B., Syka, J. E., Dryhurst, D. D., Ausio, J., Shabanowitz, J. & Hunt, D. F. 2005. Protein identification using sequential ion/ion reactions and tandem mass spectrometry. *Proc Natl Acad Sci U S A,* 102**,** 9463-8.

Corrado, M. & Pearce, E. L. 2022. Targeting memory T cell metabolism to improve immunity. *Journal of Clinical Investigation,* 132.

Corrado, M., Samardzic, D., Giacomello, M., Rana, N., Pearce, E. L. & Scorrano, L. 2021. Deletion of the mitochondria-shaping protein during early thymocyte maturation impacts mature memory T cell metabolism. *Cell Death and Differentiation,* 28**,** 2194-2206.

Cree, L. M., Samuels, D. C., Lopes, S. C. D. S., Rajasimha, H. K., Wonnapinij, P., Mann, J. R., Dahl, H. H. M. & Chinnery, P. F. 2008. A reduction of mitochondrial DNA molecules during embryogenesis explains the rapid segregation of genotypes. *Nature Genetics,* 40**,** 249-254.

Cros, J., Cagnard, N., Woollard, K., Patey, N., Zhang, S. Y., Senechal, B., Puel, A., Biswas, S. K., Moshous, D., Picard, C., Jais, J. P., D'Cruz, D., Casanova, J. L., Trouillet, C. & Geissmann, F. 2010. Human CD14dim Monocytes Patrol and Sense Nucleic Acids and Viruses via TLR7 and TLR8 Receptors. *Immunity,* 33**,** 375-386.

Czabotar, P. E., Westphal, D., Dewson, G., Ma, S., Hockings, C., Fairlie, W. D., Lee, E. F., Yao, S. G., Robin, A. Y., Smith, B. J., Huang, D. C. S., Kluck, R. M., Adams, J. M. & Colman, P. M. 2013. Bax Crystal Structures Reveal How BH3 Domains Activate Bax and Nucleate Its Oligomerization to Induce Apoptosis. *Cell,* 152**,** 519-531.

D'Erchia, A. M., Atlante, A., Gadaleta, G., Pavesi, G., Chiara, M., De Virgilio, C., Manzari, C., Mastropasqua, F., Prazzoli, G. M., Picardi, E., Gissi, C., Horner, D., Reyes, A., Sbisa, E., Tullo, A. & Pesole, G. 2015. Tissue-specific mtDNA abundance from exome data and its correlation with mitochondrial transcription, mass and respiratory activity. *Mitochondrion,* 20**,** 13-21.

Dadamio, L., Awad, K. M. & Reinherz, E. L. 1993. Thymic and Peripheral Apoptosis of Antigen-Specific T-Cells Might Cooperate in Establishing Self Tolerance. *European Journal of Immunology,* 23**,** 747-753.

Danielson, S. R., Carelli, V., Tan, G., Martinuzzi, A., Schapira, A. H., Savontaus, M. L. & Cortopassi, G. A. 2005. Isolation of transcriptomal changes attributable to LHON mutations and the cybridization process. *Brain,* 128**,** 1026-37.

de Carvalho, C. C. C. R. & Caramujo, M. J. 2018. The Various Roles of Fatty Acids. *Molecules,* 23.

de Laat, P., Janssen, M. C., Alston, C. L., Taylor, R. W., Rodenburg, R. J. & Smeitink, J. A. 2016. Three families with 'de novo' m.3243A > G mutation. *BBA Clin,* 6**,** 19-24.

de Laat, P., Koene, S., Heuvel, L. P., Rodenburg, R. J., Janssen, M. C. & Smeitink, J. A. 2013. Inheritance of the m.3243A>G mutation. *JIMD Rep,* 8**,** 47-50.

de Laat, P., Koene, S., van den Heuvel, L. P., Rodenburg, R. J., Janssen, M. C. & Smeitink, J. A. 2012. Clinical features and heteroplasmy in blood, urine and saliva in 34 Dutch families carrying the m.3243A > G mutation. *J Inherit Metab Dis,* 35**,** 1059-69.

Delettre, C., Griffoin, J. M., Kaplan, J., Dollfus, H., Lorenz, B., Faivre, L., Lenaers, G., Belenguer, P. & Hamel, C. P. 2001. Mutation spectrum and splicing variants in the OPA1 gene. *Human Genetics,* 109**,** 584-591.

Devenish, R. J., Prescott, M. & Rodgers, A. J. W. 2008. The structure and function of mitochondrial F1F0-ATP synthases. *International Review of Cell and Molecular Biology, Vol 267,* 267**,** 1-+.

DeWitt, W. S., Emerson, R. O., Lindau, P., Vignali, M., Snyder, T. M., Desmarais, C., Sanders, C., Utsugi, H., Warren, E. H., McElrath, J., Makar, K. W., Wald, A. & Robins, H. S. 2015. Dynamics of the Cytotoxic T Cell Response to a Model of Acute Viral Infection. *Journal of Virology,* 89**,** 4517-4526.

Dewson, G., Kratina, T., Czabotar, P., Day, C. L., Adams, J. M. & Kluck, R. M. 2009. Bak Activation for Apoptosis Involves Oligomerization of Dimers via Their α6 Helices. *Molecular Cell,* 36**,** 696-703.

Dewson, G., Kratina, T., Sim, H. W., Puthalakath, H., Adams, J. M., Colman, P. M. & Kluck, R. M. 2008. To trigger apoptosis, Bak exposes its BH3 domain and homodimerizes via BH3: Groove interactions. *Molecular Cell,* 30**,** 369-380.

Dhir, A., Dhir, S., Borowski, L. S., Jimenez, L., Teitell, M., Rötig, A., Crow, Y. J., Rice, G. I., Duffy, D., Tamby, C., Nojima, T., Munnich, A., Schiff, M., de Almeida, C. R., Rehwinkel, J., Dziembowski, A., Szczesny, R. J. & Proudfoot, N. J. 2018. Mitochondrial double-stranded RNA triggers antiviral signalling in humans. *Nature,* 560**,** 238-+.

Diaz, F., Bayona-Bafaluy, M. P., Rana, M., Mora, M., Hao, H. & Moraes, C. T. 2002a. Human mitochondrial DNA with large deletions repopulates organelles faster than full-length genomes under relaxed copy number control. *Nucleic Acids Research,* 30**,** 4626-4633.

Diaz, F., Bayona-Bafaluy, M. P., Rana, M., Mora, M., Hao, H. & Moraes, C. T. 2002b. Human mitochondrial DNA with large deletions repopulates organelles faster than full-length genomes under relaxed copy number control. *Nucleic Acids Research,* 30.

Diaz, F., Fukui, H., Garcia, S. & Moraes, C. T. 2006. Cytochrome c oxidase is required for the assembly/stability of respiratory complex I in mouse fibroblasts. *Molecular and Cellular Biology,* 26**,** 4872-4881.

Dolgalev, I. 2022. msigdbr: MSigDB Gene Sets for Multiple Organisms in a Tidy Data Format.

Dombi, E., Diot, A., Morten, K., Carver, J., Lodge, T., Fratter, C., Shiau Ng, Y., Liao, C., Muir, R., Blakely, E. L., Hargreaves, I., Al-Dosary, M., Sarkar, G., Hickman, S. J., Downes, S. M., Jayawant, S., Yu-Wai-Man, P., Taylor, R. W. & Poulton, J. 2016. The m.13051G>A mitochondrial DNA mutation results in variable neurology and activated mitophagy. *Neurology,* 86.

Dumke, B. R. & Lees, S. J. 2011. Age-related impairment of T cell-induced skeletal muscle precursor cell function. *American Journal of Physiology-Cell Physiology,* 300**,** C1226-C1233.

Durek, P., Nordstroem, K., Gasparoni, G., Salhab, A., Kressler, C., De Almeida, M., Bassler, K., Ulas, T., Schmidt, F., Xiong, J., Glazar, P., Klironomos, F., Sinha, A., Kinkley, S., Yang, X., Arrigoni, L., Amirabad, A. D., Ardakani, F. B., Feuerbach, L., Gorka, O., Ebert, P., Mueller, F., Li, N., Frischbutter, S., Schlickeiser, S., Cendon, C., Froehler, S., Felder, B., Gasparoni, N., Imbusch, C. D., Hutter, B., Zipprich, G., Tauchmann, Y., Reinke, S., Wassilew, G., Hoffmann, U., Richter, A. S., Sieverling, L., Chang, H. D., Syrbe, U., Kalus, U., Eils, J., Brors, B., Manke, T., Ruland, J., Lengauer, T., Rajewsky, N., Chen, W., Dong, J., Sawitzki, B., Chung, H. R., Rosenstiel, P., Schulz, M. H., Schultze, J. L., Radbruch, A., Walter, J., Hamann, A., Polansky, J. K. & Consortium, D. 2016. Epigenomic Profiling of Human CD4 T Cells Supports a Linear Differentiation Model and Highlights Molecular Regulators of Memory Development. *Immunity,* 45**,** 1148-1161.

Durinck, S., Moreau, Y., Kasprzyk, A., Davis, S., De Moor, B., Brazma, A. & Huber, W. 2005. BioMart and Bioconductor: a powerful link between biological databases and microarray data analysis. *Bioinformatics,* 21**,** 3439-40.

Ecker, C., Guo, L. L., Voicu, S., Gil-de-Gómez, L., Medvec, A., Cortina, L., Pajda, J., Andolina, M., Torres-Castillo, M., Donato, J. L., Mansour, S., Zynda, E. R., Lin, P. Y., Varela-Rohena, A., Blair, I. A. & Riley, J. L. 2018. Differential Reliance on Lipid Metabolism as a Salvage Pathway Underlies Functional Differences of T Cell Subsets in Poor Nutrient Environments. *Cell Reports,* 23**,** 741-755.

Elliott, H. R., Samuels, D. C., Eden, J. A., Relton, C. L. & Chinnery, P. F. 2008. Pathogenic mitochondrial DNA mutations are common in the general population. *American Journal of Human Genetics,* 83**,** 254-260.

Elson, J. L., Samuels, D. C., Turnbull, D. M. & Chinnery, P. F. 2001. Random intracellular drift explains the clonal expansion of mitochondrial DNA mutations with age. *Am J Hum Genet,* 68**,** 802-6.

ElTanbouly, M. A. & Noelle, R. J. 2021. Rethinking peripheral T cell tolerance: checkpoints across a T cell's journey. *Nature Reviews Immunology,* 21**,** 257-267.

Estaquier, J. & Arnoult, D. 2007. Inhibiting Drp1-mediated mitochondrial fission selectively prevents the release of cytochrome *c* during apoptosis. *Cell Death and Differentiation,* 14**,** 1086-1094.

Fagnoni, F. F., Vescovini, R., Passeri, G., Bologna, G., Pedrazzoni, M., Lavagetto, G., Casti, A., Franceschi, C., Passeri, M. & Sansoni, P. 2000. Shortage of circulating naive CD8+ T cells provides new insights on immunodeficiency in aging. *Blood,* 95**,** 2860-2868.

Falkenberg, M. 2018. Mitochondrial DNA replication in mammalian cells: overview of the pathway. *Mitochondrial Diseases,* 62**,** 287-296.

Falkenberg, M., Gaspari, M., Rantanen, A., Trifunovic, A., Larsson, N. G. & Gustafsson, C. M. 2002. Mitochondrial transcription factors B1 and B2 activate transcription of human mtDNA. *Nature Genetics,* 31**,** 289-294.

Farahi, N., Singh, N. R., Heard, S., Loutsios, C., Summers, C., Solanki, C. K., Solanki, K., Balan, K. K., Ruparelia, P., Peters, A. M., Condliffe, A. M. & Chilvers, E. R. 2012. Use of 111-Indium-labeled autologous eosinophils to establish the in vivo kinetics of human eosinophils in healthy subjects. *Blood,* 120**,** 4068-4071.

Farruggia, P., Di Cataldo, A., Pinto, R. M., Palmisani, E., Macaluso, A., Valvo, L. L., Cantarini, M. E., Tornesello, A., Corti, P., Fioredda, F., Varotto, S., Martire, B., Moroni, I., Puccio, G., Russo, G., Dufour, C. & Pillon, M. 2016. Pearson

Syndrome: A Retrospective Cohort Study from the Marrow Failure Study Group of A.I.E.O.P. (Associazione Italiana Emato-Oncologia Pediatrica). *JIMD Rep,* 26**,** 37-43.
Faxén, K., Gilderson, G., Adelroth, P. & Brzezinski, P. 2005. A mechanistic principle for proton pumping by cytochrome *c* oxidase. *Nature,* 437**,** 286-289.
Fernandez-Vizarra, E. & Zeviani, M. 2018. Mitochondrial complex III Rieske Fe-S protein processing and assembly. *Cell Cycle,* 17**,** 681-687.
Fields, P. E., Gajewski, T. F. & Fitch, F. W. 1996. Blocked ras activation in anergic CD4(+) T cells. *Science,* 271**,** 1276-1278.
Filograna, R., Koolmeister, C., Upadhyay, M., Pajak, A., Clemente, P., Wibom, R., Simard, M. L., Wredenberg, A., Freyer, C., Stewart, J. B. & Larsson, N. G. 2019. Modulation of mtDNA copy number ameliorates the pathological consequences of a heteroplasmic mtDNA mutation in the mouse. *Science Advances,* 5.
Flescher, E., Ledbetter, J. A., Schieven, G. L., Velaroch, N., Fossum, D., Dang, H., Ogawa, N. & Talal, N. 1994. Longitudinal Exposure of Human T-Lymphocytes to Weak Oxidative Stress Suppresses Transmembrane and Nuclear Signal-Transduction. *Journal of Immunology,* 153**,** 4880-4889.
Flierl, A., Reichmann, H. & Seibel, P. 1997. Pathophysiology of the MELAS 3243 transition mutation. *J Biol Chem,* 272**,** 27189-96.
Floros, V. I., Pyle, A., Dietmann, S., Wei, W., Tang, W. C. W., Irie, N., Payne, B., Capalbo, A., Noli, L., Coxhead, J., Hudson, G., Crosier, M., Strahl, H., Khalaf, Y., Saitou, M., Ilic, D., Surani, M. A. & Chinnery, P. F. 2018. Segregation of mitochondrial DNA heteroplasmy through a developmental genetic bottleneck in human embryos. *Nature cell biology,* 20.
Folmes, C. D. L., Martinez-Fernandez, A., Perales-Clemente, E., Li, X., Mcdonald, A., Oglesbee, D., Hrstka, S. C., Perez-Terzic, C., Terzic, A. & Nelson, T. J. 2013. Disease-Causing Mitochondrial Heteroplasmy Segregated Within Induced Pluripotent Stem Cell Clones Derived from a Patient with MELAS. *Stem Cells,* 31**,** 1298-1308.
Ford, C. E., Hamerton, J. L., Barnes, D. W. H. & Loutit, J. F. 1956. Cytological Identification of Radiation-Chimæras. *Nature,* 177.
Fox, C. J., Hammerman, P. S. & Thompson, C. B. 2005. Fuel feeds function: Energy metabolism and the T-cell response. *Nature Reviews Immunology,* 5**,** 844-852.
Franco, M., Pickett, S. J., Fleischmann, Z., Khrapko, M., Cote-L'Heureux, A., Aidlen, D., Stein, D., Markuzon, N., Popadin, K., Braverman, M., Woods, D. C., Tilly, J. L., Turnbull, D. M. & Khrapko, K. 2022. Dynamics of the most common pathogenic mtDNA variant m.3243A > G demonstrate frequency-dependency in blood and positive selection in the germline. *Human Molecular Genetics,* 31**,** 4075-4086.
Franklin, I. G., Milne, P., Childs, J., Boggan, R. M., Barrow, I., Lawless, C., Gorman, G. S., Ng, Y. S., Collin, M., Russell, O. M. & Pickett, S. J. 2023. T cell differentiation drives the negative selection of pathogenic mitochondrial DNA variants. *Life Science Alliance,* 6.
Frederiksen, A. L., Andersen, P. H., Kyvik, K. O., Jeppesen, T. D., Vissing, J. & Schwartz, M. 2006. Tissue specific distribution of the 3243A->G mtDNA mutation. *J Med Genet,* 43**,** 671-7.
Freeman, M. L., Oyebanji, O. A., Moisi, D., Payne, M., Sheehan, M. L., Balazs, A. B., Bosch, J., King, C. L., Gravenstein, S., Lederman, M. M. & Canaday, D. H. 2023. Association of Cytomegalovirus Serostatus With Severe Acute Respiratory Syndrome Coronavirus 2 Vaccine Responsiveness in Nursing Home Residents and Healthcare Workers. *Open Forum Infectious Diseases,* 10.

Friedman, J. R., Lackner, L. L., West, M., DiBenedetto, J. R., Nunnari, J. & Voeltz, G. K. 2011. ER Tubules Mark Sites of Mitochondrial Division. *Science,* 334**,** 358-362.

Fu, J., Ma, M., Pang, M., Yang, L., Li, G., Song, J. & Zhang, J. 2019. Broadening the phenotype of m.5703G>A mutation in mitochondrial tRNAAsn gene from mitochondrial myopathy to myoclonic epilepsy with ragged red fibers syndrome. *Chinese Medical Journal,* 132.

Fukuoh, A., Cannino, G., Gerards, M., Buckley, S., Kazancioglu, S., Scialo, F., Lihavainen, E., Ribeiro, A., Dufour, E. & Jacobs, H. T. 2014. Screen for mitochondrial DNA copy number maintenance genes reveals essential role for ATP synthase. *Molecular Systems Biology,* 10.

Galkin, A. & Moncada, S. 2017. Modulation of the conformational state of mitochondrial complex I as a target for therapeutic intervention. *Interface Focus,* 7.

Gallimore, A., Glithero, A., Godkin, A., Tissot, A. C., Plückthun, A., Elliott, T., Hengartner, H. & Zinkernagel, R. 1998. Induction and exhaustion of lymphocytic choriomeningitis virus-specific cytotoxic T lymphocytes visualized using soluble tetrameric major histocompatibility complex class I peptide complexes. *Journal of Experimental Medicine,* 187**,** 1383-1393.

Gandre-Babbe, S. & van der Bliek, A. M. 2008. The novel tail-anchored membrane protein Mff controls mitochondrial and peroxisomal fission in mammalian cells. *Molecular Biology of the Cell,* 19**,** 2402-2412.

Gao, Y. J., Deason, K., Jain, A., Irizarry-Caro, R. A., Dozmorov, I., Coughlin, L. A., Rauch, I., Evers, B. M., Koh, A. Y., Wakeland, E. K. & Pasare, C. 2020. Transcriptional profiling identifies caspase-1 as a T cell-intrinsic regulator of Th17 differentiation. *Journal of Experimental Medicine,* 217.

García-Alcalde, F., Okonechnikov, K., Carbonell, J., Cruz, L. M., Götz, S., Tarazona, S., Dopazo, J., Meyer, T. F. & Conesa, A. 2012. Qualimap: evaluating next-generation sequencing alignment data. *Bioinformatics,* 28**,** 2678-2679.

Gardeitchik, T., Mohamed, M., Ruzzenente, B., Karall, D., Guerrero-Castillo, S., Dalloyaux, D., van den Brand, M., van Kraaij, S., van Asbeck, E., Assouline, Z., Rio, M., de Lonlay, P., Scholl-Buergi, S., Wolthuis, D. F. G. J., Hoischen, A., Rodenburg, R. J., Sperl, W., Urban, Z., Brandt, U., Mayr, J. A., Wong, S., de Brouwer, A. P. M., Nijtmans, L., Munnich, A., Rötig, A., Wevers, R. A., Metodiev, M. D. & Morava, E. 2018. Bi-allelic Mutations in the Mitochondrial Ribosomal Protein MRPS2 Cause Sensorineural Hearing Loss, Hypoglycemia, and Multiple OXPHOS Complex Deficiencies. *American Journal of Human Genetics,* 102**,** 685-695.

Gargano, M. A., Matentzoglu, N., Coleman, B., Addo-Lartey, E. B., Anagnostopoulos, A., Anderton, J., Avillach, P., Bagley, A. M., Bakstein, E., Balhoff, J. P., Baynam, G., Bello, S. M., Berk, M., Bertram, H., Bishop, S., Blau, H., Bodenstein, D. F., Botas, P., Boztug, K., Cady, J., Callahan, T. J., Cameron, R., Carbon, S. J., Castellanos, F., Caufield, J. H., Chan, L. E., Chute, C. G., Cruz-Rojo, J., Dahan-Oliel, N., Davids, J. R., de Dieuleveult, M., de Souza, V., de Vries, B. B. A., de Vries, E., DePaulo, J. R., Derfalvi, B., Dhombres, F., Diaz-Byrd, C., Dingemans, A. J. M., Donadille, B., Duyzend, M., Elfeky, R., Essaid, S., Fabrizzi, C., Fico, G., Firth, H., Freudenberg-Hua, Y., Fullerton, J. M., Gabriel, D. L., Gilmour, K., Giordano, J., Goes, F. S., Moses, R. G., Green, I., Griese, M., Groza, T., Gu, W. H., Guthrie, J., Gyori, B., Hamosh, A., Hanauer, M., Hanusová, K., He, Y. Q., Hegde, H., Helbig, I., Holasová, K., Hoyt, C. T., Huang, S. Z., Hurwitz, E., Jacobsen, J. O. B., Jiang, X. F., Joseph, L., Keramatian, K., King, B., Knoflach, K., Koolen, D. A., Kraus, M. L., Kroll, C., Kusters, M., Ladewig, M. S., Lagorce,

D., Lai, M. C., Lapunzina, P., Laraway, B., Lewis-Smith, D., Li, X. R., Lucano, C., Majd, M., Marazita, M. L., Martinez-Glez, V., McHenry, T. H., McInnis, M. G., McMurry, J. A., Mihulová, M., Millett, C. E., Mitchell, P. B., Moslerová, V., Narutomi, K., Nematollahi, S., Nevado, J., et al. 2023. The Human Phenotype Ontology in 2024: phenotypes around the world. *Nucleic Acids Research*.

Garlanda, C., Dinarello, C. A. & Mantovani, A. 2013. The Interleukin-1 Family: Back to the Future. *Immunity,* 39**,** 1003-1018.

Garrido-Maraver, J., Paz, M. V., Cordero, M. D., Bautista-Lorite, J., Oropesa-Avila, M., de la Mata, M., Pavón, A. D., de Lavera, I., Alcocer-Gómez, E., Galán, F., González, P. Y., Cotán, D., Jackson, S. & Sánchez-Alcázar, J. A. 2015. Critical role of AMP-activated protein kinase in the balance between mitophagy and mitochondrial biogenesis in MELAS disease. *Biochimica Et Biophysica Acta-Molecular Basis of Disease,* 1852**,** 2535-2553.

Garrido, N., Griparic, L., Jokitalo, E., Wartiovaara, J., van der Bliek, A. M. & Spelbrink, J. N. 2003. Composition and dynamics of human mitochondrial nucleoids. *Molecular Biology of the Cell,* 14**,** 1583-1596.

Geginat, J., Lanzavecchia, A. & Sallusto, F. 2003. Proliferation and differentiation potential of human CD8+ memory T-cell subsets in response to antigen or homeostatic cytokines. *Blood,* 101**,** 4260-6.

Geisler, S., Holmström, K. M., Skujat, D., Fiesel, F. C., Rothfuss, O. C., Kahle, P. J. & Springer, W. 2010. PINK1/Parkin-mediated mitophagy is dependent on VDAC1 and p62/SQSTM1. *Nature Cell Biology,* 12**,** 119-U70.

Geltink, R. I. K., O'Sullivan, D., Corrado, M., Bremser, A., Buck, M. D., Buescher, J. M., Firat, E., Zhu, X. K., Niedermann, G., Caputa, G., Kelly, B., Warthorst, U., Rensing-Ehl, A., Kyle, R. L., Vandersarren, L., Curtis, J. D., Patterson, A. E., Lawless, S., Grzes, K., Qiu, J., Sanin, D. E., Kretz, O., Huber, T. B., Janssens, S., Lambrecht, B. N., Rambold, A. S., Pearce, E. J. & Pearce, E. L. 2017. Mitochondrial Priming by CD28. *Cell,* 171**,** 385-+.

Gene Ontology, C., Aleksander, S. A., Balhoff, J., Carbon, S., Cherry, J. M., Drabkin, H. J., Ebert, D., Feuermann, M., Gaudet, P., Harris, N. L., Hill, D. P., Lee, R., Mi, H., Moxon, S., Mungall, C. J., Muruganugan, A., Mushayahama, T., Sternberg, P. W., Thomas, P. D., Van Auken, K., Ramsey, J., Siegele, D. A., Chisholm, R. L., Fey, P., Aspromonte, M. C., Nugnes, M. V., Quaglia, F., Tosatto, S., Giglio, M., Nadendla, S., Antonazzo, G., Attrill, H., Dos Santos, G., Marygold, S., Strelets, V., Tabone, C. J., Thurmond, J., Zhou, P., Ahmed, S. H., Asanitthong, P., Luna Buitrago, D., Erdol, M. N., Gage, M. C., Ali Kadhum, M., Li, K. Y. C., Long, M., Michalak, A., Pesala, A., Pritazahra, A., Saverimuttu, S. C. C., Su, R., Thurlow, K. E., Lovering, R. C., Logie, C., Oliferenko, S., Blake, J., Christie, K., Corbani, L., Dolan, M. E., Drabkin, H. J., Hill, D. P., Ni, L., Sitnikov, D., Smith, C., Cuzick, A., Seager, J., Cooper, L., Elser, J., Jaiswal, P., Gupta, P., Jaiswal, P., Naithani, S., Lera-Ramirez, M., Rutherford, K., Wood, V., De Pons, J. L., Dwinell, M. R., Hayman, G. T., Kaldunski, M. L., Kwitek, A. E., Laulederkind, S. J. F., Tutaj, M. A., Vedi, M., Wang, S. J., D'Eustachio, P., Aimo, L., Axelsen, K., Bridge, A., Hyka-Nouspikel, N., Morgat, A., Aleksander, S. A., Cherry, J. M., Engel, S. R., Karra, K., Miyasato, S. R., Nash, R. S., Skrzypek, M. S., Weng, S., Wong, E. D., Bakker, E., et al. 2023. The Gene Ontology knowledgebase in 2023. *Genetics,* 224.

Giles, R. E., Blanc, H., Cann, H. M. & Wallace, D. C. 1980. Maternal inheritance of human mitochondrial DNA. *Proc Natl Acad Sci U S A,* 77**,** 6715-9.

Glynos, A., Bozhilova, L. V., Frison, M., Burr, S., Stewart, J. B. & Chinnery, P. F. 2023. High-throughput single-cell analysis reveals progressive mitochondrial DNA mosaicism throughout life. *Sci Adv,* 9**,** eadi4038.

Goldrath, A. W. & Bevan, M. J. 1999. Selecting and maintaining a diverse T-cell repertoire. *Nature,* 402**,** 255-262.

Gorman, G. S., Schaefer, A. M., Ng, Y., Gomez, N., Blakely, E. L., Alston, C. L., Feeney, C., Horvath, R., Yu-Wai-Man, P., Chinnery, P. F., Taylor, R. W., Turnbull, D. M. & McFarland, R. 2015. Prevalence of nuclear and mitochondrial DNA mutations related to adult mitochondrial disease. *Ann Neurol,* 77**,** 753-9.

Goto, Y., Nonaka, I. & Horai, S. 1990. A mutation in the tRNA(Leu)(UUR) gene associated with the MELAS subgroup of mitochondrial encephalomyopathies. *Nature,* 348**,** 651-3.

Grady, J. P., Murphy, J. L., Blakely, E. L., Haller, R. G., Taylor, R. W., Turnbull, D. M. & Tuppen, H. A. L. 2014. Accurate Measurement of Mitochondrial DNA Deletion Level and Copy Number Differences in Human Skeletal Muscle. *PLOS ONE,* 9.

Grady, J. P., Pickett, S. J., Ng, Y. S., Alston, C. L., Blakely, E. L., Hardy, S. A., Feeney, C. L., Bright, A. A., Schaefer, A. M., Gorman, G. S., McNally, R. J., Taylor, R. W., Turnbull, D. M. & McFarland, R. 2018. mtDNA heteroplasmy level and copy number indicate disease burden in m.3243A>G mitochondrial disease. *EMBO Mol Med,* 10.

Gray, M. W., Burger, G. & Lang, B. F. 1999. Mitochondrial evolution. *Science,* 283**,** 1476-1481.

Gubbay, S. S., Hankey, G. J., Tan, N. T. S. & Fry, J. M. 1989. Mitochondrial Encephalomyopathy with Corticosteroid Dependence. *Medical Journal of Australia,* 151**,** 100-&.

Gustafsson, C. M., Falkenberg, M. & Larsson, N. G. 2016. Maintenance and Expression of Mammalian Mitochondrial DNA. *Annu Rev Biochem,* 85**,** 133-60.

Hallberg, B. M. & Larsson, N. G. 2011. TFAM forces mtDNA to make a U-turn. *Nature Structural & Molecular Biology,* 18**,** 1179-1181.

Hamann, D., Kostense, S., Wolthers, K. C., Otto, S. A., Baars, P. A., Miedema, F. & van Lier, R. A. W. 1999. Evidence that human CD8+ CD45RA+ CD27- cells are induced by antigen and evolve through extensive rounds of division. *International Immunology,* 11**,** 1027-1033.

Hamazaki, S., Koshiba, M. & Sugiyama, T. 1993. Organ distribution of mutant mitochondrial tRNA(leu(UUR)) gene in a MELAS patient. *Acta pathologica japonica,* 43.

Hammarlund, E., Thomas, A., Amanna, I. J., Holden, L. A., Slayden, O. D., Park, B., Gao, L. N. & Slifka, M. K. 2017. Plasma cell survival in the absence of B cell memory. *Nature Communications,* 8.

Hanna, M. G., Nelson, I., Sweeney, M. G., Cooper, J. M., Watkins, P. J., Morgan-Hughes, J. A. & Harding, A. E. 1995. Congenital encephalomyopathy and adult-onset myopathy and diabetes mellitus: different phenotypic associations of a new heteroplasmic mtDNA tRNA glutamic acid mutation. *Am J Hum Genet.,* 56**,** 1026-33.

Hao, Y., Stuart, T., Kowalski, M. H., Choudhary, S., Hoffman, P., Hartman, A., Srivastava, A., Molla, G., Madad, S., Fernandez-Granda, C. & Satija, R. 2024. Dictionary learning for integrative, multimodal and scalable single-cell analysis. *Nat Biotechnol,* 42**,** 293-304.

Hart, P. C., Mao, M., de Abreu, A. L. P., Ansenberger-Fricano, K., Ekoue, D. N., Ganini, D., Kajdacsy-Balla, A., Diamond, A. M., Minshall, R. D., Consolaro, M. E. L.,

Santos, J. H. & Bonini, M. G. 2015. MnSOD upregulation sustains the Warburg effect via mitochondrial ROS and AMPK-dependent signalling in cancer. *Nature Communications,* 6.
Haze, K., Yoshida, H., Yanagi, H., Yura, T. & Mori, K. 1999. Mammalian transcription factor ATF6 is synthesized as a transmembrane protein and activated by proteolysis in response to endoplasmic reticulum stress. *Molecular Biology of the Cell,* 10**,** 3787-3799.
He, L., Luo, L., Proctor, S. J., Middleton, P. G., Blakely, E. L. & Taylor, R. W. 2003. Somatic mitochondrial DNA mutations in adult-onset leukaemia. *Leukemia,* 17**,** 2487-2491.
Heinemeyer, J., Braun, H. P., Boekema, E. J. & Kouril, R. 2007. A structural model of the cytochrome c reductase/oxidase supercomplex from yeast mitochondria. *Journal of Biological Chemistry,* 282**,** 12240-12248.
Heinzel, K., Benz, C., Martins, V. C., Haidl, I. D. & Bleul, C. C. 2007. Bone marrow-derived hemopoietic precursors commit to the T cell lineage only after arrival in the thymic microenvironment. *Journal of Immunology,* 178**,** 858-868.
Hellebrekers, D. M., Wolfe, R., Hendrickx, A. T., de Coo, I. F., de Die, C. E., Geraedts, J. P., Chinnery, P. F. & Smeets, H. J. 2012. PGD and heteroplasmic mitochondrial DNA point mutations: a systematic review estimating the chance of healthy offspring. *Hum Reprod Update,* 18**,** 341-9.
Helm, M., Florentz, C., Chomyn, A. & Attardi, G. 1999. Search for differences in post-transcriptional modification patterns of mitochondrial DNA-encoded wild-type and mutant human tRNALys and tRNALeu(UUR). *Nucleic Acids Research,* 27**,** 756-763.
Hess, J. F., Parisi, M. A., Bennett, J. L. & Clayton, D. A. 1991a. Impairment of mitochondrial transcription termination by a point mutation associated with the MELAS subgroup of mitochondrial encephalomyopathies. *Nature,* 351**,** 236-9.
Hess, J. F., Parisi, M. A., Bennett, J. L. & Clayton, D. A. 1991b. Impairment of Mitochondrial Transcription Termination by a Point Mutation Associated with the Melas Subgroup of Mitochondrial Encephalomyopathies. *Nature,* 351**,** 236-239.
Hikmat, O., Charalampos, T., Klingenberg, C., Rasmussen, M., Tallaksen, C. M. E., Brodtkorb, E., Fiskerstrand, T., McFarland, R., Rahman, S. & Bindoff, L. A. 2017. The presence of anaemia negatively influences survival in patients with POLG disease. *Journal of Inherited Metabolic Disease,* 40**,** 861-866.
Hooftman, A., Peace, C. G., Ryan, D. G., Day, E. A., Yang, M., McGettrick, A. F., Yin, M. R., Montano, E. N., Huo, L. H., Toller-Kawahisa, J. E., Zecchini, V., Ryan, T. A. J., Bolado-Carrancio, A., Casey, A. M., Prag, H. A., Costa, A. S. H., de los Santos, G., Ishimori, M., Wallace, D. J., Venuturupalli, S., Nikitopoulou, E., Frizzell, N., Johansson, C., Von Kriegsheim, A., Murphy, M. P., Jefferies, C., Frezza, C. & O'Neill, L. A. J. 2023. Macrophage fumarate hydratase restrains mtRNA-mediated interferon production. *Nature,* 615**,** 490-+.
Hornig-Do, H. T., Montanari, A., Rozanska, A., Tuppen, H. A., Almalki, A. A., Abg-Kamaludin, D. P., Frontali, L., Francisci, S., Lightowlers, R. N. & Chrzanowska-Lightowlers, Z. M. 2014. Human mitochondrial leucyl tRNA synthetase can suppress non cognate pathogenic mt-tRNA mutations. *EMBO Molecular Medicine,* 6.
Horvath, S. E. & Daum, G. 2013. Lipids of mitochondria. *Prog Lipid Res,* 52**,** 590-614.
Hoth, M., Button, D. C. & Lewis, R. S. 2000. Mitochondrial control of calcium-channel gating: A mechanism for sustained signaling and transcriptional activation in T

lymphocytes. *Proceedings of the National Academy of Sciences of the United States of America,* 97**,** 10607-10612.
Huang, Y., Jiang, W., Zhou, R., Huang, Y., Jiang, W. & Zhou, R. 2024. DAMP sensing and sterile inflammation: intracellular, intercellular and inter-organ pathways. *Nature Reviews Immunology,* 24.
Hutchison, C. A., 3rd, Newbold, J. E., Potter, S. S. & Edgell, M. H. 1974. Maternal inheritance of mammalian mitochondrial DNA. *Nature,* 251**,** 536-8.
Inoue, T. & Kurosaki, T. 2024. Memory B cells. *Nature Reviews Immunology,* 24**,** 5-17.
Irazoki, A., Gordaliza-Alaguero, I., Frank, E., Giakoumakis, N. N., Seco, J., Palacín, M., Gumà, A., Sylow, L., Sebastián, D., Zorzano, A., Irazoki, A., Gordaliza-Alaguero, I., Frank, E., Giakoumakis, N. N., Seco, J., Palacín, M., Gumà, A., Sylow, L., Sebastián, D. & Zorzano, A. 2023. Disruption of mitochondrial dynamics triggers muscle inflammation through interorganellar contacts and mitochondrial DNA mislocation. *Nature Communications,* 14.
Ishihara, N., Fujita, Y., Oka, T. & Mihara, K. 2006. Regulation of mitochondrial morphology through proteolytic cleavage of OPA1. *Embo Journal,* 25**,** 2966-2977.
Ito, K., Hirao, A., Arai, F., Takubo, K., Matsuoka, S., Miyamoto, K., Ohmura, M., Naka, K., Hosokawa, K., Ikeda, Y. & Suda, T. 2006. Reactive oxygen species act through p38 MAPK to limit the lifespan of hematopoietic stem cells. *Nature Medicine,* 12**,** 446-451.
Itoh, Y., Andréll, J., Choi, A., Richter, U., Maiti, P., Best, R. B., Barrientos, A., Battersby, B. J. & Amunts, A. 2021. Mechanism of membrane-tethered mitochondrial protein synthesis. *Science,* 371**,** 846-+.
Jacobs, S. R., Michalek, R. D. & Rathmell, J. C. 2010. IL-7 Is Essential for Homeostatic Control of T Cell Metabolism In Vivo. *Journal of Immunology,* 184**,** 3461-3469.
Jain, A., Song, R., Wakeland, E. K. & Pasare, C. 2018. T cell intrinsic IL-1R signaling licenses effector cytokine production by memory CD4 T cells. *Journal of Immunology,* 200.
Janeway, C. A., Jr. 1989. Approaching the asymptote? Evolution and revolution in immunology. *Cold Spring Harb Symp Quant Biol,* 54 Pt 1**,** 1-13.
Janssen, G. M., Hensbergen, P. J., van Bussel, F. J., Balog, C. I., Maassen, J. A., Deelder, A. M. & Raap, A. K. 2007. The A3243G tRNALeu(UUR) mutation induces mitochondrial dysfunction and variable disease expression without dominant negative acting translational defects in complex IV subunits at UUR codons. *Hum Mol Genet,* 16**,** 2472-81.
Janssen, G. M. C., Maassen, J. A. & van den Ouweland, J. M. W. 1999. The diabetes-associated 3243 mutation in the mitochondrial tRNAleuUUR gene causes severe mitochondrial dysfunction without a strong decrease in protein synthesis rate. *Journal of Biological Chemistry,* 274**,** 29744-29748.
Jellusova, J., Cato, M. H., Apgar, J. R., Ramezani-Rad, P., Leung, C. R., Chen, C. D., Richardson, A. D., Conner, E. M., Benschop, R. J., Woodgett, J. R. & Rickert, R. C. 2017. Gsk3 is a metabolic checkpoint regulator in B cells. *Nature Immunology,* 18**,** 303-312.
Jenuth, J. P., Peterson, A. C., Fu, K. & Shoubridge, E. A. 1996. Random genetic drift in the female germline explains the rapid segregation of mammalian mitochondrial DNA. *Nat Genet,* 14**,** 146-51.
Jiang, X., Jiang, H., Shen, Z. R. & Wang, X. D. 2014. Activation of mitochondrial protease OMA1 by Bax and Bak promotes cytochrome c release during apoptosis. *Proceedings of the National Academy of Sciences of the United States of America,* 111**,** 14782-14787.

Jiménez-Menéndez, N., Fernández-Millán, P., Rubio-Cosials, A., Arnan, C., Montoya, J., Jacobs, H. T., Bernadó, P., Coll, M., Usón, I. & Solà, M. 2010. Human mitochondrial mTERF wraps around DNA through a left-handed superhelical tandem repeat. *Nature Structural & Molecular Biology,* 17**,** 891-893.

Jouaville, L. S., Pjnton, P., Bastianutto, C., Rutter, G. A. & Rizzuto, R. 1999. Regulation of mitochondrial ATP synthesis by calcium: Evidence for a long-term metabolic priming. *Proceedings of the National Academy of Sciences of the United States of America,* 96**,** 13807-13812.

Kai, Y., Takamatsu, C., Tokuda, K., Okamoto, M., Irita, K. & Takahashi, S. 2006. Rapid and random turnover of mitochondrial DNA in rat hepatocytes of primary culture. *Mitochondrion,* 6**,** 299-304.

Kaji, T., Ishige, A., Hikida, M., Taka, J., Hijikata, A., Kubo, M., Nagashima, T., Takahashi, Y., Kurosaki, T., Okada, M., Ohara, O., Rajewsky, K. & Takemori, T. 2012. Distinct cellular pathways select germline-encoded and somatically mutated antibodies into immunological memory. *Journal of Experimental Medicine,* 209**,** 2079-2097.

Kamath, A. T., Henri, S., Battye, F., Tough, D. F. & Shortman, K. 2002. Developmental kinetics and lifespan of dendritic cells in mouse lymphoid organs. *Blood,* 100**,** 1734-1741.

Kamerkar, S. C., Kraus, F., Sharpe, A. J., Pucadyil, T. J. & Ryan, M. T. 2018. Dynamin-related protein 1 has membrane constricting and severing abilities sufficient for mitochondrial and peroxisomal fission. *Nature Communications,* 9.

Karan, K. R., Trumpff, C., Cross, M., Engelstad, K. M., Marsland, A. L., McGuire, P. J., Hirano, M. & Picard, M. 2022. Leukocyte cytokine responses in adult patients with mitochondrial DNA defects. *Journal of Molecular Medicine-Jmm,* 100**,** 963-971.

Karppa, M., Herva, R., Moslemi, A. R., Oldfors, A., Kakko, S. & Majamaa, K. 2005. Spectrum of myopathic findings in 50 patients with the 3243A>G mutation in mitochondrial DNA. *Brain,* 128**,** 1861-9.

Kasamatsu, H., Robberson, D. L. & Vinograd, J. 1971. Novel Closed-Circular Mitochondrial DNA with Properties of a Replicating Intermediate. *Proceedings of the National Academy of Sciences of the United States of America,* 68**,** 2252-+.

Kauppila, J. H. K., Baines, H. L., Bratic, A., Simard, M. L., Freyer, C., Mourier, A., Stamp, C., Filograna, R., Larsson, N. G., Greaves, L. C. & Stewart, J. B. 2016. A Phenotype-Driven Approach to Generate Mouse Models with Pathogenic mtDNA Mutations Causing Mitochondrial Disease. *Cell Rep,* 16**,** 2980-2990.

Keating, S. E., Zaiatz-Bittencourt, V., Loftus, R. M., Keane, C., Brennan, K., Finlay, D. K. & Gardiner, C. M. 2016. Metabolic Reprogramming Supports IFN-γ Production by CD56

NK Cells. *Journal of Immunology,* 196**,** 2552-2560.

Keyer, K. & Imlay, J. A. 1996. Superoxide accelerates DNA damage by elevating free-iron levels. *Proceedings of the National Academy of Sciences of the United States of America,* 93**,** 13635-13640.

King, M. P. & Attardi, G. 1989. Human-Cells Lacking Mtdna - Repopulation with Exogenous Mitochondria by Complementation. *Science,* 246**,** 500-503.

King, M. P., Koga, Y., Davidson, M. & Schon, E. A. 1992. Defects in mitochondrial protein synthesis and respiratory chain activity segregate with the tRNA(Leu(UUR)) mutation associated with mitochondrial myopathy,

encephalopathy, lactic acidosis, and strokelike episodes. *Mol Cell Biol,* 12**,** 480-90.
Kirino, Y., Goto, Y.-i., Campos, Y., Arenas, J., Suzuki, T., Kirino, Y., Goto, Y.-i., Campos, Y., Arenas, J. & Suzuki, T. 2005. Specific correlation between the wobble modification deficiency in mutant tRNAs and the clinical features of a human mitochondrial disease. *Proceedings of the National Academy of Sciences,* 102.
Kisielow, P., Teh, H. S., Bluthmann, H. & Vonboehmer, H. 1988. Positive Selection of Antigen-Specific T-Cells in Thymus by Restricting Mhc Molecules. *Nature,* 335**,** 730-733.
Klein Gunnewiek, T. M., Verboven, A. H. A., Pelgrim, I., Hogeweg, M., Schoenmaker, C., Renkema, H., Beyrath, J., Smeitink, J., de Vries, B. B. A., Hoen, P. A. C., Kozicz, T. & Nadif Kasri, N. 2021. Sonlicromanol improves neuronal network dysfunction and transcriptome changes linked to m.3243A>G heteroplasmy in iPSC-derived neurons. *Stem Cell Reports,* 16**,** 2197-2212.
Klenerman, P. & Oxenius, A. 2016. T cell responses to cytomegalovirus. *Nature Reviews Immunology,* 16**,** 367-377.
Koboldt, D. C., Chen, K., Wylie, T., Larson, D. E., McLellan, M. D., Mardis, E. R., Weinstock, G. M., Wilson, R. K. & Ding, L. 2009. VarScan: variant detection in massively parallel sequencing of individual and pooled samples. *Bioinformatics,* 25**,** 2283-2285.
Korhonen, J. A., Pham, X. H., Pellegrini, M. & Falkenberg, M. 2004. Reconstitution of a minimal mtDNA replisome in vitro. *EMBO J,* 23**,** 2423-9.
Kotrys, A. V., Durham, T. J., Guo, X. A., Vantaku, V. R., Parangi, S. & Mootha, V. K. 2024. Single-cell analysis reveals context-dependent, cell-level selection of mtDNA. *Nature,* 629**,** 458-466.
Krueger, F. 2024. Trimgalore.
Krüger, A., Remes, C., Shiriaev, D. I., Liu, Y., Spåhr, H., Wibom, R., Atanassov, I., Nguyen, M. D., Cooperman, B. S., Rorbach, J., Krüger, A., Remes, C., Shiriaev, D. I., Liu, Y., Spåhr, H., Wibom, R., Atanassov, I., Nguyen, M. D., Cooperman, B. S. & Rorbach, J. 2023. Human mitochondria require mtRF1 for translation termination at non-canonical stop codons. *Nature Communications,* 14.
Kudin, A. P., Bimpong-Buta, N. Y. B., Vielhaber, S., Elger, C. E. & Kunz, W. S. 2004. Characterization of superoxide-producing sites in isolated brain mitochondria. *Journal of Biological Chemistry,* 279**,** 4127-4135.
Kujoth, G. C., Hiona, A., Pugh, T. D., Someya, S., Panzer, K., Wohlgemuth, S. E., Hofer, T., Seo, A. Y., Sullivan, R., Jobling, W. A., Morrow, J. D., Van Remmen, H., Sedivy, J. M., Yamasoba, T., Tanokura, M., Weindruch, R., Leeuwenburgh, C. & Prolla, T. A. 2005. Mitochondrial DNA mutations, oxidative stress, and apoptosis in mammalian aging. *Science,* 309**,** 481-484.
Kumar, S. & Dikshit, M. 2019. Metabolic Insight of Neutrophils in Health and Disease. *Frontiers in Immunology,* 10.
Künzli, M. & Masopust, D. 2023. CD4+ T cell memory. *Nature Immunology,* 24**,** 903-914.
Kuswanto, W., Burzyn, D., Panduro, M., Wang, K. K., Jang, Y. C., Wagers, A. J., Benoist, C. & Mathis, D. 2016. Poor Repair of Skeletal Muscle in Aging Mice Reflects a Defect in Local, Interleukin-33-Dependent Accumulation of Regulatory T Cells. *Immunity,* 44**,** 355-367.
Lambert, A. J. & Brand, M. D. 2004. Superoxide production by NADH: ubiquinone oxidoreductase (complex I) depends on the pH gradient across the mitochondrial inner membrane. *Biochemical Journal,* 382**,** 511-517.

Langdahl, J. H., Larsen, M., Frost, M., Andersen, P. H., Yderstraede, K. B., Vissing, J., Duno, M., Thomassen, M. & Frederiksen, A. L. 2018. Lecocytes mutation load declines with age in carriers of the m.3243A>G mutation: A 10-year Prospective Cohort. *Clin Genet,* 93**,** 925-928.

Lareau, C. A., Dubois, S. M., Buquicchio, F. A., Hsieh, Y. H., Garg, K., Kautz, P., Nitsch, L., Praktiknjo, S. D., Maschmeyer, P., Verboon, J. M., Gutierrez, J. C., Yin, Y., Fiskin, E., Luo, W., Mimitou, E. P., Muus, C., Malhotra, R., Parikh, S., Fleming, M. D., Oevermann, L., Schulte, J., Eckert, C., Kundaje, A., Smibert, P., Vardhana, S. A., Satpathy, A. T., Regev, A., Sankaran, V. G., Agarwal, S. & Ludwig, L. S. 2023. Single-cell multi-omics of mitochondrial DNA disorders reveals dynamics of purifying selection across human immune cells. *Nat Genet,* 55**,** 1198-1209.

Lareau, C. A., Ludwig, L. S., Muus, C., Gohil, S. H., Zhao, T., Chiang, Z., Pelka, K., Verboon, J. M., Luo, W., Christian, E., Rosebrock, D., Getz, G., Boland, G. M., Chen, F., Buenrostro, J. D., Hacohen, N., Wu, C. J., Aryee, M. J., Regev, A. & Sankaran, V. G. 2021. Massively parallel single-cell mitochondrial DNA genotyping and chromatin profiling. *Nat Biotechnol,* 39**,** 451-461.

Latorre-Pellicer, A., Lechuga-Vieco, A. V., Johnston, I. G., Hämäläinen, R. H., Pellico, J., Justo-Méndez, R., Fernández-Toro, J. M., Clavería, C., Guaras, A., Sierra, R., Llop, J., Torres, M., Criado, L. M., Suomalainen, A., Jones, N. S., Ruíz-Cabello, J. & Enríquez, J. A. 2019. Regulation of Mother-to-Offspring Transmission of mtDNA Heteroplasmy. *Cell Metabolism,* 30**,** 1120-+.

Lechuga-Vieco, A. V., Latorre-Pellicer, A., Johnston, I. G., Prota, G., Gileadi, U., Justo-Méndez, R., Acín-Pérez, R., Martínez-de-Mena, R., Fernández-Toro, J. M., Jimenez-Blasco, D., Mora, A., Nicolás-Avila, J. A., Santiago, D. J., Priori, S. G., Bolaños, J. P., Sabio, G., Criado, L. M., Ruíz-Cabello, J., Cerundolo, V., Jones, N. S. & Enríquez, J. A. 2020. Cell identity and nucleo-mitochondrial genetic context modulate OXPHOS performance and determine somatic heteroplasmy dynamics. *Science Advances,* 6.

Lee, J. E., Westrate, L. M., Wu, H. X., Page, C. & Voeltz, G. K. 2016. Multiple dynamin family members collaborate to drive mitochondrial division. *Nature,* 540**,** 139-+.

Lee, W., Zamudio-Ochoa, A., Buchel, G., Podlesniy, P., Marti Gutierrez, N., Puigros, M., Calderon, A., Tang, H. Y., Li, L., Mikhalchenko, A., Koski, A., Trullas, R., Mitalipov, S. & Temiakov, D. 2023. Molecular basis for maternal inheritance of human mitochondrial DNA. *Nat Genet,* 55**,** 1632-1639.

Lewkowicz, N., Klink, M., Mycko, M. P. & Lewkowicz, P. 2013. Neutrophil – CD4+CD25+ T regulatory cell interactions: A possible new mechanism of infectious tolerance. *Immunobiology,* 218.

Li, H., Handsaker, B., Wysoker, A., Fennell, T., Ruan, J., Homer, N., Marth, G., Abecasis, G., Durbin, R. & Proc, G. P. D. 2009. The Sequence Alignment/Map format and SAMtools. *Bioinformatics,* 25**,** 2078-2079.

Li, P., Nijhawan, D., Budihardjo, I., Srinivasula, S. M., Ahmad, M., Alnemri, E. S. & Wang, X. D. 1997. Cytochrome c and dATP-dependent formation of Apaf-1/caspase-9 complex initiates an apoptotic protease cascade. *Cell,* 91**,** 479-489.

Li, W., Bai, Z., Liu, J., Tang, Y., Yin, C., Jin, M., Mu, L. & Li, X. 2023. Mitochondrial ROS-dependent CD4+PD-1+T cells are pathological expansion in patients with primary immune thrombocytopenia. *International Immunopharmacology,* 122.

Li, W., Whaley, C. D., Mondino, A. & Mueller, D. L. 1996. Blocked signal transduction to the ERK and JNK protein kinases in anergic CD4(+) T cells. *Science,* 271**,** 1272-1276.

Liao, Y., Smyth, G. K. & Shi, W. 2014. featureCounts: an efficient general purpose program for assigning sequence reads to genomic features. *Bioinformatics,* 30**,** 923-930.
Libri, V., Azevedo, R. I., Jackson, S. E., Di Mitri, D., Lachmann, R., Fuhrmann, S., Vukmanovic-Stejic, M., Yong, K., Battistini, L., Kern, F., Soares, M. V. D. & Akbar, A. N. 2011. Cytomegalovirus infection induces the accumulation of short-lived, multifunctional CD4+CD45RA+CD27-T cells: the potential involvement of interleukin-7 in this process. *Immunology,* 132**,** 326-339.
Lin, D. S., Huang, Y. W., Ho, C. S., Huang, T. S., Lee, T. H., Wu, T. Y., Huang, Z. D. & Wang, T. J. 2023. Impact of Mitochondrial A3243G Heteroplasmy on Mitochondrial Bioenergetics and Dynamics of Directly Reprogrammed MELAS Neurons. *Cells,* 12.
Linder, A., Bauernfried, S., Cheng, Y., Albanese, M., Jung, C., Keppler, O. T. & Hornung, V. 2020. CARD8 inflammasome activation triggers pyroptosis in human T cells. *EMBO J,* 39**,** e105071.
Liu, C. S., Cheng, W. L., Lee, C. F., Ma, Y. S., Lin, C. Y., Huang, C. C. & Wei, Y. H. 2006. Alteration in the copy number of mitochondrial DNA in leukocytes of patients with mitochondrial encephalomyopathies. *Acta Neurologica Scandinavica,* 113**,** 334-341.
Liu, C. Y. & Kaufman, R. J. 2003. The unfolded protein response. *Journal of Cell Science,* 116**,** 1861-1862.
Liu, Y., Makarova, K. S., Huang, W. C., Wolf, Y. I., Nikolskaya, A. N., Zhang, X. X., Cai, M. W., Zhang, C. J., Xu, W., Luo, Z. H., Cheng, L., Koonin, E. V. & Li, M. 2021. Expanded diversity of Asgard archaea and their relationships with eukaryotes. *Nature,* 593**,** 553-+.
Losón, O. C., Song, Z. Y., Chen, H. C. & Chan, D. C. 2013. Fis1, Mff, MiD49, and MiD51 mediate Drp1 recruitment in mitochondrial fission. *Molecular Biology of the Cell,* 24**,** 659-667.
Love, M. I., Huber, W. & Anders, S. 2014. Moderated estimation of fold change and dispersion for RNA-seq data with DESeq2. *Genome Biol,* 15**,** 550.
Ludwig, L. S., Lareau, C. A., Ulirsch, J. C., Christian, E., Muus, C., Li, L. H., Pelka, K., Ge, W., Oren, Y., Brack, A., Law, T., Rodman, C., Chen, J. H., Boland, G. M., Hacohen, N., Rozenblatt-Rosen, O., Aryee, M. J., Buenrostro, J. D., Regev, A. & Sankaran, V. G. 2019. Lineage Tracing in Humans Enabled by Mitochondrial Mutations and Single-Cell Genomics. *Cell,* 176**,** 1325-1339 e22.
Luo, H. Z., Mu, W. C., Karki, R., Chiang, H. H., Mohrin, M., Shin, J. Y. J., Ohkubo, R., Ito, K., Kanneganti, T. D. & Chen, D. 2019. Mitochondrial Stress-Initiated Aberrant Activation of the NLRP3 Inflammasome Regulates the Functional Deterioration of Hematopoietic Stem Cell Aging. *Cell Reports,* 26**,** 945-+.
Luo, S., Valencia, C. A., Zhang, J., Lee, N. C., Slone, J., Gui, B., Wang, X., Li, Z., Dell, S., Brown, J., Chen, S. M., Chien, Y. H., Hwu, W. L., Fan, P. C., Wong, L. J., Atwal, P. S. & Huang, T. 2018. Biparental Inheritance of Mitochondrial DNA in Humans. *Proc Natl Acad Sci U S A,* 115**,** 13039-13044.
Lutz, C. T., Karapetyan, A., Al-Attar, A., Shelton, B. J., Holt, K. J., Tucker, J. H. & Presnell, S. R. 2011. Human natural killer cells proliferate and die in vivo more rapidly than T cells in healthy young and elderly adults. *Journal of immunology,* 186.
Macallan, D. C., Asquith, B., Irvine, A. J., Wallace, D. L., Worth, A., Ghattas, H., Zhang, Y., Griffin, G. E., Tough, D. F. & Beverley, P. C. 2003. Measurement and

modeling of human T cell kinetics. *European Journal of Immunology,* 33**,** 2316-2326.

Mancuso, M., Orsucci, D., Angelini, C., Bertini, E., Carelli, V., Comi, G. P., Donati, A., Minetti, C., Moggio, M., Mongini, T., Servidei, S., Tonin, P., Toscano, A., Uziel, G., Bruno, C., Ienco, E. C., Filosto, M., Lamperti, C., Catteruccia, M., Moroni, I., Musumeci, O., Pegoraro, E., Ronchi, D., Santorelli, F. M., Sauchelli, D., Scarpelli, M., Sciacco, M., Valentino, M. L., Vercelli, L., Zeviani, M. & Siciliano, G. 2014. The m.3243A>G mitochondrial DNA mutation and related phenotypes. A matter of gender? *Journal of Neurology,* 261**,** 504-510.

Mancuso, M., Orsucci, D., Ienco, E. C., Ricci, G., Ali, G., Servadio, A., Fontanini, G., Filosto, M., Vielmi, V., Rocchi, A., Petrozzi, L., LoGerfo, A. & Siciliano, G. 2013. An "inflammatory" mitochondrial myopathy. A case report. *Neuromuscular Disorders,* 23**,** 907-910.

Mansergh, F. C., Millington-Ward, S., Kennan, A., Kiang, A. S., Humphries, M., Farrar, G. J., Humphries, P. & Kenna, P. F. 1999. Retinitis pigmentosa and progressive sensorineural hearing loss caused by a C12258A mutation in the mitochondrial MTTS2 gene. *American Journal of Human Genetics,* 64.

Mantel, C. R., O'Leary, H. A., Chitteti, B. R., Huang, X. X., Cooper, S., Hangoc, G., Brustovetsky, N., Srour, E. F., Lee, M. R., Messina-Graham, S., Haas, D. M., Falah, N., Kapur, R., Pelus, L. M., Bardeesy, N., Fitamant, J., Ivan, M., Kim, K. S. & Broxmeyer, H. E. 2015. Enhancing Hematopoietic Stem Cell Transplantation Efficacy by Mitigating Oxygen Shock. *Cell,* 161**,** 1553-1565.

Maranzana, E., Barbero, G., Falasca, A. I., Lenaz, G. & Genova, M. L. 2013. Mitochondrial respiratory supercomplex association limits production of reactive oxygen species from complex I. *Antioxid Redox Signal,* 19**,** 1469-80.

Margulis, L. 1971. Symbiosis and evolution. *Scientific American,* 225.

Marina, A. D., Bertolini, A., Wegener-Panzer, A., Flotats-Bastardas, M., Reinhardt, T., Naggar, I. E., Distelmaier, F., Blaschek, A., Schara-Schmidt, U., Brunet, T., Wagner, M., Smirnov, D., Prokisch, H., Wortmann, S. B. & Rostasy, K. 2022. Mitochondrial diseases mimicking autoimmune diseases of the CNS and good response to steroids initially. *European Journal of Paediatric Neurology,* 41.

Martijn, J., Vosseberg, J., Guy, L., Offre, P. & Ettema, T. J. G. 2018. Deep mitochondrial origin outside the sampled alphaproteobacteria. *Nature,* 557**,** 101-+.

Martin, B. N., Wang, C. H., Zhang, C. J., Kang, Z. Z., Gulen, M. F., Zepp, J. A., Zhao, J. J., Bian, G. L., Do, J. S., Min, B., Pavicic, P. G., El-Sanadi, C., Fox, P. L., Akitsu, A., Iwakura, Y., Sarkar, A., Wewers, M. D., Kaiser, W. J., Mocarski, E. S., Rothenberg, M. E., Hise, A. G., Dubyak, G. R., Ransohoff, R. M. & Li, X. X. 2016. T cell-intrinsic ASC critically promotes Th17-mediated experimental autoimmune encephalomyelitis. *Nature Immunology,* 17**,** 583-+.

Mathew, A., Lindsley, T. A., Sheridan, A., Bhoiwala, D. L., Hushmendy, S. F., Yager, E. J., Ruggiero, E. A. & Crawford, D. R. 2012. Degraded Mitochondrial DNA is a Newly Identified Subtype of the Damage Associated Molecular Pattern (DAMP) Family and Possible Trigger of Neurodegeneration. *Journal of Alzheimer's Disease,* 30.

Matsuda, N., Sato, S., Shiba, K., Okatsu, K., Saisho, K., Gautier, C. A., Sou, Y., Saiki, S., Kawajiri, S., Sato, F., Kimura, M., Komatsu, M., Hattori, N. & Tanaka, K. 2010. PINK1 stabilized by mitochondrial depolarization recruits Parkin to damaged mitochondria and activates latent Parkin for mitophagy. *Journal of Cell Biology,* 189**,** 211-221.

McCormack, J. G. & Denton, R. M. 1979. The effects of calcium ions and adenine nucleotides on the activity of pig heart 2-oxoglutarate dehydrogenase complex. *Biochem J,* 180**,** 533-44.
McFarland, R., Schaefer, A. M., Gardner, J. L., Lynn, S., Hayes, C. M., Barron, M. J., Walker, M., Chinnery, P. F., Taylor, R. W. & Turnbull, D. M. 2004. Familial myopathy: New insights into the T14709C mitochondrial tRNA mutation. *Annals of Neurology,* 55.
Medzhitov, R. & Janeway, C. A., Jr. 1997. Innate immunity: impact on the adaptive immune response. *Curr Opin Immunol,* 9**,** 4-9.
Mengel-From, J., Thinggaard, M., Dalgard, C., Kyvik, K. O., Christensen, K. & Christiansen, L. 2014. Mitochondrial DNA copy number in peripheral blood cells declines with age and is associated with general health among elderly. *Hum Genet,* 133**,** 1149-59.
Milacic, M., Beavers, D., Conley, P., Gong, C., Gillespie, M., Griss, J., Haw, R., Jassal, B., Matthews, L., May, B., Petryszak, R., Ragueneau, E., Rothfels, K., Sevilla, C., Shamovsky, V., Stephan, R., Tiwari, K., Varusai, T., Weiser, J., Wright, A., Wu, G., Stein, L., Hermjakob, H. & D'Eustachio, P. 2024. The Reactome Pathway Knowledgebase 2024. *Nucleic Acids Res,* 52**,** D672-D678.
Milasta, S., Dillon, C. P., Sturm, O. E., Verbist, K. C., Brewer, T. L., Quarato, G., Brown, S. A., Frase, S., Janke, L. J., Perry, S. S., Thomas, P. G. & Green, D. R. 2016. Apoptosis-Inducing-Factor-Dependent Mitochondrial Function Is Required for T Cell but Not B Cell Function. *Immunity,* 44**,** 88-102.
Milenkovic, D., Misic, J., Hevler, J. F., Molinié, T., Chung, I., Atanassov, I., Li, X. P., Filograna, R., Mesaros, A., Mourier, A., Heck, A. J. R., Hirst, J. & Larsson, N. G. 2023. Preserved respiratory chain capacity and physiology in mice with profoundly reduced levels of mitochondrial respirasomes. *Cell Metabolism,* 35.
Mills, D. B., Boyle, R. A., Daines, S. J., Sperling, E. A., Pisani, D., Donoghu, I. C. J. & Lenton, T. M. 2022. Eukaryogenesis and oxygen in Earth history. *Nature Ecology & Evolution,* 6**,** 520-532.
Milovanovic, M., Volarevic, V., Radosavljevic, G., Jovanovic, I., Pejnovic, N., Arsenijevic, N. & Lukic, M. L. 2012. IL-33/ST2 axis in inflammation and immunopathology. *Immunologic Research,* 52**,** 89-99.
Minczuk, M., He, J. Y., Duch, A. M., Ettema, T. J., Chlebowski, A., Dzionek, K., Nijtmans, L. G. J., Huynen, M. A. & Holt, I. J. 2011. TEFM (c17orf42) is necessary for transcription of human mtDNA. *Nucleic Acids Research,* 39**,** 4284-4299.
Miralles Fuste, J., Shi, Y., Wanrooij, S., Zhu, X., Jemt, E., Persson, O., Sabouri, N., Gustafsson, C. M. & Falkenberg, M. 2014. In vivo occupancy of mitochondrial single-stranded DNA binding protein supports the strand displacement mode of DNA replication. *PLoS Genet,* 10**,** e1004832.
Mitchell, P. 1961. Coupling of phosphorylation to electron and hydrogen transfer by a chemi-osmotic type of mechanism. *Nature,* 191**,** 144-8.
Moldoveanu, T., Grace, C. R., Llambi, F., Nourse, A., Fitzgerald, P., Gehring, K., Kriwacki, R. W. & Green, D. R. 2013. BID-induced structural changes in BAK promote apoptosis. *Nature Structural & Molecular Biology,* 20**,** 589-+.
Monnot, S., Gigarel, N., Samuels, D. C., Burlet, P., Hesters, L., Frydman, N., Frydman, R., Kerbrat, V., Funalot, B., Martinovic, J., Benachi, A., Feingold, J., Munnich, A., Bonnefont, J. P. & Steffann, J. 2011. Segregation of mtDNA throughout human embryofetal development: m.3243A>G as a model system. *Hum Mutat,* 32**,** 116-25.

Monroe, K. M., Yang, Z. Y., Johnson, J. R., Geng, X., Doitsh, G., Krogan, N. J. & Greene, W. C. 2014. IFI16 DNA Sensor Is Required for Death of Lymphoid CD4 T Cells Abortively Infected with HIV. *Science,* 343**,** 428-432.

Montoya, J., Christianson, T., Levens, D., Rabinowitz, M. & Attardi, G. 1982. Identification of initiation sites for heavy-strand and light-strand transcription in human mitochondrial DNA. *Proc Natl Acad Sci U S A,* 79**,** 7195-9.

Montoya, J., Gaines, G. L. & Attardi, G. 1983. The pattern of transcription of the human mitochondrial rRNA genes reveals two overlapping transcription units. *Cell,* 34**,** 151-9.

Moraes, C. T. 2001. What regulates mitochondrial DNA copy number in animal cells? *Trends in Genetics,* 17**,** 199-205.

Moraes, C. T., Ciacci, F., Bonilla, E., Jansen, C., Hirano, M., Rao, N., Lovelace, R. E., Rowland, C. T., Schon, E. A. & DiMauro, S. 1993. Two novel pathogenic mitochondrial DNA mutations affecting organelle number and protein synthesis. Is the tRNA(Leu(UUR)) gene an etiologic hot spot? *Journal of Clinical Investigation,* 92.

Moraes, C. T. & Hao, H. 1997. A disease-associated G5703A mutation in human mitochondrial DNA causes a conformational change and a marked decrease in steady-state levels of mitochondrial tRNA(Asn). *Molecular and cellular biology,* 17.

Moreno-Lastres, D., Fontanesi, F., García-Consuegra, I., Martín, M. A., Arenas, J., Barrientos, A. & Ugalde, C. 2012. Mitochondrial Complex I Plays an Essential Role in Human Respirasome Assembly. *Cell Metabolism,* 15**,** 324-335.

Morten, K. J., Cooper, J. M., Brown, G. K., Lake, B. D., Pike, D. & Poulton, J. 1993. A new point mutation associated with mitochondrial encephalomyopathy. *Human molecular genetics,* 2.

Nagaike, T., Suzuki, T., Tomari, Y., Takemoto-Hori, C., Negayama, F., Watanabe, K. & Ueda, T. 2001. Identification and characterization of mammalian mitochondrial tRNA nucleotidyltransferases. *Journal of Biological Chemistry,* 276**,** 40041-40049.

Narendra, D. P., Jin, S. M., Tanaka, A., Suen, D., Gautier, C. A., Shen, J., Cookson, M. R. & Youle, R. J. 2010. PINK1 Is Selectively Stabilized on Impaired Mitochondria to Activate Parkin. *PLOS Biology,* 8.

Naviaux, R. K. & Nguyen, K. V. 2004. mutations associated with Alpers' syndrome and mitochondrial DNA depletion. *Annals of Neurology,* 55**,** 706-712.

Naylor, K., Li, G. J., Vallejo, A. N., Lee, W. W., Koetz, K., Bryl, E., Witkowski, J., Fulbright, J., Weyand, C. M. & Goronzy, J. J. 2005. The influence of age on T cell generation and TCR diversity. *Journal of Immunology,* 174**,** 7446-7452.

Needs, H. I., Glover, E., Pereira, G. C., Witt, A., Hübner, W., Dodding, M. P., Henley, J. M. & Collinson, I. 2024. Rescue of mitochondrial import failure by intercellular organellar transfer. *Nature Communications,* 15.

Nemazee, D. 2017. Mechanisms of central tolerance for B cells. *Nature Reviews Immunology,* 17.

Nesbitt, V., Pitceathly, R. D., Turnbull, D. M., Taylor, R. W., Sweeney, M. G., Mudanohwo, E. E., Rahman, S., Hanna, M. G. & McFarland, R. 2013. The UK MRC Mitochondrial Disease Patient Cohort Study: clinical phenotypes associated with the m.3243A>G mutation--implications for diagnosis and management. *J Neurol Neurosurg Psychiatry,* 84**,** 936-8.

Netz, D. J. A., Stith, C. M., Stümpfig, M., Köpf, G., Vogel, D., Genau, H. M., Stodola, J. L., Lill, R., Burgers, P. M. J. & Pierik, A. J. 2012. Eukaryotic DNA polymerases

require an iron-sulfur cluster for the formation of active complexes. *Nature Chemical Biology,* 8**,** 125-132.
Ngo, H. B., Kaiser, J. T. & Chan, D. C. 2011. The mitochondrial transcription and packaging factor Tfam imposes a U-turn on mitochondrial DNA. *Nat Struct Mol Biol,* 18**,** 1290-6.
Nowell, P. C., Cole, L. J., Habermeyer, J. G. & Roan, P. L. 1956. Growth and Continued Function of Rat Marrow Cells in X-radiated Mice. *Cancer Res,* 16**,** 258-261.
O'Brien, K. L. & Finlay, D. K. 2019. Immunometabolism and natural killer cell responses. *Nature Reviews Immunology,* 19**,** 282-290.
Ohnmacht, C. & Voehringer, D. 2009. Basophil effector function and homeostasis during helminth infection. *Blood,* 113**,** 2816-25.
Ojala, D., Montoya, J. & Attardi, G. 1981. tRNA punctuation model of RNA processing in human mitochondria. *Nature,* 290**,** 470-4.
Olivo, P. D., Vandewalle, M. J., Laipis, P. J. & Hauswirth, W. W. 1983. Nucleotide-Sequence Evidence for Rapid Genotypic Shifts in the Bovine Mitochondrial-DNA D-Loop. *Nature,* 306**,** 400-402.
Otera, H., Wang, C. X., Cleland, M. M., Setoguchi, K., Yokota, S., Youle, R. J. & Mihara, K. 2010. Mff is an essential factor for mitochondrial recruitment of Drp1 during mitochondrial fission in mammalian cells. *Journal of Cell Biology,* 191**,** 1141-1158.
Palmer, C. S., Elgass, K. D., Parton, R. G., Osellame, L. D., Stojanovski, D. & Ryan, M. T. 2013. Adaptor Proteins MiD49 and MiD51 Can Act Independently of Mff and Fis1 in Drp1 Recruitment and Are Specific for Mitochondrial Fission. *Journal of Biological Chemistry,* 288**,** 27584-27593.
Panduro, M., Benoist, C. & Mathis, D. 2018. Treg cells limit IFN-γ production to control macrophage accrual and phenotype during skeletal muscle regeneration. *Proceedings of the National Academy of Sciences of the United States of America,* 115**,** E2585-E2593.
Patel, A. A., Zhang, Y., Fullerton, J. N., Boelen, L., Rongvaux, A., Maini, A. A., Bigley, V., Flavell, R. A., Gilroy, D. W., Asquith, B., Macallan, D. & Yona, S. 2017. The fate and lifespan of human monocyte subsets in steady state and systemic inflammation. *J Exp Med,* 214**,** 1913-1923.
Perandini, L. A., Chimin, P., Lutkemeyer, D. d. S. & Câmara, N. O. S. 2018. Chronic inflammation in skeletal muscle impairs satellite cells function during regeneration: can physical exercise restore the satellite cell niche? *The FEBS Journal,* 285.
Petruzzella, V., Moraes, C. T., Sano, M. C., Bonilla, E., DiMauro, S. & Schon, E. A. 1994. Extremely high levels of mutant mtDNAs co-localize with cytochrome c oxidase-negative ragged-red fibers in patients harboring a point mutation at nt 3243. *Hum Mol Genet,* 3**,** 449-54.
Picard, M., Zhang, J., Hancock, S., Derbeneva, O., Golhar, R., Golik, P., O'Hearn, S., Levy, S., Potluri, P., Lvova, M., Davila, A., Lin, C. S., Perin, J. C., Rappaport, E. F., Hakonarson, H., Trounce, I. A., Procaccio, V. & Wallace, D. C. 2014. Progressive increase in mtDNA 3243A>G heteroplasmy causes abrupt transcriptional reprogramming. *Proc Natl Acad Sci U S A,* 111**,** E4033-42.
Pickett, S. J., Grady, J. P., Ng, Y. S., Gorman, G. S., Schaefer, A. M., Wilson, I. J., Cordell, H. J., Turnbull, D. M., Taylor, R. W. & McFarland, R. 2018. Phenotypic heterogeneity in m.3243A > G mitochondrial disease: The role of nuclear factors. *Annals of Clinical and Translational Neurology,* 5**,** 333-345.

Pietras, E. M., Mirantes-Barbeito, C., Fong, S., Loeffler, D., Kovtonyuk, L. V., Zhang, S., Lakshminarasimhan, R., Chin, C. P., Techner, J.-M., Will, B., Nerlov, C., Steidl, U., Manz, M. G., Schroeder, T. & Passegué, E. 2016. Chronic interleukin-1 drives haematopoietic stem cells towards precocious myeloid differentiation at the expense of self-renewal. *Nature cell biology,* 18.

Pillay, J., den Braber, I., Vrisekoop, N., Kwast, L. M., de Boer, R. J., Borghans, J. A. M., Tesselaar, K. & Koenderman, L. 2010. In vivo labeling with 2H2O reveals a human neutrophil lifespan of 5.4 days. *Blood,* 116**,** 625-627.

Pinheiro J, B. D., DebRoy S, Sarkar D, R Core Team 2019. nlme: Linear and Nonlinear Mixed Effects Models. R package version 3.1-140.

Plitas, G. & Rudensky, A. Y. 2016. Regulatory T Cells: Differentiation and Function. *Cancer Immunology Research,* 4**,** 721-725.

Plummer, M. 2018. rjags: Bayesian graphical models using MCMC. R package version 4.13.

Pollizzi, K. N., Sun, I. H., Patel, C. H., Lo, Y. C., Oh, M. H., Waickman, A. T., Tam, A. J., Blosser, R. L., Wen, J. Y., Delgoffe, G. M. & Powell, J. D. 2016. Asymmetric inheritance of mTORC1 kinase activity during division dictates CD8+ T cell differentiation. *Nature Immunology,* 17**,** 704-+.

Porter, L., Toepfner, N., Bashant, K. R., Guck, J., Ashcroft, M., Farahi, N. & Chilvers, E. R. 2018. Metabolic Profiling of Human Eosinophils. *Frontiers in Immunology,* 9.

Posse, V., Shahzad, S., Falkenberg, M., Hällberg, B. M. & Gustafsson, C. M. 2015. TEFM is a potent stimulator of mitochondrial transcription elongation. *Nucleic Acids Research,* 43**,** 2615-2624.

Previte, D. M., O'Connor, E. C., Novak, E. A., Martins, C. P., Mollen, K. P. & Piganelli, J. D. 2017. Reactive oxygen species are required for driving efficient and sustained aerobic glycolysis during CD4

T cell activation. *Plos One,* 12.

Pronman, L., Rondinelli, M., Burkardt, D. D., Velayuthan, S., Khalili, A. S. & Bedoyan, J. K. 2019. Pearson Syndrome: A Rare Cause of Failure to Thrive in Infants. *Clin Pediatr (Phila),* 58**,** 819-824.

Pyle, A., Burn, D. J., Gordon, C., Swan, C., Chinnery, P. F. & Baudouin, S. V. 2010. Fall in circulating mononuclear cell mitochondrial DNA content in human sepsis. *Intensive Care Medicine,* 36**,** 956-962.

Pyle, A., Taylor, R. W., Durham, S. E., Deschauer, M., Schaefer, A. M., Samuels, D. C. & Chinnery, P. F. 2007. Depletion of mitochondrial DNA in leucocytes harbouring the 3243A→G mtDNA mutation. *Journal of Medical Genetics,* 44**,** 69-74.

Rahman, S., Poulton, J., Marchington, D. & Suomalainen, A. 2001. Decrease of 3243 A→G mtDNA mutation from blood in MELAS syndrome:: A longitudinal study. *American Journal of Human Genetics,* 68**,** 238-240.

Rajasimha, H. K., Chinnery, P. F. & Samuels, D. C. 2008a. Selection against pathogenic mtDNA mutations in a stem cell population leads to the loss of the 3243A-->G mutation in blood. *Am J Hum Genet,* 82**,** 333-43.

Rajasimha, H. K., Chinnery, P. F. & Samuels, D. C. 2008b. Selection against Pathogenic mtDNA Mutations in a Stem Cell Population Leads to the Loss of the 3243A→G Mutation in Blood. *Am J Hum Genet.*

Randolph, D. A., Huang, G. M., Carruthers, C. J. L., Bromley, L. E. & Chaplin, D. D. 1999. The role of CCR7 in TH1 and TH2 cell localization and delivery of B cell help in vivo. *Science,* 286**,** 2159-2162.

Rath, S., Sharma, R., Gupta, R., Ast, T., Chan, C., Durham, T. J., Goodman, R. P., Grabarek, Z., Haas, M. E., Hung, W. H. W., Joshi, P. R., Jourdain, A. A., Kim, S. H., Kotrys, A. V., Lam, S. S., McCoy, J. G., Meisel, J. D., Miranda, M., Panda, A., Patgiri, A., Rogers, R., Sadre, S., Shah, H., Skinner, O. S., To, T. L., Walker, M. A., Wang, H., Ward, P. S., Wengrod, J., Yuan, C. C., Calvo, S. E. & Mootha, V. K. 2021. MitoCarta3.0: an updated mitochondrial proteome now with sub-organelle localization and pathway annotations. *Nucleic Acids Research,* 49**,** D1541-D1547.

Rath, S. P., Gupta, R., Todres, E., Wang, H., Jourdain, A. A., Ardlie, K. G., Calvo, S. E., Mootha, V. K., Rath, S. P., Gupta, R., Todres, E., Wang, H., Jourdain, A. A., Ardlie, K. G., Calvo, S. E. & Mootha, V. K. 2024. Mitochondrial genome copy number variation across tissues in mice and humans. *Proceedings of the National Academy of Sciences,* 121.

Remick, B. C., Gaidt, M. M. & Vance, R. E. 2023. Effector-Triggered Immunity. *Annual Review of Immunology,* 41**,** 453-481.

Retter, M. W. & Nemazee, D. 1998. Receptor editing occurs frequently during normal B cell development. *Journal of Experimental Medicine,* 188**,** 1231-1238.

Richter, U., McFarland, R., Taylor, R. W. & Pickett, S. J. 2021. The molecular pathology of pathogenic mitochondrial tRNA variants. *Febs Letters,* 595**,** 1003-1024.

Riedl, S. J., Li, W. Y., Chao, Y., Schwarzenbacher, R. & Shi, Y. G. 2005. Structure of the apoptotic protease-activating factor 1 bound to ADP. *Nature,* 434**,** 926-933.

Rodriguez-Meira, A., O'Sullivan, J., Rahman, H. & Mead, A. J. 2020. TARGET-Seq: A Protocol for High-Sensitivity Single-Cell Mutational Analysis and Parallel RNA Sequencing. *STAR Protoc,* 1**,** 100125.

Roger, A. J., Muñoz-Gómez, S. A. & Kamikawa, R. 2017. The Origin and Diversification of Mitochondria. *Current Biology,* 27**,** R1177-R1192.

Romero-Garcia, S. & Prado-Garcia, H. 2019. Mitochondrial calcium: Transport and modulation of cellular processes in homeostasis and cancer (Review). *International Journal of Oncology,* 54**,** 1155-1167.

Ron-Harel, N., Santos, D., Ghergurovich, J. M., Sage, P. T., Reddy, A., Lovitch, S. B., Dephoure, N., Satterstrom, F. K., Sheffer, M., Spinelli, J. B., Gygi, S., Rabinowitz, J. D., Sharpe, A. H. & Haigis, M. C. 2016. Mitochondrial Biogenesis and Proteome Remodeling Promote One-Carbon Metabolism for T Cell Activation. *Cell Metabolism,* 24**,** 104-117.

Rossi, F. H., Okun, M., Yachnis, A., Quisling, R. & Triggs, W. J. 2002. Corticosteroid treatment of mitochondrial encephalomyopathies. *Neurologist,* 8**,** 313-315.

Rossignol, R., Faustin, B., Rocher, C., Malgat, M., Mazat, J. P. & Letellier, T. 2003. Mitochondrial threshold effects. *Biochemical Journal,* 370**,** 751-762.

Rotig, A., Bourgeron, T., Chretien, D., Rustin, P. & Munnich, A. 1995. Spectrum of mitochondrial DNA rearrangements in the Pearson marrow-pancreas syndrome. *Hum Mol Genet,* 4**,** 1327-30.

Roussou, R., Metzler, D., Padovani , F., Thoma, F., Schwarz, R., Shraiman, B., Schmoller, K. M. & Osman, C. 2024. Real-time assessment of mitochondrial DNA heteroplasmy dynamics at the single-cell level. *The EMBO Journal*.

Rufer, N., Zippelius, A., Batard, P., Pittet, M. J., Kurth, I., Corthesy, P., Cerottini, J. C., Leyvraz, S., Roosnek, E., Nabholz, M. & Romero, P. 2003. Ex vivo characterization of human CD8

T subsets with distinct replicative history and partial effector functions. *Blood,* 102**,** 1779-1787.

Sabre 2011. A Barcode Demultiplexing and Trimming Tool for FastQ Files.

Sagan, L. 1967. On the origin of mitosing cells. *J. Theor. Biol.,* 14**,** 225-274.
Sallusto, F., Lenig, D., Förster, R., Lipp, M. & Lanzavecchia, A. 1999. Two subsets of memory T lymphocytes with distinct homing potentials and effector functions. *Nature,* 401**,** 708-712.
Saneto, R. P. & Singh, K. K. 2010. Illness-induced exacerbation of Leigh syndrome in a patient with the MTATP6 mutation, m. 9185 T>C. *Mitochondrion,* 10.
Sasarman, F., Antonicka, H. & Shoubridge, E. A. 2008. The A3243G tRNALeu(UUR) MELAS mutation causes amino acid misincorporation and a combined respiratory chain assembly defect partially suppressed by overexpression of EFTu and EFG2. *Hum Mol Genet,* 17**,** 3697-707.
Satpathy, A. T., Granja, J. M., Yost, K. E., Qi, Y., Meschi, F., McDermott, G. P., Olsen, B. N., Mumbach, M. R., Pierce, S. E., Corces, M. R., Shah, P., Bell, J. C., Jhutty, D., Nemec, C. M., Wang, J., Wang, L., Yin, Y., Giresi, P. G., Chang, A. L. S., Zheng, G. X. Y., Greenleaf, W. J. & Chang, H. Y. 2019. Massively parallel single-cell chromatin landscapes of human immune cell development and intratumoral T cell exhaustion. *Nat Biotechnol,* 37**,** 925-936.
Schaefer, A. M., Phoenix, C., Elson, J. L., McFarland, R., Chinnery, P. F. & Turnbull, D. M. 2006. Mitochondrial disease in adults: A scale to monitor progression and treatment. *Neurology,* 66**,** 1932-1934.
Schmidl, C., Renner, K., Peter, K., Eder, R., Lassmann, T., Balwierz, P. J., Itoh, M., Nagao-Sato, S., Kawaji, H., Carninci, P., Suzuki, H., Hayashizaki, Y., Andreesen, R., Hume, D. A., Hoffmann, P., Forrest, A. R. R., Kreutz, M. P., Edinger, M., Rehli, M. & Consortium, F. 2014. Transcription and enhancer profiling in human monocyte subsets. *Blood,* 123**,** E90-E99.
Scholle, L. M., Zierz, S., Mawrin, C., Wickenhauser, C. & Urban, D. L. 2020. Heteroplasmy and Copy Number in the Common m.3243A>G Mutation-A Post-Mortem Genotype-Phenotype Analysis. *Genes,* 11.
Schreck, R., Rieber, P. & Baeuerle, P. A. 1991. Reactive Oxygen Intermediates as Apparently Widely Used Messengers in the Activation of the Nf-Kappa-B Transcription Factor and Hiv-1. *Embo Journal,* 10**,** 2247-2258.
Schriever, S. C., Deutsch, M. J., Adamski, J., Roscher, A. A. & Ensenauer, R. 2013. Cellular signaling of amino acids towards mTORC1 activation in impaired human leucine catabolism. *Journal of Nutritional Biochemistry,* 24**,** 824-831.
Schwartz, R. H. 2012. Historical Overview of Immunological Tolerance. *Cold Spring Harbor Perspectives in Biology,* 4.
Searcy, D. G. 2003. Metabolic integration during the evolutionary origin of mitochondria. *Cell Research,* 13**,** 229-238.
Sena, L. A., Li, S., Jairaman, A., Prakriya, M., Ezponda, T., Hildeman, D. A., Wang, C. R., Schumacker, P. T., Licht, J. D., Perlman, H., Bryce, P. J. & Chandel, N. S. 2013. Mitochondria Are Required for Antigen-Specific T Cell Activation through Reactive Oxygen Species Signaling. *Immunity,* 38**,** 225-236.
Shen, J. S., Chen, X., Hendershot, L. & Prywes, R. 2002. ER stress regulation of ATF6 localization by dissociation of BiP/GRP78 binding and unmasking of golgi localization signals. *Developmental Cell,* 3**,** 99-111.
Shoffner, J. M., Lott, M. T., Lezza, A. M. S., Seibel, P., Ballinger, S. W. & Wallace, D. C. 1990. Myoclonic epilepsy and ragged-red fiber disease (MERRF) is associated with a mitochondrial DNA tRNALys mutation. *Cell,* 61.
Sies, H. & Jones, D. P. 2020. Reactive oxygen species (ROS) as pleiotropic physiological signalling agents. *Nature Reviews Molecular Cell Biology,* 21**,** 363-383.

Sikorska, M., Sandhu, J. K., Simon, D. K., Pathiraja, V., Sodja, C., Li, Y., Ribecco-Lutkiewicz, M., Lanthier, P., Borowy-Borowski, H., Upton, A., Raha, S., Pulst, S. M. & Tarnopolsky, M. A. 2009. Identification of ataxia-associated mtDNA mutations (m.4052T>C and m.9035T>C) and evaluation of their pathogenicity in transmitochondrial cybrids. *Muscle & Nerve,* 40.

Siminovitch, L., McCulloch, E. A. & Till, J. E. 1963. The distribution of colony forming cells among spleen colonies. *Journal of cellular and comparative physiology,* 62.

Simons, B. D. & Karin, O. 2024. Tuning of plasma cell lifespan by competition explains the longevity and heterogeneity of antibody persistence. *Immunity,* 57.

Sinclair, L. V., Rolf, J., Emslie, E., Shi, Y. B., Taylor, P. M. & Cantrell, D. A. 2013. Control of amino-acid transport by antigen receptors coordinates the metabolic reprogramming essential for T cell differentiation. *Nat Immunol,* 14**,** 500-8.

Siota, M., Lim, J. B., Dang, Y. & Disis, M. L. 2011. ELISpot for measuring human immune responses to vaccines. *Expert Review of Vaccines,* 10**,** 299-306.

Slifka, M. K., Antia, R., Whitmire, J. K. & Ahmed, R. 1998. Humoral immunity due to long-lived plasma cells. *Immunity,* 8**,** 363-372.

Smirnova, E., Griparic, L., Shurland, D. L. & van der Bliek, A. M. 2001. Dynamin-related protein Drp1 is required for mitochondrial division in mammalian cells. *Molecular Biology of the Cell,* 12**,** 2245-2256.

Soleimanpour-Lichaei, H. R., Kühl, I., Gaisne, M., Passos, J. F., Wydro, M., Rorbach, J., Temperley, R., Bonnefoy, N., Tate, W., Lightowlers, R. & Chrzanowska-Lightowlers, Z. 2007. mtRF1a Is a Human Mitochondrial Translation Release Factor Decoding the Major Termination Codons UAA and UAG. *Molecular Cell,* 27.

Spang, A., Saw, J. H., Jorgensen, S. L., Zaremba-Niedzwiedzka, K., Martijn, J., Lind, A. E., van Eijk, R., Schleper, C., Guy, L. & Ettema, T. J. G. 2015. Complex archaea that bridge the gap between prokaryotes and eukaryotes. *Nature,* 521**,** 173-+.

Spencer, A. C. & Spremulli, L. L. 2004. Interaction of mitochondrial initiation factor 2 with mitochondrial fMet-tRNA. *Nucleic Acids Research,* 32.

Spinazzola, A., Invernizzi, F., Carrara, F., Lamantea, E., Donati, A., Dirocco, M., Giordano, I., Meznaric-Petrusa, M., Baruffini, E., Ferrero, I. & Zeviani, M. 2009. Clinical and molecular features of mitochondrial DNA depletion syndromes. *J Inherit Metab Dis,* 32**,** 143-58.

Spremulli, L. L., Coursey, A., Navratil, T. & Hunter, S. E. 2004. Initiation and elongation factors in mammalian mitochondrial protein biosynthesis. *Progress in Nucleic Acid Research and Molecular Biology, Vol 77,* 77**,** 211-261.

Stavnezer, J. & Schrader, C. E. 2014. Ig heavy chain class switch recombination: mechanism and regulation. *Journal of immunology,* 193.

Stehling, O. & Lill, R. 2013. The Role of Mitochondria in Cellular Iron-Sulfur Protein Biogenesis: Mechanisms, Connected Processes, and Diseases. *Cold Spring Harbor Perspectives in Biology,* 5.

Steinmann, G. G., Klaus, B. & Mullerhermelink, H. K. 1985. The Involution of the Aging Human Thymic Epithelium Is Independent of Puberty - a Morphometric Study. *Scandinavian Journal of Immunology,* 22**,** 563-575.

Stewart, J. B., Freyer, C., Elson, J. L., Wredenberg, A., Cansu, Z., Trifunovic, A. & Larsson, N. G. 2008. Strong purifying selection in transmission of mammalian mitochondrial DNA. *Plos Biology,* 6**,** 63-71.

Stokes, J. C., Bornstein, R. L., James, K., Park, K. Y., Spencer, K. A., Vo, K., Snell, J. C., Johnson, B. M., Morgan, P. G., Sedensky, M. M., Baertsch, N. A. & Johnson, S. C.

2022. Leukocytes mediate disease pathogenesis in the Ndufs4(KO) mouse model of Leigh syndrome. *Jci Insight,* 7.

Stroud, D. A., Surgenor, E. E., Formosa, L. E., Reljic, B., Frazier, A. E., Dibley, M. G., Osellame, L. D., Stait, T., Beilharz, T. H., Thorburn, D. R., Salim, A. & Ryan, M. T. 2016. Accessory subunits are integral for assembly and function of human mitochondrial complex I. *Nature,* 538**,** 123-+.

Su, T., Grady, J. P., Afshar, S., McDonald, S. A., Taylor, R. W., Turnbull, D. M. & Greaves, L. C. 2018. Inherited pathogenic mitochondrial DNA mutations and gastrointestinal stem cell populations. *J Pathol,* 246**,** 427-432.

Subburaj, Y., Cosentino, K., Axmann, M., Pedrueza-Villalmanzo, E., Hermann, E., Bleicken, S., Spatz, J. & García-Sáez, A. J. 2015. Bax monomers form dimer units in the membrane that further self-assemble into multiple oligomeric species. *Nature Communications,* 6.

Sue, C. M., Quigley, A., Katsabanis, S., Kapsa, R., Crimmins, D. S., Byrne, E. & Morris, J. G. L. 1998. Detection of MELAS A3243G point mutation in muscle, blood and hair follicles. *Journal of the Neurological Sciences,* 161**,** 36-39.

Sukumar, M., Liu, J., Mehta, Gautam U., Patel, Shashank J., Roychoudhuri, R., Crompton, Joseph G., Klebanoff, Christopher A., Ji, Y., Li, P., Yu, Z., Whitehill, Greg D., Clever, D., Eil, Robert L., Palmer, D. C., Mitra, S., Rao, M., Keyvanfar, K., Schrump, D. S., Wang, E., Marincola, F. M., Gattinoni, L., Leonard, Warren J., Muranski, P., Finkel, T. & Restifo, Nicholas P. 2016. Mitochondrial Membrane Potential Identifies Cells with Enhanced Stemness for Cellular Therapy. *Cell Metabolism,* 23.

Sumbayev, V. V., Nicholas, S. A., Streatfield, C. L. & Gibbs, B. F. 2009. Involvement of hypoxia-inducible factor-1 (HiF-1α) in IgE-mediated primary human basophil responses. *European Journal of Immunology,* 39**,** 3511-3519.

Sun, F., Huo, X., Zhai, Y. J., Wang, A. J., Xu, J. X., Su, D., Bartlam, M. & Rao, Z. H. 2005. Crystal structure of mitochondrial respiratory membrane protein complex II. *Cell,* 121**,** 1043-1057.

Supek, F., Bosnjak, M., Skunca, N. & Smuc, T. 2011. REVIGO summarizes and visualizes long lists of gene ontology terms. *PLoS One,* 6**,** e21800.

Suzuki, T., Suzuki, T., Wada, T., Saigo, K. & Watanabe, K. 2002. Taurine as a constituent of mitochondrial tRNAs: new insights into the functions of taurine and human mitochondrial diseases. *The EMBO Journal,* 21.

Tabara, L. C., Burr, S. P., Frison, M., Chowdhury, S. R., Paupe, V., Nie, Y., Johnson, M., Villar-Azpillaga, J., Viegas, F., Segawa, M., Anand, H., Petkevicius, K., Chinnery, P. F. & Prudent, J. 2024. MTFP1 controls mitochondrial fusion to regulate inner membrane quality control and maintain mtDNA levels. *Cell,* 187**,** 3619-3637 e27.

Takahashi, R., Macchini, M., Sunagawa, M., Jiang, Z. Y., Tanaka, T., Valenti, G., Renz, B. W., White, R. A., Hayakawa, Y., Westphalen, C. B., Tailor, Y., Iuga, A. C., Gonda, T. A., Genkinger, J., Olive, K. P. & Wang, T. C. 2021. Interleukin-1β-induced pancreatitis promotes pancreatic ductal adenocarcinoma via B lymphocyte-mediated immune suppression. *Gut,* 70**,** 330-341.

Takubo, K., Goda, N., Yamada, W., Iriuchishima, H., Ikeda, E., Kubota, Y., Shima, H., Johnson, R. S., Hirao, A., Suematsu, M. & Suda, T. 2010. Regulation of the HIF-1α Level Is Essential for Hematopoietic Stem Cells. *Cell Stem Cell,* 7.

Takubo, K., Nagamatsu, G., Kobayashi, Chiharu I., Nakamura-Ishizu, A., Kobayashi, H., Ikeda, E., Goda, N., Rahimi, Y., Johnson, Randall S., Soga, T., Hirao, A., Suematsu, M. & Suda, T. 2013. Regulation of Glycolysis by Pdk Functions as a

Metabolic Checkpoint for Cell Cycle Quiescence in Hematopoietic Stem Cells. *Cell Stem Cell,* 12.

Tan, B. G., Mutti, C. D., Shi, Y. H., Xie, X., Zhu, X. F., Silva-Pinheiro, P., Menger, K. E., Díaz-Maldonado, H., Wei, W., Nicholls, T. J., Chinnery, P. F., Minczuk, M., Falkenberg, M. & Gustafsson, C. M. 2022. The human mitochondrial genome contains a second light strand promoter. *Molecular Cell,* 82**,** 3646-+.

Tan, H., Yang, K., Li, y., Shaw, T. I., Wang, Y., Bastardo Blanco, D., Wang, X., Cho, J., Wang, H., Rankin, S., Guy, C., Peng, J. & Chi, H. 2017. Integrative Proteomics and Phosphoproteomics Profiling Reveals Dynamic Signaling Networks and Bioenergetics Pathways Underlying T Cell Activation. *Immunity,* 46.

Tarasenko, T. N., Pacheco, S. E., Koenig, M. K., Gomez-Rodriguez, J., Kapnick, S. M., Diaz, F., Zerfas, P. M., Barca, E., Sudderth, J., DeBerardinis, R. J., Covian, R., Balaban, R. S., DiMauro, S. & McGuire, P. J. 2017a. Cytochrome *c* Oxidase Activity Is a Metabolic Checkpoint that Regulates Cell Fate Decisions During T Cell Activation and Differentiation. *Cell Metabolism,* 25**,** 1254-+.

Tarasenko, T. N., Pacheco, S. E., Koenig, M. K., Gomez-Rodriguez, J., Kapnick, S. M., Diaz, F., Zerfas, P. M., Barca, E., Sudderth, J., DeBerardinis, R. J., Covian, R., Balaban, R. S., DiMauro, S. & McGuire, P. J. 2017b. Cytochrome c Oxidase Activity Is a Metabolic Checkpoint that Regulates Cell Fate Decisions During T Cell Activation and Differentiation. *Cell Metab,* 25**,** 1254-1268 e7.

Taylor, J. J., Pape, K. A. & Jenkins, M. K. 2012. A germinal center-independent pathway generates unswitched memory B cells early in the primary response. *Journal of Experimental Medicine,* 209**,** 597-606.

Temperley, R. J., Wydro, M., Lightowlers, R. N. & Chrzanowska-Lightowlers, Z. M. 2010. Human mitochondrial mRNAs-like members of all families, similar but different. *Biochimica Et Biophysica Acta-Bioenergetics,* 1797**,** 1081-1085.

Terzioglu, M., Ruzzenente, B., Harmel, J., Mourier, A., Jemt, E., López, M. D., Kukat, C., Stewart, J. B., Wibom, R., Meharg, C., Habermann, B., Falkenberg, M., Gustafsson, C. M., Park, C. B. & Larsson, N. G. 2013. MTERF1 Binds mtDNA to Prevent Transcriptional Interference at the Light-Strand Promoter but Is Dispensable for rRNA Gene Transcription Regulation. *Cell Metabolism,* 17**,** 618-626.

Tiegs, S. L., Russell, D. M. & Nemazee, D. 2011. Receptor Editing in Self-reactive Bone Marrow B Cells (Reprinted from vol 177, pg 1009, 1993). *Journal of Immunology,* 186**,** 1009-1020.

To, T. L., Mccoy, J. G., Ostriker, N. K., Sandler, L. S., Mannella, C. A. & Mootha, V. K. 2024. PMF-seq: a highly scalable screening strategy for linking genetics to mitochondrial bioenergetics. *Nature Metabolism,* 6.

Todt, F., Cakir, Z., Reichenbach, F., Emschermann, F., Lauterwasser, J., Kaiser, A., Ichim, G., Tait, S. W. G., Frank, S., Langer, H. F. & Edlich, F. 2015. Differential retrotranslocation of mitochondrial Bax and Bak. *Embo Journal,* 34**,** 67-80.

Tokunaga, M., Mita, S., Murakami, T., Kumamoto, T., Uchino, M., Nonaka, I. & Ando, M. 1994. Single muscle fiber analysis of mitochondrial myopathy, encephalopathy, lactic acidosis, and stroke-like episodes (MELAS). *Ann Neurol,* 35**,** 413-9.

Tokuyama, T., Hirai, A., Shiiba, I., Ito, N., Matsuno, K., Takeda, K., Saito, K., Mii, K., Matsushita, N., Fukuda, T., Inatome, R. & Yanagi, S. 2020. Mitochondrial Dynamics Regulation in Skin Fibroblasts from Mitochondrial Disease Patients. *Biomolecules,* 10.

Tomecki, R., Dmochowska, A., Gewartowski, K., Dziembowski, A. & Stepien, P. P. 2004. Identification of a novel human nuclear-encoded mitochondrial poly(A) polymerase. *Nucleic Acids Research,* 32.

Trifunovic, A., Wredenberg, A., Falkenberg, M., Spelbrink, J. N., Rovio, A. T., Bruder, C. E., Bohlooly-Y, M., Gidlöf, S., Oldfors, A., Wibom, R., Törnell, J., Jacobs, H. T. & Larsson, N. G. 2004. Premature ageing in mice expressing defective mitochondrial DNA polymerase. *Nature,* 429**,** 417-423.

Upton, J. P., Wang, L. K., Han, D., Wang, E. S., Huskey, N. E., Lim, L., Truitt, M., McManus, M. T., Ruggero, D., Goga, A., Papa, F. R. & Oakes, S. A. 2012. IRE1α Cleaves Select microRNAs During ER Stress to Derepress Translation of Proapoptotic Caspase-2. *Science,* 338**,** 818-822.

Vahsen, N., Candé, C., Brière, J. J., Bénit, P., Joza, N., Larochette, N., Mastroberardino, P. G., Pequignot, M. O., Casares, N., Lazar, V., Feraud, O., Debili, N., Wissing, S., Engelhardt, S., Madeo, F., Piacentini, M., Penninger, J. M., Schägger, H., Rustin, P. & Kroemer, G. 2004. AIF deficiency compromises oxidative phosphorylation. *Embo Journal,* 23**,** 4679-4689.

Van Goethem, G., Schwartz, M., Löfgren, A., Dermaut, B., Van Broeckhoven, C. & Vissing, J. 2003. Novel POLG mutations in progressive external ophthalmoplegia mimicking mitochondrial neurogastrointestinal encephalomyopathy. *European Journal of Human Genetics,* 11**,** 547-549.

Vardhana, S. A., Hwee, M. A., Berisa, M., Wells, D. K., Yost, K. E., King, B., Smith, M., Herrera, P. S., Chang, H. Y., Satpathy, A. T., van den Brink, M. R. M., Cross, J. R. & Thompson, C. B. 2020a. Impaired mitochondrial oxidative phosphorylation limits the self-renewal of T cells exposed to persistent antigen. *Nature Immunology,* 21**,** 1022-+.

Vardhana, S. A., Hwee, M. A., Berisa, M., Wells, D. K., Yost, K. E., King, B., Smith, M., Herrera, P. S., Chang, H. Y., Satpathy, A. T., van den Brink, M. R. M., Cross, J. R. & Thompson, C. B. 2020b. Impaired mitochondrial oxidative phosphorylation limits the self-renewal of T cells exposed to persistent antigen. *Nat Immunol,* 21**,** 1022-1033.

Veitia, R. A. 2018. How the most common mitochondrial DNA mutation (m.3243A>G) vanishes from leukocytes: a mathematical model. *Hum Mol Genet,* 27**,** 1565-1571.

Verbist, K. C., Guy, C. S., Milasta, S., Liedmann, S., Kaminski, M. M., Wang, R. N. & Green, D. R. 2016. Metabolic maintenance of cell asymmetry following division in activated T lymphocytes. *Nature,* 532**,** 389-+.

Verma, K., Ogonek, J., Varanasi, P. R., Luther, S., Bünting, I., Thomay, K., Behrens, Y. L., Mischak-Weissinger, E. & Hambach, L. 2017. Human CD8+CD57-T cells: Too young to be called "old". *Plos One,* 12.

Viant, C., Weymar, G. H. J., Escolano, A., Chen, S., Hartweger, H., Cipolla, M., Gazumyan, A. & Nussenzweig, M. C. 2020. Antibody Affinity Shapes the Choice between Memory and Germinal Center B Cell Fates. *Cell,* 183**,** 1298-+.

Victora, G. D. & Nussenzweig, M. C. 2022. Germinal Centers. *Annual Review of Immunology,* 40**,** 413-442.

Villanueva, R. A. M. & Chen, Z. J. 2019. ggplot2: Elegant Graphics for Data Analysis, 2nd edition. *Measurement-Interdisciplinary Research and Perspectives,* 17**,** 160-167.

Vinograd, J., Morris, J., Davidson, N. & Dove, W. F., Jr. 1963. The bouyant behavior of viral and bacterial DNA in alkaline CsCl. *Proc Natl Acad Sci U S A,* 49**,** 12-7.

Vrisekoop, N., den Braber, I., de Boer, A. B., Ruiter, A. F. C., Ackermans, M. T., van der Crabben, S. N., Schrijver, E. H. R., Spierenburg, G., Sauerwein, H. P., Hazenberg,

M. D., de Boer, R. J., Miedema, F., Borghans, J. A. M. & Tesselaar, K. 2008. Sparse production but preferential incorporation of recently produced naive T cells in the human peripheral pool. *Proceedings of the National Academy of Sciences of the United States of America,* 105**,** 6115-6120.

Wai, T., Teoli, D. & Shoubridge, E. A. 2008. The mitochondrial DNA genetic bottleneck results from replication of a subpopulation of genomes. *Nature Genetics,* 40**,** 1484-1488.

Walberg, M. W. & Clayton, D. A. 1981. Sequence and Properties of the Human Kb-Cell and Mouse L-Cell D-Loop Regions of Mitochondrial-DNA. *Nucleic Acids Research,* 9**,** 5411-5421.

Walcott, B. P., Edlow, B. L., Xia, Z. Q., Kahle, K. T., Nahed, B. V. & Schmahmann, J. D. 2012. Steroid Responsive A3243G Mutation MELAS. *Neurologist,* 18**,** 159-170.

Walker, M. A., Lareau, C. A., Ludwig, L. S., Karaa, A., Sankaran, V. G., Regev, A. & Mootha, V. K. 2020. Purifying Selection against Pathogenic Mitochondrial DNA in Human T Cells. *N Engl J Med,* 383**,** 1556-1563.

Walker, M. A., Li, S., Livak, K. J., Karaa, A., Wu, C. J. & Mootha, V. K. 2024. T cell activation contributes to purifying selection against the MELAS-associated m.3243A>G pathogenic variant in blood. *J Inherit Metab Dis,* 47**,** 757-765.

Wang, R., Dillon, C. P., Zhichang Shi, L., Milasta, S., Carter, R., Finkelstein, D., McCormick, L. L., Fitzgerald, P., Chi, H., Munger, J. & Green, D. R. 2011. The Transcription Factor Myc Controls Metabolic Reprogramming upon T Lymphocyte Activation. *Immunity,* 35.

Wang, Z. & Wu, M. 2015. An integrated phylogenomic approach toward pinpointing the origin of mitochondria. *Scientific Reports,* 5.

Warburg, O. 1956. On the Origin of Cancer Cells. *Science,* 123.

Watt, I. N., Montgomery, M. G., Runswick, M. J., Leslie, A. G. W. & Walker, J. E. 2010. Bioenergetic cost of making an adenosine triphosphate molecule in animal mitochondria. *Proceedings of the National Academy of Sciences of the United States of America,* 107**,** 16823-16827.

Wei, W., Pagnamenta, A. T., Gleadall, N., Sanchis-Juan, A., Stephens, J., Broxholme, J., Tuna, S., Odhams, C. A., Genomics England Research, C., BioResource, N., Fratter, C., Turro, E., Caulfield, M. J., Taylor, J. C., Rahman, S. & Chinnery, P. F. 2020. Nuclear-mitochondrial DNA segments resemble paternally inherited mitochondrial DNA in humans. *Nat Commun,* 11**,** 1740.

Wei, Y., Wang, L., Wei, Y. & Wang, L. 2018. Adult-onset Leigh syndrome with central fever and peripheral neuropathy due to mitochondrial 9176T>C mutation. *Neurological Sciences 2018 39:12,* 39.

Weiskopf, D., Bangs, D. J., Sidney, J., Kolla, R. V., De Silva, A. D., de Silva, A. M., Crotty, S., Peters, B. & Sette, A. 2015. Dengue virus infection elicits highly polarized CX3CR1+ cytotoxic CD4+T cells associated with protective immunity. *Proceedings of the National Academy of Sciences of the United States of America,* 112**,** E4256-E4263.

West, A. P., Khoury-Hanold, W., Staron, M., Tal, M. C., Pineda, C. M., Lang, S. M., Bestwick, M., Duguay, B. A., Raimundo, N., MacDuff, D. A., Kaech, S. M., Smiley, J. R., Means, R. E., Iwasaki, A. & Shadel, G. S. 2015. Mitochondrial DNA stress primes the antiviral innate immune response. *Nature,* 520**,** 553-+.

Westermann, B. 2010. Mitochondrial fusion and fission in cell life and death. *Nature Reviews Molecular Cell Biology,* 11**,** 872-884.

Wherry, E. J. 2011. T cell exhaustion. *Nature Immunology,* 12**,** 492-499.

Wieten, R. W., Jonker, E. F. F., van Leeuwen, E. M. M., Remmerswaal, E. B. M., ten Berge, I. J. M., de Visser, A. W., van Genderen, P. J. J., Goorhuis, A., Visser, L. G., Grobusch, M. P. & de Bree, G. J. 2016. A Single 17D Yellow Fever Vaccination Provides Lifelong Immunity; Characterization of Yellow-Fever-Specific Neutralizing Antibody and T-Cell Responses after Vaccination. *Plos One,* 11.

Wilkins, H. M., Carl, S. M., Weber, S. G., Ramanujan, S. A., Festoff, B. W., Linseman, D. A. & Swerdlow, R. H. 2015. Mitochondrial Lysates Induce Inflammation and Alzheimer's Disease-Relevant Changes in Microglial and Neuronal Cells. *Journal of Alzheimer's Disease,* 45.

Williams, H., Mack, C., Baraz, R., Marimuthu, R., Naralashetty, S., Li, S. P. & Medbury, H. 2023. Monocyte Differentiation and Heterogeneity: Inter-Subset and Interindividual Differences. *International Journal of Molecular Sciences,* 24.

Windt, G. J. W. V. d., Everts, B., Chang, C.-H., Curtis, J. D., Freitas, T. C., Amiel, E., Pearce, E. J. & Pearce, E. L. 2012. Mitochondrial Respiratory Capacity Is A Critical Regulator Of CD8+ T Cell Memory Development. *Immunity,* 36.

Wittenhagen, L. M. & Kelley, S. O. 2002. Dimerization of a pathogenic human mitochondrial tRNA. *Nat Struct Biol,* 9**,** 586-90.

Wu, D. J., Sanin, D. E., Everts, B., Chen, Q. Y., Qiu, J., Buck, M. D., Patterson, A., Smith, A. M., Chang, C. H., Liu, Z. P., Artyomov, M. N., Pearce, E. L., Cella, M. & Pearce, E. J. 2016. Type 1 Interferons Induce Changes in Core Metabolism that Are Critical for Immune Function. *Immunity,* 44**,** 1325-1336.

Wu, L. L., Yan, Z. Q., Jiang, Y. Y., Chen, Y. Y., Du, J., Guo, L. J., Xu, J. J., Luo, Z. H. & Liu, Y. 2023. Metabolic regulation of dendritic cell activation and immune function during inflammation. *Frontiers in Immunology,* 14.

Xia, D., Yu, C. A., Kim, H., Xia, J. Z., Kachurin, A. M., Zhang, L., Yu, L. & Deisenhofer, J. 1997. Crystal structure of the cytochrome bc1 complex from bovine heart mitochondria. *Science,* 277**,** 60-6.

Xiong, Y. J., Chen, H. T., Lin, P. F., Wang, A. H., Wang, L. & Jin, Y. P. 2017. ATF6 knockdown decreases apoptosis, arrests the S phase of the cell cycle, and increases steroid hormone production in mouse granulosa cells. *American Journal of Physiology-Cell Physiology,* 312**,** C341-C353.

Xu, F., Ackerley, C., Maj, M. C., Addis, J. B. L., Levandovskiy, V., Lee, J., MacKay, N., Cameron, J. M. & Robinson, B. H. 2008. Disruption of a mitochondrial RNA-binding protein gene results in decreased cytochrome *c* expression and a marked reduction in ubiquinol-cytochrome *c* reductase activity in mouse heart mitochondria. *Biochemical Journal,* 416**,** 15-26.

Xu, K., Yin, N., Peng, M., Stamatiades, E. G., Shyu, A., Li, P., Zhang, X., Do, M. H., Wang, Z. Q., Capistrano, K. J., Chou, C., Levine, A. G., Rudensky, A. Y. & Li, M. O. 2021. Glycolysis fuels phosphoinositide 3-kinase signaling to bolster T cell immunity. *Science,* 371**,** 405-+.

Yakubovskaya, E., Mejia, E., Byrnes, J., Hambardjieva, E. & Garcia-Diaz, M. 2010. Helix unwinding and base flipping enable human MTERF1 to terminate mitochondrial transcription. *Cell,* 141**,** 982-93.

Yamamoto, K., Sato, T., Matsui, T., Sato, M., Okada, T., Yoshida, H., Harada, A. & Mori, K. 2007. Transcriptional induction of mammalian ER quality control proteins is mediated by single or combined action of ATF6α and XBP1. *Developmental Cell,* 13**,** 365-376.

Yang, K., Blanco, D. B., Chen, X., Dash, P., Neale, G., Rosencrance, C., Easton, J., Chen, W. A., Cheng, C. D., Dhungana, Y., Anil, K. C., Awad, W., Guo, X. Z. J., Thomas,

P. G. & Chi, H. B. 2018. Metabolic signaling directs the reciprocal lineage decisions of αβ and γδ T cells. *Science Immunology,* 3.

Yang, K., Shrestha, S., Zeng, H., Karmaus, P. W. F., Neale, G., Vogel, P., Guertin, D. A., Lamb, R. F. & Chi, H. 2013. T Cell Exit from Quiescence and Differentiation into Th2 Cells Depend on Raptor-mTORC1-Mediated Metabolic Reprogramming. *Immunity,* 39.

Yasukawa, T., Suzuki, T., Suzuki, T., Ueda, T., Ohta, S. & Watanabe, K. 2000. Modification defect at anticodon wobble nucleotide of mitochondrial tRNAs

(UUR) with pathogenic mutations of mitochondrial myopathy, encephalopathy, lactic acidosis, and stroke-like episodes. *Journal of Biological Chemistry,* 275**,** 4251-4257.

Ye, F., Huang, W. T. & Guo, G. J. 2017. Studying hematopoiesis using single-cell technologies. *Journal of Hematology & Oncology,* 10.

Ye, J., Rawson, R. B., Komuro, R., Chen, X., Davé, U. P., Prywes, R., Brown, M. S. & Goldstein, J. L. 2000. ER stress induces cleavage of membrane-bound ATF6 by the same proteases that process SREBPs. *Molecular Cell,* 6**,** 1355-1364.

Ye, Y. S., Gaugler, B., Mohty, M. & Malard, F. 2020. Plasmacytoid dendritic cell biology and its role in immune-mediated diseases. *Clinical & Translational Immunology,* 9.

Yen, M. Y., Lee, H. C., Wang, A. G., Chang, W. L., Liu, J. H. & Wei, Y. H. 1999. Exclusive homoplasmic 11778 mutation in mitochondrial DNA of Chinese patients with Leber's hereditary optic neuropathy. *Jpn J Ophthalmol,* 43**,** 196-200.

Yi, J. S., Holbrook, B. C., Michalek, R. D., Laniewski, N. G. & Grayson, J. M. 2006a. Electron transport complex I is required for CD8+ T cell function. *Journal of Immunology,* 177**,** 852-862.

Yi, J. S., Holbrook, B. C., Michalek, R. D., Laniewski, N. G. & Grayson, J. M. 2006b. Electron transport complex I is required for CD8+ T cell function. *J Immunol,* 177**,** 852-62.

Yokota, M., Hatakeyama, H., Okabe, S., Ono, Y. & Goto, Y. I. 2015. Mitochondrial respiratory dysfunction caused by a heteroplasmic mitochondrial DNA mutation blocks cellular reprogramming. *Human Molecular Genetics,* 24**,** 4698-4709.

Yoneda, M., Chomyn, A., Martinuzzi, A., Hurko, O. & Attardi, G. 1992. Marked Replicative Advantage of Human Mtdna Carrying a Point Mutation That Causes the Melas Encephalomyopathy. *Proceedings of the National Academy of Sciences of the United States of America,* 89**,** 11164-11168.

Yoshikawa, S., Shinzawa-Itoh, K. & Tsukihara, T. 1998. Crystal structure of bovine heart cytochrome c oxidase at 2.8 Å resolution. *Journal of Bioenergetics and Biomembranes,* 30**,** 7-14.

Yoshimi, A., Grunert, S. C., Cario, H., Fisch, A., Gross-Wieltsch, U., Timmermann, K., Kontny, U., Lobitz, S., Odenthal, H. S., Schmid, I., Uetz, B., Holl, T., Rotig, A., Lucke, T., Borkhardt, A., Strauss, G., Hohnecker, A., Metzler, M., Karall, D. & Niemeyer, C. M. 2021. Haematological characteristics and spontaneous haematological recovery in Pearson syndrome. *Br J Haematol,* 193**,** 1283-1287.

Zhang, H. F. M., Ye, X., Su, Y., Yuan, J., Liu, Z., Stein, D. A. & Yang, D. C. 2010. Coxsackievirus B3 Infection Activates the Unfolded Protein Response and Induces Apoptosis through Downregulation of p58

and Activation of CHOP and SREBP1. *Journal of Virology,* 84**,** 8446-8459.

Zhang, J., Koolmeister, C., Han, J., Filograna, R., Hanke, L., Àdori, M., Sheward, D. J., Teifel, S., Gopalakrishna, S., Shao, Q., Liu, Y., Zhu, K., Harris, R. A., McInerney,

G., Murrell, B., Aoun, M., Bäckdahl, L., Holmdahl, R., Pekalski, M., Wedell, A., Engvall, M., Wredenberg, A., Karlsson Hedestam, G. B., Castro Dopico, X. & Rorbach, J. 2023. Antigen receptor stimulation induces purifying selection against pathogenic mitochondrial tRNA mutations. *JCI insight,* 8.

Zheng, G. Q., Qin, Y. D., Clark, W. C., Dai, Q., Yi, C. Q., He, C., Lambowitz, A. M. & Pan, T. 2015. Efficient and quantitative high-throughput tRNA sequencing. *Nature Methods,* 12**,** 835-+.

Zheng, Y., Collins, S. L., Lutz, M. A., Allen, A. N., Kole, T. P., Zarek, P. E. & Powell, J. D. 2007. A role for mammalian target of rapamycin in regulating T cell activation versus anergy. *Journal of Immunology,* 178**,** 2163-2170.

Zhong, Z. Y., Liang, S., Sanchez-Lopez, E., He, F., Shalapour, S., Lin, X. J., Wong, J., Ding, S. Y., Seki, E., Schnabl, B., Hevener, A. L., Greenberg, H. B., Kisseleva, T. & Karin, M. 2018. New mitochondrial DNA synthesis enables NLRP3 inflammasome activation. *Nature,* 560**,** 198-+.

Zhu, H. B., Bhatt, B., Sivaprakasam, S., Cai, Y. F., Liu, S. Y., Kodeboyina, S. K., Patel, N., Savage, N. M., Sharma, A., Kaufman, R. J., Li, H. L. & Singh, N. 2019. Ufbp1 promotes plasma cell development and ER expansion by modulating distinct branches of UPR. *Nature Communications,* 10.

Zickermann, V., Wirth, C., Nasiri, H., Siegmund, K., Schwalbe, H., Hunte, C. & Brandt, U. 2015. Mechanistic insight from the crystal structure of mitochondrial complex I. *Science,* 347**,** 44-49.